

Molecular Characterization of ***Mycobacterium chelonae* biofilms**

By

Perla Jazmín Vega Domínguez

A thesis submitted to the University of Birmingham

for the degree of

DOCTOR OF PHILOSOPHY

Institute of Microbiology and Infection

School of Biosciences

University of Birmingham

September of 2019

UNIVERSITY OF
BIRMINGHAM

University of Birmingham Research Archive

e-theses repository

This unpublished thesis/dissertation is copyright of the author and/or third parties. The intellectual property rights of the author or third parties in respect of this work are as defined by The Copyright Designs and Patents Act 1988 or as modified by any successor legislation.

Any use made of information contained in this thesis/dissertation must be in accordance with that legislation and must be properly acknowledged. Further distribution or reproduction in any format is prohibited without the permission of the copyright holder.

ABSTRACT

Mycobacterium chelonae is a non-tuberculous mycobacteria that is ubiquitously found in the environment. It can cause infections in humans, and it is regarded as one of the most drug-resistant mycobacteria, attribute partially explained due to the poor permeability of its cell wall. Because *M. chelonae* causes infections and persists in the environment as a biofilm, we studied pellicular biofilms, aiming to elucidate its molecular components and structure. Using scanning electron microscopy, we detected the presence of an extracellular matrix coating the bacilli residing in a pellicle, and also detected the presence of pores. With fluorescent microscopy, biochemical analysis, and Raman spectroscopy, we characterized the components of the extracellular matrix, identifying proteins and lipids as the principal components. We also identified an accumulation of free mycolic acids and phosphatidylglycerol in *M. chelonae* pellicles. After analyzing the transcripts of *M. chelonae* pellicles, we identified down regulation of transporters, and upregulation of genes belonging to the REDOX metabolism, and the oxidative phosphorylation pathway. The characterization of *M. chelonae* pellicles in this thesis will contribute to the understanding of biofilm formation in this pathogen for the development of anti-biofilm strategies.

DECLARATION

The work presented in this thesis was carried out in the School of Biosciences at the University of Birmingham, U.K., B15 2TT, during the period September 2015 to September 2019. The work in this thesis is original except where acknowledged by reference. No part of the work is being, or has been submitted for a degree, diploma or any other qualification at any other University.

ACKNOWLEDGMENTS

First and foremost, I would like to thank Apoorva Bhatt, my supervisor, for giving me the opportunity to conduct this research project. I am thankful for his constant support and guidance through the development of this thesis.

I would also like to thank the Mexican Science and Technology Council (CONACYT) for funding this Ph. D. (scholarship number 411092).

A special thanks to Eliza Peterson, Nitin Baliga, and Min Pan, from the Institute of Systems Biology, Seattle; for their thorough assistance on the transcriptome analysis. I also would like to thank Alessandro DiMaio from the Birmingham Advanced Light Microscopy facility at the University of Birmingham for his guidance in confocal microscopy. A special thanks to Saumya Singh and Siva Umapathy from the Indian Institute of Science, Bangalore; for the Raman spectra acquisition. I would also like to thank Laurent Kremer from the Institut de Recherche en Infectiologie de Montpellier, FR; for providing the pMV306-eGFP plasmid used in this work.

I am also thankful to Luke Alderwick and Timothy Overton, for their feedback during the supervision meetings. I am grateful to the members from the Bhatt Lab, Rebeca Bailo, Nabiela Moolla, Albel Singh, Anja Djockic, Hayleah Pickford, Charlotte Cooper, and Helen Clayton, for their support and advice. I would also like to thank Natacha Verapeen and other members of the Besra's and Alderwick's for their continuous help.

Finally, I would like to thank my parents, sister, and boyfriend for their encouragement and unconditional support through this Ph. D.

This thesis is dedicated to my parents.

Esta tesis está dedicada a mis padres.

TABLE OF CONTENTS

Chapter 1	General introduction	1
1.1	The genus <i>Mycobacterium</i>	2
1.2	Non-tuberculous mycobacteria	3
1.3	Importance of NTM for human health	4
1.4	<i>Mycobacterium chelonae</i>	6
1.1.1	<i>M. chelonae</i> as a human pathogen	7
1.4.1	Skin and soft tissue infections	8
1.4.2	Catheter and port- associated infections	9
1.4.3	Endocarditis	10
1.4.4	Eye infections	10
1.5	Management of <i>M. chelonae</i> infections	11
1.6	Mycobacterial cell envelope	12
1.6.1	The structure of the mycobacterial envelope	13
1.7	Biofilms	28
1.7.1	The development of the biofilm	29
1.8	Biofilms of mycobacteria	30
1.8.1	Lipid metabolism during biofilm formation	31
1.8.2	Carbohydrates and biofilm formation	33
1.8.3	Role of extracellular DNA in biofilms	34

1.8.4	Proteins in mycobacterial biofilms_____	35
1.9	Is there a unified mechanism for biofilm formation in mycobacteria? ____	35
1.10	Aim _____	38
1.10.1	Specific objectives _____	38
Chapter 2	Microscopy of <i>Mycobacterium chelonae</i> pellicular biofilms _____	39
2.1	Introduction _____	40
2.2	Aim _____	42
2.2.1	Specific objectives _____	42
2.3	Results _____	42
2.3.1	<i>Mycobacterium chelonae</i> pellicles have similar ultrastructure to other mycobacterial biofilms. _____	42
2.3.2	<i>Mycobacterium chelonae</i> pellicles are composed of lipids, eDNA, carbohydrates, and proteins. _____	45
2.4	Discussion _____	53
Chapter 3	Analysis of the extra polymeric substances of <i>Mycobacterium chelonae</i> biofilms	56
3.1	Introduction _____	57
3.2	Aim _____	58
3.2.1	Specific objectives: _____	58
3.3	Results _____	58
3.3.1	The lipid profile of <i>M. chelonae</i> biofilms is different from its planktonic counterpart _____	59

3.3.2	The glucose content of surface-exposed of <i>M. chelonae</i> biofilm decreases as the biofilm ages.	68
3.4	Discussion	71
Chapter 4 Raman spectroscopy for the study of <i>Mycobacterium chelonae</i> biofilms		74
4.1	Introduction	75
4.2	Aim	76
4.2.1	Specific objectives	76
4.3	Results	77
4.3.1	Characteristic Raman spectra of <i>M. chelonae</i> cultures	77
4.3.2	PCA discerns between Raman spectra from <i>M. chelonae</i> pellicles and planktonic bacteria	79
4.3.3	PCA discerns between <i>M. chelonae</i> planktonic bacteria at OD ₆₀₀ =1 and OD ₆₀₀ =3.	89
4.3.4	PCA discerns between <i>M. chelonae</i> planktonic bacteria at OD ₆₀₀ =1 and OD ₆₀₀ =3.	95
4.4	Discussion	100
Chapter 5 A study of the <i>Mycobacterium chelonae</i> biofilm transcriptome		101
5.1	Introduction	102
5.2	Aim	103
5.2.1	Specific objectives	103
5.3	Results	104

5.3.1	The gene expression profiles of <i>Mycobacterium chelonae</i> biofilms are different from planktonic cultures. _____	104
5.3.2	The enriched metabolic pathways in <i>M. chelonae</i> biofilms are different. _____	110
5.4	Discussion _____	122
Chapter 6	General discussion _____	123
6.1	General discussion and future work _____	124
Chapter 7	Materials and methods _____	130
7.1	Chemicals and reagents _____	131
7.2	Culture media preparation _____	131
7.2.1	7H9/OADC broth _____	131
7.2.2	7H11/OADC _____	131
7.2.3	Sauton's media _____	132
7.3	Preparation of stocks of fluorescent dyes _____	132
7.3.1	Nile Red stock _____	132
7.3.2	Propidium Iodide Stock _____	133
7.3.3	Concanavalin A Alexa Fluor 647 stock _____	133
7.4	Culture conditions _____	133
7.4.1	Propagation of <i>M. chelonae</i> _____	133
7.4.2	Biofilm formation _____	133
7.4.3	Planktonic cultures _____	134
7.5	Transformation of <i>M. chelonae</i> _____	134

7.5.1	Preparation of electrocompetent <i>Mycobacterium chelonae</i> _____	135
7.5.2	Electroporation of <i>Mycobacterium chelonae</i> _____	135
7.6	Microscopy _____	136
7.6.1	Scanning electron microscopy of <i>M. chelonae</i> biofilms _____	136
7.6.2	CLSM of <i>M. chelonae</i> biofilms _____	136
7.7	RNAseq _____	139
7.7.1	RNA extraction _____	139
7.7.2	rRNA depletion _____	140
7.7.3	Library preparation _____	141
7.7.4	Sequencing _____	143
7.7.5	DEG and pathway enrichment analysis _____	143
7.7.6	Data interpretation and visualization _____	144
7.8	Raman spectroscopy _____	144
7.8.1	Sample preparation _____	144
7.8.2	Spectra acquisition _____	145
7.8.3	Data visualization and analysis _____	145
7.9	Lipid analysis _____	146
7.9.1	Radiolabelling of <i>M. chelonae</i> cultures _____	146
7.9.2	Lipid extraction _____	146
7.9.3	Mycolic acid derivatization _____	147
7.9.4	Quantification of radioactivity _____	148
7.9.5	Thin layer chromatography _____	149

7.10	Analysis of the extracellular carbohydrates	149
7.10.1	Extraction of extracellular polysaccharides	150
7.10.2	Synthesis of alditol acetates	151
7.10.3	Gas chromatography of alditol acetates	152
Appendices		153
Appendix 1: Chromatograms of alditol acetates from capsular polysaccharides from 5-day old <i>M. chelonae</i> pellicles		154
Appendix 2: Chromatograms of alditol acetates from capsular polysaccharides from 10-day old <i>M. chelonae</i> pellicles		155
Appendix 3: Chromatograms of alditol acetates from capsular polysaccharides from <i>M. chelonae</i> planktonic cultures OD ₆₀₀ =1.		156
Appendix 3: Chromatograms of alditol acetates from capsular polysaccharides from <i>M. chelonae</i> planktonic cultures OD ₆₀₀ =3.		157
Appendix 4: Common DEG in Plancktonic t2, Biofilm t1, and Biofilm t2.		158
Appendix 5: Common DEG in Plancktonic t2 and Biofilm t1, but not DE in Biofilm t2.		159
Appendix 6: Common DEG in Planktonic t2 and Biofilm t2, but not DE in Biofilm t1.		160
Appendix 7: Common DEG in Biofilm t1 and Biofilm t2, but not in Planktonic t2		161
Appendix 8: DEG only in Planktonic t2.		166
Appendix 9: DEG only in Biofilm t1.		167
Appendix 10: DEG only in Biofilm t2.		168

LIST OF FIGURES

<i>Figure 1-1. Seven-day old colony of Mycobacterium chelonae.</i>	7
<i>Figure 1-2. Schematic representation of the mycobacterial cell envelope.</i>	14
<i>Figure 1-3. Phospholipids present in the MIM.</i>	16
<i>Figure 1-4. Schematic representation of mycolic acids.</i>	20
<i>Figure 1-5. Trehalose dimycolate.</i>	23
<i>Figure 1-6. Generic structure of glycopeptidolipids.</i>	24
<i>Figure 1-7. Generic structure of capsular α-glucan from mycobacterial species.</i>	26
<i>Figure 1-8. The biofilm life cycle</i>	30
<i>Figure 2-1. Five-day old M. chelonae pellicle growth in Sauton's media at 30°C.</i>	43
<i>Figure 2-2. SEM micrographs of M. chelonae cultures.</i>	45
<i>Figure 2-3. CLSM images of M. chelonae planktonic bacteria.</i>	47
<i>Figure 2-4. CLSM images of M. chelonae pellicles.</i>	49
<i>Figure 2-5. Relative volumes of components of M. chelonae ECM</i>	52
<i>Figure 3-1. M. chelonae biofilms growth for five (A) and ten (B) days in Sauton's media at 30°C.</i>	59
<i>Figure 3-2. TLC of M. chelonae apolar lipids resolved using system A.</i>	61
<i>Figure 3-3. TLC of M. chelonae apolar lipids resolved using system B.</i>	62
<i>Figure 3-4. TLC of M. chelonae apolar lipids resolved using system C.</i>	63
<i>Figure 3-5. TLC of M. chelonae apolar lipids resolved using system D.</i>	64
<i>Figure 3-6. TLC of M. chelonae polar lipids resolved using system D.</i>	65
<i>Figure 3-7. TLC of M. chelonae polar lipids resolved using system E.</i>	66
<i>Figure 3-8. Argentation TLC of M. chelonae mycolic acid methylesters.</i>	67

<i>Figure 3-9. The relative abundance of sugars and Myo-inositol extracted from EPS of M. chelonae cultures.</i>	71
<i>Figure 4-1. Average Raman spectra from M. chelonae cultures.</i>	78
<i>Figure 4-2. Scree plot showing the percentage of the explained variance by the first twenty PCs in the PCA involving Raman spectra from M. chelonae pellicles and planktonic cultures.</i>	80
<i>Figure 4-3. Visual representation of Raman spectra from M. chelonae cultures in terms of PC1, PC2, and PC3.</i>	81
<i>Figure 4-4. Annotated average Raman spectra obtained from M. chelonae pellicles and planktonic cultures.</i>	84
<i>Figure 4-5. Selected Raman shifts associated with the glycosidic bond.</i>	88
<i>Figure 4-6. Scree plot showing the percentage of the explained variance by the first twenty PCs in the PCA involving Raman spectra from M. chelonae planktonic cultures OD₆₀₀=1 and OD₆₀₀=3.</i>	89
<i>Figure 4-7. Visual representation of Raman spectra from M. chelonae planktonic cultures in terms of PC1 and PC2.</i>	90
<i>Figure 4-8 Annotated average Raman spectra obtained from M. chelonae pellicles and planktonic cultures.</i>	92
<i>Figure 4-9. Scree plot showing the percentage of the explained variance by the first twenty PCs in the PCA involving Raman spectra from 5 and 10-day M. chelonae pellicles.</i>	95
<i>Figure 4-10 Visual representation of Raman spectra from M. chelonae pellicles in terms of PC1 and PC2.</i>	96
<i>Figure 4-11. Annotated average Raman spectra obtained from M. chelonae pellicles.</i>	97

<i>Figure 5-1. Heat map depicting the Log2FC of the DEG in 5 (Biofilm t1) and 10-day (Biofilm t2) old M. chelonae pellicles, and M. chelonae Planktonic culture OD=3 (Planktonic t2).</i>	105
<i>Figure 5-2. Venn diagram of the DEG in 5 and 10-day old M. chelonae pellicles and planktonic cultures OD=3.</i>	110
<i>Figure 5-3 Enriched metabolic subsystems in 5-day old M. chelonae pellicles.</i>	117
<i>Figure 5-4. Enriched metabolic subsystems in 10-day old M. chelonae pellicles</i>	118
<i>Figure 6-1. Model for M. chelonae biofilm formation.</i>	125

LIST OF TABLES

<i>Table 2-1. Relative biovolumes and colocalization coefficients of the components of the M. chelonae pellicles ECM.</i>	51
<i>Table 3-1. The relative content of sugars and Myo-inositol in M. chelonae EPS.</i>	70
<i>Table 3-2. Relative molar ratio of arabinose, mannose, and Glucose, extracted from M. chelonae EPS.</i>	70
<i>Table 4-1. Top 20 Raman shifts with a high contribution to the PCs.</i>	82
<i>Table 4-2. Representative Raman shifts with a high contribution to the three PCs selected to describe M. chelonae pellicles and planktonic cultures.</i>	85
<i>Table 4-3. Raman shifts with high contribution to PC1 and PC2 in the PCA of M. chelonae planktonic cultures.</i>	91
<i>Table 4-4. Representative Raman shifts with a high contribution to the two PCs selected to describe M. chelonae planktonic cultures.</i>	93
<i>Table 4-5 Representative Raman shifts with a high contribution to the three PCs selected to describe M. chelonae pellicles.</i>	98
<i>Table 5-2 Top 50 differentially expressed genes with the highest absolute fold change from M. chelonae planktonic culutres OD₆₀₀=3.</i>	105
<i>Table 5-3 Top 50 differentially expressed genes with the highest absolute fold change from 5-day old M. chelonae pellicles.</i>	106
<i>Table 5-4. Top 50 differentially expressed genes with the highest absolute fold change from 10-day old M. chelonae pellicles.</i>	108
<i>Table 5-5. Enriched metabolic pathways in 5-day old M. chelonae pellicles.</i>	111
<i>Table 5-6. Enriched metabolic pathways in 10-day old M. chelonae pellicles.</i>	113
<i>Table 7-1. Sauton's media composition.</i>	132

<i>Table 7-2. Conditions for biofilm formation.</i>	<i>134</i>
<i>Table 7-3. Staining conditions.</i>	<i>137</i>
<i>Table 7-4. Acquisition parameters.</i>	<i>138</i>
<i>Table 7-5. Solvents systems for TLC.</i>	<i>149</i>

LIST OF ABBREVIATIONS

ACP	Acyl carrier protein
AcPIM	Acetylated phosphatidylinositom mannoside
ADP	Adenosindiphosphate
AG	Arabinogalactan
AGP	Arabinogalactan-peptidoglycan complex
AM	Arabinomannan
Araf	Arabinofuranose
ATP	Adenosintriphosphate
CLSM	Confocal laser scanning microscopy
ConcA	Concanavalin A
DE	Differentially expressed
DEG	Differentially expressed genes
DNA	Deoxyribonucleic acid
ECM	Extracellular matrix
EDTA	Ethylenediaminetetraacetic acid
eDNA	Extracellular DNA
EPS	Extra polymeric substances
FMA	Free mycolic acids
g	Gram
Galf	Galactofuranose
GC	Gas chromatography

L	Litre
LAM	Lipoarabinomannan
LM	Lipomannan
M	Molar
MA	Mycolic acid
mAGP	mycolyl-arabinogalactan-peptidoglycan
Manp	Mannopyranose
MIM	Mycobacterial Inner Membrane
MOM	Mycobacterial Outer Membrane
NAD	Nicotinamide adenine dinucleotide
NADH	Reduced nicotinamide adenine dinucleotide
NTM	Non Tuberculous Mycobacteria
OD	Optical density
PC	Principal components
PCA	Principal component analysis
PG	Peptidoglycan
PI	Phosphatidylinositol
PIM	Phosphatidylinositol mannoside
pRpp	5-phosphoribofuranose pyrophosphate
RNA	Ribonucleic acid
TBAH	Tetrabutylammonium hydroxide
TDM	Trehalose dimycolate
TE	Tris-EDTA
TFA	Trifluoroacetic acid

TLC	Thin layer chromatography
-----	---------------------------

Chapter 1 General introduction

1.1 The genus *Mycobacterium*

The genus *Mycobacterium* belongs to the phylum *Actinobacteria* and consists of rod-shaped bacilli with a high content of G+C, and comprises over 170 species (Goodfellow, 2012). Most mycobacteria are non-pathogenic and occur ubiquitously in water and soil (Falkinham, 2009), and some of them are used in steroids biotechnology (Fernández-Cabezón et al., 2018). However, the most studied members of this genus are obligated pathogens, like *Mycobacterium tuberculosis* and *Mycobacterium leprae*, responsible for causing human tuberculosis (TB) and leprosy, respectively; or animal pathogens such as *Mycobacterium bovis*, responsible for bovine tuberculosis.

Because of the magnitude of the problem that TB represents for human health, *M. tuberculosis* is the most extensively studied mycobacteria. Tuberculosis is an airborne disease that affects the lungs primarily, and it is estimated that one-third of the world's population is carrying the *M. tuberculosis* bacillus, despite the absence of any apparent symptoms. From 5 to 10% of these carriers will develop symptoms of the disease during their lifetime, and this percentage increases for immunocompromised individuals, such as HIV-infected persons or those going under corticosteroid therapies (WHO, 2015).

Due to an increase in the cases of TB driven by HIV epidemics, in 1993 TB was declared by the World Health Organization as a global emergency (WHO, 1993). TB accounted for the death of 1.2 HIV-negative individuals plus 251000 HIV-positive patients worldwide during 2018, and most of the deaths occurred in sub-Saharan Africa and southeast Asia regions (World Health Organization, 2019).

There is an available vaccine against *M. tuberculosis*, and it is a live attenuated variant of *Mycobacterium bovis*, the Bacillus Calmette-Guérin (BCG). BCG owes its name to Charles Calmette and Camille Guérin, which isolated the attenuated strain after a series

of passages in their potato-glycerine-bile media (Calmette, 1922). Although BCG is very good at conferring protection against the extra-pulmonary forms of TB, it is not effective against pulmonary TB, the most common form of the disease (Poyntz et al., 2014). There are also drugs for treating tuberculosis, but the length of the required chemotherapy that needs to last at least four months translates into poor adherence to the regime and eventual relapse. To further add to TB as a global health emergency, during the past three decades, there has been an increase in the detection of strains of *M. tuberculosis* that are resistant to the currently used drugs to treat TB (Keshavjee and Farmer, 2012). All these issues together highlight the importance of investing in mycobacterial research.

1.2 Non-tuberculous mycobacteria

Apart from *M. tuberculosis* and *M. leprae*, there is a group of environmental mycobacteria that can act as opportunistic pathogens, especially in immunocompromised individuals (Katoch, 2004; Lake et al., 2016; Tebruegge et al., 2016). In 1950, Ernest Runyon introduced the term ‘Non-tuberculous mycobacteria’ (NTM) to reference these, back then, poorly characterized mycobacteria (Runyon, 1959).

Runyon also conceived a classification system based on the growth rate of these mycobacteria and their capability of producing pigments when exposed to light. Groups I, II, and III, were constituted by NTM that showed a similar growth rate to *M. tuberculosis* which typically takes around 21 days to form colonies in agar plates. Group I or *Photocromogens*, was composed of NTM that developed a yellow-red pigmentation

only when exposed to light. Group II or *Scotochromogens*, included NTM that produced yellow-red pigments even when grown under dark conditions. Group III or *Non-Photochromogens*, was formed by NTM that were not able to produce any pigmentation, even in the presence of light. Finally, Group IV or *Fast growers*, comprised NTM that developed visible colonies after only 48h of cultivation in agar (Runyon, 1959).

A recent phylogenetic analysis comprising 150 mycobacterial species, outlined the existence of five clades: the “*Tuberculosis-Simiae*”, “*Terrae*”, “*Triviale*”, “*Fortuitum-Vacaccae*”, and “*Abscessus-Chelonae*” clade (Gupta et al., 2018). The *Fast growers* mycobacteria are comprised in the “*Fortuitum-Vacaccae*” and “*Abscessus-Chelonae*” clades, while the “*Tuberculosis-Simiae*”, “*Terrae*”, and “*Triviale*” clades group the slow grower mycobacteria (Gupta et al., 2018).

1.3 Importance of NTM on human health

NTM are gaining interest from the scientific community because there has been an apparent increase in the incidence of these opportunistic pathogens (Blanc et al., 2016; Dabó et al., 2015; Kim et al., 2014; Maurya et al., 2015; Nasiri et al., 2015; Rindi and Garzelli, 2016; Streit et al., 2013; Varghese et al., 2013). NTM are known to cause disease in several parts of the human body, primarily in the lungs, followed by skin and soft tissue, eyes, and heart (Katoch, 2004; Lake et al., 2016; Piersimoni and Scarparo, 2009). Individuals with some specific conditions, such as AIDS, chronic obstructive pulmonary disease (COPD), cystic fibrosis (CF), or impaired production of IFN- γ , are especially susceptible to NTM infections (Griffith et al., 2007; Lake et al., 2016; Orme and Ordway, 2014).

During NTM diagnosis, the identification of the etiological agent at the species level is of paramount importance (Faria et al., 2015), as the susceptibility to antibiotics varies between species (Cowman et al., 2016; Falkinham, 2018). In the practice *Mycobacterium avium*, a slow grower NTM that often causes pulmonary disease is treated with a regimen consisting of three antibiotics that are clarithromycin or azithromycin, rifampicin or rifabutin, and ethambutol (Griffith et al., 2007).

On the other hand, the suggested chemotherapy for treating infections caused by *M. chelonae* and *M. abscessus*, two closely related fast growers NTM, consists on the use of amikacin or macrolides (Griffith et al., 2007), however, it is strongly advisable to test for susceptibility to antimicrobials first, as clinical isolates from these species present variable patterns of antimicrobial susceptibility (Brown-Elliott et al., 2012; Griffith et al., 2007).

Another interesting topic of research is the potential interference of NTM with the effectiveness of the *M. tuberculosis* vaccine. The available TB vaccine is a live attenuated strain of *Mycobacterium bovis*: the bacillus Calmette-Guerin or *M. bovis* BCG (BCG). As mentioned above, vaccination with BCG is good at protecting against extra-pulmonary forms of TB, but the protection against pulmonary TB varies widely according to the world region (Mangtani et al., 2014).

There is not yet a consensus on how NTM impacts on BCG vaccination, as different NTM species and different administration routes seem to impact differently on the protective capacity of BCG (Shah et al., 2019). For example, a study in a murine model found that the protection of the BCG vaccine against pulmonary TB in mice that have been pre-exposed orally to *M. avium* is impaired, compared to mice that have not been pre-exposed to this NTM (Poyntz et al., 2014). Another study shows that aerogenic pre-exposure to

M. avium does not affect the capacity of BCG vaccination for controlling *M. tuberculosis* bacterial burden (de Lisle et al., 2005). This evidence shows that more research needs to be carried to clarify the potential impact of NTM exposure to BCG vaccination.

Also is interesting assessing if vaccination with BGC could also offer some protection against pathogenic NTM. For instance, there is a report suggesting that BCG vaccination may offer some protection against *M. avium* and *M. abscessus* (Abate et al., 2019), supporting the data on the increase of prevalence of NTM infections after changes of the policy of BCG administration (Poyntz et al., 2014).

1.4 *Mycobacterium chelonae*

Mycobacterium chelonae, the subject of this study, belongs to the “*Abscessus-Chelonae*” clade, and the type strain NCTC946 (ATCC35752) has a genome size of 5.03 Mbp, and a G+C content of 63.9% (Nouioui et al., 2018). It is a fast grower mycobacteria that can grow in a temperature range from 22 to 40°C, although some strains may grow poorly, or not grow at all at 37°C (Goodfellow, 2012). As all other mycobacteria, *M. chelonae* is an acid-fast bacteria, and form colonies that are typically round and glossy (Figure 1-1), although some strains showing colonies with a waxy, irregular appearance, have been described (Fogelson et al., 2019; Hsueh et al., 1998; Manzoor et al., 1999). It was first isolated in 1903 by Friedman from a turtle, the reason for its original name *Mycobacterium chelonae* (Goodfellow, 2012).



Figure 1-1. Seven-day old colony of *Mycobacterium chelonae*.

A representative colony of *M. chelonae* growth in 7H11/OADC agar for 7 days at 30°C. The colony is round with undulated margins, and it has a white pigmentation, with a pale-yellow center.

1.1.1 *M. chelonae* as a human pathogen

M. chelonae is regarded as an opportunistic pathogen that can infect several parts of the body, being skin and soft tissue, followed by eye infections. Infections caused by *M. chelonae* tend to be localized, and arise after trauma, iatrogenic, or cosmetic procedures, although disseminated infections have been observed in individuals with underlying. The infections caused by *M. chelonae* and other NTMs are often associated with impairment of the immune system (Lake et al., 2016), but *M. chelonae* is also capable of causing disease in individuals with no underlying immunosuppressive conditions (Campbell et al., 2013; Jagadeesan et al., 2013).

It is difficult to determine the incidence of *M. chelonae*, because reporting infections due to NTM is not mandatory in many countries. However, there is some epidemiology data available on NTM infections from some countries, and was recently summarized by Wagner et al., 2019. Overall, there seems to be a relatively low reported NTM incidence,

ranging from 0.72-0.74 cases per 100,000 habitants in Germany between 2009 and 2014 (Ringshausen et al., 2016), to 3.2 per 100,000 population in Australia during 2005 (Thomson, 2010). The incidence of NTM in England, Wales, and North Ireland is 7.6 cases per 100,000 inhabitants, putting *M. chelonae* as the second most commonly isolated NTM, identified in 9% of the isolated cultures (Shah et al., 2016). The incidence of *M. chelonae* varies according to the world region. For instance, in India *M. chelonae* was the fourth most commonly isolated NTM from clinical samples from 2013 and 2015 (Umrao et al., 2016), while in NTM strains collected from selected European countries (this study does not include the UK), *M. chelonae* was the seventh most commonly isolated (van der Werf et al., 2014).

Unlike *M. tuberculosis* and *M. leprae* that are only found on their hosts, *M. chelonae* is ubiquitously found in the environment, from water sources and soil to house and hospital plumbs (Falkinham, 2009; Manzoor et al., 1999; Stormer and Falkinham, 1989), and these environmental niches are thought to be the sources of the latter infecting bacilli. In the following sections, the type of infections caused by *M. chelonae* will be outlined.

1.4.1 Skin and soft tissue infections

M. chelonae can cause skin and soft tissue infection usually after a trauma (Mali et al., 2014) or iatrogenic procedures (Kannaiyan et al., 2015; Kim and Mascola, 2010; Murback et al., 2015). There are also cases where *M. chelonae* skin infections arose after cosmetic procedures such as dermal fillers (Rodriguez et al., 2013), fat injections and biomesotherapy (Ivan et al., 2013), piercings (Pearlman, 1995), and ink tattoos (Binić et al., 2011). Interestingly, there is also one report from an immunocompetent patient

lacking previous story of trauma and with no comorbidities associated with susceptibility to mycobacteriosis, that presented erythema due to *M. chelonae* (Campbell et al., 2013).

While in immunocompetent patients the infections by *M. chelonae* are usually localized; in immunocompromised individuals, the infections often spread, for example, there are reports of disseminated cutaneous infection has in patients with acute myeloid leukemia (Roukens et al., 2014), mixed connective tissue disease (Lage et al., 2012), diabetes (Patnaik et al., 2013), or those under corticosteroids therapy (McCallum and Johnson, 2016; Pinto-Gouveia et al., 2015).

1.4.2 Catheter and port- associated infections

Often the devices used to facilitate the delivery of therapeutics can be colonized by bacteria, and the consequential infections interfere with the treatment of the original disease. There is report of *M. chelonae* colonizing the dialysis machines and the catheters used by the patients, leading to peritonitis, and in most cases, the infections did not resolve by the sole use of antibiotics, and the catheters were replaced (Van Ende et al., 2016; Lo et al., 2013; Okado et al., 2015; Yamada et al., 2015).

1.4.3 Endocarditis

M. chelonae, along with *M. fortuitum* and *M. abscessus*, are the predominant *Mycobacteria* causing endocarditis (Yuan, 2014). Early reports have linked endocarditis caused by *M. chelonae* after surgical implant of prosthetic heart valves (Narasimhan and Austin, 1978), but also on pacemakers (Hooda et al., 2014), and cardioverter defibrillators (Whitaker et al., 2016). Surprisingly, *M. chelonae* caused endocarditis in an immunocompetent patient without a history of previous trauma (Jagadeesan et al., 2013).

1.4.4 Eye infections

The most commonly isolated mycobacteria from eye infections is *M. chelonae*, accounting for around 42% of the reported cases (Kheir et al., 2015). *M. chelonae* often causes keratitis which is the inflammation of the cornea (Kheir et al., 2015), usually after a corneal grafts (Aylward et al., 1987; Chowdhury et al., 2016; Mirate et al., 1983; Murthy et al., 2013). Apart from the cornea, *M. chelonae* also causes infections on the white part of the eye (scleritis) (Holland et al., 2017), dacryocystitis (inflammation on the lacrimal sac) (Meyer et al., 2011), and eye lids (Moorthy and Rao, 1995).

1.5 Management of *M. chelonae* infections

The clinical management of *M. chelonae*, is challenging, as *M. chelonae* is regarded as one of the drug resistant NTMs (Brown-Elliott et al., 2012; Cowman et al., 2016). The standard therapy for *M. chelonae* involves the use of a macrolide, usually clarithromycin, along with a fluoroquinolone (Griffith et al., 2007). Unlike amikacin, the aminoglycoside tobramycin is effective against *M. chelonae*, as well as the oxazolidinone linezolid (Brown-Elliott and Philley, 2017).

This resistance to antibiotics in *M. chelonae* could be attributed to the poor permeability of the mycobacterial envelope, as well as the low expression of porins (Garcia et al., 2019) and the presence of beta lactamases and other efflux pumps (Brown-Elliott et al., 2012) encoded in its genome. In addition to these genetic traits, *M. chelonae* is able to form biofilms *in vivo* (Aung et al., 2017; Chandra et al., 2001), which are communities of bacteria encased into extra polymeric substances (EPS), known to foster an increased drug-tolerance on its residents (Falkinham, 2018; Ojha and Hatfull, 2012). *M. chelonae* forms biofilms in medically relevant surfaces (Hall-Stoodley et al., 1999) and in the cornea of infected mice (Holland et al., 2017). The object of the study of this thesis is *M. chelonae* biofilms. Still, due to the leading role of the mycobacterial cell envelope during biofilm formation, the components and organization of this organelle will be reviewed in the following sections.

1.6 Mycobacterial cell envelope

The mycobacterial cell envelope is, without doubt, the most distinct feature of mycobacteria. It is responsible for giving the bacilli structural support and acting as an impermeable barrier that confers protection from the environment (Brennan and Nikaido, 1995).

For pathogenic mycobacteria such as *M. tuberculosis*, some components of the mycobacterial cell envelope have immunomodulatory properties that allow the bacilli to evade the immune response from the host (Gago et al., 2018). Such is the relevance of this organelle that two of the first-line drugs against tuberculosis, isoniazid and ethambutol, target the synthesis of components of the cell wall (Abrahams and Besra, 2018). Isoniazid inhibits the action of Inh (Banerjee et al., 1994), an enzyme part of the complex that elongates mycolic acids (Marrakchi et al., 2000), while ethambutol targets EmbC, an arabinosyltransferase involved in the synthesis of arabinogalactan (Goude et al., 2009).

The mycobacterial cell envelope is an organelle with relatively low permeability, and this partly explains the mycobacterial intrinsic resistance to some drugs. For instance, *M. chelonae* cell envelope is extremely impermeable to hydrophilic molecules (Jarlier and Nikaido, 1990), being at least ten times less permeable than *M. smegmatis* or *M. tuberculosis* cell envelopes (Brennan and Nikaido, 1995). Although most of the components of the cell envelope are well conserved across mycobacteria, others are species-specific, and these traits seem to have an impact on the bacilli antimicrobial susceptibility as well as the interaction with the environment (Brennan and Nikaido, 1995).

Most information on the mycobacterial cell wall derives from studies done in *M. tuberculosis* or *Mycobacterium smegmatis*, a fast grower NTM used as a surrogate for *M. tuberculosis*. The following sections detail the available information on the components of the mycobacterial cell wall, highlighting the particular traits about fast growers NTM.

1.6.1 The structure of the mycobacterial envelope

The mycobacterial cell envelope is formed of four segments, and each one of them is depicted in Figure 1-2. The first segment is the plasma membrane composed of phospholipids, referred as mycobacterial inner membrane (MIM). The second segment consists of peptidoglycan that is covalently linked to arabinogalactan, forming the arabinogalactan complex, the core of the cell wall. The arabinogalactan chains are in turn esterified to mycolic acids (MAs), a characteristic long-chain α -alkyl β -hydroxy acid produced by the genus *Mycobacterium* and other actinobacteria (Marrakchi et al., 2014; Nataraj et al., 2015).

MAs, along with non-covalently bound lipids, form a bilayer known as mycobacterial outer membrane (MOM), the third segment of the mycobacterial cell envelope. Finally a capsule composed of polysaccharides, proteins, and glycolipids, forms the fourth and outermost section of the mycobacterial cell envelope (Daffé et al., 2014; Jankute et al., 2015; Kaur et al., 2009a; Minnikin et al., 2015).

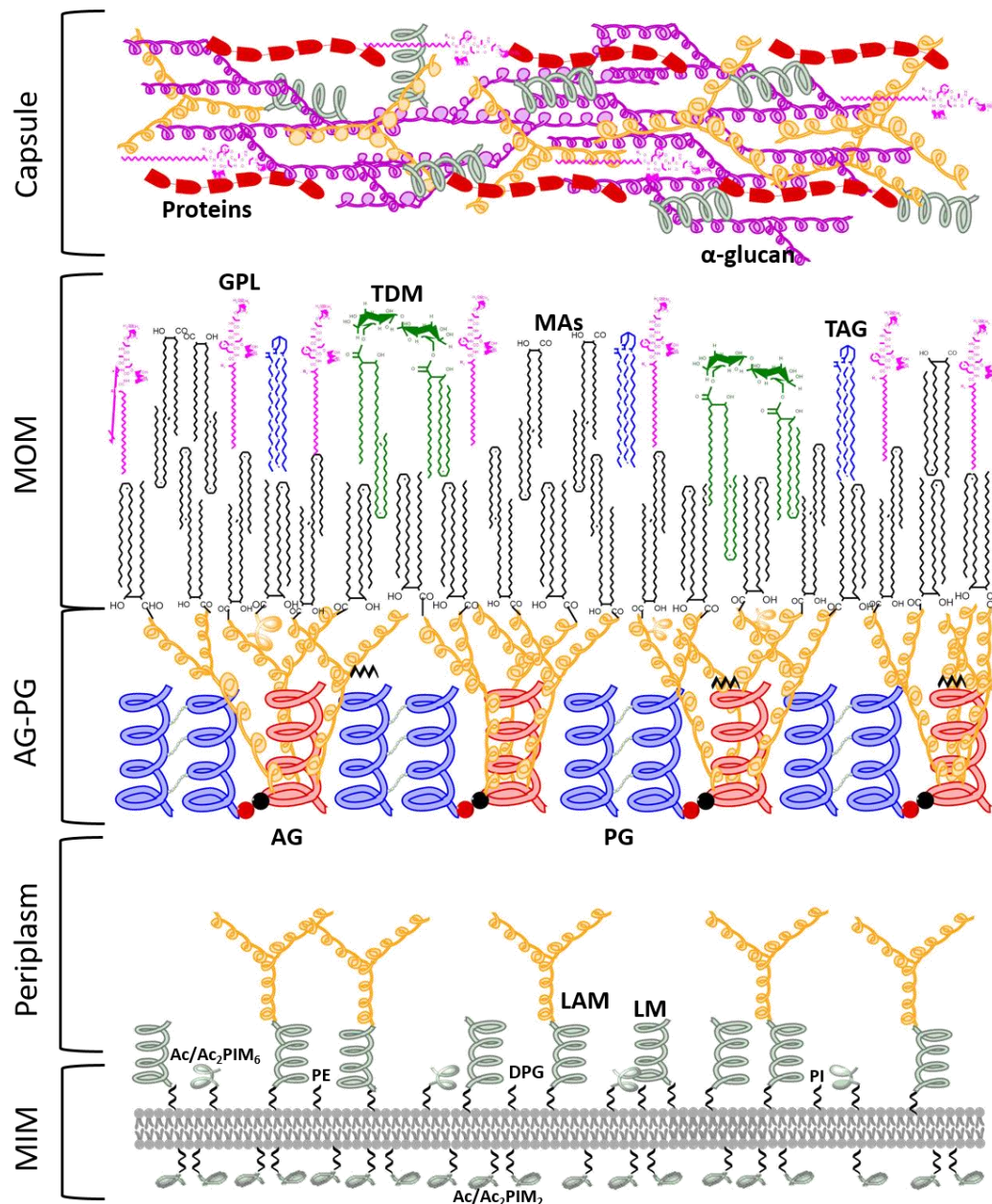


Figure 1-2. Schematic representation of the mycobacterial cell envelope.

The mycobacterial cell envelope is composed of four segments, a plasma membrane often referred as mycobacterial inner membrane (MIM), composed mainly of phospholipids. The core of the mycobacterial cell envelope is formed by peptidoglycan bound to arabinogalactan, which in turn is esterified to mycolic acids (MAs). The mycobacterial outer membrane (MOM) is formed by glycolipids and free MA that are intercalated with the MAs bound to the arabinogalactan. The outermost structure of the mycobacterial cell envelope is a capsule formed mainly by proteins and carbohydrates. GPL- glycopeptidolipids, TDM- trehalosedimycolate, MAs- mycolic acids, TAG- triacylglycerides, AG- arabinogalactan, PG- peptidoglycan, LAM-lipoarabinomannan, LM- lipomannan, PE- phosphatidylethanolamine, DPG- diphosphatidylglycerol, PI-phosphatidylinositol, Ac/Ac₂PIM₆, Ac/Ac₂PIM₂- mannosylated phosphatidylinositol.

1.6.1.1 Mycobacterial inner membrane

The MIM of *M. smegmatis* is made up of several phospholipids, and their structures are depicted in Figure 1-3. Among the phospholipids present in the MIM are phosphatidylglycerol (DPG), phosphatidylethanolamine (PE), phosphatidylinositol (PI), but the most abundant phospholipid is a specie of phosphatidylinositol mannoside (PIM), the diacyl phosphatidylinositol dimannoside (Ac₂PIM₂) (Bansal-mutalik and Nikaido, 2014). One considerable difference of mycobacterial plasma membrane to other bacterial plasma membranes is the relatively low proportion of the phospholipid phosphatidylglycerol (Jackson et al., 2000). The MIM of *M. smegmatis* also contains other PIMs species, such as the acyl phosphatidylinositol dimannoside (AcPIM₂), mono- and di- acetylated phosphatidylinositol tetramannosides (AcPIM₄/Ac₂PIM₄), and mono- and di- acetylated phosphatidyl inositol hexamannosides (AcPIM₆/Ac₂PIM₆) (Bansal-mutalik and Nikaido, 2014). In addition to the phospholipids, the hypermannosylated forms of PIMs, named lipomannans (LM) and lipoarabinomannans (LAM) are anchored on the MIM (Crellin et al., 2013).

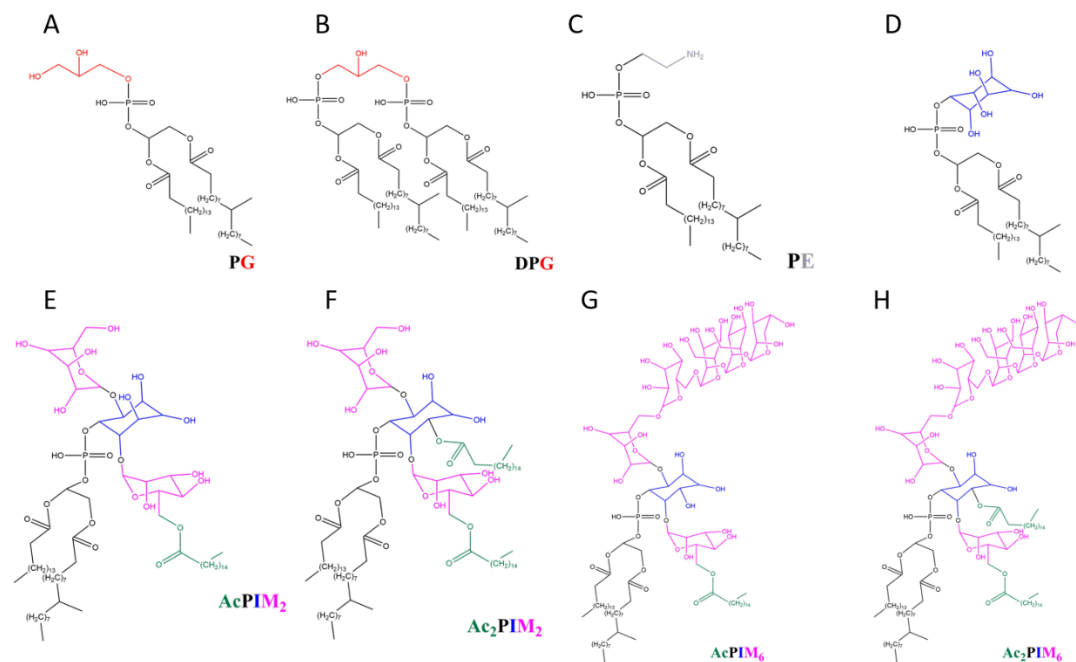


Figure 1-3. Phospholipids present in the MIM. The phospholipids present in the *M. smegmatis* MIM are Diphosphatidylglycerol (B), PE- phosphatidylethanolamine (C), PI- phosphatidylinositol (D), and its mannosylated derivatives, acetyl phosphatidylinositol dimannoside (E), diacetyl phosphatidylinositol dimannoside (F), acetyl phosphatidylinositol hexamannoside (G), and diacetyl phosphatidylinositol hexamannoside (H). The phospholipid phosphatidylglycerol (A) is also present in the MIM, although in low quantities.

PIMs, LM, and LAM share a conserved PI anchor, which consists of *sn*-glycero-3-(1-D-*myo*-inositol) that is further mannosylated at the O-2 and O-6 residues of the *myo*-inositol residue (Kaur et al., 2009b). In addition to the anchor, LM and LAM possess a mannan core composed of 21-34 *Manp* residues linked by an $\alpha(1\rightarrow6)$ glycosidic bond, with branches of a single $\alpha(1\rightarrow2)$ *Manp* residues (Misaki et al., 1977), with the notable exception of LAM and LM of *M. chelonae*, where the branching occurs at the C-3 position (Guérardel et al., 2002a). The length and the degree of branching vary according to the mycobacterial specie (Kaur et al., 2009a). For LAM, the mannan core is further glycosylated with linear chains of $\alpha(1\rightarrow5)$ *Araf* residues, decorated with $\alpha(3\rightarrow5)$ *Araf* branches (Jankute et al., 2015). The non-reducing end of the arabinan domain is capped by different motifs that are species-dependent (Kaur et al., 2009a). *M. chelonae* lacks a capping motif (Guérardel et al., 2002b); while the capping motif in other fast growers NTM, such as *M. smegmatis* and *M. fortuitum* is phospho-*myo*-inositol (Khoo et al.,

1995), the capping motif of some slow-growing mycobacteria (*M. tuberculosis*, *M. bovis*, *M. leprae*, *M. avium*), consists of $\alpha(1\rightarrow2)$ -linked Manp residues (Chatterjee et al., 1992).

1.6.1.2 Arabinogalactan-peptidoglycan (AGP) complex

The arabinogalactan-peptidoglycan complex surrounds the mycobacterial inner membrane. It provides structural stability to the MOM and, and also regulates the osmotic stress on the bacilli (Brennan and Nikaido, 1995). It is composed of a mesh-like structure of peptidoglycan that is covalently linked to the arabinogalactan complex; however, the exact spatial conformation of the components is still under debate (Alderwick et al., 2015).

1.6.1.2.1 Peptidoglycan

The peptidoglycan (PG) localizes outside the plasma membranes in most bacteria. The peptidoglycan from mycobacteria is formed of repetitive units of N-acetylglucosamine (GlcNac) and N-acetylmuramic acid (MurNac) via a $\beta(1\rightarrow4)$ linkage (McNeil et al., 1990b). The peptidoglycan from mycobacteria has a distinctive feature, as a proportion of MurNac residues are modified to N-glycolylmuramic acid (N-MurGlyc) (Raymond et al., 2005), that is believed to increase the overall strength of the peptidoglycan (Alderwick et al., 2015).

The mycobacterial peptidoglycan chains possess a linker unit formed of the tetrapeptide L-alanyl-D-isoglutaminyl-*meso*-diaminopimelic-D-alanine that is cross-linked between

meso-diaminopimelic acid(*m*-DAP)and D-alanine(3→4), allowing the formation of mesh-like structures with the PG chains (Alderwick et al., 2015; Jankute et al., 2015). The PG is covalently bound to the galactan domain of the arabinogalactan complex, where the -OH residues from the C6 of muramic acid residues bind to C-5 of the β (1→6) Gal_f residues (Besra et al., 1995) from arabinogalactan forming a phosphodiester bond, via a unique linker unit consisting of α -L-rhamnopranose-(1→3)- α -D-GlcNAc-(1-P) (McNeil et al., 1990b).

1.6.1.2.2 Arabinogalactan complex

The heteropolysaccharide arabinogalactan (AG) is acknowledged as the principal cell wall polysaccharide in mycobacteria (Kaur et al., 2009a). It is composed of galactose (Gal) and arabinose (Ara), both in the furanose (*f*) form (McNeil et al., 1987). The galactan component consists of a chain of about 30 units of 5- and 6- β -D-Gal_f (McNeil et al., 1990a). The arabinans chains are made of α -1,5-linked Ara_f, and the branches are introduced by α -3,5- bond in some of the Ara_f units (Daffe et al., 1990). The inner core of the arabinan domain is decorated with up to three succinyl esters, and interestingly, only those chains that are not bound to mycolic acids are succinylated (Bhamidi et al., 2008).

The nonreducing ends of the arabinan chains consist of an hexa-arabinoside motif [β -D-Ara_f-(1→2)- α -D-Ara_f]2-3,5- α -D-Ara_f-(1→5)- α -D-Ara_f], where the C5 of the terminal β -D-Ara_f and the penultimate 2- α -D-Ara_f serves as an attachment site for mycolic acids (McNeil et al., 1991).

1.6.1.3 Mycobacterial outer membrane

The mycobacterial outer membrane has a thickness of 7-8nm (Sani et al., 2010). The inner leaflet is made of the mycolic acids that are bound to the arabinogalactan complex, while the outer leaflet consists of diverse lipids intercalated to the tails of the mycolic acids of the inner leaflet (Bansal-mutalik and Nikaido, 2014).

Recently, a study using a reverse micellar approach found that the non-covalently bound lipids from the *M. smegmatis* MOM are glycopeptidolipids (GPLs), trehalose dimycolate (TDM), free mycolic acids (FMA), and diacyl and triacylglycerols (DAG, TAG) (Bansal-mutalik and Nikaido, 2014).

1.6.1.3.1 Mycolic acids

Mycolic acids (MA) are 2-alkyl, 3-hydroxy long-chain fatty acids (Marrakchi et al., 2014). The breakdown of a molecule of MA yields an intact fatty acid, also known as the α -branch, and a longer aldehyde, often referred as the merochain (Figure 1-4) (Barry et al., 1998).

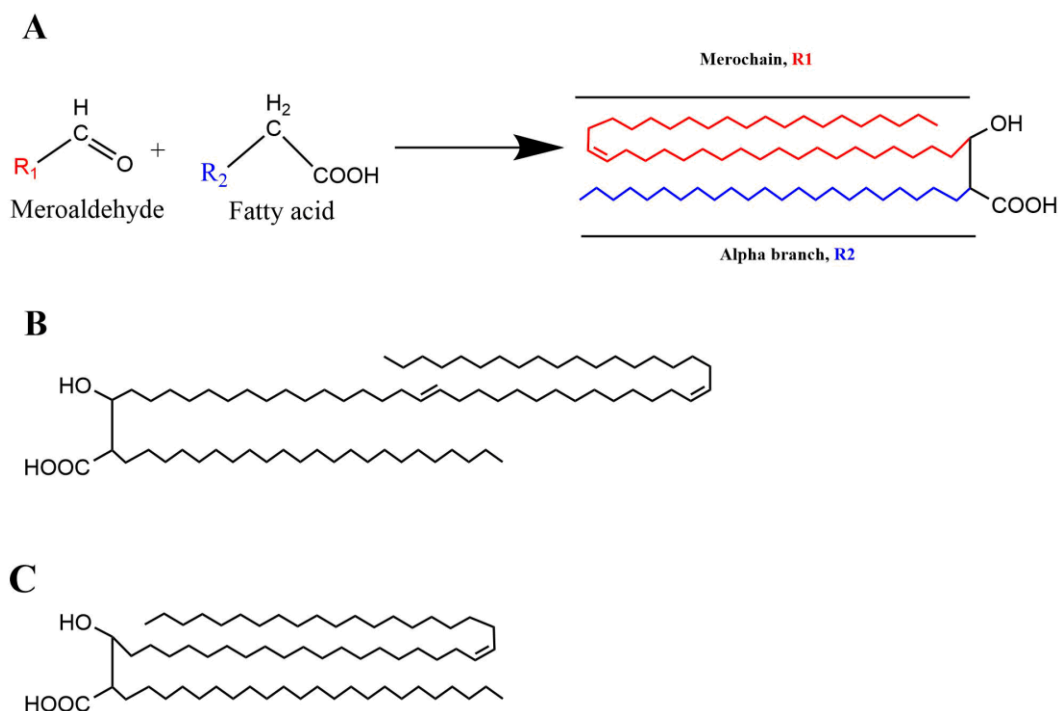


Figure 1-4. Schematic representation of mycolic acids.

The molecule of a mycolic acid originates by the condensation of a meroaldehyde and a fatty acid (A). The merochain moiety (red) of the mycolic acid molecule originates from the meroaldehyde, while the alpha branch (blue) comes from the fatty acid molecule. *M. chelonae* produces two classes of mycolic acids, the α -mycolic acid (B), and α' - (C) mycolic acid. The α - and α' -mycolic acids differ in the length of their mero chain, being shorter in α' -mycolic acids.

According to the functionalization and length of the merochain, seven different types of mycolic acids have been identified in mycobacteria. α -mycolic acids, which contain from 70 to 74 carbon units, and typically have *cis*-cyclopropyl groups or two double bonds in the meromycolic branch. The α' -mycolic acids, which have a single *cis*-double bond and are shorter in length (from 60 to 62 carbon atoms). There are also five types of oxygenated mycolic acids and are classified according to the functional group adjacent to a methyl group within the meromycolate branch. The oxygenated mycolic acids are keto-, methoxy, epoxy-, wax ester-, and hydroxyl-mycolic acids (Marrakchi et al., 2014). All the studied mycobacteria are found to produce α -mycolic acids, and most of the mycobacteria produce keto-mycolic acids. Although α' -mycolic acids are produced by a vast amount of mycobacteria, this mycolic acid species is absent in *M. tuberculosis* (Barry

et al., 1998). *M. chelonae* produces only α and α' mycolic acids (Barry et al., 1998). The α -branch of all mycolic acids from *M. chelonae* has a length of 24 carbon units, while the merochain for the α -mycolic has a length of 48-54 carbon units (Kaneda et al., 1986).

Mycolic acid biosynthesis requires two types of fatty acyl synthases, the eukaryotic-like type I fatty acid synthase (Fas-I) that synthesize *de novo* short-chain fatty acids, and a prokaryotic-like type II fatty acid synthase (Fas-II) which elongates fatty acids to form the distinctively long merochain of mycolic acids (Marrakchi et al., 2014; Nataraj et al., 2015). In *M. tuberculosis*, Fas-I is encoded by the gene *fas* and consists of a single polypeptide (Zimhony et al., 2004), while Fas-II involves discrete dissociable enzymes that catalyze the elongation of the fatty acids (Barry et al., 1998).

The activity of Fas-I and Fas-II involves the four sequential enzymatic activities: β -ketoacyl synthase (KAS), β -ketoacyl reductase (KR), β -hydroxy acyl dehydratase (DE), and an enoyl reductase (ER) (Nataraj et al., 2015). The synthesis of mycolic acids is initiated by Fas-I that elongates *de novo* fatty acids of 18 or 24-26 carbon units, and these short-chain fatty acids are likely to act as substrates for Fas-II to be further elongated to 60 carbon units chains (Marrakchi et al., 2014; Nataraj et al., 2015), because mycobacterial Fas-II cannot synthesize fatty acids *de novo* (Odriozola et al., 1977).

The elongating of the fatty acids in Fas-I and Fas-II requires of the successive addition of two-carbon units from malonyl-coenzyme A (CoA) (Daniel et al., 2007). In Fas-II, the malonyl moiety from malonyl-CoA is transferred to an acyl carrier protein (ACP) by FabD (Kremer et al., 2001) to form β -ketoacyl-ACP. From that point, the chain will go through four iterative steps for elongating the nascent chain. First, the keto group is reduced by the action of MabA (Marrakchi et al., 2002) to form a β -hydroxyl intermediate, and the subsequent dehydration of the β -hydroxyl intermediate to form enoyl-ACP is carried by the heterodimers HadAB or HadBC (Brown et al., 2007; Sacco

et al., 2007). The enoyl-ACP is further reduced by InhA (Vilchéze et al., 2000) to form an Acyl-CoA. The following elongation rounds will be then initiated by KasA or KasB, β -ketoacyl synthases (Bhatt et al., 2007; Gao et al., 2003) until the acyl chains reach the required length.

The α -branch and the merochain are condensed by Pks13 (Gande et al., 2004; Portevin et al., 2004) to yield an oxo-mycolic acid. This latter is further reduced by the action of Rv2509 (in *M. tuberculosis*) to yield a fully mature mycolic acid (Bhatt et al., 2008). DesA1 introduces the double bonds in the merochain of α -mycolic acids, and this modification likely occurs during the merochain elongation (Singh et al., 2016).

Prior exportation from the cytosol, mycolic acids are bound to trehalose, although the mechanism has not yet been identified (Takayama et al., 2005). TMM is then transported to the cytoplasm by Mmp13 (Varela et al., 2012; Xu et al., 2017), where the mycoloyl residues are transferred to the cell wall acceptors, in a process mediated by the proteins from the Antigen85 (Belisle et al., 1997; Puech et al., 2002).

1.6.1.3.2 *Trehalose dimycolate*

Trehalose dimycolate (TDM, Figure 1-5) is present on the outer leaflet of the *M. smegmatis* MOM (Bansal-mutalik and Nikaido, 2014). It was one of the first identified lipids from mycobacteria and is known to have several immunomodulatory properties. TDM is synthesized by the proteins of the Antigen 85 that transfer a mycoloyl group from one molecule of TMM to another molecule of TMM (Belisle et al., 1997).

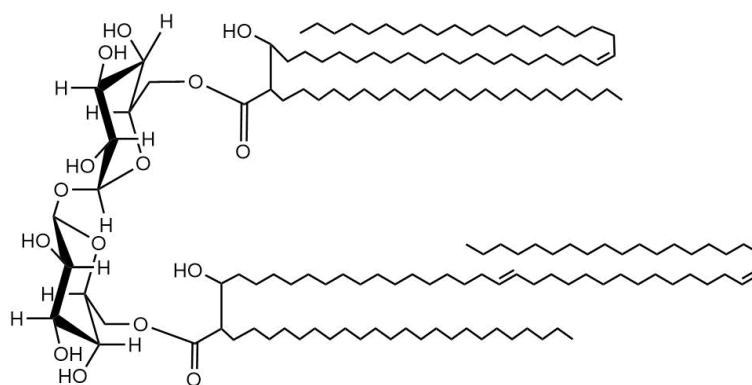


Figure 1-5. Trehalose dimycolate. The glycolipid trehalose dimycolate (TDM) is present on the MOM. It is composed by two mycolic acid molecules esterified to C6 of each glucose residue from the trehalose.

1.6.1.3.3 Glycopeptidolipids

Glycopeptidolipids (GPLs), formerly known as c-mycosides, are a group of lipids present in some NTM such as *M. avium*, *M. smegmatis*, *M. abscessus*, *M. fortuitum*, and *M. chelonae* (Fujiwara et al., 2015). In *M. smegmatis*, GPLs account for almost half of the lipids of the non-covalently bound lipids from the MOM (Bansal-mutalik and Nikaido, 2014). The structure of a GPL (Figure 1-6) consists of a 3-hydroxylated or a 3-methoxylated fatty acid, usually from 26 to 36 carbons long, linked to the tripeptide D-Phe-D-alloThr-D-Ala by an amide bond. The tripeptide is in turn terminated with an L-alaninol residue. The D-alloThr residue is glycosylated with a di-*O*-acetylated 6-deoxytalosyl unit, and the L-alaninol residue is glycosylated with a 3,4-*O*-methyl-rhamnose (Daffé et al., 2014).

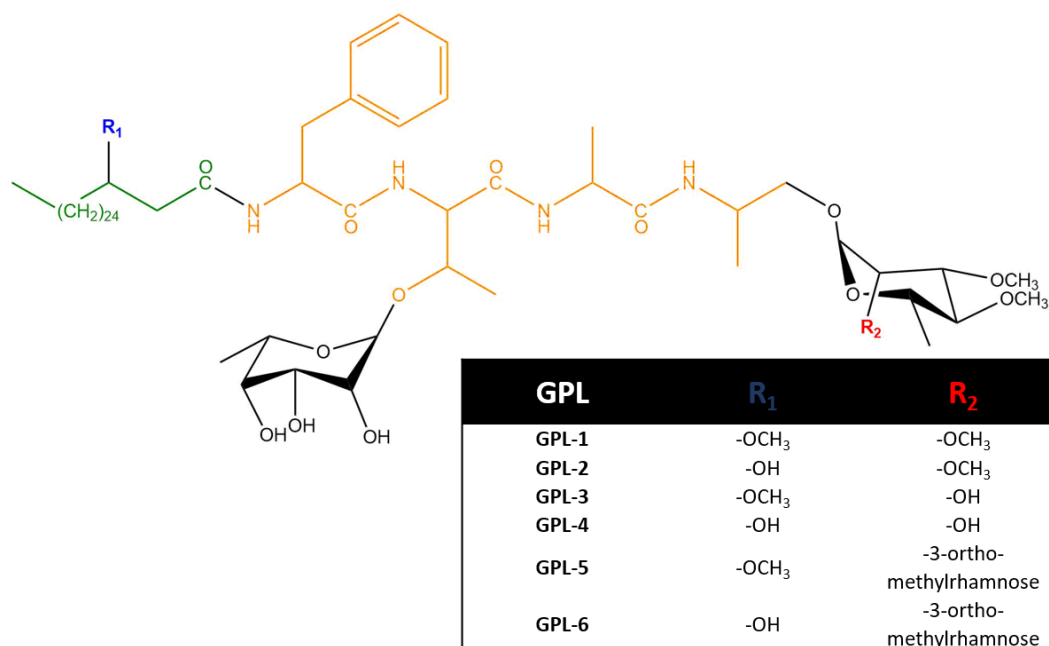


Figure 1-6. Generic structure of glycopeptidolipids. The GPLs are composed by either a fatty acid (blue) bound to the tripeptide Phe-D-alloThr-D-Ala (orange). The C3 from the fatty acid moiety is either methoxylated in or hydroxylated (R₁, blue). The D-alloThr residue from the tripeptide is further glycosylated with a di-O-acetylated 6-deoxytalosyl unit, and the L-alaninol residue is glycosylated with a 3,4-O-methyl-rhamnose. The C2 from the 3,4-O-methyl-rhamnose residue is methoxylated in GPL-1 and GPL-2, while in GPL-5 and GPL-6 the substituent is a 3-O-methylrhamnose.

According to the number of sugars linked to the lipopeptide core, two major types of GPLs can be distinguished. The non-polar GPLs, GPL-(1-4), contain only two sugars, while the polar GPLs contain more than two. Unlike the polar GPLs of *M. avium*, where the extra sugars are bound to the 6-deoxy-talose (Daffé et al., 2014), The polar GPLs of *M. smegmatis* (GPL-5 and GPL-6) have the second 3-O-methyl-rhamnose linked to the one bound to the alaninol residue (Villeneuve et al., 2003). These triglycosylated GPLs (GPL-5 and GPL-6) were only observed in *M. smegmatis* when it was cultured in carbon starvation media (Ojha et al., 2002), although triacetylated GPLs had been observed first in *M. fortuitum* (López Marin et al., 1991), and *M. abscessus* and *M. chelonae* (Lopez-Marín et al., 1994). The GPLs produced by *M. chelonae* and *M. abscessus* are indistinguishable from the GPLs produced by *M. smegmatis*, but their relative abundance differs among the three species (Ripoll et al., 2007).

In *M. smegmatis*, the synthesis of the GPLs is currently thought to involve around 24 genes (Daffé et al., 2014), and some of them have already been characterized (Schorey and Sweet, 2008). The non-ribosomal peptide synthases Mps1 and Mps2 are responsible for the synthesis of the peptidic moiety (Billman-Jacobe et al., 1999), while Pks1 is thought to synthesize the acyl chain linked to the peptidic moiety (Sonden et al., 2005). The glycosyltransferases involved in the addition of the 6-deoxytalose is Gft1 (Eckstein et al., 2003; Miyamoto et al., 2006), while Gft2 catalyzes the addition of the 3,4-di-*O*-methyl-rhamnose to the alalinol residue (Eckstein et al., 2003; Miyamoto et al., 2006). Gft3 adds the second 3,4-di-*O*-methyl-rhamnose for the formation of the polar GPL-5 and GPL-6 (Miyamoto et al., 2006). Finally, the translocation of GPLs in *M. smegmatis* and *M. abscessus*, is mediated by MmpL4 (Deshayes et al., 2010; Nessar et al., 2011; Recht et al., 2000).

1.6.1.4 Capsule

Mycobacteria possess a capsule that has a thickness of ~30nm (Sani et al., 2010). Although its composition varies among mycobacterial species (Lemassu et al., 1996b), in general it is formed by neutral polysaccharides, proteins, and in a minor proportion, lipids (Ortalo-Magne et al., 1995). This structure is easily shed from the bacilli when grown in the presence of detergents (Sani et al., 2010), which is the standard protocol for culturing mycobacteria in the laboratory.

1.6.1.4.1 α -glucan

The most abundant polysaccharide in all the studied mycobacterial capsules is α -glucan (Lemassu et al., 1996b; Lemassu and Daffé, 1994; Ortalo-Magne et al., 1995). The synthesis of this polymer is the product of the iterative action of GlgB and GlgE. First, the maltosyl transferase GlgE creates linear chains of $\rightarrow 4\text{-}\alpha\text{-D-Glcp-1}\rightarrow$ residues, using maltose-1-phosphate (Kalscheuer et al., 2010a). Once GlgE has elongated the chain to about 16 units, GlgB introduces a branch by cleaving 7-8 residues from the non-reducing end of the elongated maltooligosaccharide, and creates the branch by transferring the cleaved residues back into the chain via an α -1,6 bond (Rashid et al., 2016). The final α -glucan has an apparent molecular weight of 120kDA (Dinadayala et al., 2008; Lemassu and Daffé, 1994; Ortalo-Magne et al., 1995), and its generic structure is depicted in Figure 1-7. Although the synthesis of capsular α -glucan is carried out in the cytosol (Koliwer-brandl et al., 2016), the mechanism involved in the export of this polymer to the capsule remains unknown.

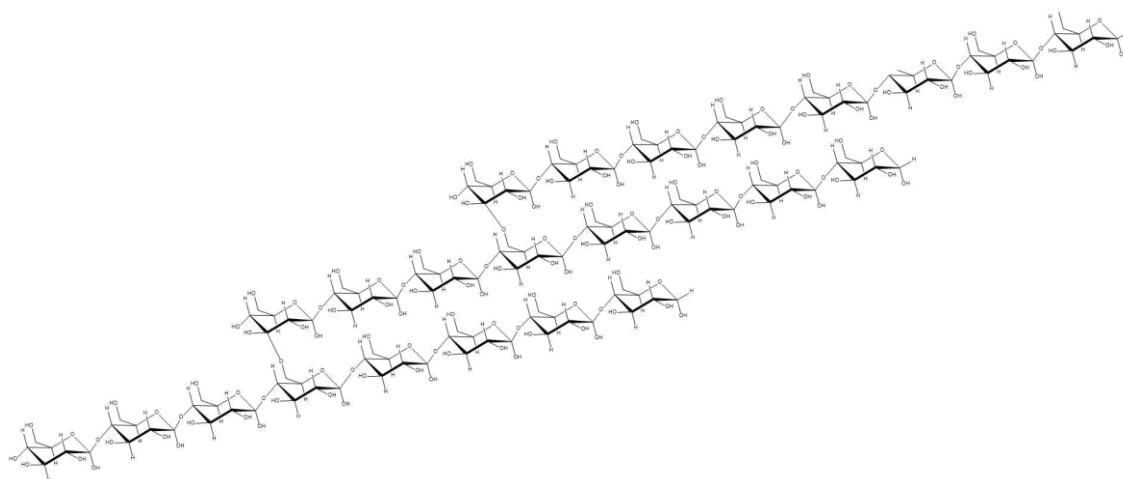


Figure 1-7. Generic structure of capsular α -glucan from mycobacterial species. The glucan from mycobacterial species is composed of chains of glucose bound by an $\alpha\rightarrow 1,4$ glycosidic bonds and decorated with ramifications arising from the C6 of some residues.

1.6.1.4.2 Mannans and arabinomannans

Mannans and arabinomannans are also present in the mycobacterial capsule (Lemassu et al., 1996b; Lemassu and Daffé, 1994; Ortalo-Magne et al., 1995), and share the same structure as the moieties from LAM and LM (Guérardel et al., 2002b), so it is likely that these originate from the cleavage of LAM and LM by a mechanism yet to be determined.

1.6.1.4.3 Lipids in the mycobacterial capsule

Lipids are a minor component of the mycobacterial capsules (Ortalo-Magné et al., 1996) except in *M. leprae* (Hunter et al., 1982) and *M. lepraemurium* (Draper and Rees, 1973), mycobacterial species which capsules possess large amounts of phenolglycolipids (PGLs) and GPLs respectively. The study of the lipids present in the capsule of several mycobacteria determined that the lipid composition varies according to each specie (Ortalo-Magné et al., 1996). *M. tuberculosis* capsule harbours species-specific lipids, such as phenolglycolipids (PGLs), lipooligosaccharydes (LOS), dimycoserolates, phthiocerols, as well as the non-species specific PIMs (Ortalo-Magné et al., 1996). The lipids present in the *M. smegmatis* capsule, TMM, TAG, PE, and PIMs, are non-species specific, with the notable exception of GPLs (Ortalo-Magné et al., 1996; Villeneuve et al., 2003).

1.7 Biofilms

Biofilms are communities of bacteria that grow surrounded by a matrix of extra-polymeric substances (EPS). Biofilms seem to be the preferred mode of growth for many bacteria (Davey and O'toole, 2000), as around only 0.1% of the world's bacteria live as planktonic (free-living) bacteria (Mah and O'Toole, 2001; Potera, 1998).

Biofilms in the clinical settings have tremendous importance, as up to 80% of the human bacterial infections are associated with biofilm formation (Römling and Balsalobre, 2012). Microorganisms can colonize the human host and implantable devices, forming pathogenic biofilms, that derive into infections that are difficult to eradicate (Aparna and Yadav, 2008)

A typical example of pathogenic biofilms formed in human tissues is periodontitis, where bacteria colonize the supporting structure of the teeth, causing chronic inflammation that may lead to tooth loss (Kinane et al., 2017). Other diseases caused by pathogenic biofilm are urinary tract infections caused by uropathogenic *Escherichia coli* (Anderson et al., 2001), chronic wounds infected with *Pseudomonas aeruginosa* (James et al., 2007), osteomyelitis caused by *Staphylococcus aureus* (Brady et al., 2007), and lung infection by *P. aeruginosa* in cystic fibrosis patients (Singh et al., 2000).

Medical and implantable devices can also be colonized by microorganisms, causing posterior infections that often resolve only after the removal of the implanted device (Römling and Balsalobre, 2012). Among the most common bacteria that colonize implantable devices are *Enterococcus faecalis*, *Staphylococcus aureus*, *Staphylococcus epidermis*, *Streptococcus viridans*, *Escherichia coli*, *Klebsiella pneumonia*, *Proteus mirabilis*, and *Pseudomonas aeruginosa* (Khatoon et al., 2018).

Although the biofilms formed by the pathogens mentioned before differ vastly in composition, the resulting infections share some similar traits, such as recalcitrance to antibiotics. Biofilms are known for fostering drug-tolerance on the residing microorganisms, perhaps, because the environmental heterogeneity within the biofilm structures results in the arising of populations of microorganisms with different metabolic activities, and thus different susceptibility to drugs (Bjarnsholt et al., 2013).

1.7.1 The development of the biofilm

Prior biofilm formation, planktonic bacteria sense extracellular signals that result in the synthesis of second messengers (intracellular molecules) that lead to the modulation of the metabolism for biofilm formation (Tamayo et al., 2007). In many bacteria the second messenger cyclic diguanylate (c-di-GMP) modulates the transition from planktonic bacteria to biofilms (Tamayo et al., 2007).

Biofilms can occur either attached to biotic or abiotic surfaces, submerged under fluids, or also in the liquid-air interphase, and are then called pellicles (Kovács and Dragoš, 2019). Although there is a high heterogeneity on the signals or molecular components contributing to biofilm formation across bacteria (López et al., 2010), all biofilms go through five distinctive stages from their formation to the dispersion of the structure (Sauer, 2003), as shown in Figure 1-8.

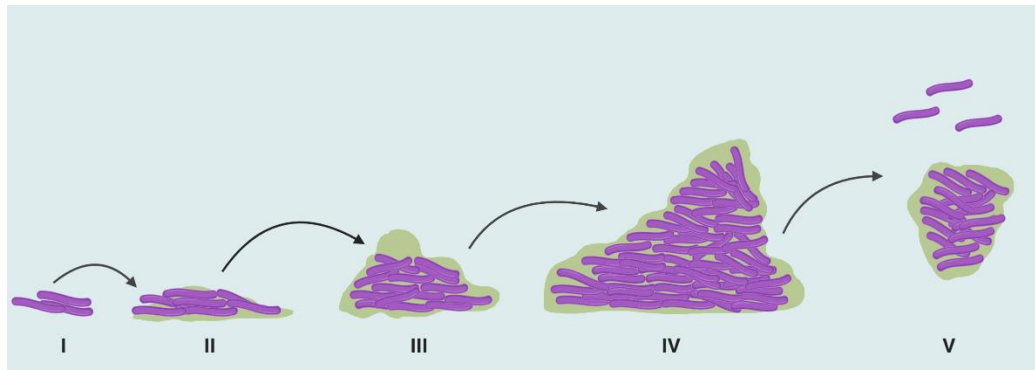


Figure 1-8. The biofilm life cycle

In Stage I, planktonic bacteria deposits into a surface. The attachment becomes irreversible when the deposited bacteria start secreting EPS (Stage II), and the structure develops into a mature state (Stage III). When the biofilm is fully mature (Stage IV), it goes through processes that lead to the dispersion of the structure (Stage V).

During Stage I, the bacterial cells attach in a reversible mode to a surface. In Stage II, the attachment becomes irreversible due to the secretion of extra-polymeric substances (EPS). At stage III, the biofilm enters into an early maturation stage, where its architecture is defined. When the biofilm has reached a sufficiently mature structure, then it has reached Stage IV. Finally, during Stage V, several mechanisms on the biofilm are activated and lead to the dispersal of the structure (Aparna and Yadav, 2008; Sauer, 2003).

1.8 Biofilms of mycobacteria

The spontaneous formation of pellicles for mycobacteria has been observed since the very first years of mycobacteriology. Mycobacteria usually form clumps when grown in the absence of detergents, and perhaps this predisposition to self-associate facilitates the biofilm formation (Islam et al., 2012; Zambrano and Kolter, 2005). For instance, *M. bovis* BCG, the available vaccine for TB, is sometimes grown as a pellicle (Dietrich et al., 2002).

While most mycobacteria form pellicles (Ojha et al., 2008), some mycobacteria, as *M. chelonae*, *M. smegmatis* and, *M. abscessus*, can also form surface-attached biofilms (Recht and Kolter, 2001; Rose et al., 2015), and colonize a wide array of surfaces, being found in household plumbing and implantable medical devices (Falkinham, 2009). Among the mycobacteria that form biofilms in the environment as well as in the human host we found *M. chelonae* (Holland et al., 2017), *M. abscessus* (Qvist et al., 2015), and *M. ulcerans* (Marsollier et al., 2007); and it has even been suggested that *M. tuberculosis* could form biofilm-like structures *in vivo*, nevertheless this is still under debate (Lenaerts et al., 2007; Orme, 2013).

Most of the studies in mycobacterial biofilms have been done in pellicles, as this spontaneously-formed structure yields a fair amount of biomass that facilitates further analysis. The biochemical characterization of mycobacterial biofilms has highlighted cell wall components as the major components of the biofilms EPS (Chakraborty and Kumar, 2019). In the following sections the available information on the role of different molecules during biofilm formation is reviewed.

1.8.1 Lipid metabolism during biofilm formation

Lipid metabolism plays a leading role in mycobacterial biofilm formation (Ojha et al., 2008; Pacheco et al., 2013; Pang et al., 2012; Recht and Kolter, 2001; Röse et al., 2004; Sambandan et al., 2013), and have been the most extensively studied components of the mycobacterial biofilm matrix.

One of the most distinctive phenotypes in mycobacterial biofilms is the accumulation of free mycolic acids, observed in *M. tuberculosis* (Ojha et al., 2008; Sambandan et al., 2013) and *M. smegmatis* (Ojha et al., 2010). The increase in the production of mycolic acids during biofilm formation in *M. smegmatis* is mediated by GroEL1, which binds to KasA and aids in the synthesis of long-chain fatty acids (Ojha et al., 2005). In *M. smegmatis*, the accumulation of FMA is partly consequence of the enzymatic hydrolysis of TDM (Ojha et al., 2010), and this glycolipid is also essential for biofilm formation (Ojha et al., 2010). Interestingly, *M. avium* biofilms show a decrease in the TDM content but do not appear to accumulate FMA (Totani et al., 2017).

In addition to TDM, mycolyldiacylglycerols (MDAGs) have also been associated with biofilm formation in *M. smegmatis* (Chen et al., 2006; Pacheco et al., 2013). The essentiality for biofilm formation of MDAG was first identified in an *M. smegmatis* mutant lacking Lsr2, a global transcriptional regulator present in several mycobacteria (Chen et al., 2006). The mycobacteria membrane protein large 11 (MmpL11) was then identified to be the transporter of MDAGs and mycolate wax ester in *M. smegmatis*, and thus essential for biofilm formation (Pacheco et al., 2013). MmpL11 is also required for biofilm formation in *M. tuberculosis*, although only mycolate wax ester was identified as a substrate for this transporter (Wright et al., 2017).

Glycopeptidolipids contribute to biofilm formation in NTMs (Freeman et al., 2006; Howard et al., 2006; Nessar et al., 2011; Recht et al., 2000; Recht and Kolter, 2001). In *M. smegmatis* acetylated GPLs mediate the attachment of the bacilli to several surfaces (Recht and Kolter, 2001; Yang et al., 2017), and although the absence of GPLs delays pellicle formation in *M. smegmatis*, these are dispensable for the formation of this type of biofilm (Yang et al., 2017).

1.8.2 Carbohydrates and biofilm formation

Polysaccharides are the major components of the extracellular matrix (ECM) in most types of biofilms (Flemming and Wingender, 2010). In mycobacterial biofilms, lipids are often regarded as the major components of mycobacterial biofilms; however confocal laser scanning microscopy (CLSM) analysis and biochemical analysis of the ECM show that carbohydrates are the bulk component of the mycobacterial biofilms (Lemassu et al., 1996b; Lemassu and Daffé, 1994; Trivedi et al., 2016).

In all of the studied mycobacterial pellicles, the ECM is composed of neutral polysaccharides, and α -glucan was identified as the predominant species, followed by arabinomannans, and mannans (Lemassu et al., 1996a; Lemassu and Daffé, 1994), the same polysaccharides present in the mycobacterial capsule (Dinadayala et al., 2008; Ortalo-Magne et al., 1995). More recent studies show that thiol-induced *M. tuberculosis* biofilms and *M. smegmatis* pellicles contain cellulose-like polysaccharides (Trivedi et al., 2016; Wyk et al., 2017), somehow conflicting with previous observations, where the glycosidic bond of the glucans was determined to have an α configuration (Dinadayala et al., 2008).

1.8.3 Role of extracellular DNA in biofilms

In many biofilms, extracellular DNA (eDNA) is an essential structural component of the ECM (Okshevsky and Meyer, 2015), and in some microorganisms, triggers responses that contribute to drug tolerance from the residing microorganisms (Okshevsky and Meyer, 2015). The biofilms formed by *M. chelonae*, *M. abscessus*, *M. avium*, and *M. tuberculosis*, contain extracellular DNA (eDNA) (Rose et al., 2015; Rose and Bermudez, 2016; Trivedi et al., 2016), and in surface-attached biofilms formed by *M. chelonae*, *M. abscessus*, and *M. avium*, HCO_3^- triggers the release of eDNA (Rose and Bermudez, 2016).

M. tuberculosis is capable of forming colonies of drug-tolerant bacilli attached to DNA from lysed leukocytes (Ackart et al., 2014a). These microcolonies had a thickness of $\approx 28\mu\text{m}$ and were surrounded by complex polysaccharides (Ackart et al., 2014a), very much resembling biofilms. The drug tolerance of these microcolonies was reverted after treatment with tween 80 or DNase (Ackart et al., 2014a) or by adding imidazole-based compounds, that inhibit pellicle formation in *M. smegmatis* (Ackart et al., 2014b). Detailed observation of these structures by confocal laser scanning microscopy (CLSM), showed that eDNA served as an attachment scaffold for *M. tuberculosis* microcolonies to the culture well surface (Ackart et al., 2014a), and this observation is in agreement with the study by Trivedi et al. 2016 in *M. tuberculosis* biofilms, where the eDNA seems to mediate the attachment of the bacilli to the culture flasks in thiol-induced biofilms (Trivedi et al., 2016).

1.8.4 Proteins in mycobacterial biofilms

There is limited information regarding the role of proteins present in the mycobacterial ECM. Proteins play a structural role in thiol-induced *M. tuberculosis* biofilms (Trivedi et al., 2016), and in *M. avium* SA-biofilms, the most abundant proteins present on the ECM (Rose and Bermudez, 2016) include Wag31, a protein that regulates cell wall biosynthesis in mycobacteria (Kang et al., 2008); SodA and KatG, enzymes associated with the maintenance of the REDOX homeostasis in mycobacteria (Kumar et al., 2011); a DNA binding protein (MAVA6_16770); and the Antigen 85B.

1.9 Is there a unified mechanism for biofilm formation in mycobacteria?

The biofilms formed by *M. smegmatis* have been extensively studied, and this has allowed the identification of components and mechanisms required for the development of this structure. GPLs are required for the initial attachment of the bacilli to the substratum making them essential for SA-biofilm formation in NTM (Recht and Kolter, 2001), and although they facilitate the formation of the pellicle *in vitro*, the intercellular aggregation is more relevant during pellicle formation. Interestingly the intercellular aggregation is modulated in *M. smegmatis* by Lsr2, a transcriptional regulator that also mediates the production of MDAG (Chen et al., 2006; Yang et al., 2017).

After cells have aggregated, there is an overall increase in the synthesis of FMA mediated by GroEL1 (Ojha et al., 2005) followed by an induction on the expression of genes related with iron uptake (Yang et al., 2017), a mineral essential for the formation of mature

pellicles in *M. smegmatis* (Ojha and Hatfull, 2007). The increase in the synthesis of free mycolic acids and the up-regulation of iron acquisition genes define the early maturation stage of *M. smegmatis* biofilms (Yang et al., 2017). The stage of late maturation is defined by induction of genes related to nitrogen acquisition (Yang et al., 2017), a process mediated in by the transcriptional regulator GlnR, which leads to a peroxide-resistant phenotype on biofilms (Yang et al., 2018).

An imbalance in the REDOX metabolism triggers various mechanisms required for biofilm formation in several microorganisms (Gambino and Cappitelli, 2016), including mycobacteria (Anand et al., 2015; Trivedi et al., 2016; Wolff et al., 2015). A way of assessing the REDOX balance in the cells is to measure the oxidation state of the nucleotide nicotinamide adenine dinucleotide, NAD(H), or its phosphorylated version NADP(H) (Liu et al., 2019). The NADH/NAD⁺ ratio in *M. smegmatis* biofilms is about three times higher than planktonic bacteria, and the adenosine triphosphate (ATP) level is halved compared to ATP in planktonic cultures (Anand et al., 2015), suggesting impaired respiration and augmented reductive stress in *M. smegmatis* pellicles (Anand et al., 2015). *M. tuberculosis* forms biofilms after exposure to dithiotreitol (DTT), a molecule widely used for producing reductive stress in bacteria (Trivedi et al., 2016). In mycobacteria, elevated levels of NADH induce the transcription of the protein kinase PknG (Wolff et al., 2015), that act on substrates known to regulate the central carbon metabolism (Rieck et al., 2017; Ventura et al., 2013), and it is required for biofilm formation (Wolff et al., 2015), further highlighting the role of reductive stress as a trigger of biofilm formation in mycobacteria.

The effect of the second messenger c-di-GMP during biofilm formation has also been assessed in mycobacteria (Flores-Valdez et al., 2012; Gupta et al., 2016). Mycobacteria possess the enzymes for metabolizing c-di-GMP (Cui and He, 2012; Hong et al., 2013;

Kumar and Chatterji, 2008), but the role of this second messenger in mycobacterial biofilm formation shows conflicting evidence, as some studies show that c-di-GMP contributes to biofilm formation in *M. smegmatis* (Gupta et al., 2015) and *M. bovis* BCG (Flores-Valdez et al., 2015), while other studies found it being dispensable for biofilm formation (Kumar and Chatterji, 2008).

Although some molecular changes occurring during biofilm formation have been defined in some mycobacteria, there is not yet a comprehensive description that integrates the role of other vital components of the ECM, such as polysaccharides or eDNA; nor the molecular traits associated with the dispersion of the mycobacterial biofilms. The presence of polysaccharides and eDNA has been observed in many of the the studied mycobacterial biofilms, suggesting that perhaps the presence of eDNA is a conserved trait in mycobacterial biofilms, so it is important to carry more research in order to elucidate the mechanisms orchestrating biofilm formation in mycobacteria, especially in pathogenic mycobacteria that form biofilms *in vivo*, such as *M. chelonae*.

1.10 Aim

The overarching aim of this thesis is to conduct a characterization of *M. chelonae* biofilms at a molecular level and a spatial level, aiming to further contribute to the elucidation of the mechanisms responsible for biofilm formation in *M. chelonae*.

1.10.1 Specific objectives

The specific objectives of the work described in this thesis are:

- To define the structural organization of *M. chelonae* pellicular biofilms.
- To characterize the changes occurring in cell wall lipids and carbohydrates during biofilm formation.
- To identify the overall changes in the composition of the biofilm through time using Raman spectroscopy.
- To investigate the changes in the *M. chelonae* transcriptome during biofilm formation.
- Amalgamate the information gained from working towards the above objectives to identify molecules and mechanisms involved in mycobacterial pellicle formation.

Chapter 2 Microscopy of ***Mycobacterium*** ***chelonae* pellicular** **biofilms**

2.1 Introduction

Scanning electron microscopy (SEM) has been widely used for imaging biofilms because it produces 3D images with high resolution (Surman et al., 1996). SEM provides invaluable information on the morphology of biofilms. SEM has been used to identify *ex vivo* biofilms in tooth root canals, allowing the identification of different morphologies according to the stage of the infection (Distel et al., 2002). SEM also allows observing the aggregation and cord formation in mycobacterial biofilms (Abidi et al., 2014; Hall-Stoodley et al., 1999; Julián et al., 2010; Sambandan et al., 2013; Sochorová et al., 2014; Sousa et al., 2015; Totani et al., 2017; Trivedi et al., 2016).

Although SEM is a technique that allows the visualization of bacterial biofilms in a high range of amplification and very high resolution, it does not provide information on the identity of biofilm components (Gomes et al., 2014). A way to visually identify the components of the biofilm matrix can be achieved by using Confocal Laser Scanning Microscopy (CSLM), using fluorophores targeting specific components of the biofilm matrix.

CLSM allows the capture of two-dimensional optical sections of a specimen that can be later used to recreate three-dimensional reconstructions (Luo et al., 2018) by scanning the specimen with a focused beam of light (usually a laser). The generated fluorescent signal is detected by a photomultiplier tube through a pinhole, and the resulting signal is finally built into an image by a computer (Rai and Dey, 2011).

CLSM is hugely versatile as we can select specific fluorescent stains and genetically engineered organisms for visualizing specific components of the studied sample. Many fluorophores have been functionalized changing their permeability and increasing its specificity, and are commercially available.

The availability of fluorophores, and the possibility to genetically modify microorganisms to express fluorescent proteins, make CLSM a gold standard for the study of biofilms. When quantitative image analysis follows image acquisition, the resulting information can also provide quantitative data on different properties of the biofilm matrix (Schlafer and Meyer, 2017). There is software that facilitates the calculus of geometrical parameters such as biovolume and colocalization coefficients, which can help researchers to describe biofilms objectively (Schlafer and Meyer, 2017). The calculus of geometrical parameters from bacterial biofilms made possible to assess the changes on the biofilm biovolume under different conditions (Guilbaud et al., 2015), or in response to antimicrobials (Jung et al., 2014), and have also made possible the monitoring of specific components of the ECM through time (González-Machado et al., 2018).

In mycobacteria, CLSM has allowed the observation of the morphology of the biofilm and the components of the biofilm matrix (Aung et al., 2016; Hall-stoodley et al., 2006; Julián et al., 2010; Martín-de-Hijas et al., 2009; Trivedi et al., 2016; Wouters et al., 2010). CLSM made possible the measuring of the NADH/NAD⁺ ratio across the structure (Anand et al., 2015), and biovolumes of components of the ECM (Trivedi et al., 2016). The quantitative description components of the ECM using CLSM could allow the comparison of mycobacterial biofilm development through time, between species, and in response to antimicrobials, which could be useful in the development of strategies against mycobacterial biofilms.

2.2 Aim

The aim of this chapter is to describe the structure of *M. chelonae* biofilms and determine the presence of extra polymeric substances by using microscopy.

2.2.1 Specific objectives

- Describe the morphology of *M. chelonae* biofilms using SEM.
- Identify the presence of extra polymeric substances in *M. chelonae* biofilms CLSM.
- Calculate geometric parameters to describe the polymers present in the *M. chelonae* biofilm.

2.3 Results

2.3.1 *Mycobacterium chelonae* pellicles have similar ultrastructure to other mycobacterial biofilms.

Mycobacterial pellicles have been widely cultured in Sauton's media (Esteban and García-Coca, 2018; Ojha et al., 2008; Trivedi et al., 2016) because its primary carbon source is glycerol, which allows copious growth of many mycobacterial species (Keating

et al., 2005). Aiming to facilitate the comparisons with information available in the study of other mycobacterial biofilms, we chose Sauton's media for growing *M. chelonae* pellicles and planktonic bacteria (see section 7.4.2 and 7.4.3).

M. chelonae pellicles grown in Sauton's media for 5 days are opaque, and possess a creamy coloration (Figure 1-1), and also display the typical wrinkles, as observed in other mycobacterial pellicles (Ojha et al., 2008).

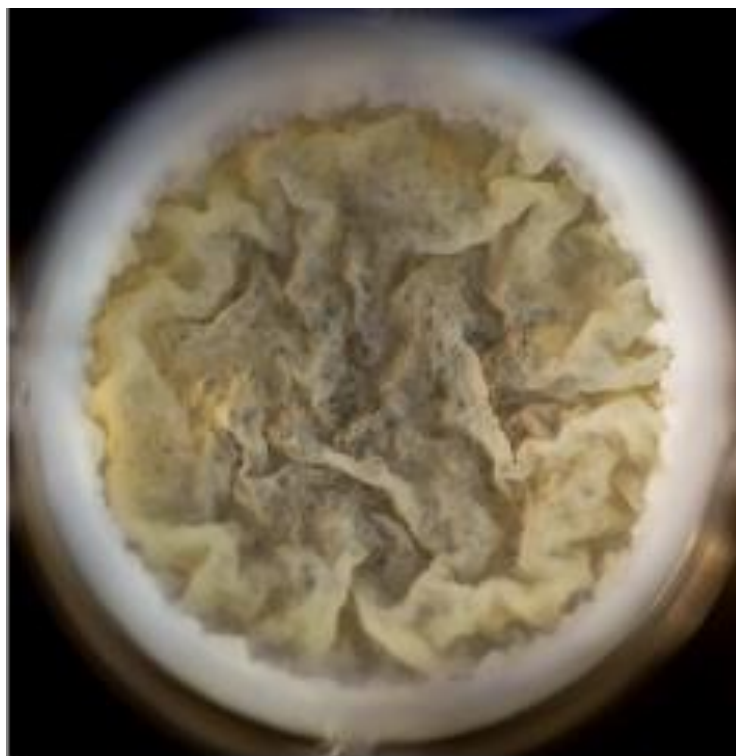


*Figure 2-1. Five-day old *M. chelonae* pellicle growth in Sauton's media at 30°C.*

Detail of a 5-day old *M. chelonae* pellicle growth in Sauton's media a 24-well plate at 30°C. The coloration of the pellicle is creamy, and displays the characteristic wrinkling of other mycobacterial pellicles.

To gain a deeper understanding of the morphology *M. chelonae* pellicle, we imaged them using SEM. We grew planktonic bacteria and pellicles as described in section 7.4.3 and 7.4.2 respectively. For the *M. chelonae* pellicles, before the removal of the aqueous phase

for further fixation, a sterile coverslip was placed in the bottom of the well, as this allowed a more gentle collection of the pellicle, aiming to preserve better the structure of the pellicle. The pellicle was then fixed with 6% paraformaldehyde overnight, and latter imaged in a Philips XL-30 FEG ESEM. The obtained micrographs showed that *M. chelonae* planktonic bacteria (Figure 2-2, panel A) is not covered by extracellular material, unlike bacilli residing in pellicles (Figure 2-2, panel B) that are coated by a substance that prevents to distinguish individual bacilli. As we zoomed out into the structure, we noticed that *M. chelonae* pellicles have pores (Figure 2-2, panels C and D, white arrows), and display cord-like structures (Figure 2-2, panel E, white box), very similar to the observed cording in other mycobacterial agar colonies (Julián et al., 2010).

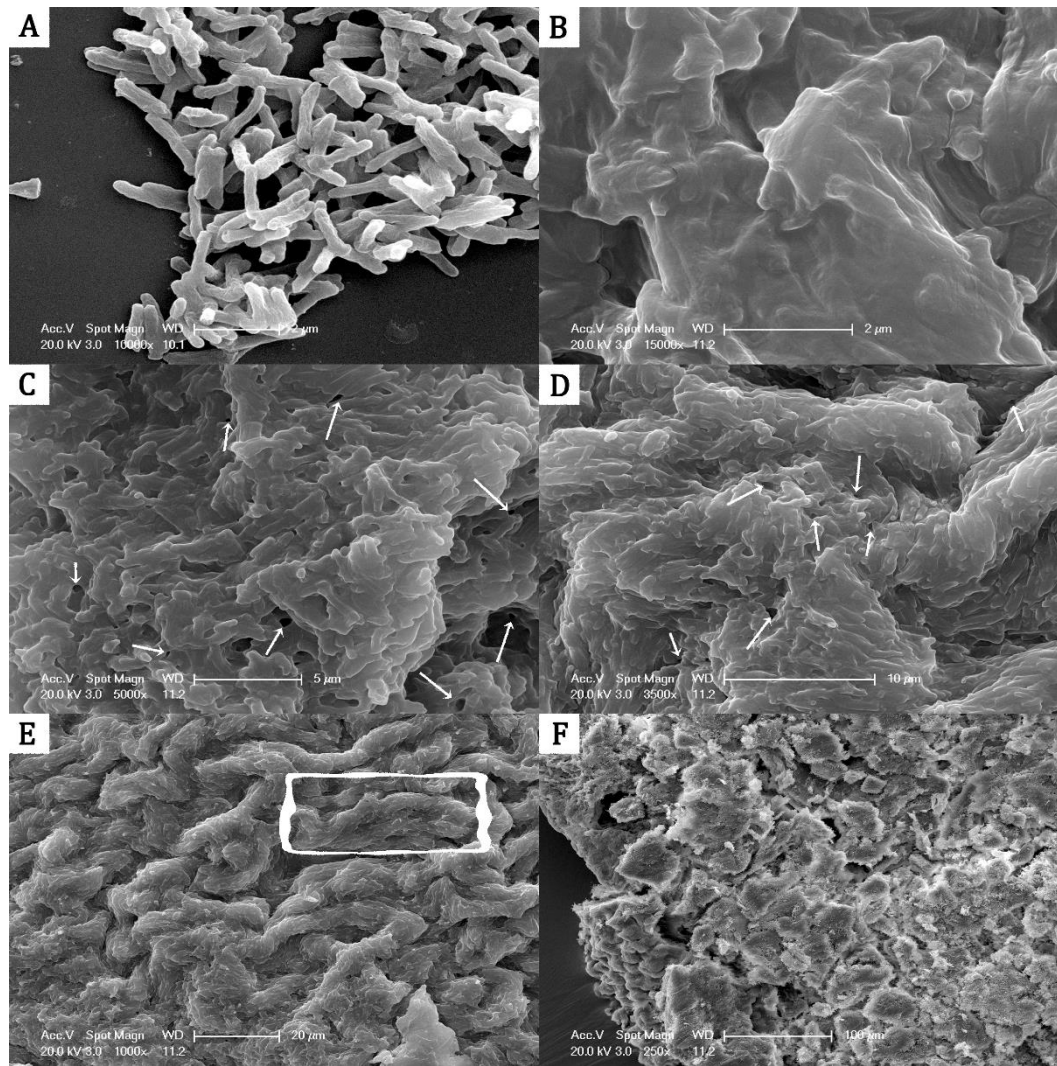


Figure 2-2. SEM micrographs of *M. chelonae* cultures.

M. chelonae planktonic bacteria (A) and 5-day old pellicles (B-F) were imaged using SEM. Unlike planktonic bacteria (A), biofilm-residing bacteria is coated by a layer of extracellular material (B). As the magnification decreases in the structure, the presence of pores becomes evident (white arrows, C and D). Similarly to other mycobacterial biofilms, *M. chelonae* pellicles show the characteristic cord-like pattern (white rectangle, E).

2.3.2 *Mycobacterium chelonae* pellicles are composed of lipids, eDNA, carbohydrates, and proteins.

After generating high-resolution 3D images of *M. chelonae* pellicles, we stained *M. chelonae* pellicles using CLSM to visualize specific biopolymers present in the biofilm matrix. The eGFP-expressing *M. chelonae* pellicles were stained with an impermeable fluorophore targeting a specific component of the biofilm matrix. Once fixed, *M.*

chelonae cultures were incubated in a solution containing a single fluorophore. We used Nile Red (NR) for staining lipids, Concanavalin A conjugated with Alexa Fluor 647 (ConcA) for staining carbohydrates, Propidium Iodide (PI) for nucleic acids, and FilmTracer™ SYPRO® Ruby biofilm matrix stain (SR) for proteins. We selected this set of fluorophores because with the exception of NR, they are all impermeable to cells, and their emission wavelength does not overlap with the emission wavelength of eGFP. The concentration and staining time for each of the fluorophores is summarized in table Table 7-3.

We started imaging *M. chelonae* planktonic cultures. The signals from the bacilli (eGFP) and lipids (NR), show the rod-shaped characteristic bacilli (Figure 2-3, panel A). The signals from carbohydrates (ConcA), and proteins (SR), are also present, although more faint (Figure 2-3, panels C and D, respectively). The signal from eDNA (PI) was barely detectable (Figure 2-3, panel B). Our confocal images of planktonic *M. chelonae* show that there is not a large accumulation of proteins, carbohydrates, or eDNA, in the outermost surface of the bacteria, or that these polymers may have been released to the culture media due to the agitation and the presence of tyloxapol used for growing planktonic bacteria (see section 7.4.3).

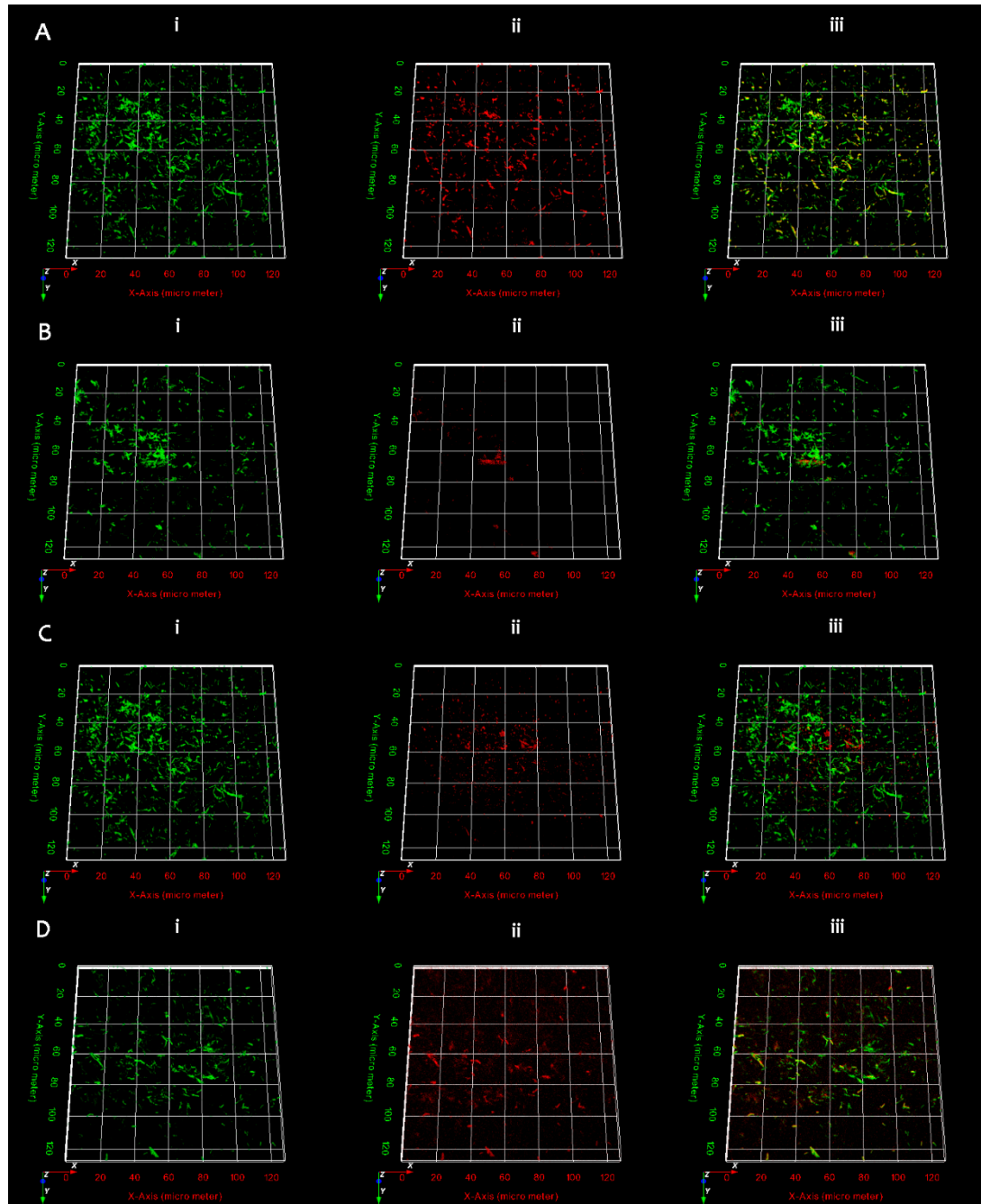


Figure 2-3. CLSM images of *M. chelonae* planktonic bacteria.

The figure shows a 5 μ m-thick stack acquired from *M. chelonae* planktonic bacilli growth in Sauton's media + 0.05% tyloxapol, until an OD₆₀₀=1. Panel **A** shows pellicles stained with NR (lipids), **B** with PI (eDNA), **C** with ConCA (carbohydrates), and **D** with SR (proteins). eGFP-expressing bacilli is depicted in column **i**, column **ii** shows the signal corresponding to the specific fluorophore, and column **iii** is the overlay of the signals from eGFP and the fluorophore.

We next imaged 5-day old pellicles, and in Figure 2-4 we observe a representative figure of the imaged pellicles. Similar to planktonic bacteria (Figure 2-3, panel A), the signal from lipids and bacilli were intense in *M. chelonae* pellicles (Figure 2-4, panel A), and unlike planktonic *M. chelonae* (Figure 2-3), we were able to detect a good signal from carbohydrates (Figure 2-4, panel C), eDNA (Figure 2-4, panel B), and proteins (Figure 2-4, panel D). Overall, CLSM allowed us to visually identify lipids, carbohydrates, proteins, and eDNA, as a component of the *M. chelonae* pellicle matrix.

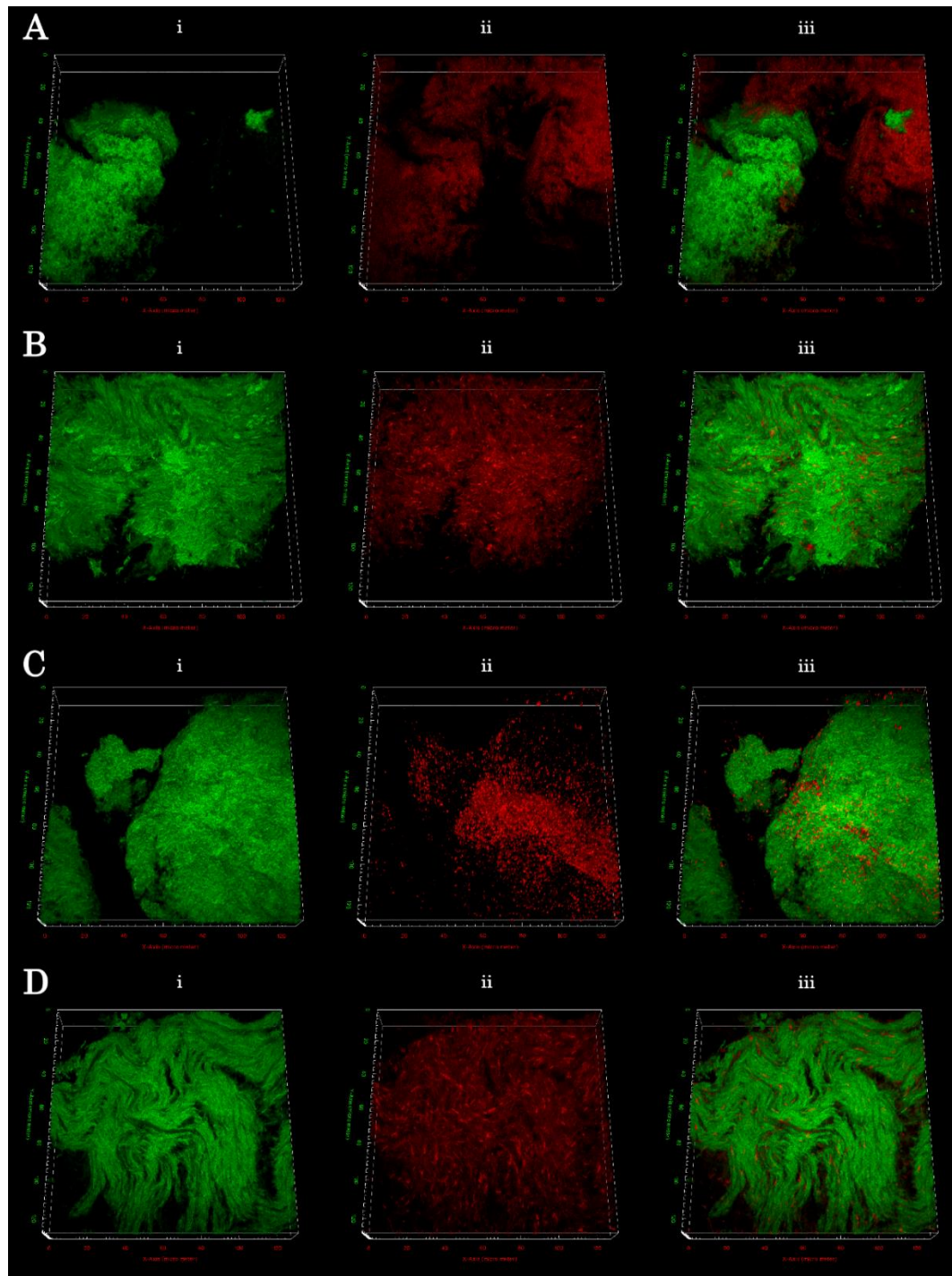


Figure 2-4. CLSM images of *M. chelonae* pellicles.

The figure shows a 20 μ m-thick stack acquired from *M. chelonae* pellicles. Panel **A** shows pellicles stained with NR (lipids), **B** with PI (eDNA), **C** with ConCA (carbohydrates), and **D** with SR (proteins). eGFP-expressing bacilli is depicted in column **i**, column **ii** shows the signal corresponding to the specific fluorophore, and column **iii** is the overlay of the signals from eGFP and the fluorophore.

To further describe the distribution of the biopolymers on the biofilm matrix, we calculated geometrical parameters that would aid to the description of the localization of the biopolymer. We imaged four different locations in four biological replicates (16 acquisitions per fluorophore in total). First, we calculated the relative volume of each of the biopolymers using as a reference the volume of the eGFP-expressing bacilli (see section 7.6.2.3), using the stats module in Icy (de Chaumont et al., 2012). We also evaluated co-localization by calculating the Pearson's correlation coefficient (r) and the Mander's co-occurrence coefficients (M1 and M2), using the ColocalizationStudio PlugIn in Icy (de Chaumont et al., 2012). The Pearson's correlation coefficient allows us to evaluate how well two signals (eGFP and one of the other fluorophores) linearly correlate to each other. This parameter is useful for evaluating if we measure more of the signal of a fluorophore (a specific component of the biofilm matrix) due to an increased concentration of bacteria (eGFP signal). The Pearson's coefficient does not give information on the fraction of a given signal that overlaps with another one, meaning that we would not be able to measure how much of the bacilli in the biofilm is covered by a specific component of the ECM. To overcome this problem, we calculated the Mander's co-occurrence coefficients (M1 and M2) as they calculate the fraction of the signal from a defined fluorophore co-occurring with the signal from another fluorophore. In this thesis, M1 always refers to the fraction of the eGFP signal co-occurring with any of the used fluorophores (NR, SR, ConcA, and PI), while M2 always refers to the fraction of the signal from a given fluorophore (a component of the extracellular matrix) that co-occurs with the eGFP signal (bacilli). The median of the calculated relative volumes are summarized in Table 2-1 and Figure 2-5, and the medians for each of the coefficients are summarized in Table 2-1.

Table 2-1. Relative biovolumes and colocalization coefficients of the components of the *M. chelonae* pellicles ECM.

Component of the ECM	Relative biovolume	Pearson's correlation coefficient	Mander's coefficient	
			M1 (fraction of the eGFP signal co-occurring with the fluorophore signal)	M2 (fraction of the signal of the fluorophore co-occurring with the eGFP signal)
Nile Red (Lipids)	1.030	0.717	0.926	0.898
Propidium iodide (eDNA)	1.081	0.85	0.984	0.924
Concanavalin A Alexa Fluor 647 (Carbohydrates)	0.688	0.271	0.640	0.966
SYPRO Ruby (Proteins)	1.073	0.678	0.832	0.732

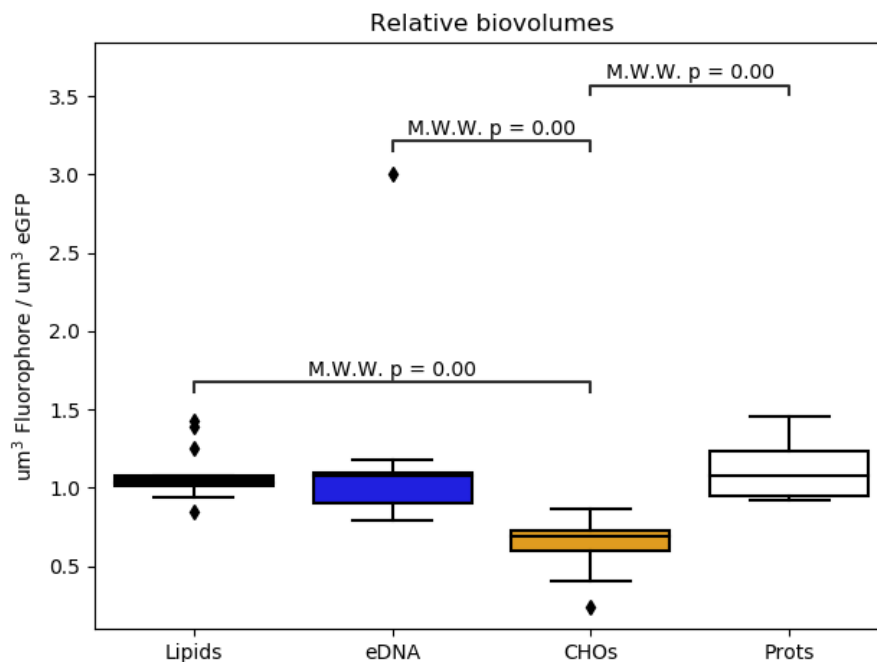


Figure 2-5. Relative volumes of components of *M. chelonae* ECM

The relative volumes of each of the components of the mycobacterial biofilms were calculated using the fluorescent signal from stained *M. chelonae* pellicles and the signal from fluorescent bacilli (eGFP), was used as the reference. Lipids, eDNA, and proteins have a relative volume closer to 1 μ^3 fluorophore/ μ^3 eGFP, while the relative volume from carbohydrates, 0.688 μ^3 carbohydrates/ μ^3 eGFP (Table 2-1), is significantly lower than the rest of the components (Mann-Whitney test, pval<0.01).

The correlation between the PI and eGFP signals is high (0.859, Table 2-1), and even more, most of the signals overlap with each other (M1=0.984 and M2=0.924, Table 2-1). These parameters indicate that eDNA is likely to be in the proximity of the bacilli.

The signal from NR and eGFP have a good ($r=0.717$, Table 2-1), and as expected, most of the eGFP signal overlaps with the signal from NR (M1= 0.926, Table 2-1), but around 10% of the signal of NR does not overlap with the bacilli on the biofilm (M2=0.898, Table 2-1). This data suggests that, to some degree, lipids are components of the ECM.

Although most of the eGFP signal overlaps with SR ($M1=0.832$, Table 2-1), around 30% of the SR signal does not overlap with eGFP ($M2=0.732$, Table 2-1). However, the correlation between the signals is relatively high ($r=0.678$, Table 2-1). These calculations suggest that proteins are scattered across the biofilm matrix and are the bulk component of the *M. chelonae* biofilm ECM.

The signals from ConcA and eGFP correlate poorly ($r=0.271$, Table 2-1), and although around 96% of ConcA signal overlaps with eGFP ($M2=0.966$, Table 2-1), only 73% of the eGFP signal overlaps with ConcA ($M1=0.732$, Table 2-1). The calculations suggest that carbohydrates are accumulating in specific areas of the biofilms, or that some of the carbohydrate content may have been removed during the repeated washes during the staining. It is also worth taking into account that unlike NR, PI, and SR, Concanavalin A is a protein and perhaps does not diffuse across the biofilm matrix as freely as the rest of the dyes, that are relatively smaller molecules.

2.4 Discussion

Microscopy is a powerful tool that not only allows us to get a closer, detailed look at the morphology of mycobacterial biofilms but also has the power of revealing quantitative data on the components of the ECM. When the experimental design incorporates good practices for image acquisition and includes the calculation of geometrical parameters, such as biovolume and colocalization coefficients, the resulting information can be compared between studies, facilitating the description of biofilms, and easing the evaluation of anti-biofilm strategies.

The information obtained by imaging *M. chelonae* pellicles is similar to other studies (Lemassu et al., 1996b; Lemassu and Daffé, 1994; Ortalo-Magne et al., 1995; Rose et al., 2015; Rose and Bermudez, 2016), and eased the description of how the ECM components distribute on the biofilm. *Mycobacterium chelonae* pellicles form cord-like structures and have pores, and the resident bacilli are coated by a layer of extra-polymeric substances that make up the ECM. The composition of the ECM of some mycobacterial pellicles has been addressed before and showed that the most abundant components are carbohydrates and proteins, eDNA and to a minor degree lipids (Lemassu et al., 1996b; Lemassu and Daffé, 1994; Ortalo-Magne et al., 1995; Ortalo-Magné et al., 1996; Rose et al., 2015; Rose and Bermudez, 2016; Trivedi et al., 2016).

After detecting proteins, lipids, carbohydrates, and eDNA, in the ECM of *M. chelonae* pellicles, the relative biovolume was calculated using as a reference the volume of the bacilli in the pellicle. The relative biovolumes for all components are all close to 1, except for carbohydrates, which is 0.69. While eDNA and lipids appear to be closer to the bacilli, carbohydrates and proteins are in the outermost part of the *M. chelonae*. eDNA, proteins, and carbohydrates have a structural role in mycobacterial biofilm biofilms (Aung et al., 2017; Rose et al., 2015; Trivedi et al., 2016). Lipids are also present in the ECM (Ortalo-Magne et al., 1995; Ortalo-Magné et al., 1996), but they do not seem to be responsible for the structure of the biofilm (Trivedi et al., 2016). Carbohydrates, at least the ones detected by Concanavalin A, appear to be concentrated in some parts of the pellicles, instead of uniformly distributed. This observation may be due to removal of the carbohydrate-content during the washes involved in the staining, or poor penetration of the used dye, as Concanavalin A is protein, and it is bigger than the other used dyes. *M. tuberculosis* and *M. smegmatis* produce cellulose when forming biofilms (Trivedi et al., 2016; Van Wyk et al., 2017), despite the genus mycobacteria lacking the genes for

cellulose synthase, and these observations contrast with previous studies, where the configuration of the glycosidic bond characterized polysaccharides from mycobacterial pellicles, including *M. tuberculosis* and *M. smegmatis*, was α , not β (Lemassu and Daffé, 1994). Perhaps, further experiments will help us to clarify the role of carbohydrates during pellicle formation in *M. chelonae*.

**Chapter 3 Analysis of the
extra polymeric
substances of
*Mycobacterium
chelonae* biofilms**

3.1 Introduction

The extra polymeric substances (EPS) of bacterial biofilms are responsible for mediating the first steps of the attachment during biofilm formation. Once the structure is formed, the EPS confers protection to the resident bacteria to a wide variety of stresses (Flemming and Wingender, 2010), including attacks from the immune system in infection-associated biofilms. However, the response following the encounter of the components of the immune system and pathogenic biofilms is often complicated and depends significantly on the components of the EPS and the anatomical location of the biofilm (Watters et al., 2016).

Some EPS are known to impair the functions of components of the immune system. EPS produced by a clinical strain of *Burkholderia cepacia* inhibits neutrophils chemotaxis and the production of reactive oxygen species (Bylund et al., 2006), while the alginate produced by *Pseudomonas aeruginosa* interferes with the killing effects of the macrophages (Leid et al., 2005) and opsonization by the complement system (Pier et al., 2001).

The composition of the EPS of several mycobacterial biofilms has been described (Lemassu and Daffé, 1994; Ojha et al., 2005; Ortalo-Magne et al., 1995; Ortalo-Magné et al., 1996; Rose et al., 2015; Rose and Bermudez, 2016; Trivedi et al., 2016), finding an accumulation of free mycolic acids during pellicle formation, and identifying carbohydrates as the bulk components of the ECM. However, the components of *M. chelonae* pellicles have not yet been characterized fully.

3.2 Aim

The aim of this chapter is to elucidate the changes occurring of carbohydrates and cell wall lipids from *M. chelonae* due to biofilm formation.

3.2.1 Specific objectives:

- Determine the lipid profiles of *M. chelonae* biofilms and planktonic cultures.
- Identify changes in cell wall lipids associated with biofilm formation.
- Elucidate the composition of the carbohydrates present in *M. chelonae* extracellular material.
- Identify changes in the composition of carbohydrates during biofilm formation.

3.3 Results

In the past chapter, we analyzed the structure of *M. chelonae* pellicles and identified the presence of lipids, eDNA, carbohydrates, and proteins, as components of the extracellular matrix. Due to the extensive washing required for fluorescent staining, we did not pursue the imaging of 10-day old biofilms (Figure 3-1, panel B), as they are easily disrupted by mechanical movement. However, in the current chapter, we include the lipid and carbohydrate composition of *M. chelonae* pellicles growth for five (Biofilm t1) and ten days (Biofilm t2), as well as planktonic bacilli at OD₆₀₀=1 (Planktonic t1) and OD₆₀₀=3 (Planktonic t2), to assess the changes occurring in the pellicles through time.

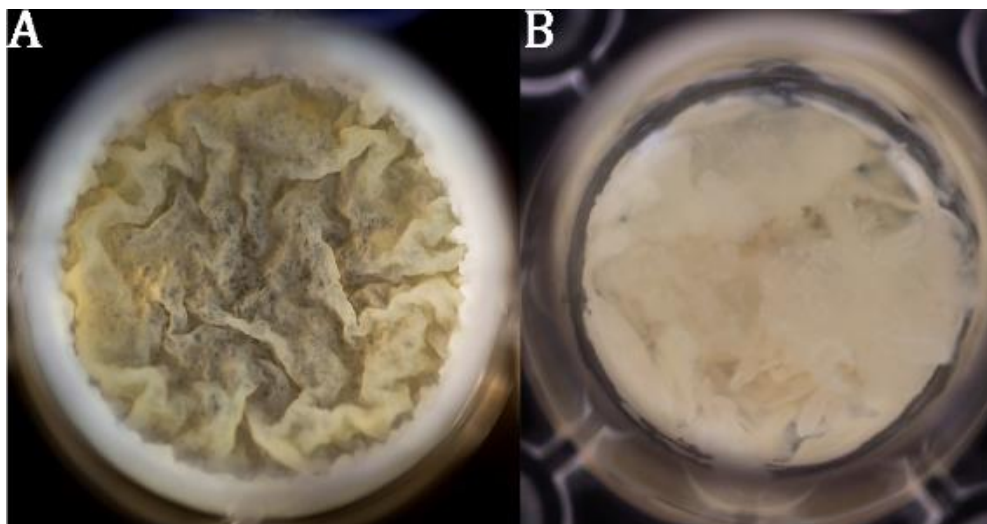


Figure 3-1. *M. chelonae* biofilms growth for five (A) and ten (B) days in Sauton's media at 30°C.

Detail of a single well of a 24-well plate where *M. chelonae* pellicles have been growing for five (A) and ten (B) days. The five-day old pellicle displays the characteristic cording of mycobacterial pellicles, while the ten-day old pellicle has collapsed and sunk into the bottom of the well.

3.3.1 The lipid profile of *M. chelonae* biofilms is different from its planktonic counterpart

Lipids are an integral component of the mycobacterial outer envelope, and they have been studied in detail in several mycobacterial biofilms (Ojha et al., 2008; Ortalo-Magné et al., 1996; Pacheco et al., 2013; Recht and Kolter, 2001; Sambandan et al., 2013; Wright et al., 2017). We grew *M. chelonae* pellicles and planktonic bacteria in Sauton's media supplemented with a small amount of ^{14}C -acetate, for it to be incorporated into the synthesized lipids (for more details, see section 7.9.1). The ^{14}C -labelled lipids from *M. chelonae* cultures were extracted into three different lipid fractions using a mix of solvents with different polarities (section 7.9.2). We obtained solvent-extractable apolar lipids,

inner apolar lipids, and polar lipids. In addition to the fractionation of lipids from *M. chelonae* cultures, we hydrolyzed the de-lipidated bacterial pellet to extract the cell wall-bound mycolic acids, which in turn were derivatized to their respective methyl-ester (see section 7.9.3). All the obtained lipid fractions were resolved using thin-layer chromatography systems described by Dobson, et.al. (Dobson et al., 1985; see Table 7-5), and the obtained TLC lipid profiles are depicted from Figure 3-2 to Figure 3-8.

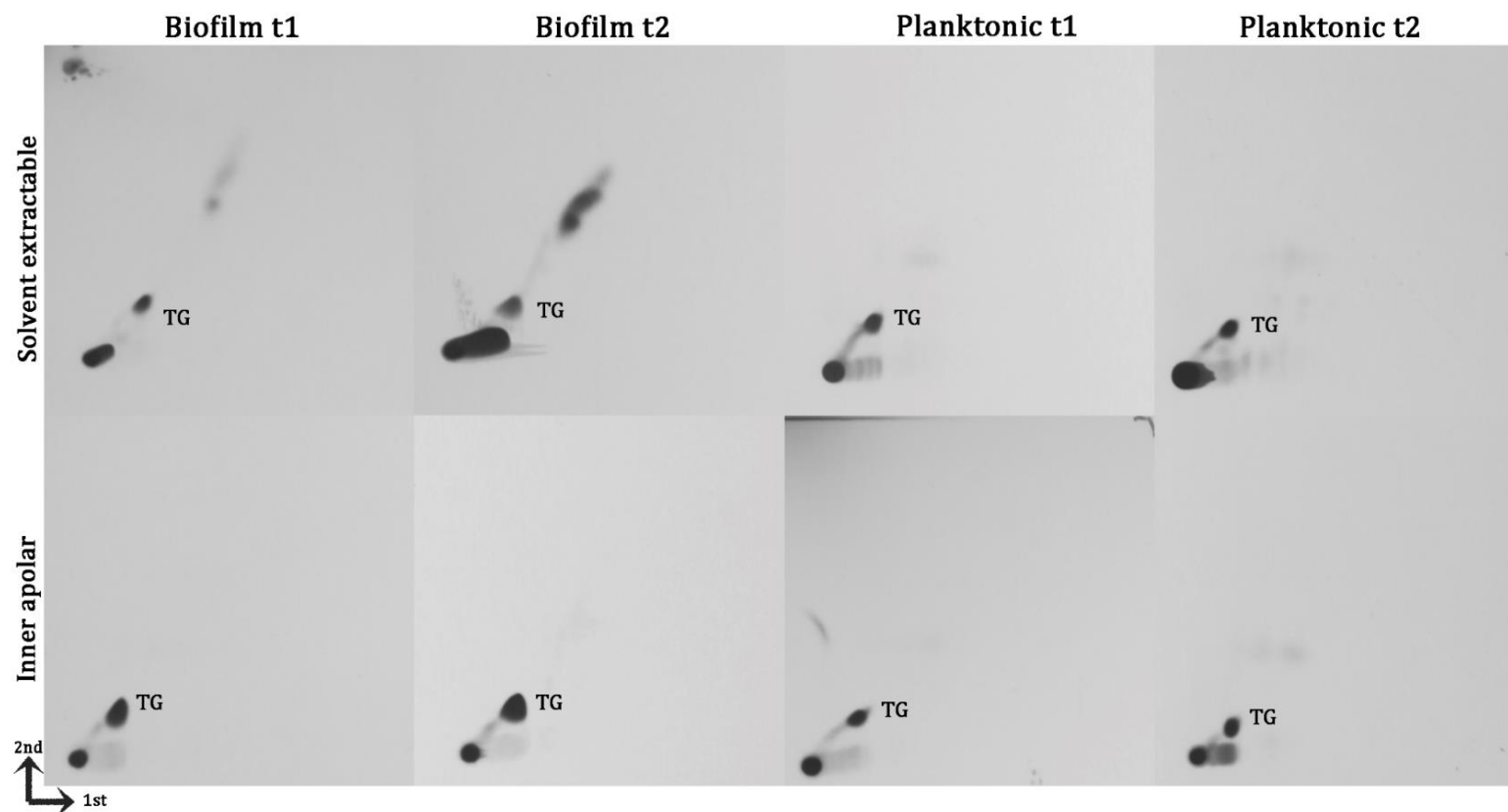


Figure 3-2. TLC of *M. chelonae* apolar lipids resolved using system A.

Solvent extractable and inner apolar lipids from 5 (Biofilm t1) and 10-day old (Biofilm t2) and *M. chelonae* planktonic cultures $OD_{600}=1$ (Planktonic t1) and $OD_{600}=3$ (Planktonic t2) were resolved by TLC using system A (Table 7-5). This solvent allows to resolve triacylglycerol (TG) from the rest of the lipids present in the analyzed fractions.

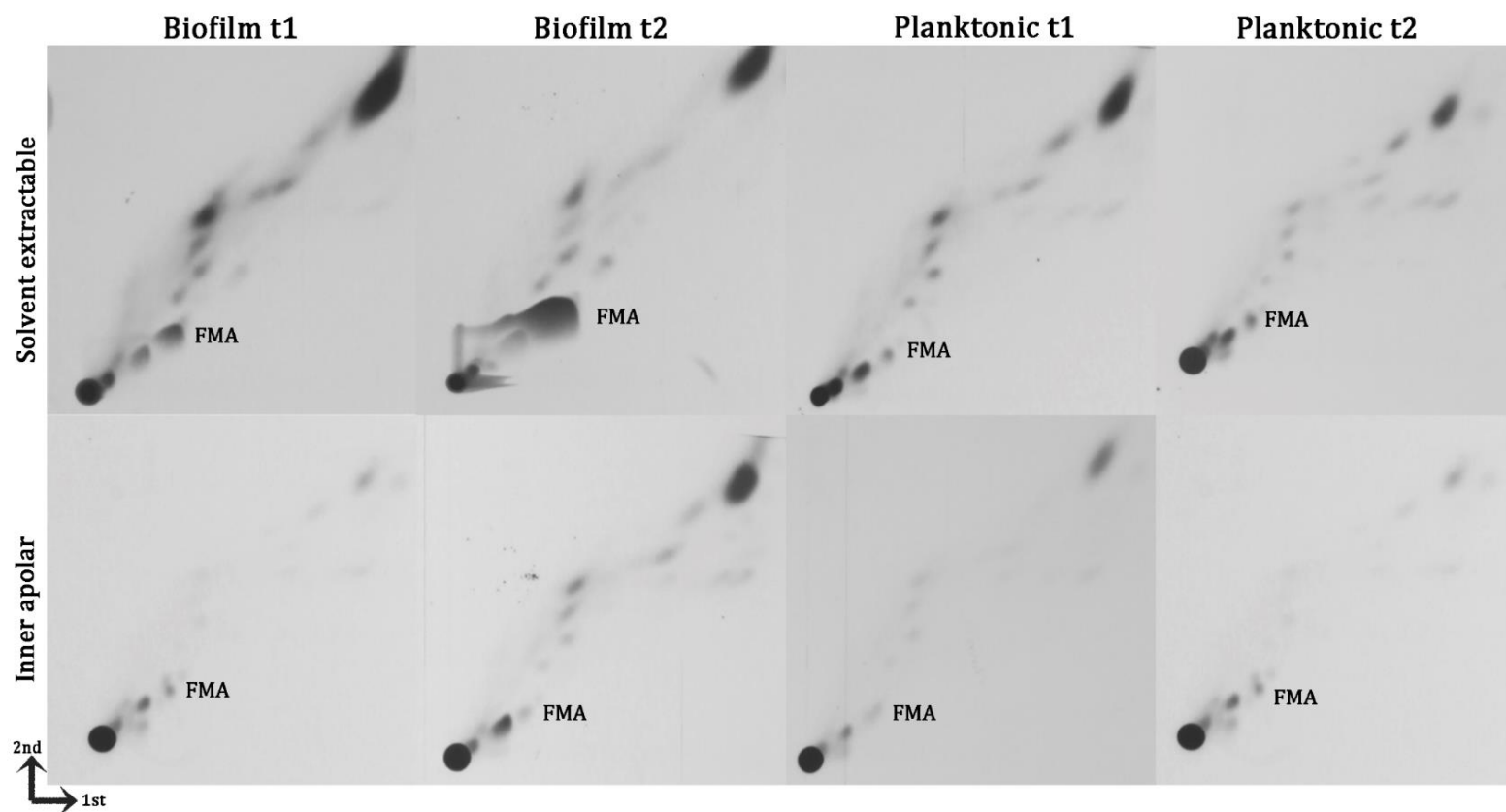


Figure 3-3. TLC of *M. chelonae* apolar lipids resolved using system B.

Solvent extractable and inner apolar lipids from 5 (Biofilm t1) and 10-day old (Biofilm t2) and *M. chelonae* planktonic cultures OD600=1 (Planktonic t1) and OD600=3 (Planktonic t2) were resolved by TLC using system B (Table 7-5). This solvent allows to resolve free mycolic acids(FMA) from the rest of the lipids present in the analyzed fractions. We observed an accumulation of FMA on the solvent extractable lipid fraction from *M. chelonae* pellicles, compared to their planktonic counterparts. The accumulation of FMA is even more evident in 10-day old *M. chelonae* pellicles.

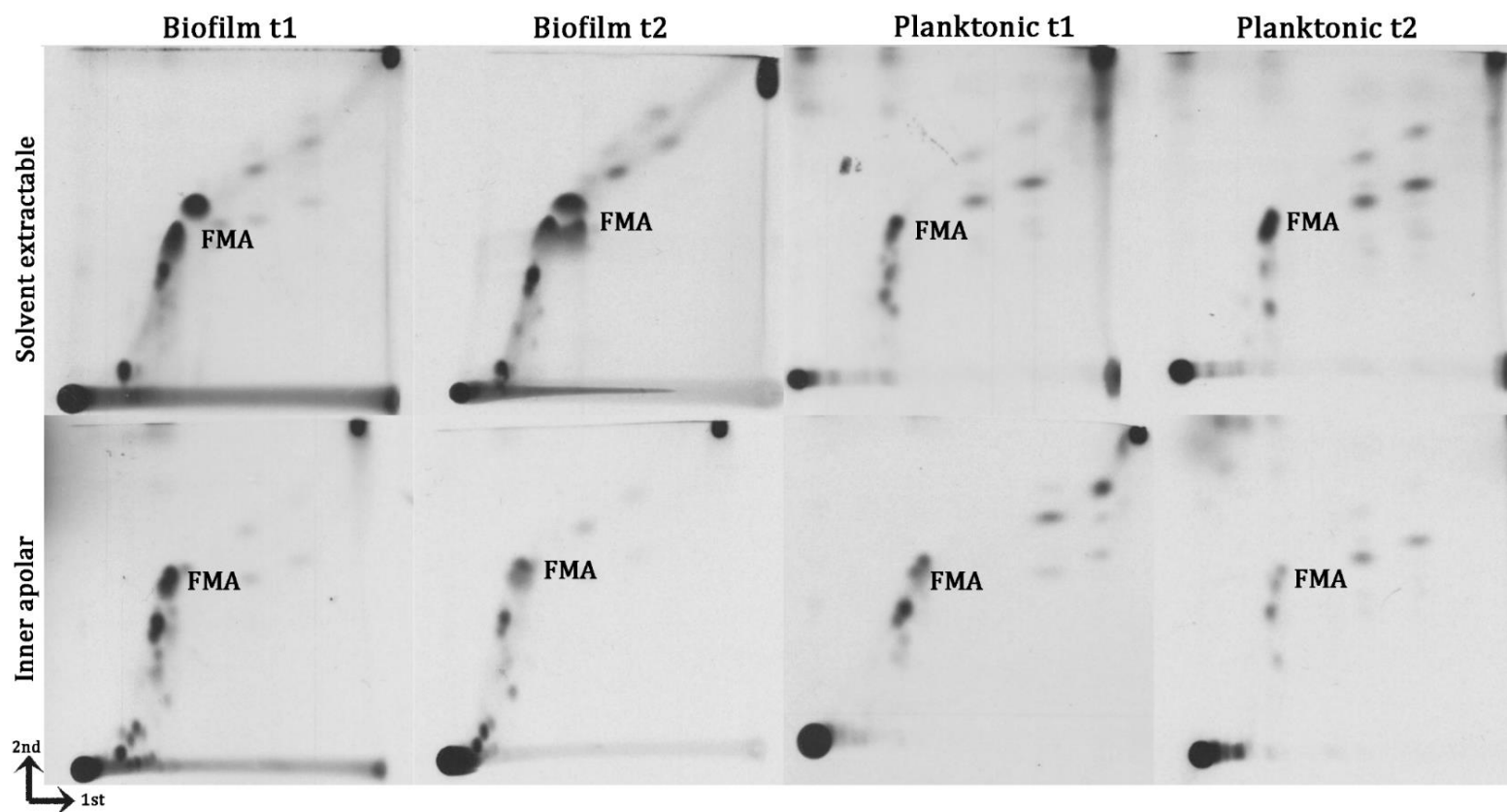


Figure 3-4. TLC of *M. chelonae* apolar lipids resolved using system C.

Solvent extractable and inner apolar lipids from 5 (Biofilm t1) and 10-day old (Biofilm t2) and *M. chelonae* planktonic cultures OD600=1 (Planktonic t1) and OD600=3 (Planktonic t2) were resolved by TLC using system C (Table 7-5). This solvent allowed us to resolve free mycolic acids (FMA) from the rest of the lipids present in the analyzed fractions. As observed in Figure 3-3, the accumulation of FMA on the solvent extractable lipid fraction from *M. chelonae* pellicles is evident, and this system even allowed the resolution of two different spots of FMA (Solvent extractable lipids, Biofilm t2), perhaps two different subclasses of FMA.

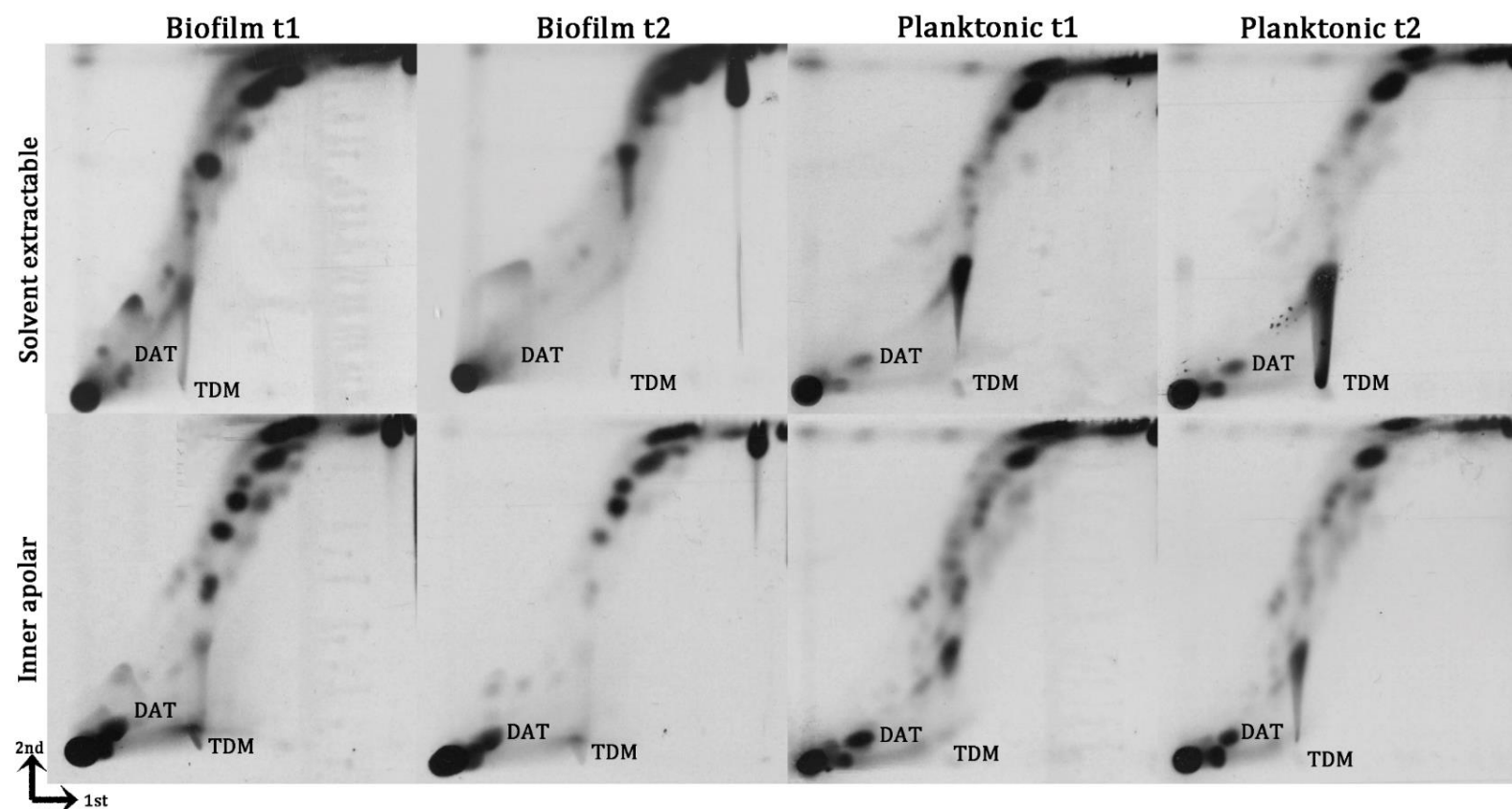


Figure 3-5. TLC of *M. chelonae* apolar lipids resolved using system D.

Solvent extractable and inner apolar lipids from 5 (Biofilm t1) and 10-day old (Biofilm t2) and *M. chelonae* planktonic cultures $OD_{600}=1$ (Planktonic t1) and $OD_{600}=3$ (Planktonic t2) were resolved by TLC using system D (Table 7-5). This solvent system allowed us to resolve trehalose dimycolate (TDM) and diacyl trehalose (DAT) from the rest of the lipids present in the analyzed fractions. While the presence of the glycolipid TDM increases from Planktonic t1 to Planktonic t2, it decreases from Biofilm t1 to Biofilm t2.

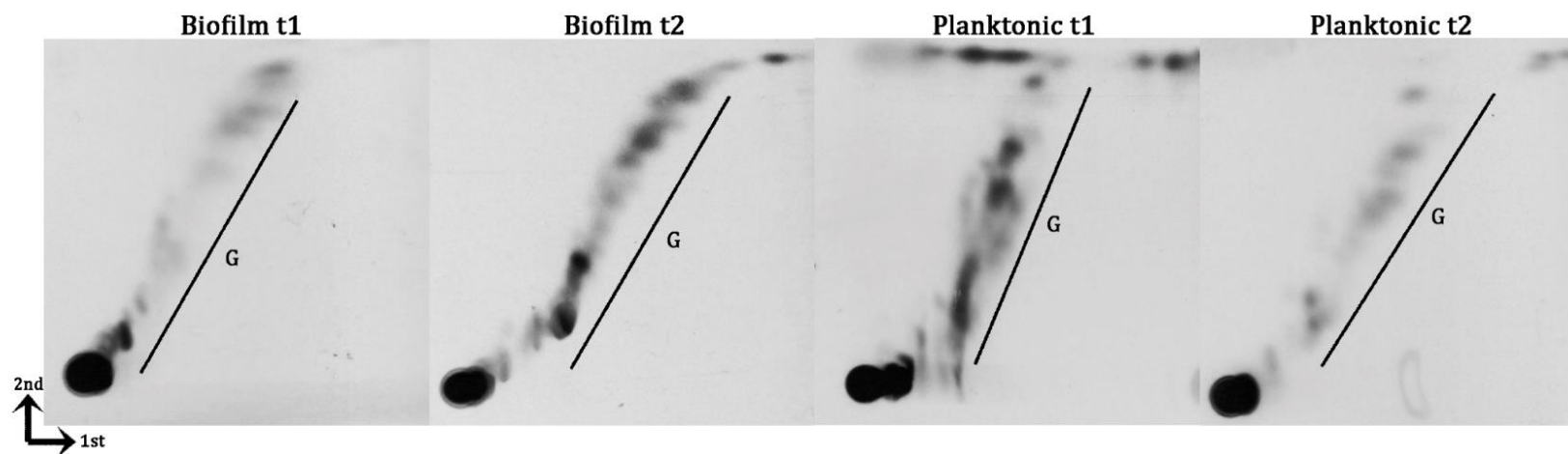


Figure 3-6. TLC of *M. chelonae* polar lipids resolved using system D.

Polar lipids from 5 (Biofilm t1) and 10-day old (Biofilm t2) and *M. chelonae* planktonic cultures $OD_{600}=1$ (Planktonic t1) and $OD_{600}=3$ (Planktonic t2) were resolved by TLC using system D (Table 7-5). This solvent system allowed us to resolve glycolipids (G) from the rest of the lipids present in the analyzed fractions.

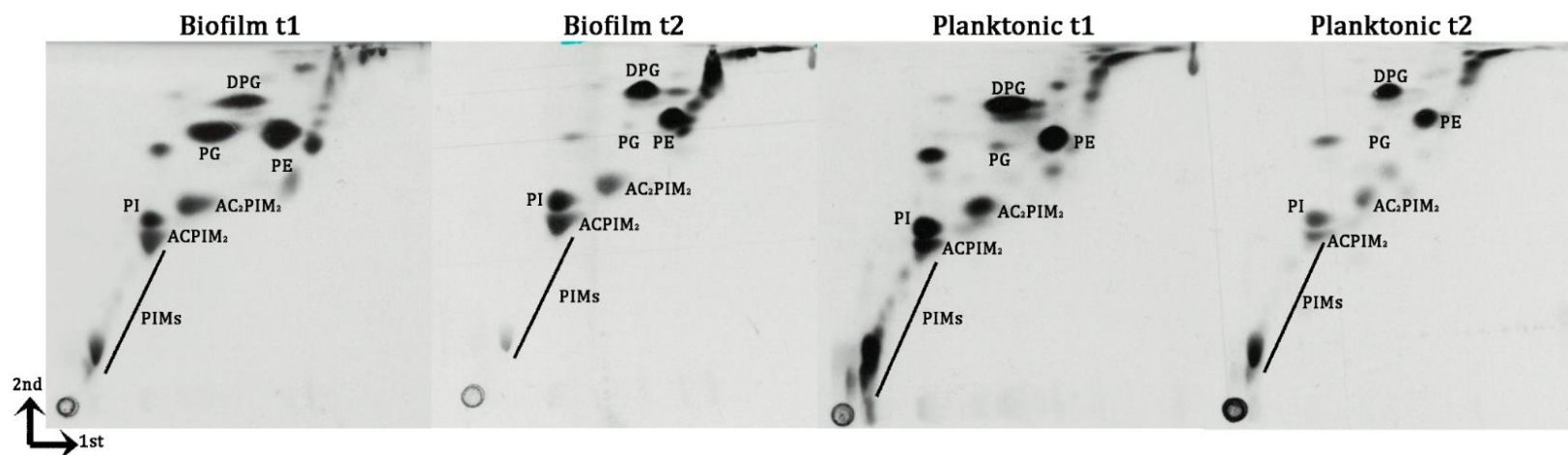


Figure 3-7. TLC of *M. chelonae* polar lipids resolved using system E.

Polar lipids from 5 (Biofilm t1) and 10-day old (Biofilm t2) and *M. chelonae* planktonic cultures $OD_{600}=1$ (Planktonic t1) and $OD_{600}=3$ (Planktonic t2) were resolved by TLC using system E (Table 7-5). This solvent system allowed us to resolve the phospholipids diphosphatidylglycerol (DPG), phosphatidylethanolamine (PE), phosphatidylglycerol (PG), phosphatidylinositol, the phosphatidylinositolmannosides (PIMs) and its acetylated variants (ACPIM₂, AC₂PIM₂). We detected an accumulation of PG in polar lipids from Biofilm t1, although PG is a minor component of the mycobacterial inner membrane.

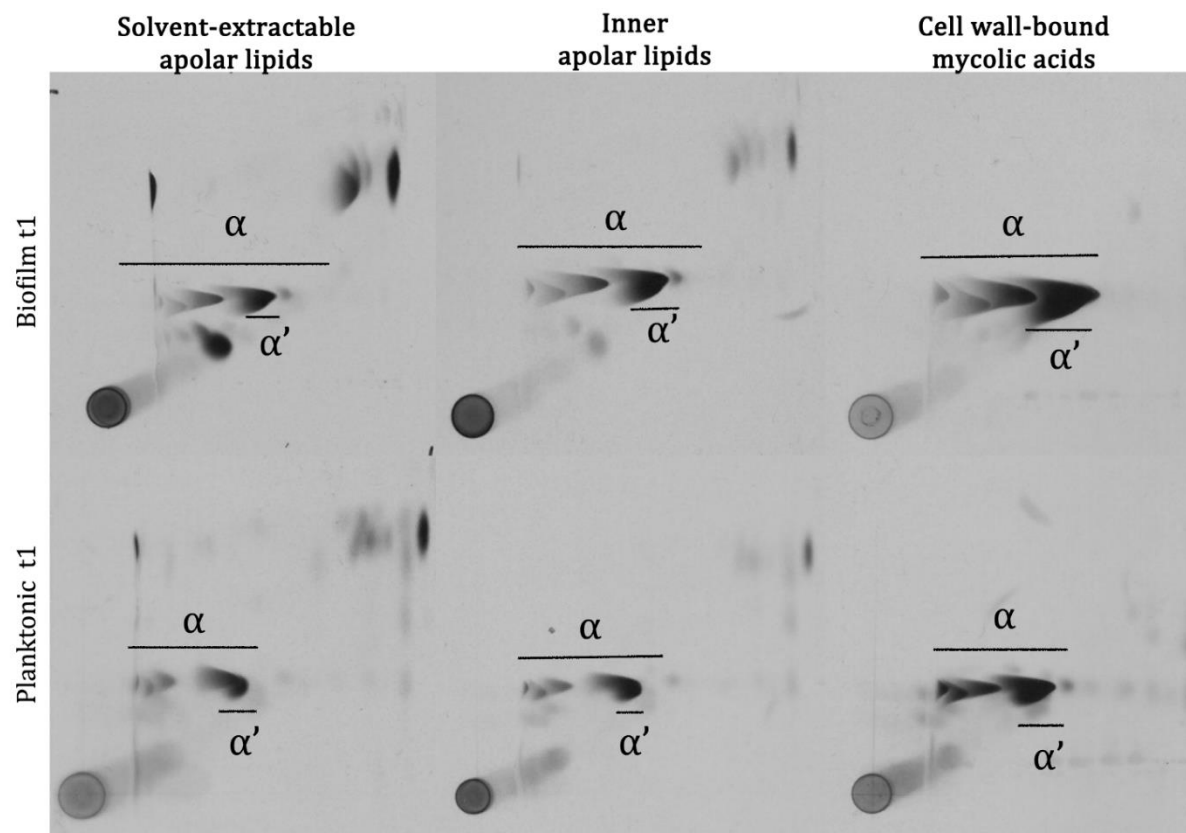


Figure 3-8. Argentation TLC of *M. chelonae* mycolic acid methylesters.

The mycolic acids present in apolar lipid fractions (solvent extractable apolar lipids and inner apolar lipids) and the cell wall-bound mycolic acids were derivatized to their methyl ester form and resolved using argentation TLC. This silica plates have been treated with silver nitrate (see sections 7.9.3 and 7.9.5), this allows to resolve subspecies from the mycolic acids, according to the degree of insaturations. We were able to discern between α and α' mycolic acids methylesters, but we did not observe any difference between *M. chelonae* pellicles or planktonic cultures.

After comparing the patterns of lipids, we were able to identify profiles that have been identified in other mycobacterial biofilms that are also present in *M. chelonae* biofilms. We observed an accumulation of free mycolic acids on solvent extractable lipids from biofilm samples (Figure 3-4 and Figure 3-4, FMA), and we also have noted that this accumulation is more evident as the biofilm ages (Figure 3-4, see FMA in solvent extractable lipids from Biofilm t1 and Biofilm t2). The accumulation of free mycolic acids has been observed in all the studied mycobacterial biofilms, except in *M. avium* (Totani et al., 2017). In *M. smegmatis*, the release of free mycolic acids is partly attributed to the enzymatic hydrolysis of TDM by the action of the TDM serine-esterase Msmeg_1529 (Ojha et al., 2010). As occurring in *M. smegmatis*, we have observed a transient decrease of TDM in *M. chelonae* biofilms (Figure 3-5, see TDM in Solvent extractable lipids for Biofilm t1 and Biofilm t2), while TDM is easily detected in planktonic bacteria (Figure 3-5, see TDM in solvent extractable lipids for Planktonic t1 and t2), suggesting a similar mechanism as the one observed in *M. smegmatis*.

In addition to the changes in the abundance of free mycolic acids and TDM, we have observed that the amount of phosphatidylglycerol, a phospholipid present in the plasma membrane, is increased in Biofilm t1 compared to planktonic cultures or Biofilm t2 (Figure 3-7, PG).

3.3.2 The glucose content of surface-exposed of *M. chelonae* biofilm decreases as the biofilm ages.

Early studies in mycobacterial pellicles have shown that the most abundant carbohydrate present as a surface exposed material is α -glucan, followed by arabinomannans and mannans (Lemassu et al., 1996a; Lemassu and Daffé, 1994; Ortalo-Magne et al., 1995).

We extracted surface-exposed material from *M. chelonae* cultures (3 biological replicates), for further hydrolysis and synthesis of the respective alditol acetates. The synthesized alditol acetates were quantified using gas chromatography (GC). The obtained chromatographs are attached in Appendices 1-4. We used the areas for the peaks corresponding to arabinose, mannose, glucose, and myo-inositol, to calculate the relative abundance of these three species, and the median of the relative abundance of each component is summarized in **Table 3-1** and depicted in **Figure 3-9. The relative abundance of sugars and Myo-inositol extracted from EPS of *M. chelonae* cultures..** We also determined the molar ratio of each sugar, using Myo-inositol as a reference and the results are summarized in

Table 3-2. The molar ratios calculated for 5-day old *M. chelonae* pellicles (Biofilm t2) must be interpreted with caution, as they were calculated using a single replicate because we were unable to detect myo-inositol in the other two replicates.

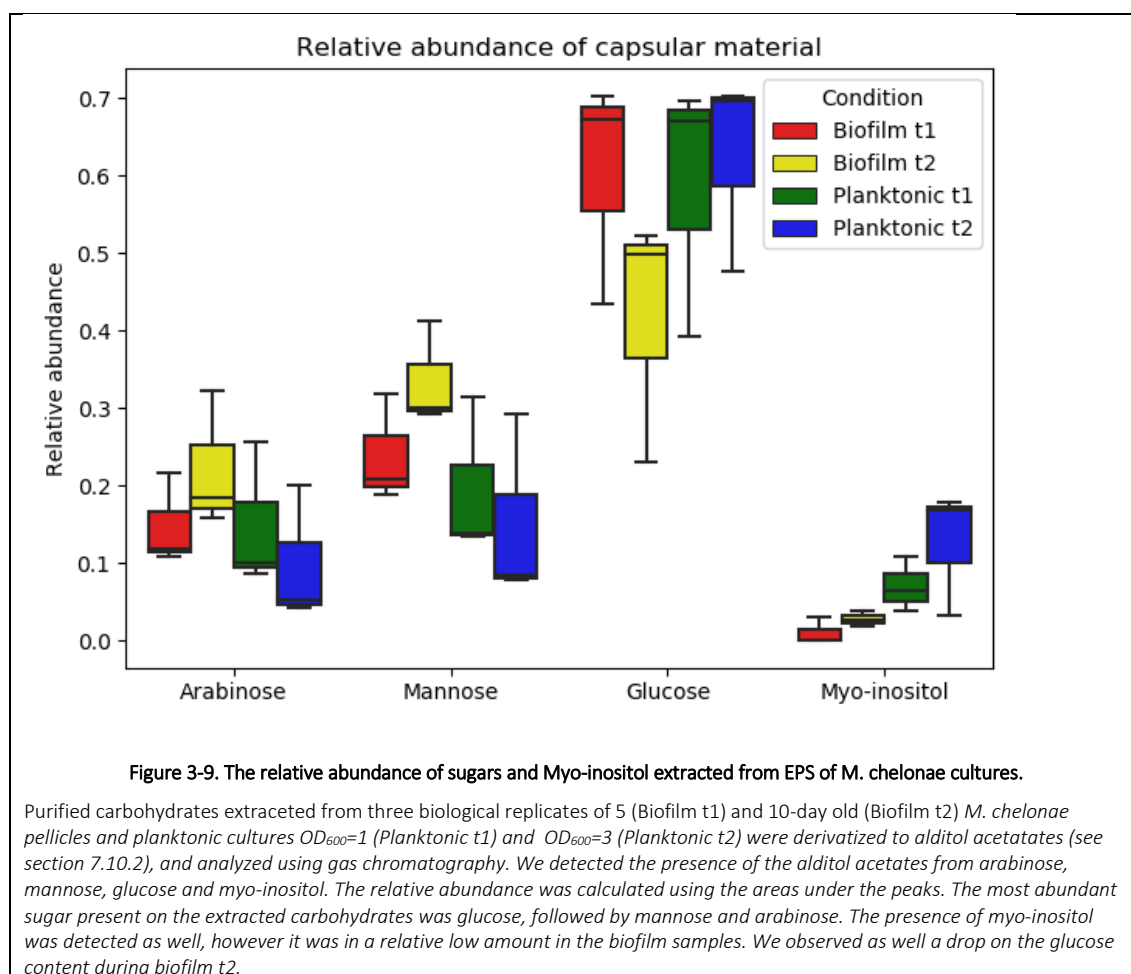
As observed in other mycobacteria, glucose is the major component of the surface exposed polysaccharides in *M. chelonae* biofilms and planktonic cultures, followed by mannose and arabinose (Figure 3-9). Myo-inositol, a polyalcohol that is a component of phosphatidylinositol and its glycosylated derivatives, was found to be more abundant in *M. chelonae* planktonic cultures (Figure 3-9). In contrast, in 5-day old pellicles, Myo-inositol was only detected in one of the three experiments. An interesting trend we observed is that the glucose content drops in Biofilm t2, with the respective increment of arabinose and mannose (Figure 3-9).

Table 3-1. The relative content of sugars and Myo-inositol in *M. chelonae* EPS.

Component	Relative abundance			
	Biofilm t1	Biofilm t2	Planktonic t1	Planktonic t2
Arabinose	0.118	0.183	0.100	0.051
Mannose	0.208	0.299	0.138	0.083
Glucose	0.672	0.497	0.671	0.696
Myo-Inositol	0	0.0272	0.064	0.167

Table 3-2. Relative molar ratio of arabinose, mannose, and Glucose, extracted from *M. chelonae* EPS.

Component	Relative molar ratio			
	Biofilm t1	Biofilm t2	Planktonic t1	Planktonic t2
Arabinose	7.06	8.02	3.07	2.24
Mannose	10.46	12.50	3.92	3.33
Glucose	14.25	17.17	9.12	7.60
Myo-inositol	1	1	1	1



3.4 Discussion

As seen in other mycobacteria, bacilli residing in biofilms display a distinct lipid phenotype compared to its planktonic counterpart (Islam et al., 2012; Ojha et al., 2008).

Possibly, one of the most characteristic traits of mycobacterial biofilms is the accumulation of free mycolic acids. This phenotype has been observed in virtually all the studied mycobacterial biofilms, and in *M. smegmatis* the accumulation of these lipids during biofilm formation has been partially attributed to the hydrolysis of trehalose dimycolate (TDM) to yield trehalose monomycolate and free mycolic acids (Ojha et al., 2010). As we also observe a reduction in the TDM content from 10-day old (Biofilm t2)

M. chelonae biofilms compared to 5-day old biofilm samples (Biofilm t1), we could hypothesize that a similar mechanism could be happening as well in *M. chelonae*.

The accumulation of free mycolic acids in the mycobacterial outer membrane is not exclusive of mycobacterial biofilms. This phenotype has also been observed in planktonic cultures of a strain of *M. tuberculosis* lacking Mez, a malic enzyme involved in the central carbon metabolism (Basu et al., 2018).

Although the signals and the mechanisms leading to the phenotypes related to biofilm formation are yet to be fully elucidated, it has been suggested that a restructure of the lipid metabolism is occurring during biofilm formation (Chen et al., 2006), and there is already some evidence pointing the importance of regulators of the central carbon metabolism on biofilm formation, specifically PknG and Lsr2 (Chen et al., 2006; Wolff et al., 2015).

Another consistent change we observed was the accumulation of phosphatidylglycerol in Biofilm t1, but not in the rest of the analyzed samples. Phosphatidylglycerol is a phospholipid present in abundance in all plasma membranes, either eukaryotic or prokaryotic organisms, but in mycobacteria is acknowledged only as a minor component of the plasma membrane (Jackson et al., 2000). Phosphatidylglycerol is one of the most abundant lipid components of *M. tuberculosis* extracellular vesicles (Prados-Rosales et al., 2011), and despite the lack of studies addressing the role of mycobacterial extracellular vesicles on biofilm formation, it would not be surprising to find they play an active role in biofilm formation, as extracellular vesicles are known to export eDNA and proteins during biofilm formation (Brown et al., 2015; Schooling and Beveridge, 2006).

Regarding carbohydrates, we have observed that the glucose content of the EPS of the *M. chelonae* biofilms decreases as the structure ages. The intracellular glycogen and capsular glucan, are synthesized by a common pathway in mycobacteria (Kalscheuer et al., 2019). Our pathway enrichment analysis shows that the transcription of genes involved in the synthesis of glucans is down-regulated in the 10-day old biofilm, which could partially explain the observed decrease in the glucose content in the EPS.

Although mycobacteria share many distinctive molecular changes associated with biofilm formation, some seem to be species-specific. Apart from the accumulation of FMA and decrease on TDM during biofilm formation, the study on the matrix components resulted in two new molecular changes associated with biofilm formation or maintenance which are the accumulation of phosphatidylglycerol in the 5-day old biofilms, and the second one, the decrease in the glucose content displayed only in 10-day old biofilms. Whether these changes are exclusive of *M. chelonae* biofilms or if they are shared by all mycobacteria is yet to be determined, as most of the studies have not focused on studying the changes of mycobacterial biofilms through time.

It is also essential to assess if these alterations of the EPS components have a further impact on the interaction with the immune system, as several components of the cell envelope are known to have immunomodulatory properties.

**Chapter 4 Raman
spectroscopy for
the study of
*Mycobacterium
chelonae* biofilms**

4.1 Introduction

When a molecule is irradiated with light (photons) into a virtual state, the light is scattered by the molecules. Often, the energy of the scattered photons is the same as the energy of the photons used for irradiating the sample, and this phenomenon is called Rayleigh scattering. However, sometimes the energy of the scattered photons is larger than the energy of the photons used for irradiating the sample, and then the event is termed Stokes Raman scattering (Diem, 2015).

The Stokes Raman scattering is an extremely rare event (Diem, 2015), but the development of the technology has made it easier to record Raman spectra (Vandenabeele, 2010). In Raman spectroscopy, the energy of the liberated photon is called Raman shift, and its value depends on the type of “vibrations” of the bonds of the molecule from where the Stokes Raman scattering originated, but it is independent of the energy of the photons used for irradiating the sample. Even more, the intensity of the generated Raman shift is proportional to the concentration of the molecule in the sample, so if done correctly, Raman spectroscopy can provide both quantitative and qualitative information about the composition of the analyzed sample (Butler et al., 2016; Diem, 2015; Vandenabeele, 2010). Unlike in Infrared spectroscopy, the presence of water on samples analyzed by Raman spectroscopy does not generate interference, so this trait makes Raman spectroscopy very attractive for the study of intact biological samples, with minimal sample requirements (Butler et al., 2016; Vandenabeele, 2010).

Raman spectroscopy is used widely for the characterization of biological samples (Butler et al., 2016; Diem, 2015; Rösch et al., 2005), and for microorganisms, it has made possible the identification of different species within mixed-communities biofilms (Beier

et al., 2010; Samek et al., 2015), as well as the effect of antibiotics on *Pseudomonas aeruginosa* biofilms (Jung et al., 2014). To our knowledge, in the mycobacterial field, Raman spectroscopy has proven to be powerful enough for discerning mycobacteria to the level of species (Stöckel et al., 2017) and thus has been suggested as a potential diagnostic tool to determine the mycobacteria species quickly without the need of culturing the microorganism (Buijters et al., 2008). Raman spectroscopy has also made it possible to identify differences in the metabolite production of *M. smegmatis* grown in different carbon sources (Kumar et al., 2015). Raman spectroscopy has also been used for generating the characteristic Raman spectra from different mycolic acids, aiming to generate characteristic patterns for diagnosis (Perumal et al., 2018).

4.2 Aim

The overall aim of the work described in this chapter is to use Raman spectroscopy to elucidate changes in the overall composition of *M. chelonae* biofilms to identify molecular changes during biofilm formation.

4.2.1 Specific objectives

- Generate Raman spectra from *M. chelonae* biofilms and planktonic cultures.
- Identify the differences between *M. chelonae* biofilms and planktonic culture Raman spectra, and
- Associate the changes in the Raman spectra to changes in the composition of the biofilm.

4.3 Results

4.3.1 Characteristic Raman spectra of *M. chelonae* cultures

After analyzing carbohydrates and lipids present in *M. chelonae* pellicles and planktonic bacteria, we applied Raman spectroscopy to further characterize these bacterial cultures. This spectroscopy technique will allow us to obtain a ‘fingerprint’ of the analyzed sample, that we can later dissect and annotate to gain further information on the biomolecules present on the sample. In collaboration with the Umapathy group from the Indian Institute of Science, Bangalore, we generated the average Raman spectra for five and 10-day old *M. chelonae* biofilms and *M. chelonae* planktonic cultures at an OD₆₀₀=1 and OD₆₀₀=3. The obtained Raman spectra are depicted in Figure 4-1.

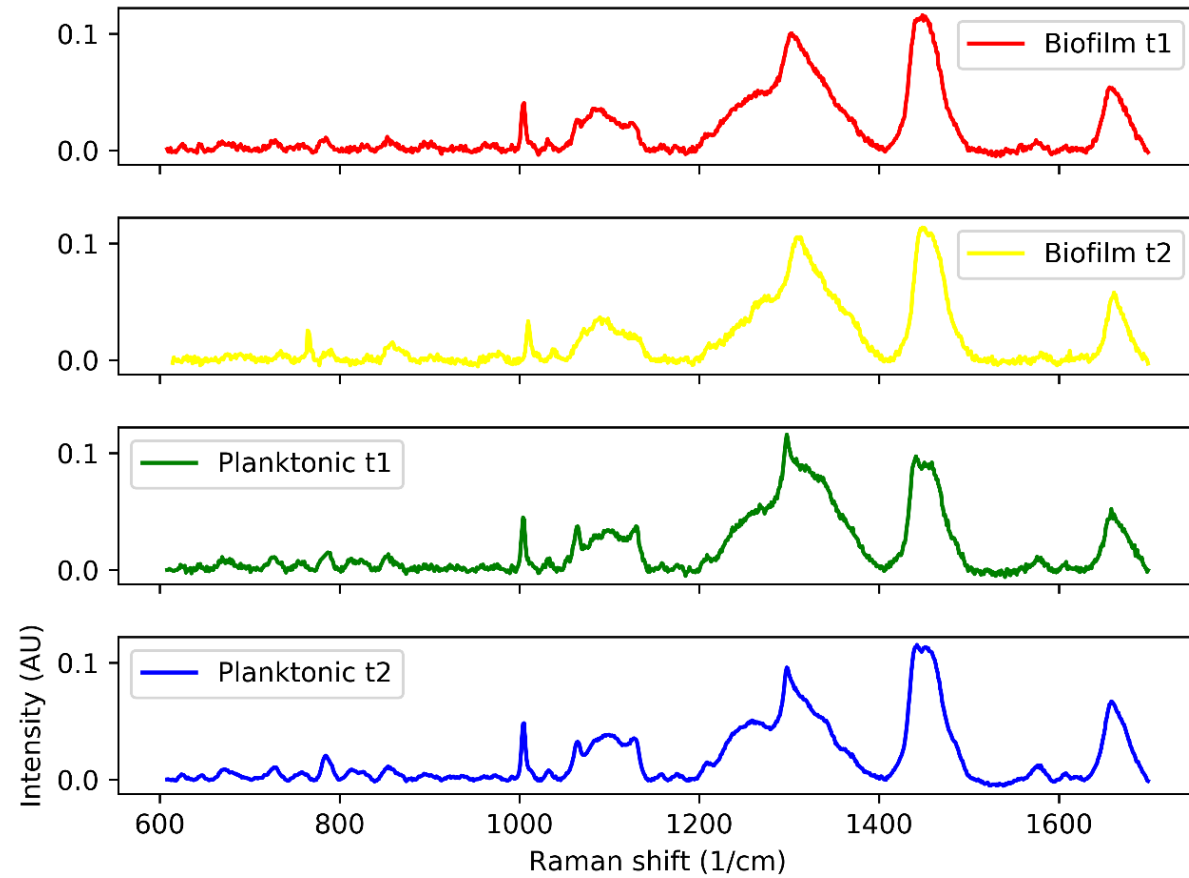


Figure 4-1. Average Raman spectra from M. chelonae cultures.

We collected the Raman shift from four different replicates of 5-day old (Biofilm t1) and 10-day old (Biofilm t2) *M. chelonae* pellicles, and planktonic bacteria at an $OD_{600}=1$ (Planktonic t1) and $OD_{600}=3$. The average intensity of each recorded Raman shift is expressed in arbitrary units (AU) and was used to generate each sample characteristic spectra.

It is challenging to identify the differences between growth conditions just by looking at the spectra, and for our work, determining the Raman shifts (and the associated biomolecules) that allow us to discern between *M. chelonae* pellicles and planktonic cultures is essential. To achieve this, we applied a Principal Component Analysis (PCA) to the generated spectra to identify zones where the samples differ the most, and further associate them to biomolecules to describe changes on the composition between pellicles and planktonic cultures.

4.3.2 PCA discerns between Raman spectra from *M. chelonae* pellicles and planktonic bacteria

A Principal Component Analysis (PCA) was applied to ease the description of the data set, and for identifying specific Raman shifts (and associated biomolecules) causing variability between samples. The PCA describes the samples in terms of new variables named Principal Components (PC), which are just linear combinations of our original measured variables (Raman shifts). Once the principal components were calculated, a scree plot was generated. A scree plot shows the percentage of the explained variance by each component, so we can select a few components that account for most of the variability between samples and use them to describe our samples.

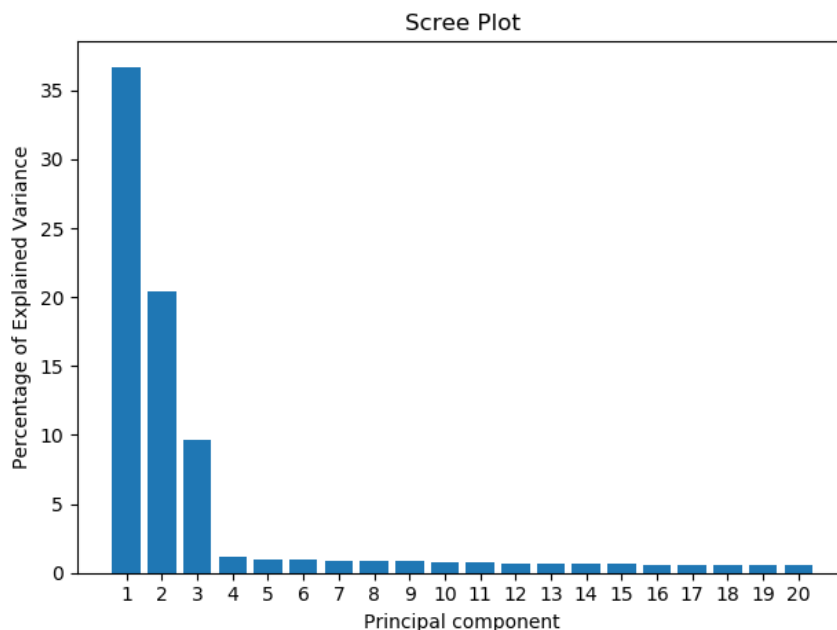


Figure 4-2. Scree plot showing the percentage of the explained variance by the first twenty PCs in the PCA involving Raman spectra from *M. chelonae* pellicles and planktonic cultures.

The first three PCs were used to describe the data set. PC1, PC2, and PC3 explain for 66.7% of the variance of the data set (Figure 4-2). After plotting each sample in terms of the principal components (Figure 4-3), we can observe that each growing condition clusters well, meaning that the PCA applied to the acquired Raman spectra allowed us to distinguish between biofilms and planktonic cultures, at different stages of growth.

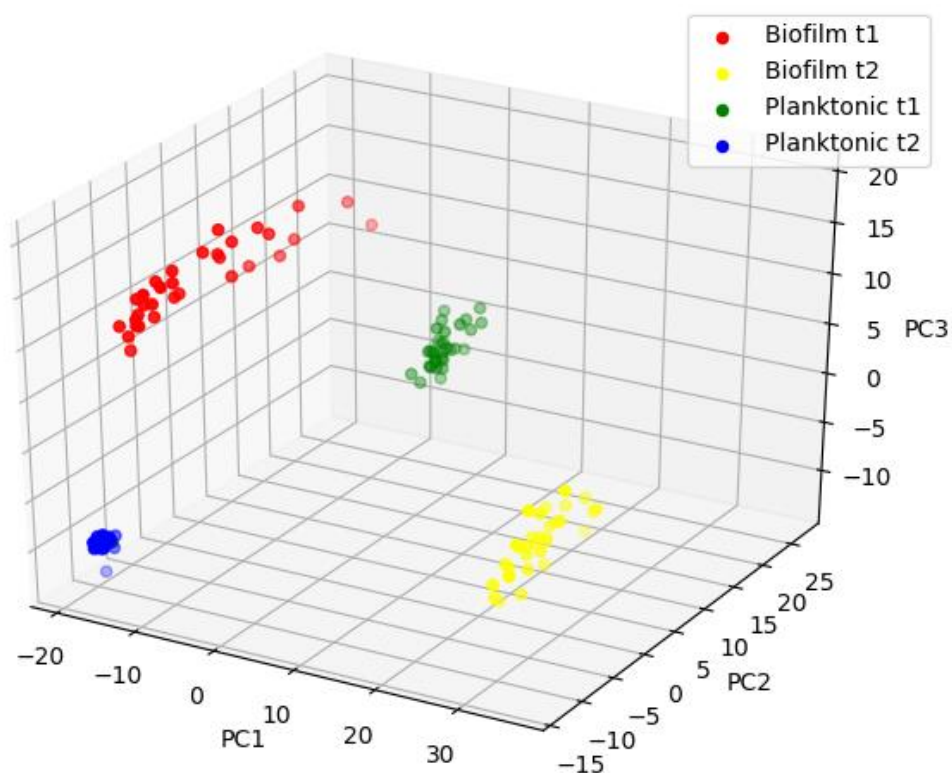


Figure 4-3. Visual representation of Raman spectra from *M. chelonae* cultures in terms of PC1, PC2, and PC3.

The scree plot (**Figure 4-2**) shows that using three principal components is sufficient for explaining most of the variability between the spectra from *M. chelonae* pellicles and planktonic cultures. By plotting each analyzed sample in terms of the three principal components, we observe that samples cluster well, meaning that the PCA is able to discern between 5 (Biofilm t1) and 10—day old (Biofilm t2) *M. chelonae* pellicles and planktonic *M. chelonae* at and OD600=1 (Planktonic t1) and OD600=3 (Planktonic t2).

4.3.2.1 *The intensities for proteins and lipid-associated signals are different between M. chelonae biofilms and planktonic cultures.*

Once that we identified the set of variables (PCs), that describe best the differences between *M. chelonae* pellicles and planktonic bacteria, we identified which Raman shifts have a higher contribution to each PC (and thus to the variability between samples), and those are summarized in Table 4-1.

Table 4-1. Top 20 Raman shifts with a high contribution to the PCs.

Principal component	Top 20 Raman shifts with the highest contribution to the PC (cm ⁻¹)
<i>PC1</i>	1006.29, 1005.16, 1436.85, 1435.80, 1434.76, 1004.02, 1437.89, 1002.89, 1240.28, 1235.94, 1438.93, 1237.03, 1238.11, 1243.53, 1239.19, 1245.69, 1433.72, 1241.36, 1247.86, 1248.94.
<i>PC2</i>	1454.54, 1455.57, 1456.61, 1288.80, 1453.50, 1450.38, 1457.65, 1444.14, 1285.58, 1451.42, 1449.34, 1458.69, 1289.87, 1286.65, 1452.46, 1445.18, 1284.50, 1446.22, 1287.73, 1448.30.
<i>PC3</i>	1132.96, 791.72, 1115.22, 794.09, 792.90, 1114.11, 1487.67, 1484.57, 1113.00, 790.53, 1483.54, 1116.33, 1134.07, 1111.89, 1485.60, 1118.55, 1117.44, 1486.64, 1110.77, 1131.85.

It is possible to associate some Raman shifts to biomolecules, and by comparing the intensities of the signals between is possible to get information on the relative abundance of the biopolymers between samples (Kuhar et al., 2018). We chose representative Raman shifts with a high contribution to the principal components and highlighted them on top of the acquired spectra (*Figure 4-4*). Next, we compared the intensities between samples for some of these Raman shifts, and associate them with previously characterized

biomolecules (Table 4-2). This association makes it is possible to explain the differences between *M. chelonae* biofilms and planktonic cultures in terms of abundance of biopolymers.

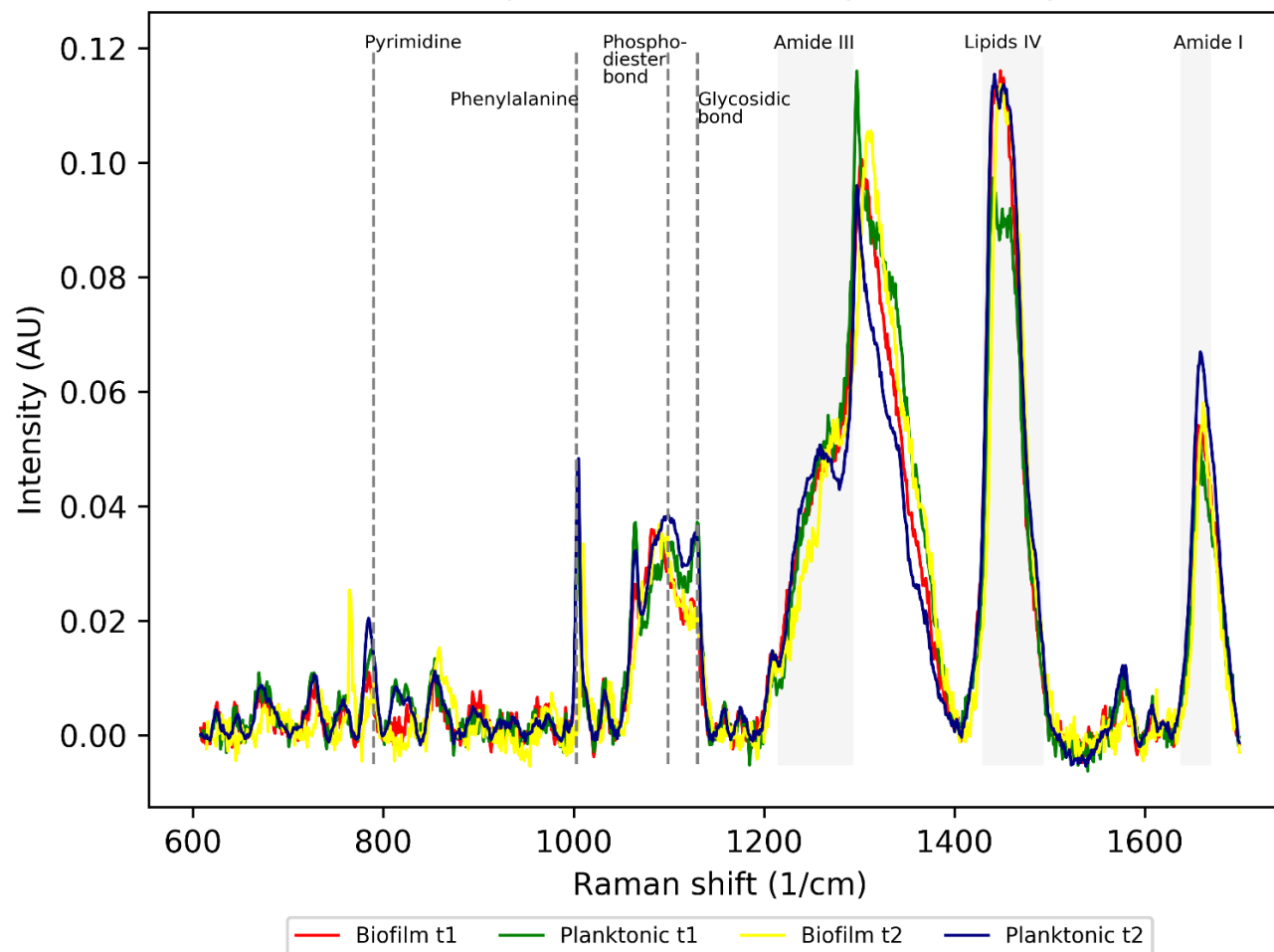
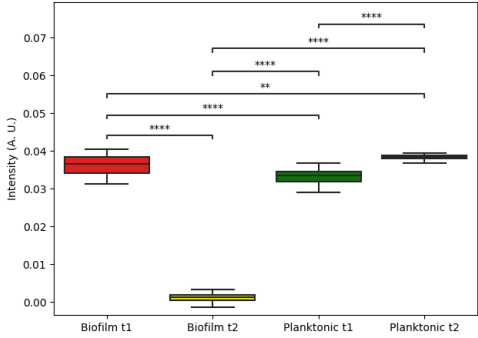
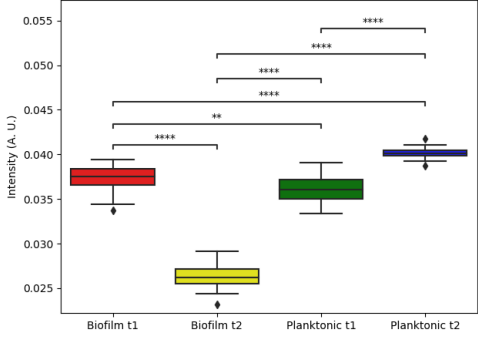
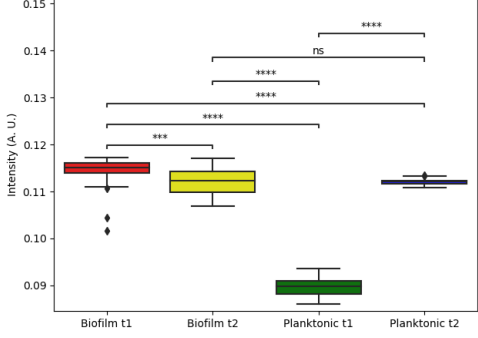
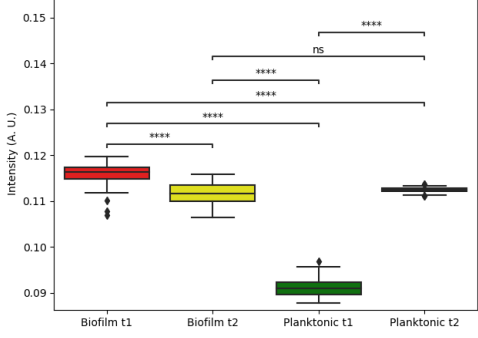
Differences between the spectra of *M. chelonae* pellicles and planktonic cultures

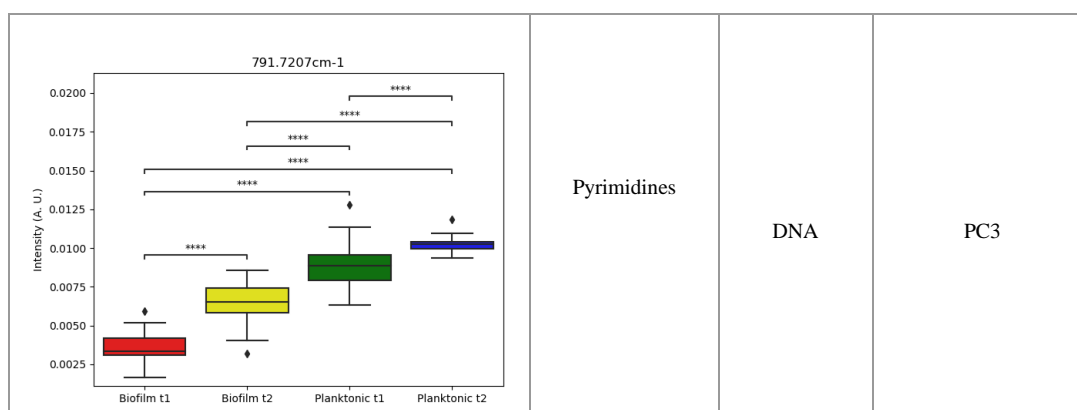
Figure 4-4. Annotated average Raman spectra obtained from *M. chelonae* pellicles and planktonic cultures.

The average Raman spectra from 5 (Biofilm t1) and 10-day (Biofilms t2) old *M. chelonae* pellicles and planktonic cultures OD600=1 (Planktonic t1) and OD600=3 (Planktonic t2) were plotted and annotated with Raman shifts with high contribution to the PCs. Each annotated region was associated with a biopolymer. Most of the variability between Raman spectra from *M. chelonae* pellicles and planktonic cultures is due to signals related to proteins (Phenylalanine, Amide region III, and Amide region I), and lipids (lipids region IV). There is also a contribution from signals associated with nucleic acids (phosphodiester bond from the DNA backbone, and pyrimidine), and carbohydrates (glycosidic linkage).

Table 4-2. Representative Raman shifts with a high contribution to the three PCs selected to describe *M. chelonae* pellicles and planktonic cultures.

Raman shift	Assignment	Biomolecule	Principal component
<p>1002.8916cm⁻¹</p> 	Phenylalanine	Proteins	PC1
<p>1240.2832cm⁻¹</p> 	Amide, region III	Proteins	PC1
<p>1454.54004cm⁻¹</p> 	Lipids, region IV	Lipids	PC2
<p>1444.14258cm⁻¹</p> 	Lipids, region IV	Lipids	PC2

<p>1436.85156cm⁻¹</p>	Lipids, region IV	Lipids	PC1
<p>1288.80371cm⁻¹</p>	Amide, region III	Proteins	PC2
<p>1132.96582cm⁻¹</p>	n(C-C), n(P-O)	Lipids	PC3
	Glycosidic linkage	Carbohydrates	
<p>1115.22461cm⁻¹</p>	n(C-C), n(P-O)	Lipids	PC3
	n(C-O), n(C-C)	Carbohydrates	



In general, we can observe two trends. First, proteins appear less abundant in Biofilm t2 (1002 and 1240 cm^{-1}) compared to the rest of the samples. Also, characteristic signals for lipids (1444 and 1454 cm^{-1}) have a lower intensity in Planktonic t1 than the rest of the samples. For nucleic acids, the signal for DNA (791 cm^{-1}) is most intense in Planktonic t2, and less intense in Biofilm t1.

Some Raman shifts from PC3 are related to carbohydrates (1115 and 1130 cm^{-1}); however, the assignment is ambiguous as they are also associated with lipids. Because no other Raman shift with high contribution to the PCs is associated exclusively with carbohydrates, we selected known signals for the glycosidic bonds (Wiercigroch et al., 2017) and looked for a general trend between samples (*Figure 4-5*). Four of the six selected Raman shifts show a decrease in the intensity of Biofilm t2 (727, 942, 938, and 1051 cm^{-1} , *Figure 4-5*). Still, two show a different trend (1130 and 1099 cm^{-1} , *Figure 4-5*), perhaps due to contribution of other molecules (lipids) to those Raman shifts.

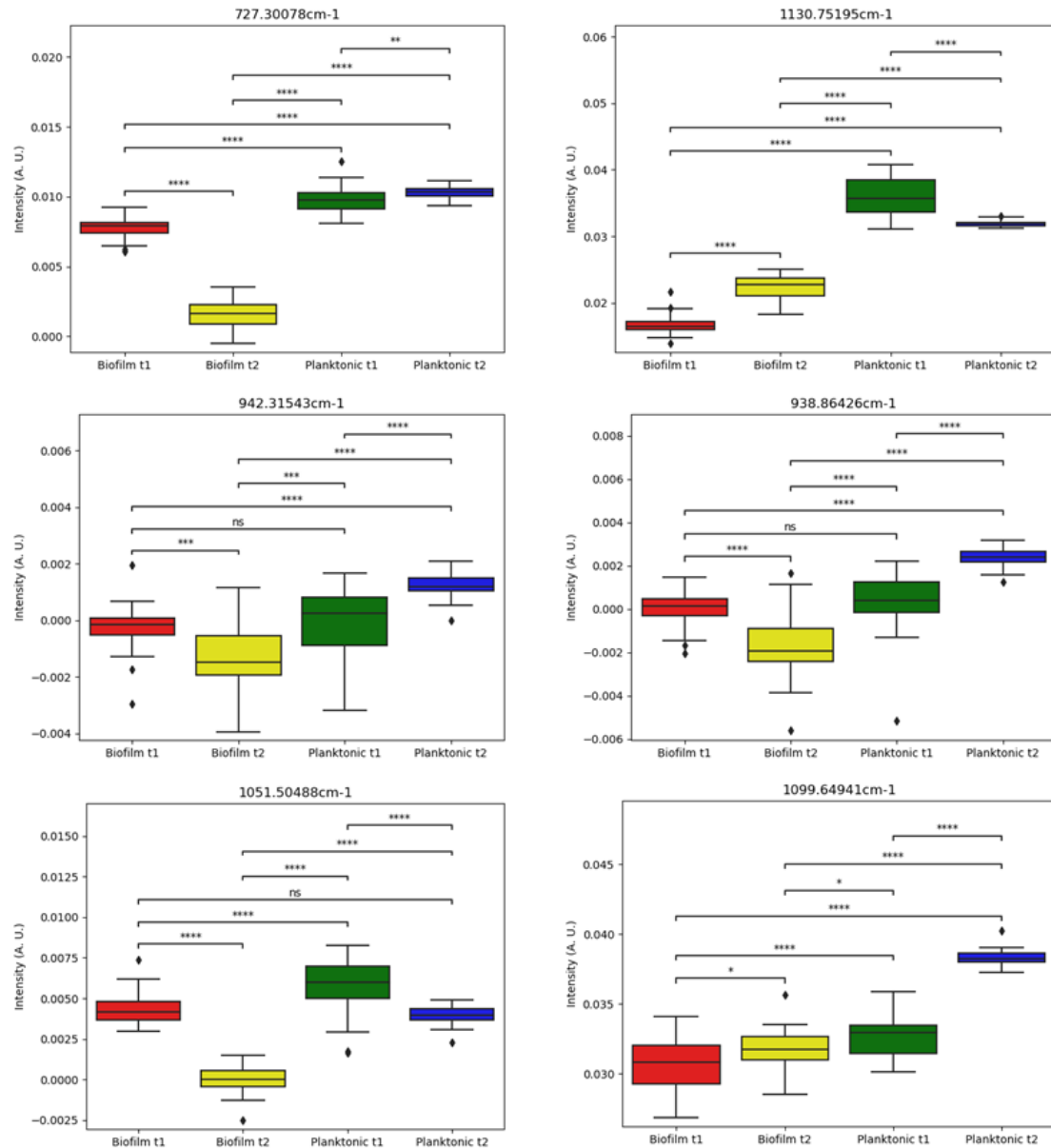


Figure 4-5. Selected Raman shifts associated with the glycosidic bond.

To further clarify the behavior of signals associated with carbohydrates, we selected a group of Raman shifts associated with carbohydrates (Kuhar et al., 2018; Talari et al., 2015; Wiercigroch et al., 2017). While in three of the selected show a similar trend (727, 942, 1051 cm⁻¹, left column), the selected Raman shifts in the right columns do not follow a uniform pattern.

4.3.3 PCA discerns between *M. chelonae* planktonic bacteria at OD₆₀₀=1 and OD₆₀₀=3.

After analyzing *M. chelonae* pellicles and planktonic cultures, we re-analyzed the Raman spectra from *M. chelonae* planktonic cultures at an OD₆₀₀=1 and OD₆₀₀=3. We applied a PCA, and we found that the first principal component explains 42.1% of the variance of the sample, while the second PC accounts for only 3.5% (Figure 4-6). We chose the two first PCs to describe our data set, and by plotting each sample in terms of the two first principal components (Figure 4-7), we can conclude that the PCA can discern between *M. chelonae* planktonic cultures at OD₆₀₀=1 and OD₆₀₀=3.

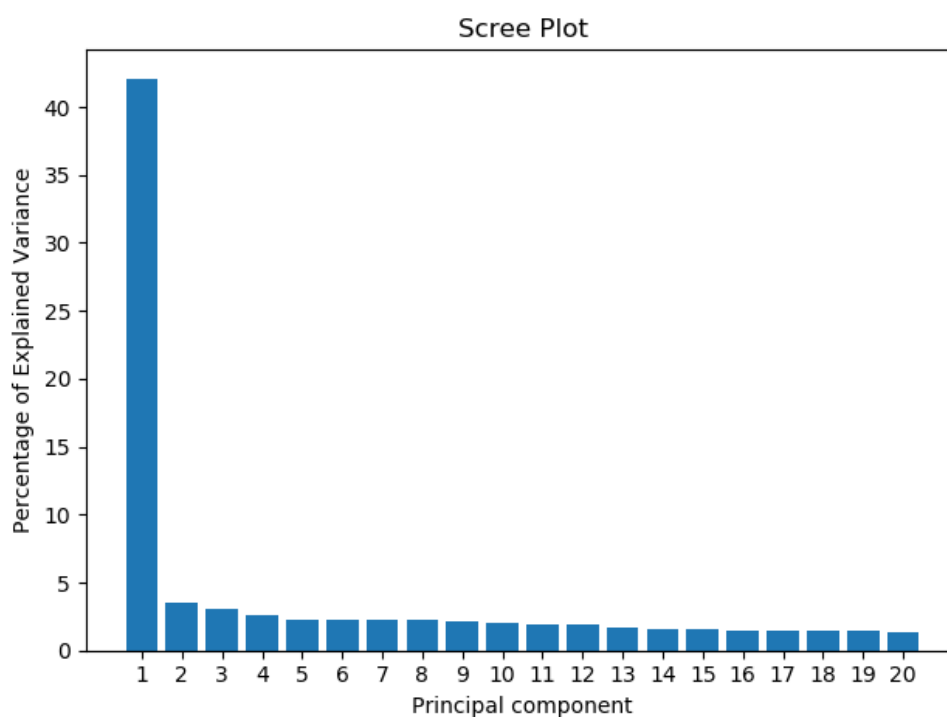


Figure 4-6. Scree plot showing the percentage of the explained variance by the first twenty PCs in the PCA involving Raman spectra from *M. chelonae* planktonic cultures OD₆₀₀=1 and OD₆₀₀=3.

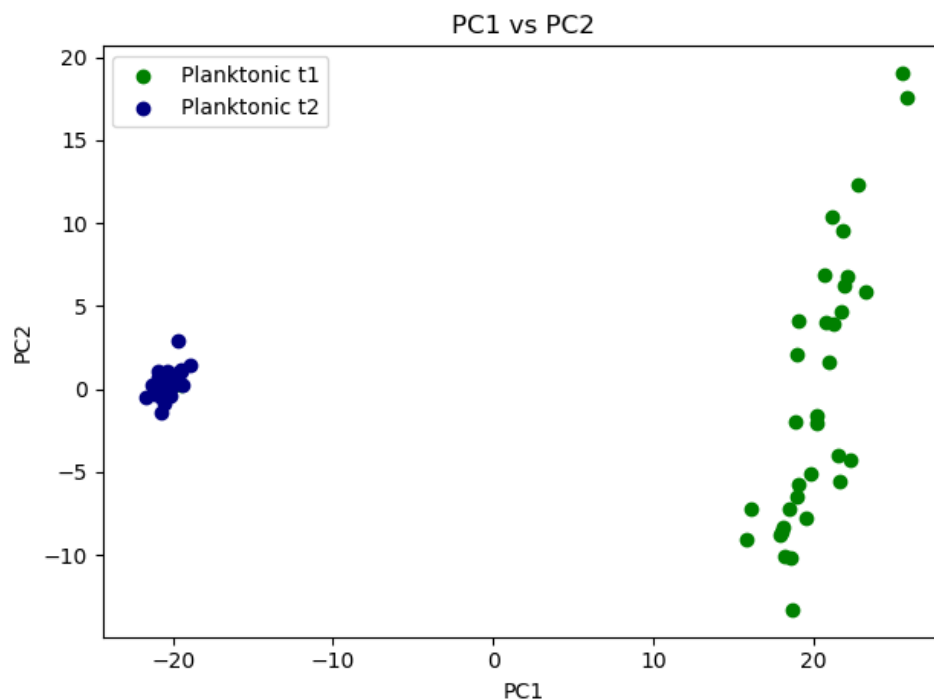


Figure 4-7. Visual representation of Raman spectra from *M. chelonae* planktonic cultures in terms of PC1 and PC2.

The scree plot (Figure 4-6) shows that using two principal components is sufficient for explaining most of the variability between the spectra from *M. chelonae* planktonic cultures. By plotting each analyzed sample in terms of the two principal components, we observe that samples cluster well, meaning that the PCA is able to discern between planktonic *M. chelonae* at and $OD_{600}=1$ (Planktonic t1) and $OD_{600}=3$ (Planktonic t2).

4.3.3.1 The intensities for carbohydrates and protein-associated signals are different between *M. chelonae* planktonic cultures.

To get a better understanding of the potential biomolecules causing the variations between planktonic *M. chelonae* $OD_{600}=1$ and $OD_{600}=3$, we identified the Raman shifts with high contribution to PC1 and PC2 (Table 4-3), associated them to biomolecules (

Figure 4-8), and compared their intensities between *M. chelonae* planktonic cultures (Table 4-4).

Table 4-3. Raman shifts with high contribution to PC1 and PC2 in the PCA of *M. chelonae* planktonic cultures.

Principal component	Top 20 Raman shifts with the highest contribution to the PC (cm ⁻¹)
<i>PC1</i>	1656.27344, 1657.27344, 1660.27148, 1355.95898, 1446.22363, 1448.30469, 1450.38379, 1655.27441, 1658.27344, 1456.61719, 1452.46289, 1353.84082, 1359.13477, 1451.42285, 1664.26758, 1346.41992, 1447.26465, 1334.73633, 1331.54492, 1354.90039.
<i>PC2</i>	1066.10938, 893.7832, 779.85449, 1127.42871, 1067.23047, 1057.12695, 1062.74219, 1608.06738, 778.66602, 931.95508, 1064.98731, 809.46777, 1130.75195, 1591.90137, 807.10547, 804.74121, 1438.93555, 1128.53613, 1437.89356, 918.1084.

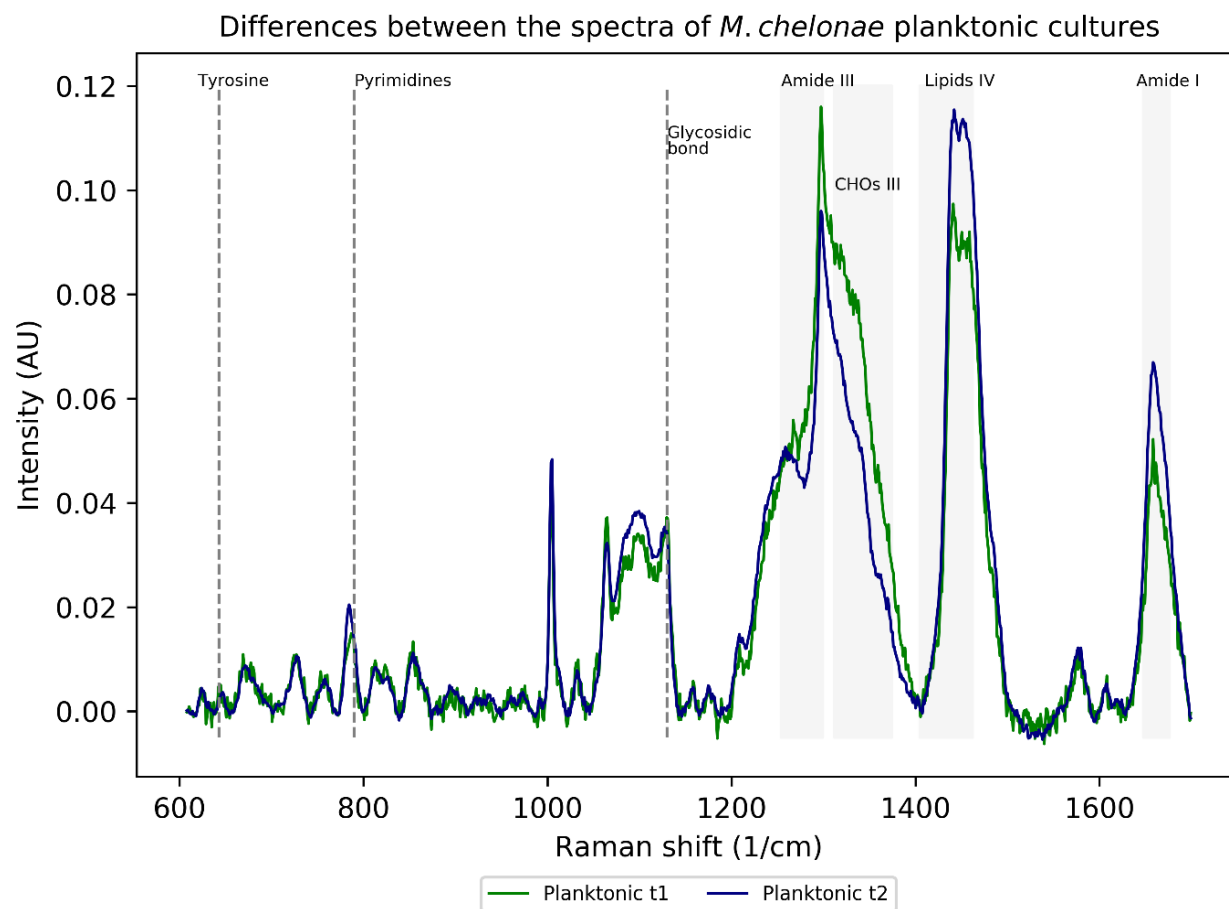
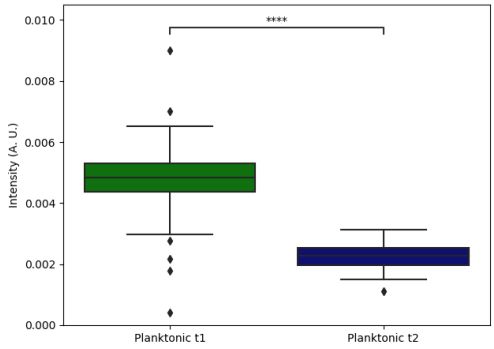
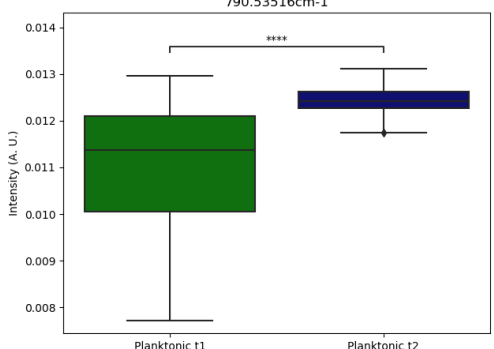
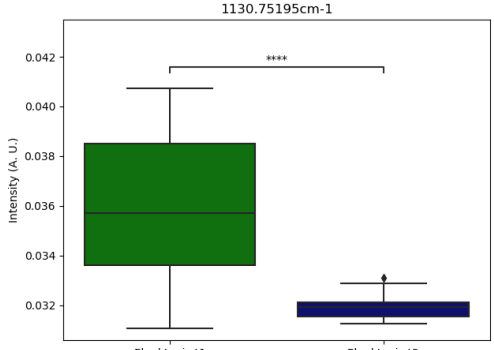
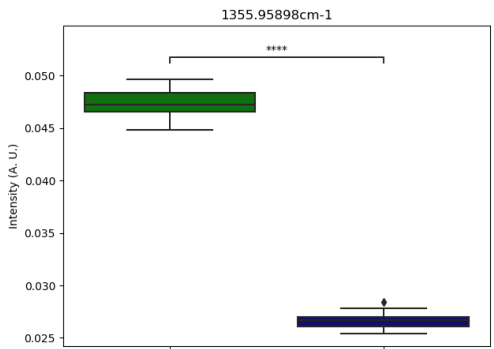


Figure 4-8 Annotated average Raman spectra obtained from *M. chelonae* pellicles and planktonic cultures.

The average Raman spectra from *M. chelonae* planktonic cultures OD600=1 (Planktonic t1) and OD600=3 (Planktonic t2) were plotted and annotated with Raman shifts with high contribution to the PCs. Each annotated region was associated with a biopolymer. Most of the variability between Raman spectra from *M. chelonae* pellicles and planktonic cultures is due to signals associated with proteins (Tyrosine, Amide region III, and Amide region I), and lipids (lipids region IV). There is also a contribution from signals associated with nucleic acids (pyrimidines) and carbohydrates (glycosidic linkage).

Table 4-4. Representative Raman shifts with a high contribution to the two PCs selected to describe *M. chelonae* planktonic cultures.

Raman shift	Assignment	Associated biomolecule	Principal component
 <p>642.52539cm⁻¹</p>	C-C twisting mode of tyrosine	Proteins	PC2
 <p>790.53516cm⁻¹</p>	Pyrimidines	Nucleic acids	PC2
 <p>1130.75195cm⁻¹</p>	Glycosidic linkage	Carbohydrates	PC2
 <p>1355.95898cm⁻¹</p>	Carbohydrates III	Carbohydrates	PC1

<p>1285.58398cm⁻¹</p> <p>Intensity (A.U.)</p> <p>Planktonic t1 Planktonic t2</p>	Amide III	Proteins	PC1
<p>1447.26465cm⁻¹</p> <p>Intensity (A.U.)</p> <p>Planktonic t1 Planktonic t2</p>	Lipids IV	Lipids	PC1
<p>1648.26953cm⁻¹</p> <p>Intensity (A.U.)</p> <p>Planktonic t1 Planktonic t2</p>	Amide I	Proteins	PC1

The intensity of the signals associated with carbohydrates decreases from *M. chelonae* planktonic cultures $OD_{600}=1$ to $OD_{600}=3$ (Table 4-4, 1130 and 1355cm⁻¹). And we observe a similar trend in some Raman shifts associated with proteins (Table 4-4, 1285 and 642cm⁻¹).

4.3.4 PCA discerns between *M. chelonae* planktonic bacteria at OD₆₀₀=1 and OD₆₀₀=3.

To finalize the analysis of *M. chelonae* Raman spectra, a PCA was applied to five and 10-day old *M. chelonae* pellicles. We noted that the first two PC accounted for 61% of the variance of the sample (Figure 4-9). When each sample was plotted in terms of PC1 and PC2 (Figure 4-10), we observed that the applied PCA is able to distinguish between *M. chelonae* pellicles, so we chose the first two PCs to describe the differences between Raman spectra from *M. chelonae* pellicles.

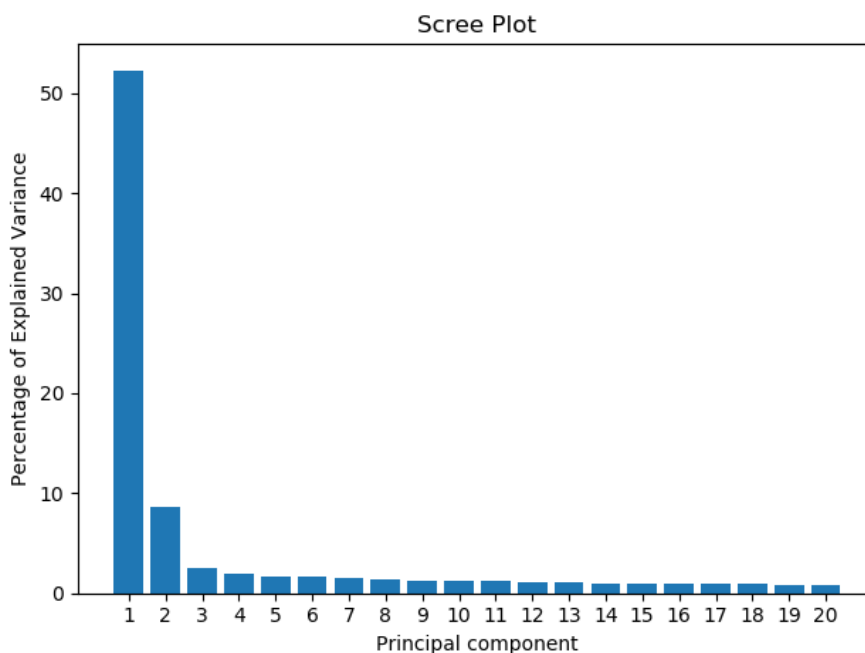


Figure 4-9. Scree plot showing the percentage of the explained variance by the first twenty PCs in the PCA involving Raman spectra from 5 and 10-day *M. chelonae* pellicles.

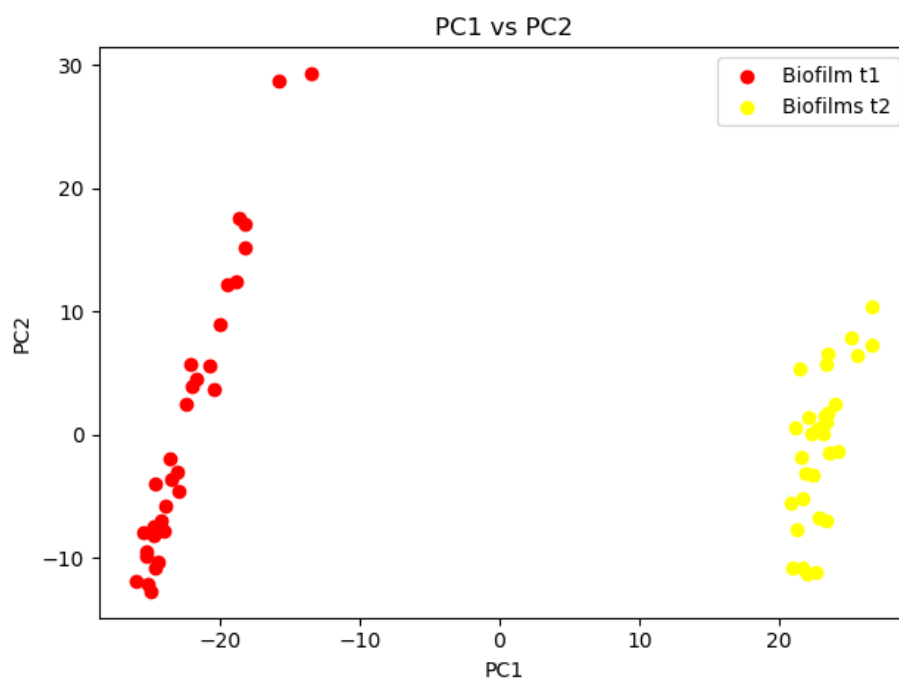


Figure 4-10 Visual representation of Raman spectra from *M. chelonae* pellicles in terms of PC1 and PC2.

The scree plot (Figure 4-9) shows that using two principal components is sufficient for explaining most of the variability between the spectra from *M. chelonae* pellicles, and by plotting each analyzed sample in terms of the two principal components, we observe that samples cluster well, meaning that the PCA is able to discern between 5 (Biofilm t1) and 10—day old (Biofilm t2) *M. chelonae* pellicles.

Principal component	Top 20 Raman shifts with the highest contribution to the PC (cm ⁻¹)
<i>PC1</i>	1004.02832, 1002.8916, 1005.16309, 1001.75586, 1436.85156, 1434.7666, 1437.89356, 1435.80957, 1438.93555, 1006.29883, 1439.97754, 1433.72363, 1000.61914, 1431.63769, 1432.68066, 1430.59375, 1647.26758, 1648.26953, 1646.26563, 0.043418945.
<i>PC2</i>	1284.50977, 1285.58398, 1447.26465, 1283.43555, 1445.18359, 1665.26563, 1449.34375, 1448.30469, 1101.87695, 1664.26758, 1666.26367, 1668.25977, 1100.76367, 1286.65723, 1282.36133, 1099.64941, 1288.80371, 1280.21191, 1455.5791, 1446.22363.

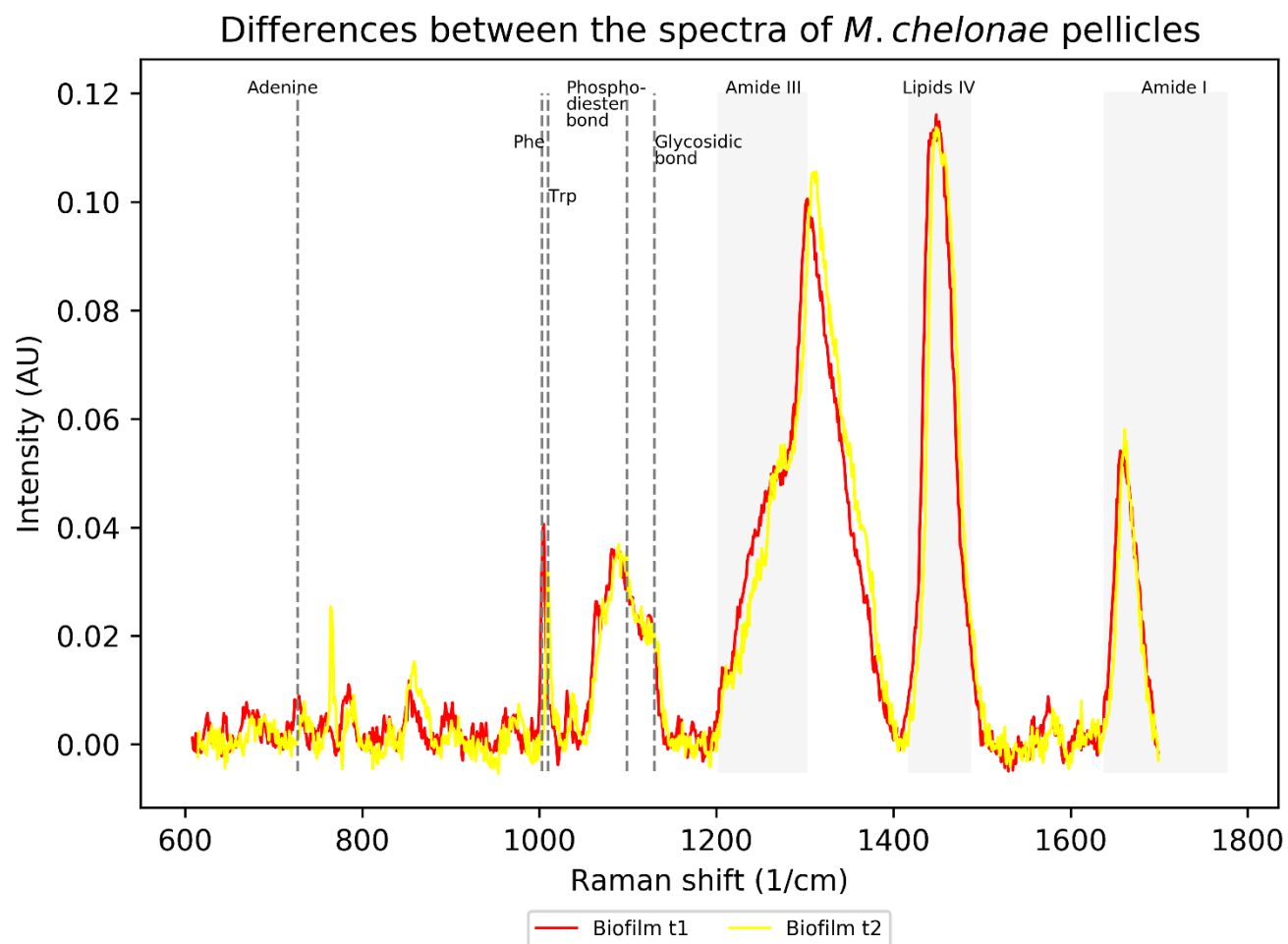
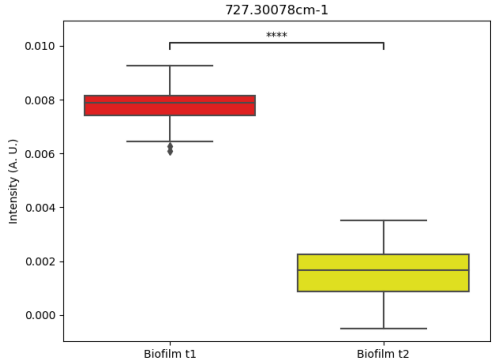
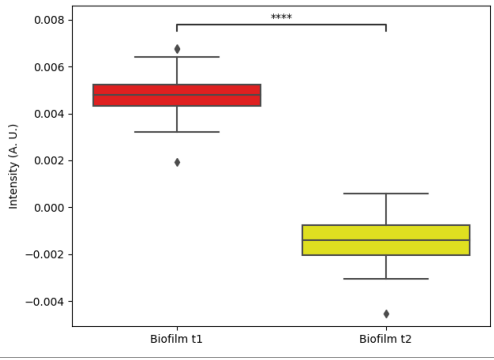
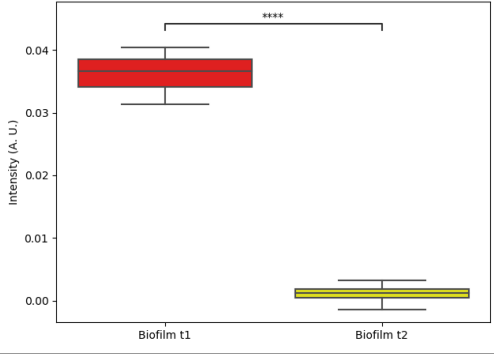
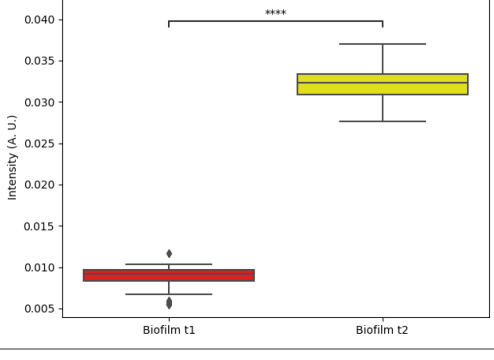
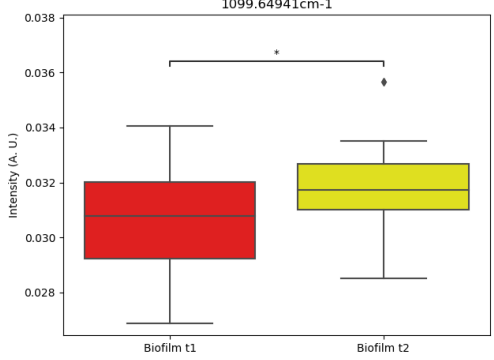
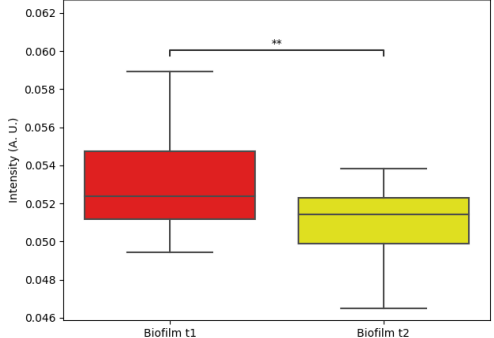
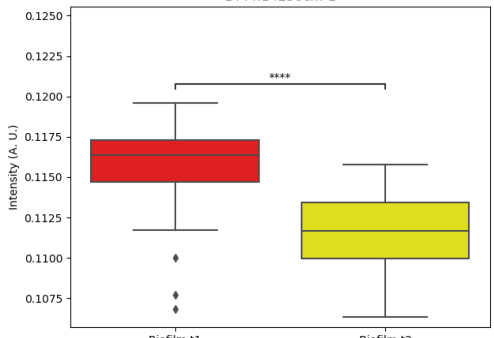
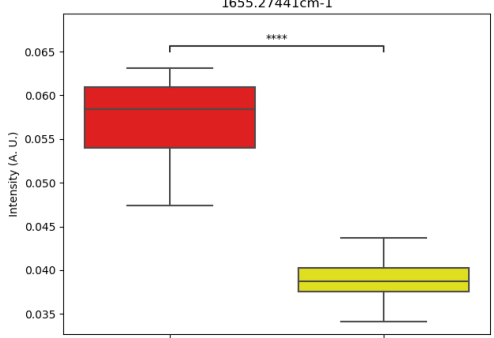


Figure 4-11. Annotated average Raman spectra obtained from *M. chelonae* pellicles.

The average Raman spectra from 5 (Biofilm t1) and 10-day (Biofilms t2) old *M. chelonae* pellicles were plotted and annotated with Raman shifts with high contribution to the PCs. Each annotated region was associated with a biopolymer. Most of the variability between Raman spectra from *M. chelonae* pellicles and planktonic cultures is due to signals associated to proteins (Phenylalanine, Tryptophan, Amide region III, and Amide region I), and lipids (lipids region IV). There is also contribution from signals associated with nucleic acids (phosphodiester bond from the DNA backbone, and adenine), and carbohydrates (glycosidic linkage).

Table 4-5 Representative Raman shifts with a high contribution to the three PCs selected to describe *M. chelonae* pellicles.

Raman shift	Assignment	Biomolecule	Principal component
	Ring breathing of adenine	Nucleic acids	PC1
	Phosphatidyl inositol	Lipids	PC1
	Phenylalanine	Proteins	PC1
	Tryptophan	Proteins	PC1

 <p>1099.64941cm-1</p> <p>Intensity (A. U.)</p> <p>Biofilm t1 Biofilm t2</p>	Symmetric stretchin PO ₄ in DNA	Nucleic acids	PC2
 <p>1285.58398cm-1</p> <p>Intensity (A. U.)</p> <p>Biofilm t1 Biofilm t2</p>	Amide region III	Proteins	PC1
 <p>1444.14258cm-1</p> <p>Intensity (A. U.)</p> <p>Biofilm t1 Biofilm t2</p>	Lipids region IV	Lipids	PC1
 <p>1655.27441cm-1</p> <p>Intensity (A. U.)</p> <p>Biofilm t1 Biofilm t2</p>	Amide region I	Proteins	PC1

4.4 Discussion

The Raman spectra generated from *M. chelonae* biofilms and its planktonic counterparts are different. Furthermore, the PCA analysis showed that samples can be distinguished from each other and that most of the variance of the data set could be explained by using two or three principal components.

Overall, Raman spectroscopy serves as an exploratory approach for detecting potential differences in the composition of bacterial biofilms and its planktonic counterparts, being able to detect changes in the relative abundance of biopolymers between biofilms and planktonic cultures, and also between different time points.

Chapter 5 A study of the *Mycobacterium chelonae* biofilm transcriptome

5.1 Introduction

The transcriptome is the complete set of transcribed RNAs on a cell population during a specific condition (Wang et al., 2009). One of the applications that derive from the study of transcriptomes is the identification of differentially expressed genes (DEG) aiming to understand which genes or pathways are associated with a defined condition (Ishii, 2014).

The study of bacterial biofilms has benefited hugely from the study of transcriptomes (Franklin et al., 2015), as it made possible the identification of key molecular components required for biofilm formation in several microorganisms, such as *Candida albicans* (Rajendran et al., 2016), *Escherichia coli* O157:H7 (Lee et al., 2011), or *Bacillus subtilis*, the model organism for studying gram-positive bacterial biofilms (Kobayashi, 2007; Pisithkul et al., 2019).

Apart from providing information on the metabolic pathways active during *in vitro* biofilm formation, transcriptomics allowed the identification of genes that are up-regulated *in vivo* in pathogenic *Pseudomonas aeruginosa* biofilms (Cornforth et al., 2018), assessing quickly and easily how the *in vitro* growth differs from biofilms in animal models or humans (Cornforth et al., 2018).

Unlike other bacteria, there are not yet many studies on the transcriptomes of mycobacterial biofilms. In *M. tuberculosis*, the transcriptome profile of thiol-induced biofilms shows an up-regulation in cysteine and iron metabolism. At the same time, genes related to cell wall biogenesis, replication, transcription, and translation are down regulated (Trivedi et al., 2016).

Transcriptomic analysis in *M. smegmatis* pellicles shows a time-dependent change on the transcription of genes related to iron uptake, being up-regulated prior biofilm maturation,

and down-regulated in fully-matured biofilms (Ojha and Hatfull, 2007; Yang et al., 2017). Also, genes related to the uptake of nitrogen are up-regulated in fully-mature biofilms (Yang et al., 2017). Interestingly, the expression of the genes related to nitrogen uptake is under control of Glnr, a transcription factor which activation during biofilms formation also translates into peroxide resistance (Yang et al., 2018).

The previous information shows that the development of mycobacterial biofilms follows defined stages that require the modulation of the transcriptome. Understanding the transcriptional network during biofilm formation for pathogenic NTM biofilms, such as the ones formed by *M. chelonae*, will provide information on the molecular requirements for the formation and maintenance of the structure.

5.2 Aim

The aim of this chapter is to characterize the transcriptional changes occurring during *M. chelonae* biofilms and identify genes that could contribute to the development of *M. chelonae* biofilms.

5.2.1 Specific objectives

- Describe the transcriptome of *M. chelonae* pellicles and planktonic cultures.
- Identify the enriched metabolic subsystems occurring during biofilm formation.

5.3 Results

5.3.1 The gene expression profiles of *Mycobacterium chelonae* biofilms are different from planktonic cultures.

We extracted RNA from five and ten-day old *M. chelonae* pellicles and *M. chelonae* planktonic cultures at an $OD_{600}=1$ and $OD_{600}=3$, and depleted the ribosomal RNA. Once the sample was purified, we synthesized a cDNA library for further sequencing. The cDNA library contains a complementary chain of the mRNA isolated (transcriptome) from the *M. chelonae* cultures. After sequencing, the obtained reads were analyzed by Dr. Eliza Peterson at the Institute for System Biology (Seattle, USA), for defining the differentially expressed genes (DEG) using the DESq2 algorithm (Love et al., 2014). The sample taken as a reference was *M. chelonae* planktonic t1 ($OD_{600}=1$), and the log2 fold-change for a given gene was calculated based on the reads obtained in the reference samples (Planktonic t1)

Overall, 1274 were differentially expressed in at least one condition. *M. chelonae* Planktonic t2 ($OD_{600}=3$) has 92 DEG, 5-day old *M. chelonae* pellicle (Biofilm t1) has 566, and 10-day old *M. chelonae* pellicle has 1137 DEG. For visualization of the expression patterns between samples, a heat map was generated using the Log2 of the fold changes (FC) of the DEG in at least one condition (Figure 5-1). The 50 DEG genes with the highest value on the absolute FC are shown Table 5-1 for *M. chelonae* $OD_{600}=3$, and Table 5-2 and Table 5-3 for five and ten-day old pellicles respectively.



Figure 5-1. Heat map depicting the Log2FC of the DEG in 5 (Biofilm t1) and 10-day (Biofilm t2) old *M. chelonae* pellicles, and *M. chelonae* Planktonic culture OD=3 (Planktonic t2).

Table 5-1 Top 50 differentially expressed genes with the highest absolute fold change from *M. chelonae* planktonic cultures OD₆₀₀=3.

Gene name	Product	Log2 Fold change	p-value
Top 25 DEG			
BB28_RS05065	pyridoxamine 5'-phosphate oxidase family protein	5.036193	0.001119
BB28_RS19640	type 1 glutamine amidotransferase	4.071299	0.000557
BB28_RS05070	cytochrome c oxidase subunit I	2.787458	2.23E-05
BB28_RS07075	23S ribosomal RNA	2.636275	0.004764
BB28_RS07070	16S ribosomal RNA	2.563874	0.006823
BB28_RS24410	hypothetical protein	1.870165	0.000593
BB28_RS01700	ammonium transporter	1.592994	0.004892
BB28_RS01605	2-isopropylmalate synthase	1.587311	0.00488
BB28_RS03135	copper chaperone	1.528366	0.004328
BB28_RS18895	cutinase family protein	1.51776	0.006762
BB28_RS07400	DUF3618 domain-containing protein	1.489112	0.000333
BB28_RS15725	23S rRNA (adenine(2503)-C(2))-methyltransferase RlmN	1.372465	8.84E-05
BB28_RS20590	resuscitation-promoting factor RpfA	1.316039	0.001582
BB28_RS13050	quinolinate synthase NadA	1.295696	0.002987

BB28_RS17700	hydroxylase	1.292062	0.000108
BB28_RS17085	DUF2275 domain-containing protein	1.24188	0.007914
BB28_RS01090	histidinol-phosphate transaminase	1.240005	0.004088
BB28_RS22740	TIGR04338 family metallohydrolase	1.230089	0.005493
BB28_RS11240	MarR family transcriptional regulator	1.220136	0.003168
BB28_RS09300	M4 family peptidase	1.207552	0.005956
BB28_RS12530	heat-shock protein Hsp20	1.172827	0.006791
BB28_RS15655	malate dehydrogenase (quinone)	1.169495	0.003624
BB28_RS03580	TetR/AcrR family transcriptional regulator	1.159861	0.000405
BB28_RS04055	DUF2537 domain-containing protein	1.151279	0.001438
BB28_RS06210	class I SAM-dependent methyltransferase	1.146762	0.009768
Bottom 25 DEG			
BB28_RS12345	hypothetical protein	-2.14966	0.000134
BB28_RS01290	hypothetical protein	-1.97396	0.002947
BB28_RS21160	hypothetical protein	-1.64299	0.002528
BB28_RS01155	hypothetical protein	-1.59252	0.007685
BB28_RS08540	hypothetical protein	-1.573	0.006691
BB28_RS19505	ECF subfamily RNA polymerase sigma-24 subunit	-1.53578	0.000157
BB28_RS18955	hypothetical protein	-1.49932	0.007281
BB28_RS18540	tautomerase family protein	-1.48569	0.00149
BB28_RS04035	DUF2530 domain-containing protein	-1.36114	0.005286
BB28_RS14770	dUTP diphosphatase	-1.35084	0.007965
BB28_RS04930	hypothetical protein	-1.25801	0.000772
BB28_RS10780	precorrin-4 C(11)-methyltransferase	-1.24844	0.006817
BB28_RS20535	hypothetical protein	-1.23867	0.001707
BB28_RS22455	glycosyltransferase family 1 protein	-1.22506	0.001108
BB28_RS05625	hypothetical protein	-1.21917	0.002603
BB28_RS15035	hypothetical protein	-1.18803	0.009193
BB28_RS13085	malate:quinone oxidoreductase	-1.18395	0.00015
BB28_RS19125	alpha/beta hydrolase	-1.18219	0.000574
BB28_RS17160	cytochrome P450	-1.18149	0.008268
BB28_RS24395	hypothetical protein	-1.16963	0.005786
BB28_RS24740	hypothetical protein	-1.16767	0.006124
BB28_RS12790	dTDP-4-keto-6-deoxy-D-glucose epimerase	-1.14886	0.006001
BB28_RS24370	hypothetical protein	-1.14727	0.000712
BB28_RS18120	acyl-CoA dehydrogenase	-1.13683	0.000475
BB28_RS13345	hypothetical protein	-1.12173	0.00099

Table 5-2 Top 50 differentially expressed genes with the highest absolute fold change from 5-day old *M. chelonae* pellicles.

Gene name	Product	Log2 Fold change	p-value
Top 25 DEG			
BB28_RS24410	hypothetical protein	8.063117	3.2E-17
BB28_RS24780	hypothetical protein	6.762328	8.3E-13

BB28_RS14405	XshC-Cox1 family protein	6.709886	2.65E-09
BB28_RS19640	type 1 glutamine amidotransferase	6.653272	9.38E-22
BB28_RS03140	class I SAM-dependent methyltransferase	6.134321	5.37E-23
BB28_RS05065	pyridoxamine 5'-phosphate oxidase family protein	5.554323	2.19E-18
BB28_RS05000	divalent metal cation transporter MntH	5.231883	5.1E-20
BB28_RS19975	1,4-dihydroxy-2-naphthoate polyprenyltransferase	5.182603	2.39E-17
BB28_RS02635	hypothetical protein	4.915092	1.03E-16
BB28_RS23240	hypothetical protein	4.755926	1.94E-09
BB28_RS05070	cytochrome c oxidase subunit I	4.745509	1.72E-18
BB28_RS18265	Lrp/AsnC family transcriptional regulator	4.644677	4.4E-16
BB28_RS03120	PE family protein	4.638839	1.3E-08
BB28_RS12215	hypothetical protein	4.391448	1.04E-13
BB28_RS18255	NADPH-dependent oxidoreductase	4.343847	3.25E-19
BB28_RS15580	HNH endonuclease	4.096421	5.04E-06
BB28_RS14545	hypothetical protein	4.028601	8.55E-06
BB28_RS03145	PPE family protein	3.982017	8.91E-13
BB28_RS02630	hypothetical protein	3.949084	1.45E-15
BB28_RS14470	molybdopterin-guanine dinucleotide biosynthesis protein MobA	3.886748	7.59E-05
BB28_RS21800	LuxR family transcriptional regulator	3.874218	2.39E-08
BB28_RS03095	TauD/TfdA family dioxygenase	3.854598	7.71E-14
BB28_RS05190	hypothetical protein	3.835867	4.22E-15
BB28_RS02680	metal ABC transporter permease	3.775164	1.99E-10
BB28_RS15365	bleomycin resistance family protein	3.732409	3.5E-11
Bottom 25 DEG			
BB28_RS13040	nicotinate-nucleotide diphosphorylase (carboxylating)	-4.8564	1.84E-16
BB28_RS08635	competence protein	-2.74031	4.13E-11
BB28_RS00165	cell division protein CrgA	-2.71257	1.95E-05
BB28_RS06700	nuclear transport factor 2 family protein	-2.43886	4.6E-05
BB28_RS16680	Lrp/AsnC family transcriptional regulator	-2.35382	0.003525
BB28_RS07345	sensor domain-containing protein	-2.22298	2.98E-08
BB28_RS15035	hypothetical protein	-2.07191	0.000529
BB28_RS18120	acyl-CoA dehydrogenase	-2.06732	3.99E-06
BB28_RS11055	MbtH family protein	-2.03382	0.003463
BB28_RS04665	TetR/AcrR family transcriptional regulator	-2.02977	0.000437
BB28_RS13025	ABC transporter ATP-binding protein	-1.99038	0.000115
BB28_RS11035	peroxiredoxin	-1.96506	0.001948
BB28_RS05570	deferrochelataase/peroxidase EfeB	-1.925	1.94E-05
BB28_RS15555	hypothetical protein	-1.90972	1.32E-05
BB28_RS07270	enoyl-CoA hydratase	-1.83859	1.76E-06
BB28_RS05500	hypothetical protein	-1.81247	6.17E-08
BB28_RS24490	cupin	-1.78874	2.06E-05
BB28_RS15295	YceI family protein	-1.78669	0.000353
BB28_RS14200	DJ-1/PfpI family protein	-1.77805	2.87E-06
BB28_RS09780	polyketide cyclase	-1.77588	0.000645
BB28_RS00910	hypothetical protein	-1.77378	0.002223

BB28_RS03055	TetR/AcrR family transcriptional regulator	-1.76973	0.003673
BB28_RS13085	malate:quinone oxidoreductase	-1.74296	2.01E-07
BB28_RS14015	haloacid dehalogenase type II	-1.73793	5.94E-05
BB28_RS11925	GlsB/YeaQ/YmgE family stress response membrane protein	-1.71861	2.07E-05

Table 5-3. Top 50 differentially expressed genes with the highest absolute fold change from 10-day old *M. chelonae* pellicles.

Gene name	Product	Log2 Fold change	p-value
Top 25 DEG			
BB28_RS24410	hypothetical protein	8.603997	5.57E-27
BB28_RS24780	hypothetical protein	7.271395	5.96E-22
BB28_RS19640	type 1 glutamine amidotransferase	7.00953	4.23E-40
BB28_RS14405	XshC-Cox1 family protein	6.706251	3.53E-20
BB28_RS05065	pyridoxamine 5'-phosphate oxidase family protein	6.606976	9.21E-28
BB28_RS18265	Lrp/AsnC family transcriptional regulator	6.222184	5.91E-39
BB28_RS03140	class I SAM-dependent methyltransferase	6.180836	4.92E-33
BB28_RS19975	1,4-dihydroxy-2-naphthoate polyprenyltransferase	6.062166	5.45E-17
BB28_RS09130	hypothetical protein	5.626574	2.48E-16
BB28_RS18280	short-chain dehydrogenase	5.423429	9.63E-35
BB28_RS14470	molybdopterin-guanine dinucleotide biosynthesis protein MobA	5.237611	1.35E-12
BB28_RS01840	glycerol kinase	5.033261	5.57E-25
BB28_RS11130	amino acid permease	5.018604	5.02E-26
BB28_RS18255	NADPH-dependent oxidoreductase	4.999078	5.25E-27
BB28_RS23625	phosphoenolpyruvate carboxylase	4.968198	4.33E-21
BB28_RS05070	cytochrome c oxidase subunit I	4.949974	1.43E-33
rrf	5S ribosomal RNA	4.906745	0.00014
BB28_RS01830	short-chain dehydrogenase	4.901315	6.34E-18
BB28_RS12870	DUF4190 domain-containing protein	4.820052	1.13E-18
BB28_RS20565	hypothetical protein	4.818612	4.57E-19
BB28_RS19940	DUF3349 domain-containing protein	4.699323	1.59E-08
BB28_RS09340	alcohol dehydrogenase	4.67926	7.7E-29
BB28_RS01820	lipid-transfer protein	4.632437	3.12E-16
BB28_RS19665	hypothetical protein	4.607207	7.73E-07
BB28_RS11125	ATP-dependent DNA helicase RecQ	4.590025	8.4E-29
Bottom 25 DEG			
BB28_RS13040	nicotinate-nucleotide diphosphorylase (carboxylating)	-6.12272	5.9E-38
BB28_RS07375	holo-ACP synthase	-3.36334	1.65E-07
BB28_RS20715	glycosyltransferase	-3.05592	1.67E-23
BB28_RS04550	hypothetical protein	-2.80231	0.000798
BB28_RS07550	hypothetical protein	-2.77308	0.003348
BB28_RS20780	membrane protein	-2.72794	0.000125
BB28_RS07835	DNA polymerase III subunit beta	-2.72708	1.38E-16
BB28_RS09250	XRE family transcriptional regulator	-2.67993	8.31E-16

BB28_RS16680	Lrp/AsnC family transcriptional regulator	-2.66573	0.001674
BB28_RS23445	methyltransferase domain-containing protein	-2.62497	0.001919
BB28_RS00145	SAM-dependent methyltransferase	-2.57556	1.08E-18
BB28_RS02080	hypothetical protein	-2.55072	6.64E-20
BB28_RS02330	wax ester/triacylglycerol synthase family O-acyltransferase	-2.53378	1.38E-14
BB28_RS10840	NAD(P)-dependent oxidoreductase	-2.47466	1.78E-14
BB28_RS09020	1-aminocyclopropane-1-carboxylate deaminase	-2.47365	4.05E-18
BB28_RS01525	hypothetical protein	-2.46563	1.33E-12
BB28_RS21165	hypothetical protein	-2.45175	4.6E-08
BB28_RS18120	acyl-CoA dehydrogenase	-2.42846	2.49E-14
BB28_RS24800	acyltransferase	-2.41719	1.41E-08
BB28_RS21500	hypothetical protein	-2.40781	4.83E-11
BB28_RS07270	enoyl-CoA hydratase	-2.37866	1.81E-09
BB28_RS19165	50S ribosomal protein L23	-2.3435	6.38E-08
BB28_RS08635	competence protein	-2.29122	5.51E-10
BB28_RS22655	CoA-binding protein	-2.27424	4.51E-07
BB28_RS02035	EamA/RhaT family transporter	-2.27408	2.28E-12

In general, the patterns of DEG on Biofilm t1 and t2 are similar, but perhaps with steeper values on the FC on DEG from Biofilm t2 (Figure 5-1). In order to ease the visualization of the DEG associated with each condition, a Venn diagram was generated (Figure 5-2), and the genes belonging to each of the generated subgroups are summarized in Appendices 4-10. Forty-one genes are differentially expressed in all conditions (Appendix 4), and only eight are differentially expressed in 5-day old *M. chelonae* pellicles and Planktonic cultures OD₆₀₀=3, and fourteen DEG are common to 10-day old *M. chelonae* pellicles and the Planktonic cultures OD₆₀₀=3. There are 416 DEGs common to five and ten-day old *M. chelonae* pellicles (Appendix 7), suggesting a core of genes differentially regulated during biofilm formation. There are also genes that are differentially expressed exclusive to each of the conditions, suggesting that each growth condition could be characterized by specific metabolic signatures (Appendices 8-10).

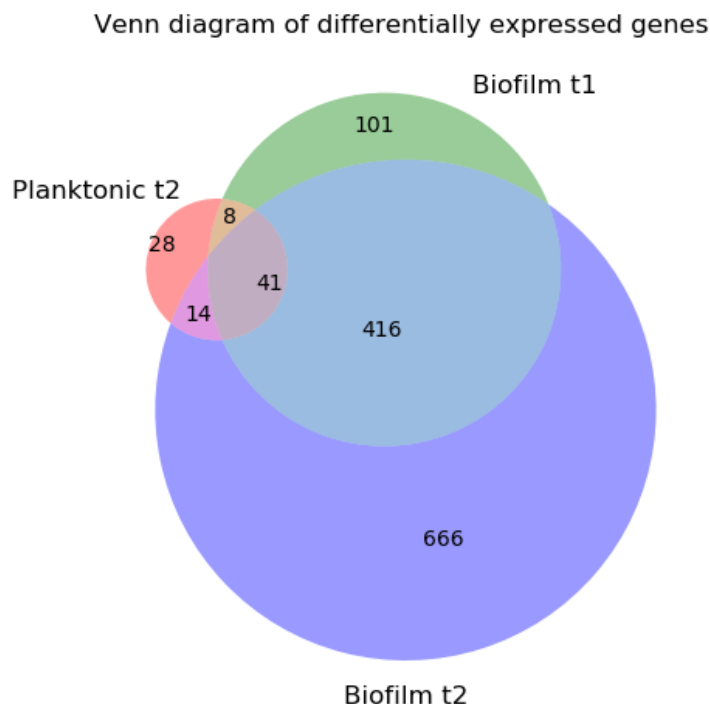


Figure 5-2. Venn diagram of the DEG in 5 and 10-day old *M. chelonae* pellicles and planktonic cultures OD=3.

The Venn diagram of the differentially expressed genes in 5 (Biofilmt1) and 10-day old (Biofilm t2) *M. chelonae* pellicles and planktonic cultures OD₆₀₀=3 (Planktonic t2) allows the visualization of the common differentially expressed genes between conditions.

5.3.2 The enriched metabolic pathways in *M. chelonae* biofilms are different.

There are 4726 predicted coding sequences in *M. chelonae* genome (Jaén-Luchoro et al., 2016); therefore, the DEG during Biofilm t2 represents around 24% of the whole genome, and such amount of data complicates the biological interpretation of the transcriptome profiles. A way to overcome this problem is by doing pathway enrichment analysis, which allows the identification of metabolic pathways that enriched in a list of genes (Hänzelman et al., 2013; Reimand et al., 2019). The pathway enrichment analysis of our transcriptomic data set was carried out by Dr. Eliza Peterson. First, the closest ortholog

in *M. tuberculosis* of the list of DEG from *M. chelonae* pellicles were mapped into the *M. tuberculosis* genome scale model iEK1011 (Kavvas et al., 2018), and then identified the metabolic pathways that were enriched. The metabolic pathways that are enriched (hypergeometric test, $p\text{-value} < 0.01$, Log_2 fold change ≥ 1 or $1 \leq$) in 5 and 10-day old *M. chelonae* pellicles are shown in Table 5-4 and Table 5-5, respectively.

Table 5-4. Enriched metabolic pathways in 5-day old *M. chelonae* pellicles.

Subsystem	Fold change	Number of genes	p-value	Genes	Closest TB ortholog	Gene name
L_AAA biosynthesis	2	1	0	BB28_RS18260	lat	Rv3290c
Oxidative phosphorylation	1	16	4.07E-07	BB28_RS05070	Rv3043c	ctaD
				BB28_RS07010	Rv1304	atpB
				BB28_RS07015	Rv1305	atpE
				BB28_RS07020	Rv1306	atpF
				BB28_RS10465	Rv3146	nuoB
				BB28_RS10470	Rv3147	nuoC
				BB28_RS10475	Rv3148	nuoD
				BB28_RS10485	Rv3150	nuoF
				BB28_RS10490	Rv3151	nuoG
				BB28_RS10495	Rv3152	nuoH
				BB28_RS10500	Rv3153	nuoI
				BB28_RS10505	Rv3154	nuoJ
				BB28_RS10515	Rv3156	nuoL
				BB28_RS11885	Rv1854c	ndh
				BB28_RS12095	Rv2196	qcrB
				BB28_RS13975	Rv1305	atpE
Redox metabolism	1	8	0.002	BB28_RS07405	Rv3045	adhC
				BB28_RS12110	Rv1908c	katG
				BB28_RS12850	Rv1623c	cydA
				BB28_RS12855	Rv1622c	cydB
				BB28_RS12860	Rv1621c	cydD
				BB28_RS12865	Rv1620c	cydC
				BB28_RS14155	Rv2605c	tesB2
				BB28_RS17655	Rv0253	nirD
Glyoxylate metabolism	1	1	0.002	BB28_RS15360	Rv2780	ald
Lipid metabolism	2	2	0.002	BB28_RS24120	Rv2495c	bkdC
				BB28_RS24125	Rv2496c	bkdB
Mycolic acid biosynthesis	2	3	0.0008	BB28_RS03100	Rv0098	fcoT
				BB28_RS06770	Rv2246	kasA
				BB28_RS06780	Rv2245	kasB
Arabinogalactan biosynthesis	-1	8	0.0005	BB28_RS00845	Rv3809c	glf
				BB28_RS00865	Rv3805c	aftB
				BB28_RS00955	Rv3793	embC
				BB28_RS00960	Rv3792	aftA
				BB28_RS01015	Rv3782	glfT1

				<i>BB28_RS10090</i>	<i>Rv2174</i>	<i>mptA</i>
				<i>BB28_RS16230</i>	<i>Rv2981c</i>	<i>ddlA</i>
				<i>BB28_RS18830</i>	<i>Rv3441c</i>	<i>mrsA</i>
Arginine-Proline metabolism	1	4	0.0016	<i>BB28_RS11450</i>	<i>Rv1653</i>	<i>argJ</i>
				<i>BB28_RS11455</i>	<i>Rv1654</i>	<i>argB</i>
				<i>BB28_RS11460</i>	<i>Rv1655</i>	<i>argD</i>
				<i>BB28_RS11465</i>	<i>Rv1656</i>	<i>argF</i>
Mycobactin biosynthesis	1	7	8.99E-06	<i>BB28_RS10375</i>	<i>Rv2382c</i>	<i>mbtC</i>
				<i>BB28_RS10385</i>	<i>Rv2380c</i>	<i>mbtE</i>
				<i>BB28_RS10390</i>	<i>Rv2379c</i>	<i>mbtF</i>
				<i>BB28_RS10395</i>	<i>Rv2383c</i>	<i>mbtB</i>
				<i>BB28_RS11030</i>	<i>Rv2386c</i>	<i>mbtI</i>
				<i>BB28_RS11045</i>	<i>Rv2380c</i>	<i>mbtE</i>
Mycolic acid biosynthesis	1	4	0.0016	<i>BB28_RS11050</i>	<i>Rv2378c</i>	<i>mbtG</i>
				<i>BB28_RS00895</i>	<i>Rv3801c</i>	<i>fadD32</i>
				<i>BB28_RS00900</i>	<i>Rv3800c</i>	<i>pks13</i>
				<i>BB28_RS09435</i>	<i>Rv2245</i>	<i>kasA</i>
Nucleotide salvage pathway	1	2	0.005	<i>BB28_RS13295</i>	<i>Rv1483</i>	<i>fabG1/mabA</i>
				<i>BB28_RS02415</i>	<i>Rv3624c</i>	<i>hpt</i>
Peptidoglycan metabolism	1	4	0.0016	<i>BB28_RS20200</i>	<i>Rv0501</i>	<i>galE2</i>
				<i>BB28_RS10140</i>	<i>Rv2158c</i>	<i>murE</i>
				<i>BB28_RS10145</i>	<i>Rv2157c</i>	<i>murF</i>
				<i>BB28_RS10155</i>	<i>Rv2155c</i>	<i>murD</i>
Transport	1	33	2.49E-11	<i>BB28_RS10165</i>	<i>Rv2153c</i>	<i>murG</i>
				<i>BB28_RS01235</i>	<i>Rv3759c</i>	<i>proX</i>
				<i>BB28_RS01240</i>	<i>Rv3758c</i>	<i>proV</i>
				<i>BB28_RS01245</i>	<i>Rv3757c</i>	<i>proW</i>
				<i>BB28_RS01250</i>	<i>Rv3756c</i>	<i>proZ</i>
				<i>BB28_RS03405</i>	<i>Rv1282c</i>	<i>oppC</i>
				<i>BB28_RS04470</i>	<i>Rv3496c</i>	<i>mce4D</i>
				<i>BB28_RS04490</i>	<i>Rv1965</i>	<i>yrbE4B</i>
				<i>BB28_RS04495</i>	<i>Rv3501c</i>	<i>yrbE1A</i>
				<i>BB28_RS06575</i>	<i>Rv1235</i>	<i>lpqY</i>
				<i>BB28_RS06580</i>	<i>Rv1236</i>	<i>sugA</i>
				<i>BB28_RS06585</i>	<i>Rv1237</i>	<i>sugB</i>
				<i>BB28_RS06590</i>	<i>Rv1238</i>	<i>sugC</i>
				<i>BB28_RS08770</i>	<i>Rv2399c</i>	<i>cysT</i>
				<i>BB28_RS08775</i>	<i>Rv2398c</i>	<i>cysW</i>
				<i>BB28_RS11060</i>	<i>Rv1349</i>	<i>irtB</i>
				<i>BB28_RS11065</i>	<i>Rv1348</i>	<i>irtA</i>
				<i>BB28_RS13025</i>	<i>Rv3758c</i>	<i>proV</i>
				<i>BB28_RS16340</i>	<i>Rv1200</i>	<i>Rv1200</i>
				<i>BB28_RS16665</i>	<i>Rv1348</i>	<i>irtA</i>
				<i>BB28_RS16670</i>	<i>Rv1349</i>	<i>irtB</i>
				<i>BB28_RS20335</i>	<i>Rv3501c</i>	<i>yrbE4A</i>
				<i>BB28_RS20340</i>	<i>Rv1965</i>	<i>yrbE4B</i>
				<i>BB28_RS20920</i>	<i>Rv3494c</i>	<i>mce4F</i>
				<i>BB28_RS20925</i>	<i>Rv3495c</i>	<i>lprN</i>
				<i>BB28_RS20930</i>	<i>Rv3496c</i>	<i>mce4D</i>
				<i>BB28_RS20935</i>	<i>Rv3497c</i>	<i>mce4C</i>
				<i>BB28_RS20940</i>	<i>Rv3498c</i>	<i>mce4B</i>
				<i>BB28_RS20945</i>	<i>Rv3499c</i>	<i>mce4A</i>
				<i>BB28_RS20950</i>	<i>Rv3500c</i>	<i>yrbE4B</i>
				<i>BB28_RS20955</i>	<i>Rv3501c</i>	<i>yrbE4A</i>
				<i>BB28_RS22480</i>	<i>Rv1200</i>	<i>Rv1200</i>

				BB28_RS22830	Rv3496c	mce4D
				BB28_RS23005	Rv1965	yrbE3B

Table 5-5. Enriched metabolic pathways in 10-day old *M. chelonae* pellicles.

Subsystem	Fold change	p-value	Genes	Closest TB ortholog	Gene name
β-oxidation of unsaturated fatty acids	1	0.001	BB28_RS02715	Rv3573c	fadE34
			BB28_RS03610	Rv1715	fadB3
			BB28_RS03880	Rv0859	fadA
			BB28_RS04445	Rv0243	fadA2
			BB28_RS05195	Rv0971c	echA7
			BB28_RS05215	Rv0975c	fadE13
			BB28_RS09385	Rv2724c	fadE20
			BB28_RS11710	Rv2789c	fadE21
			BB28_RS12250	Rv1934c	fadE17
			BB28_RS14975	Rv2724c	fadE20
			BB28_RS15455	Rv3573c	fadE34
			BB28_RS15460	Rv1933c	fadE18
			BB28_RS15465	Rv2831	echA16
			BB28_RS17275	Rv3556c	fadA6
			BB28_RS19370	Rv0672	fadE8
			BB28_RS20660	Rv0468	fadB2
			BB28_RS20970	Rv3504	fadE26
			BB28_RS20975	Rv3505	fadE27
			BB28_RS21000	Rv3516	echA19
			BB28_RS21905	Rv0271c	fadE6
			BB28_RS22260	Rv0244c	fadE5
			BB28_RS22855	Rv1142c	echA10
Cholesterol degradation	1	1.47E-05	BB28_RS02715	Rv3573c	fadE34
			BB28_RS02740	Rv3570c	hsaA
			BB28_RS02745	Rv3568c	hsaC
			BB28_RS02885	Rv3546	fadA5
			BB28_RS02890	Rv3545c	cyp125
			BB28_RS02930	Rv3538	Rv3538
			BB28_RS02935	Rv3537	kstD
			BB28_RS02945	Rv3536c	hsaE
			BB28_RS02950	Rv3535c	hsaG
			BB28_RS02955	Rv3534c	hsaF
			BB28_RS05945	Rv3409c	choD
			BB28_RS15455	Rv3573c	fadE34
			BB28_RS18630	Rv3409c	choD
			BB28_RS19125	Rv3569c	hsaD
			BB28_RS19770	Rv3571	kshB
			BB28_RS20970	Rv3504	fadE26
			BB28_RS20975	Rv3505	fadE27
			BB28_RS20995	Rv3515c	fadD19
			BB28_RS21020	Rv3522	ltp4
			BB28_RS21025	Rv3523	ltp3
			BB28_RS21050	Rv3526	kshA
L_AAA biosynthesis	2	0	BB28_RS18260	lat	Rv3290c
Oxidative phosphorylation	1	3.83E-06	BB28_RS05070	Rv3043c	ctaD
			BB28_RS07015	Rv1305	atpE
			BB28_RS10465	Rv3146	nuoB
			BB28_RS10470	Rv3147	nuoC

			<i>BB28_RS10475</i>	<i>Rv3148</i>	<i>nuoD</i>
			<i>BB28_RS10480</i>	<i>Rv3149</i>	<i>nuoE</i>
			<i>BB28_RS10485</i>	<i>Rv3150</i>	<i>nuoF</i>
			<i>BB28_RS10490</i>	<i>Rv3151</i>	<i>nuoG</i>
			<i>BB28_RS10495</i>	<i>Rv3152</i>	<i>nuoH</i>
			<i>BB28_RS10500</i>	<i>Rv3153</i>	<i>nuoI</i>
			<i>BB28_RS10505</i>	<i>Rv3154</i>	<i>nuoJ</i>
			<i>BB28_RS10510</i>	<i>Rv3155</i>	<i>nuoL</i>
			<i>BB28_RS10515</i>	<i>Rv3156</i>	<i>nuoL</i>
			<i>BB28_RS10520</i>	<i>Rv3157</i>	<i>nuoM</i>
			<i>BB28_RS10525</i>	<i>Rv3158</i>	<i>nuoN</i>
			<i>BB28_RS11885</i>	<i>Rv1854c</i>	<i>ndh</i>
			<i>BB28_RS12095</i>	<i>Rv2196</i>	<i>qcrB</i>
			<i>BB28_RS13975</i>	<i>Rv1305</i>	<i>atpE</i>
Arabinogalactan biosynthesis	-1	2.62E-09	<i>BB28_RS00845</i>	<i>Rv3809c</i>	<i>glf</i>
			<i>BB28_RS00850</i>	<i>Rv3808c</i>	<i>glfT2</i>
			<i>BB28_RS00855</i>	<i>Rv3807c</i>	<i>Rv3807c</i>
			<i>BB28_RS00860</i>	<i>Rv3806c</i>	<i>ubiA</i>
			<i>BB28_RS00865</i>	<i>Rv3805c</i>	<i>aftB</i>
			<i>BB28_RS00940</i>	<i>Rv3795</i>	<i>embB</i>
			<i>BB28_RS00955</i>	<i>Rv3793</i>	<i>embC</i>
			<i>BB28_RS00960</i>	<i>Rv3792</i>	<i>aftA</i>
			<i>BB28_RS00965</i>	<i>Rv3791</i>	<i>dprE2</i>
			<i>BB28_RS00970</i>	<i>Rv3790</i>	<i>dprE1</i>
			<i>BB28_RS01015</i>	<i>Rv3782</i>	<i>glfT1</i>
			<i>BB28_RS10090</i>	<i>Rv2174</i>	<i>mptA</i>
			<i>BB28_RS16230</i>	<i>Rv2981c</i>	<i>ddlA</i>
			<i>BB28_RS18830</i>	<i>Rv2981c</i>	<i>ddlA</i>
			<i>BB28_RS18970</i>	<i>Rv3464</i>	<i>rmlB</i>
			<i>BB28_RS18975</i>	<i>Rv3465</i>	<i>rmlC</i>
			<i>BB28_RS20760</i>	<i>Rv0334</i>	<i>rmlA</i>
Arginine proline metabolism	-1	0.0003	<i>BB28_RS11445</i>	<i>Rv1652</i>	<i>argC</i>
			<i>BB28_RS11450</i>	<i>Rv1653</i>	<i>argJ</i>
			<i>BB28_RS11455</i>	<i>Rv1654</i>	<i>argB</i>
			<i>BB28_RS11460</i>	<i>Rv1655</i>	<i>argD</i>
			<i>BB28_RS11465</i>	<i>Rv1656</i>	<i>argF</i>
			<i>BB28_RS20210</i>	<i>Rv0500</i>	<i>proC</i>
Histidine metabolism	-1	0.001	<i>BB28_RS10445</i>	<i>Rv2122c</i>	<i>hisE</i>
			<i>BB28_RS10450</i>	<i>Rv2121c</i>	<i>hisG</i>
			<i>BB28_RS12965</i>	<i>Rv1606</i>	<i>hisI</i>
			<i>BB28_RS12970</i>	<i>Rv1605</i>	<i>hisF</i>
			<i>BB28_RS12980</i>	<i>Rv1603</i>	<i>hisA</i>
Mycobactin biosynthesis	-1	5.90E-05	<i>BB28_RS10375</i>	<i>Rv2382c</i>	<i>mbtC</i>
			<i>BB28_RS10385</i>	<i>Rv2380c</i>	<i>mbtE</i>
			<i>BB28_RS10390</i>	<i>Rv2379c</i>	<i>mbtF</i>
			<i>BB28_RS10395</i>	<i>Rv2383c</i>	<i>mbtB</i>
			<i>BB28_RS11045</i>	<i>Rv2380c</i>	<i>mbtE</i>
			<i>BB28_RS11050</i>	<i>Rv2378c</i>	<i>mbtG</i>
			<i>BB28_RS20695</i>	<i>Rv2377c</i>	<i>mbtH</i>
			<i>BB28_RS23405</i>	<i>Rv2377c</i>	<i>mbtH</i>
Mycolic acids pathway	-1	0.006	<i>BB28_RS00870</i>	<i>Rv0129c</i>	<i>fbpC</i>
			<i>BB28_RS00880</i>	<i>Rv3804c</i>	<i>fbpA</i>
			<i>BB28_RS00890</i>	<i>Rv3802c</i>	<i>Rv3802c</i>
			<i>BB28_RS10830</i>	<i>Rv2051c</i>	<i>ppm1</i>
			<i>BB28_RS18245</i>	<i>Rv3285</i>	<i>accA3</i>
Peptidoglycan metabolism	-1	1.81E-05	<i>BB28_RS02395</i>	<i>Rv3627c</i>	<i>Rv3627c</i>
			<i>BB28_RS10140</i>	<i>Rv2158c</i>	<i>murE</i>
			<i>BB28_RS10145</i>	<i>Rv2157c</i>	<i>murF</i>

			<i>BB28_RS10150</i>	<i>Rv2156c</i>	<i>murX</i>
			<i>BB28_RS10155</i>	<i>Rv2155c</i>	<i>murD</i>
			<i>BB28_RS10165</i>	<i>Rv2153c</i>	<i>murG</i>
			<i>BB28_RS10170</i>	<i>Rv2152c</i>	<i>murC</i>
Purine pyrimidine biosynthesis	-1	0.006	<i>BB28_RS02235</i>	<i>Rv3645</i>	<i>Rv3645</i>
			<i>BB28_RS02415</i>	<i>Rv3624c</i>	<i>hpt</i>
			<i>BB28_RS03255</i>	<i>Rv0777</i>	<i>purB</i>
			<i>BB28_RS03270</i>	<i>Rv0780</i>	<i>purC</i>
			<i>BB28_RS03315</i>	<i>Rv0788</i>	<i>purQ</i>
			<i>BB28_RS03440</i>	<i>Rv0809</i>	<i>purM</i>
			<i>BB28_RS05170</i>	<i>Rv0956</i>	<i>purN</i>
			<i>BB28_RS05175</i>	<i>Rv0957</i>	<i>purH</i>
			<i>BB28_RS07090</i>	<i>Rv1319c</i>	<i>Rv1319c</i>
			<i>BB28_RS08795</i>	<i>Rv1286</i>	<i>cysN</i>
			<i>BB28_RS09035</i>	<i>Rv2344c</i>	<i>dgt</i>
			<i>BB28_RS11620</i>	<i>Rv1712</i>	<i>cmk</i>
			<i>BB28_RS13780</i>	<i>Rv1389</i>	<i>gmk</i>
			<i>BB28_RS13795</i>	<i>Rv1385</i>	<i>pyrF</i>
			<i>BB28_RS14085</i>	<i>Rv2584c</i>	<i>apt</i>
			<i>BB28_RS14770</i>	<i>Rv2697c</i>	<i>dut</i>
			<i>BB28_RS18005</i>	<i>Rv3247c</i>	<i>tmk</i>
			<i>BB28_RS18990</i>	<i>Rv0733</i>	<i>adk</i>
			<i>BB28_RS21525</i>	<i>Rv0382c</i>	<i>pyrE</i>
Starch sucrose metabolism	-1	0.006	<i>BB28_RS07135</i>	<i>Rv1327c</i>	<i>glgE</i>
			<i>BB28_RS16620</i>	<i>Rv3031</i>	<i>Rv3031</i>
			<i>BB28_RS16625</i>	<i>Rv3032</i>	<i>Rv3032</i>
Transport	-1	1.47E-06	<i>BB28_RS01235</i>	<i>Rv3759c</i>	<i>proX</i>
			<i>BB28_RS01240</i>	<i>Rv3758c</i>	<i>proV</i>
			<i>BB28_RS01245</i>	<i>Rv3757c</i>	<i>proW</i>
			<i>BB28_RS01745</i>	<i>Rv3331</i>	<i>sugI</i>
			<i>BB28_RS03405</i>	<i>Rv1282c</i>	<i>oppC</i>
			<i>BB28_RS04470</i>	<i>Rv3496c</i>	<i>mce4D</i>
			<i>BB28_RS04490</i>	<i>Rv1965</i>	<i>yrbE3B</i>
			<i>BB28_RS04495</i>	<i>Rv3501c</i>	<i>yrbE4A</i>
			<i>BB28_RS05180</i>	<i>Rv1819c</i>	<i>bacA</i>
			<i>BB28_RS05425</i>	<i>Rv0346c</i>	<i>ansP2</i>
			<i>BB28_RS06575</i>	<i>Rv1235</i>	<i>lpqY</i>
			<i>BB28_RS06580</i>	<i>Rv1236</i>	<i>sugA</i>
			<i>BB28_RS06585</i>	<i>Rv1237</i>	<i>sugB</i>
			<i>BB28_RS06590</i>	<i>Rv1238</i>	<i>sugC</i>
			<i>BB28_RS08770</i>	<i>Rv2399c</i>	<i>Rv2399c</i>
			<i>BB28_RS08775</i>	<i>Rv2398c</i>	<i>cysW</i>
			<i>BB28_RS09175</i>	<i>Rv2316</i>	<i>uspA</i>
			<i>BB28_RS11060</i>	<i>Rv1349</i>	<i>irtB</i>
			<i>BB28_RS13025</i>	<i>Rv3758c</i>	<i>proV</i>
			<i>BB28_RS16670</i>	<i>Rv1349</i>	<i>irtB</i>
			<i>BB28_RS20335</i>	<i>Rv3501c</i>	<i>yrbE4A</i>
			<i>BB28_RS20340</i>	<i>Rv1965</i>	<i>yrbE3B</i>
			<i>BB28_RS20920</i>	<i>Rv3494c</i>	<i>mce4F</i>
			<i>BB28_RS20925</i>	<i>Rv3495c</i>	<i>lprN</i>
			<i>BB28_RS20930</i>	<i>Rv3496c</i>	<i>mce4D</i>
			<i>BB28_RS20935</i>	<i>Rv3497c</i>	<i>mce4C</i>
			<i>BB28_RS20940</i>	<i>Rv3498c</i>	<i>mce4B</i>
			<i>BB28_RS20945</i>	<i>Rv3499c</i>	<i>mce4A</i>
			<i>BB28_RS20950</i>	<i>Rv3500c</i>	<i>yrbE4B</i>
			<i>BB28_RS20955</i>	<i>Rv3501c</i>	<i>yrbE4A</i>
			<i>BB28_RS21320</i>	<i>Rv0411c</i>	<i>glnH</i>
			<i>BB28_RS21440</i>	<i>Rv2287</i>	<i>yjcE</i>

			<i>BB28_RS22480</i>	<i>Rv1200</i>	<i>Rv1200</i>
			<i>BB28_RS22830</i>	<i>Rv3496c</i>	<i>mce4D</i>
			<i>BB28_RS23005</i>	<i>Rv1965</i>	<i>yrbE3B</i>
			<i>BB28_RS23520</i>	<i>Rv2692</i>	<i>ceoC</i>

In 5-day old *M. chelonae* pellicles there are six metabolic pathways are up-regulated, and seven of them are down-regulated. In comparison, in 10-day old *M. chelonae pellicles*, four metabolic pathways are up-regulated, and nine are down-regulated. Aiming to ease the visualization of the interaction of the proteins coded by the genes in the enriched pathways, we used String (Szilarczyk et al., 2019) to generate a network, using as a criterion for showing interaction neighborhood, gene fusion or co-occurrence. The generated networks were annotated in Cytoscape (Shannon et al., 2003), and are depicted in Figure 5-3 and Figure 5-4.

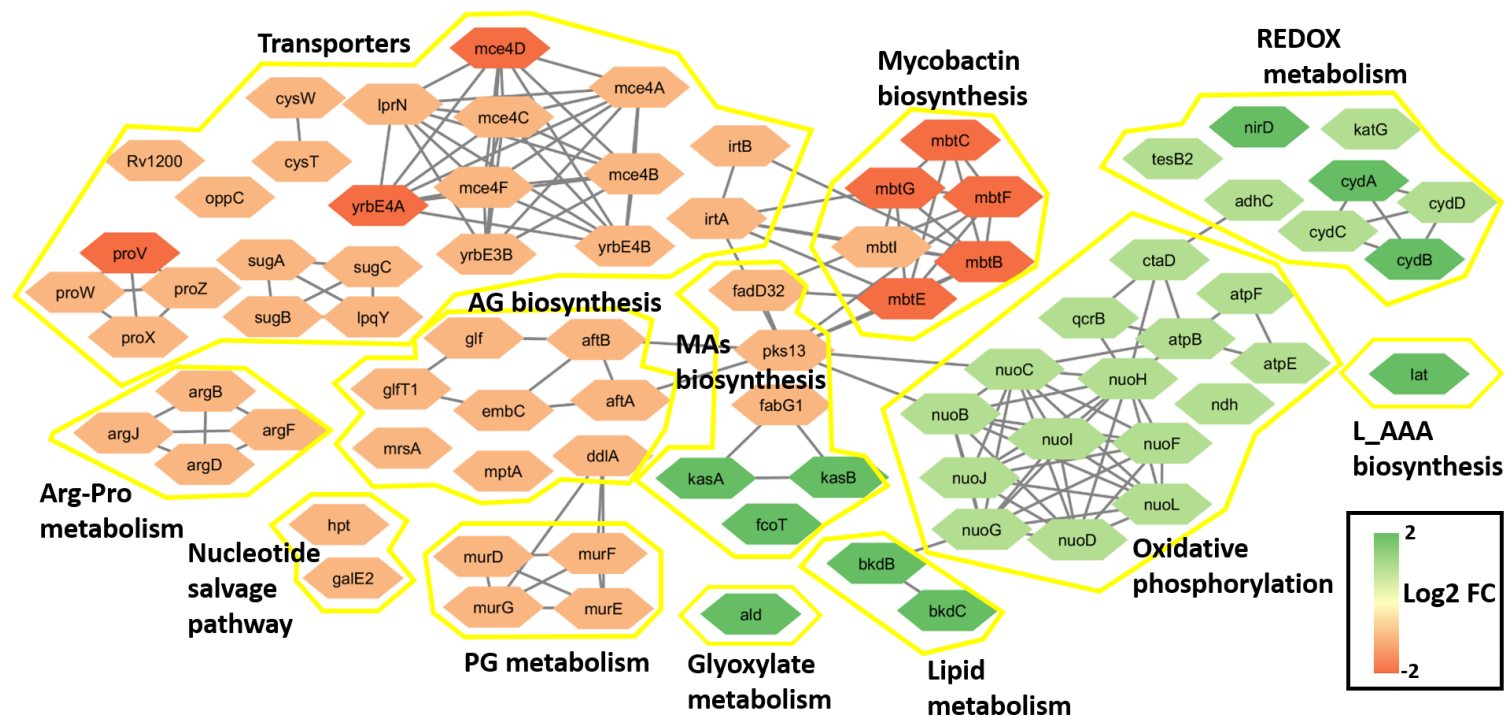


Figure 5-3 Enriched metabolic subsystems in 5-day old *M. chelonae* pellicles.

After determining the enriched metabolic pathways in 5-day old *M. chelonae* pellicles, we created a network on by defining as interaction neighborhood, gene fusion, or co-occurrence. There are thirteen enriched metabolic pathways, and the identity of each pathway is written next to it. The genes belonging to the same metabolic pathway are contained in a yellow polygon. The colour of the hexagon containing the gene names refers to the Log2 Fold change value.



118

5.3.2.1 Genes related to the cell wall biogenesis are down-regulated during biofilm formation

During Biofilm t1 and t2, there is a down-regulation of purine and pyrimidine metabolism, and in Biofilm t2, there is also a down-regulation of the histidine-proline metabolism. These pathways share in common the metabolite phosphoribosyl-1-pyrophosphate (pRpp) (Hove-Jensen, 1988). In mycobacteria pRpp is synthesized by UbiA (Alderwick et al., 2010), and derived to arabinose to be incorporated into the arabinogalactan biosynthesis (Mikusova et al., 2005).

The arabinogalactan biosynthesis and peptidoglycan metabolism are down-regulated in *M. chelonae* at Biofilmt t1 and t2, suggesting an arrest on bacilli replication in biofilm. However, bacilli in mycobacterial biofilms remain metabolically active (Anand et al., 2015), and indeed, genes involved in the oxidative phosphorylation show up-regulation in both Biofilm samples.

5.3.2.2 The oxidative phosphorylation is up-regulated during biofilm formation

In *M. bovis* BCG biofilm, genes related to respiration (oxidative phosphorylation) are down-regulated, leading to the generation of ATP via glycolysis and activation of subsequent biosynthetic pathways (Zeng et al., 2019). This process is known as the Crabtree effect (Herbert and Crabtree, 1929). A similar trend is not observed in the analyzed *M. chelonae* biofilms samples, suggesting that this organism does not favour glycolysis to respiration during biofilm formation, or else, that the Crabtree effect is a transient phenomenon in mycobacterial biofilms and our analyzed biofilm samples are not in the same developmental stage as the *M. bovis* BCG biofilms used in this study.

5.3.2.3 Genes associated with steroids degradation and β -oxidation are up-regulated in *M. chelonae* biofilms

During Biofilm t2, there is an up-regulation of genes associated with cholesterol degradation and β -oxidation of unsaturated fatty acids. *M. chelonae* is not predicted to be able to assimilate cholesterol, as it lacks some of the characteristic genes coding for enzymes required for degrading this metabolite (van Wyk et al., 2019). We also observe a down regulation of genes from the *mce4* operon, and in *M. smegmatis* this operon codes for enzymes that are required for cholesterol uptake (García-Fernández et al., 2017). In *M. smegmatis* all the mce transporters are non-essential, but deletion of all of them impair biofilm formation, likely due to alteration in the cell wall components (Klepp et al., 2012).

5.3.2.4 Genes related to iron uptake are down regulated in *M. chelonae* biofilms

The genes involved in the mycobactin biosynthesis and iron transporter (*irtA* and *irtB*) are down regulated in *M. chelonae* Biofilm t1 and t2, a phenotype consistent with observations in other mature mycobacterial biofilms (Yang et al., 2017). Prior biofilm formation there is an up-regulation of genes related to iron uptake and storage (Ojha and Hatfull, 2007), but as the biofilm matures, there is a down-regulation of these genes (Yang et al., 2017). The uptake and storage of iron are controlled processes, as iron participates in the Fenton reaction that generates free radicals that cause cell damage (Crichton and Charlotiaux-wauters, 1976; Fang et al., 2015).

5.3.2.5 *lat*, a persistence-associated gene, is up-regulated during *M. chelonae* biofilm formation.

In mycobacteria, Lat shows lysine-aminotransferase activity (Tripathi and Ramachandran, 2006). In *M. tuberculosis*, *lat* is up-regulated after nutrient starvation (Betts et al., 2002), and in *M. bovis* BCG, *lat* contributes to the arising of persister bacilli after exposure to norfloxacin (Li et al., 2016). The pathway analysis shows an up-regulation of *lat* in Biofilm t1 and t2, suggesting a potential role of *lat* in persister formation in *M. chelonae* biofilms, although this remains to be tested.

5.3.2.6 Genes related to the synthesis of α -glucan are down-regulated in 10-day old biofilms

The genes related to the synthesis of α -glucan (starch and sucrose metabolism), and a trehalose transporter (*lpqY-sugA-sugB-sugC*) are down-regulated during Biofilm t2. α -glucan is an important component of mycobacterial biofilms (Lemassu and Daffé, 1994; Ortalo-Magne et al., 1995; Ortalo-Magné et al., 1996), and is synthesized from maltose-1-phosphate (Kalscheuer et al., 2010a). Trehalose can also be incorporated to the synthesis of α -glucan, as it can be converted into maltose-1-phosphate for further elongation to α -glucan.

5.4 Discussion

The comparison of the transcriptomes of *M. chelonae* biofilms and planktonic cultures, followed by a pathway enrichment analysis, showed that *M. chelonae* biofilms share some of the transcriptional changes associated to biofilm formation in other mycobacteria, such as the down-regulation of genes associated with iron uptake and storage.

However, *M. chelonae* biofilms display specific transcriptional changes not previously described in other mycobacterial biofilms, such as the induction of *lat*, or the down-regulation of the α -glucan biosynthesis during Biofilm t2. In *M. smegmatis* biofilms, the induction of genes associated with nitrogen acquisition and glutamine metabolism leads to peroxide resistance (Yang et al., 2018), and such transcriptional changes are not observed in the analyzed *M. chelonae* biofilms.

The observed transcriptional changes associated with biofilm formation in *M. chelonae* contribute to the identification of the requirements for the maintenance (transcriptome of Biofilm t1), or dispersion of the biofilm (Biofilm t2). Whether if these transcriptional changes are also relevant when *M. chelonae* forms biofilms during infection remains to be tested.

Chapter 6 General discussion

6.1 General discussion and future work

Some NTM can form biofilms, either colonizing implantable devices or human tissues (Holland et al., 2017; Marsollier et al., 2007; Qvist et al., 2015, 2013). NTM-associated infections often require prolonged chemotherapy, and sometimes, the infection only resolves after the replacement of the colonized implantable device, or debridement the infected tissue (Blanc et al., 2016; Tebruegge et al., 2016). *M. chelonae* is one of the two most drug-resistant NTM and forms biofilms *in vivo* (Holland et al., 2017), making it extremely difficult to treat.

NTM occur in the environment as biofilms (Falkinham, 2009), and these environmental biofilms are thought to be the source of the infecting NTM. After an outbreak *M. chelonae* causing skin infections in patients that had undergone liposuction, the source of the infection was likely a strain of *M. chelonae* recovered from a biofilm formed in the pipes of the water system in one of the physicians office (Meyers et al., 2002). The identification of environmental biofilms as the source of biofilm-associated infections highlights the need for characterizing *Mycobacterium chelonae* biofilms.

In light of this information, the aim of this thesis was to characterize *M. chelonae* biofilms, associating changes in the transcriptome to changes in the biochemical composition during biofilm formation. The observed phenotypes associated with *M. chelonae* biofilm formation derived from this thesis are summarized in Figure 6-1. We have identified several phenotypes that are common to other mycobacterial biofilms, and our study on *M. chelonae* biofilms also shows biofilm-associated phenotypes that have not been described previously in other mycobacterial biofilms. Similar to other mycobacteria (Lemassu et al., 1996a; Lemassu and Daffé, 1994; Ortalo-Magne et al.,

1995; Trivedi et al., 2016), the extracellular matrix of *M. chelonae* biofilms is formed by carbohydrates, proteins, lipids, and nucleic acids, and the *M. chelonae* biofilm morphology shows the distinctive cording of other mycobacterial biofilms (Abidi et al., 2014; Hall-Stoodley et al., 1999; Julián et al., 2010; Sambandan et al., 2013; Sochorová et al., 2014; Sousa et al., 2015; Totani et al., 2017; Trivedi et al., 2016).

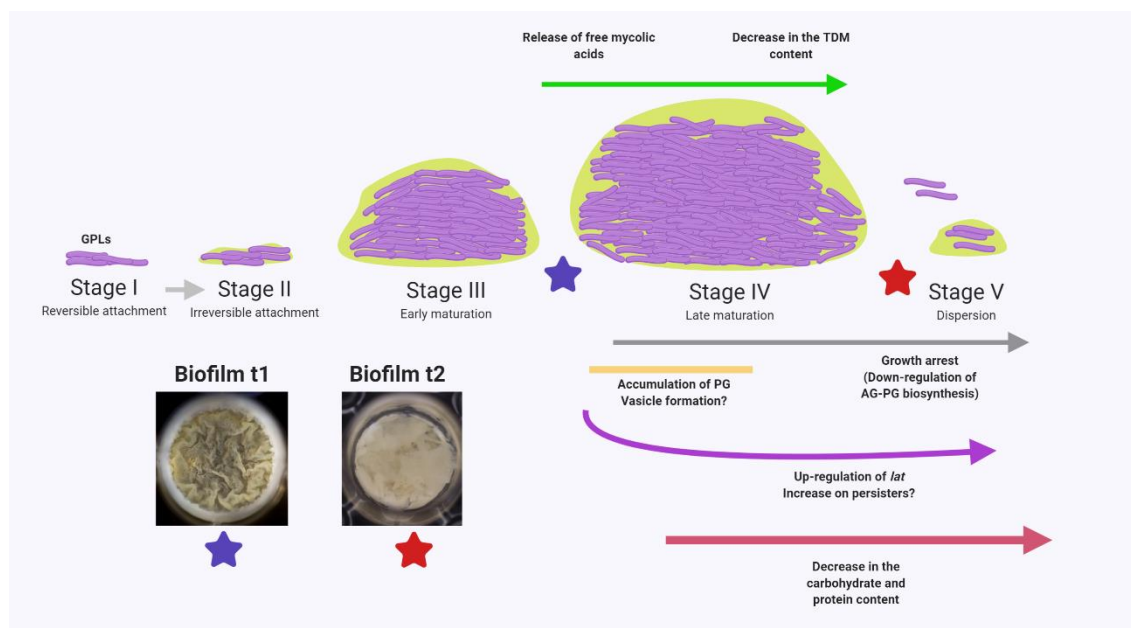


Figure 6-1. Model for *M. chelonae* biofilm formation.

Biofilm t1 correspond to *M. chelonae* biofilms in the Late maturation stage (blue star) and Biofilm t2 to biofilms prior Dispersion state (red star). As *M. chelonae* biofilms reach the dispersion stage, there is a down-regulation of the synthesis of cell wall components, as well as upregulation of genes associated with persistence. There is also a decrease in the carbohydrates and proteins that could contribute to de dispersion of the biofilms.

The lipid profiles from mycobacterial biofilms have been studied extensively (Fujiwara et al., 2015; Ojha et al., 2005, 2010; Ortalo-Magné et al., 1996; Pacheco et al., 2013; Sambandan et al., 2013; Wright et al., 2017), and one of the distinctive features of mycobacterial biofilms is the accumulation of free mycolic acids (Ojha et al., 2010, 2008). In agreement with previous observations, *M. chelonae* accumulate free mycolic acids. In *M. smegmatis*, the release of free mycolic acids is due to the hydrolysis of TDM (Ojha et al., 2010). The content of TDM in *M. chelonae* biofilms decreases from day five to day ten, suggesting a similar mechanism as in *M. smegmatis*.

In addition to the accumulation of free mycolic acids and the decrease of TDM, the lipid profile from 5-day old *M. chelonae* biofilms shows an accumulation of phosphatidylglycerol. This phospholipid is not abundant in the mycobacterial plasma membrane (Jackson et al., 2000); however, it is one of the principal phospholipids found in mycobacterial extracellular vesicles (Prados-Rosales et al., 2011). Many bacteria, both Gram-negative and Gram-positive, secrete extracellular vesicles that contribute to the formation of biofilms (Brown et al., 2015; Liao et al., 2014; Schooling and Beveridge, 2006). The accumulation of phosphatidylglycerol during biofilm formation has not been reported for other mycobacteria before, but *Mycobacterium ulcerans*, the etiological agent of Buruli ulcer, is known to form biofilms that have abundant extracellular vesicles (Marsollier et al., 2007). Although it is likely that vesicles play role in *M. chelonae* biofilms, this yet remains to be determined.

Carbohydrates, proteins, and eDNA have a structural function in mycobacterial biofilms (Aung et al., 2017; Rose et al., 2015; Trivedi et al., 2016), and the Raman spectra from 10-day old biofilms show an overall decrease in the protein content, and also suggests a possible a decrease in the carbohydrate content of 10-day old biofilms, but this result is somehow ambiguous.

There is a down-regulation of genes related to the synthesis of α -glucan and trehalose importers observed in Biofilm t2. Trehalose can be used to form α -glucan (Kalscheuer et al., 2010b), and when the synthesis of intracellular α -glucan decreases, the abundance of capsular glucan decreases as well (Sambou et al., 2008). The glucose-content of extracellular polysaccharides from *M. chelonae* decreases from day 5 to day 10, further supporting the findings from Raman spectroscopy and transcriptome analysis. This information suggests that prior/during dispersion stage, *M. chelonae* biofilms down-

regulates the synthesis of α -glucan, which could contribute to the dispersion of the structure.

Although our pathway enrichment analysis detected a down regulation of genes related to the synthesis of α -glucans during 10-day old *M. chelonae* pellicles, which we further correlated with the decrease in the glucose content measured with gas chromatography, we did not obtain further information about pathways related to the central carbon metabolism. In *Bacillus subtilis*, the dynamic remodelling of the central carbon metabolism allows the bacteria to adapt during the biofilm formation (Pisithkul et al., 2019). Our study would have benefitted from determining secreted metabolites such as pyruvate or acetate to query the active metabolic pathways in *M. chelonae* biofilm through time.

M. smegmatis and *M. tuberculosis* induce the expression of genes related to the glutamine biosynthesis during biofilm formation (Yang et al., 2018; Zeng et al., 2019), and in *M. smegmatis* this leads to peroxide resistant (Yang et al., 2018). The transcriptome of *M. chelonae* biofilms does not show similar behaviour, and perhaps other mechanisms are involved in the development of biofilms increased tolerance to antimicrobials.

The microorganisms dispersed from a biofilm do not go immediately into planktonic growth phase (Chua et al., 2014). *Pseudomonas aeruginosa* that have just been released from a biofilm are hyper-virulent to macrophages and have a different transcriptome compared to both biofilms and planktonic bacteria (Chua et al., 2014). During *M. chelonae* biofilm formation, there is an up-regulation of *lat*, a gene coding for an enzyme associated with persisters formation in *M. bovis* BCG (Li et al., 2016), and that is also up-regulated on *M. tuberculosis* in a nutrient-starved persistence model (Betts et al., 2002). Genes coding for enzymes associated with the synthesis of arginine, proline, and histidine

are down-regulated in *M. chelonae* biofilms. Mycobacterial biofilms are metabolically heterogeneous (Anand et al., 2015), and although mycobacterial biofilms have pores that could help to facilitate the distribution of nutrients through the biofilm, it is possible that the inner population of the biofilm is not receiving as many nutrients as the bacilli present in the outermost layers of the biofilms. The starvation of the inner bacilli in *M. chelonae* biofilms could be responsible for the observed up-regulation of *lat*, and perhaps, is a mechanism that could contribute to the arising of persisters in *M. chelonae* biofilms.

The information derived from this work show characteristic molecular changes occurring in *M. chelonae* biofilm formation and the methods here described could be used in other mycobacteria to compare the biofilm formation between species, aiming to identify conserved mechanisms or components necessary for biofilm formation in NTM.

The strain used in this work is *M. chelonae* NCTC 946 and was isolated from the lung of a turtle by Friedman. Although there is little genetic variability between *M. chelonae* clinical isolates and *M. chelonae* NCTC 946, the latter is slightly more susceptible to antibiotics compared to clinical isolates (Fogelson et al., 2019). There is no information available on the characteristics of the biofilms formed by clinical isolates, but using as a reference the molecular signatures associated with biofilm formation identified in this work, Raman spectroscopy could be used to quickly evaluate the biochemical composition of biofilms formed by *M. chelonae* clinical isolates, to further determine if a particular component of the biofilm is associated with the capacity of a clinical isolate to colonize a determined tissue.

It would also be interesting to study the biofilm formation of *M. chelonae* or other NTM, in *ex vivo* models (Schaudinn et al., 2017), and determine the transcriptome of both host and bacilli, as it has been done for other mycobacteria (Peterson et al., 2019). The study

of transcriptomes during biofilm formation in *ex vivo* models could lead to the identification of genes that are involved in the biofilm formation in different human tissues, providing the researchers with valuable information for further development therapies against *Mycobacterium chelonae* and other pathogenic NTM.

Chapter 7 Materials and methods

7.1 Chemicals and reagents

All chemicals and solvents were purchased from Sigma-Aldrich (U. K.) unless otherwise stated.

7.2 Culture media preparation

7.2.1 7H9/OADC broth

2.35g of 7H9 powder (DifcoTM) was dissolved in 450mL of miliQ water and sterilized by autoclaving at 121°C for 15min. After sterilization, 50mL of sterile ovoalbumin, dextrose, and catalase (OADC) enrichment (DifcoTM), 5mL of sterile 50% glycerol, and 1.25mL of sterile 20% Tween 80 were added.

7.2.2 7H11/OADC

9.5g of 7H11 powder (DIFCOTM) was dissolved in 450mL of miliQ water and sterilized by autoclaving at 121°C for 15min. After sterilization, 50mL of sterile OADC enrichment and 10mL of 50% glycerol were added. The agar was then distributed in plates aseptically.

7.2.3 Sauton's media

The compound used for preparing Sauton's media are summarized in Table 7-1. All the components were mixed in 940mL of miliQ water and 60mL of glycerol. The pH was adjusted to 7.2, when required, with KOH or HCl. The solution was autoclaved for 15min at 121°C. After sterilization, 10mL of sterile 50% glucose was added. When required, Sauton's media was supplemented with tyloxapol until a final concentration of 0.05%.

Table 7-1. Sauton's media composition.

Compound	Amount per liter
Asparagine	4g
Potassium citrate	3.18g
1% ZnSO ₄ in miliQ water	100μL
K ₂ HPO ₄	0.5
MgSO ₄	0.5
Ammonium ferric citrate	0.05g

7.3 Preparation of stocks of fluorescent dyes

7.3.1 Nile Red stock

The Nile Red powder was diluted in miliQ water until a final concentration of 15mg/mL. Then, this stock was further diluted to 0.03184mg/mL. 2μL of the final stock was diluted in 1mL of water before biofilm staining.

7.3.2 Propidium Iodide Stock

The Propidium Iodide was diluted in water until a final concentration of 10µg/mL. From this stock, 0.2mL was further diluted in water to a final volume of 1mL.

7.3.3 Concanavalin A Alexa Fluor 647 stock

5mg of Concanavalin A Alexa Fluor 647 was resuspended in 1mL of 0.1M NaHCO₃ (5mg/mL). 200µL from this solution was further diluted to 1mg/mL. Prior usage, 100µL of the 1mg/mL stock were diluted to a final volume of 1mL (100µg/mL).

7.4 Culture conditions

7.4.1 Propagation of *M. chelonae*

M. chelonae strains were routinely maintained in Middlebrook 7H9 broth or 7H11 agar. Cultures were maintained at 30°C and 100rpm or under static conditions.

7.4.2 Biofilm formation

For biofilm formation, *M. chelonae* NCTC 946 was grown in 7H9 broth, and further diluted until an OD₆₀₀ of 0.03 in Sauton's media. The volumes and containers used were different for each analysis, and the Table 7-2 summarizes the conditions for each analysis.

Table 7-2. Conditions for biofilm formation.

Analysis	Conditions for biofilm cultures	Conditions for planktonic cultures
Confocal microscopy and Scanning Electron Microscopy	16mL distributed in the central wells of a 24-well plate.	Not required.
Lipid extraction for radiolabelled lipids	16mL distributed in the central wells of a 24-well plate.	10mL
RNAseq	50mL, in a 75cm ² culture flask.	50mL
Carbohydrates	500mL, in 10 75cm ² culture flask.	1L

For all the analyses, except for the microscopy analysis (SEM and CLSM), the samples were analyzed at two different time points. For biofilm cultures, the samples were collected on day 5 (Biofilm t1) or on day10 (Biofilm t2).

7.4.3 Planktonic cultures

For biofilm formation, *M. chelonae* cultures growth in 7H9 broth were diluted until an OD₆₀₀ of 0.03 in Sauton's media supplemented with tyloxapol (0.05%). The cultures were collected at an OD₆₀₀ of 1 (Planktonic t1) or 3 (Planktonic t2).

7.5 Transformation of *M. chelonae*

For CLSM, *M. chelonae* was transformed with the plasmid

pMV306-eGFP, kindly provided by Laurent Kremer.

7.5.1 Preparation of electrocompetent *Mycobacterium chelonae*

M. chelonae cultures were grown in 50mL of 7H9 broth to an OD₆₀₀ of 0.8. The culture was pelleted by centrifugation at 3000rpm for 10min at 4°C. The supernatant was discarded, and the remaining cell pellet was washed 3 times with ice-cold 10% glycerol in MiliQ water. Once the washes were completed, the remaining bacterial pellet was suspended in 1 mL of 10% glycerol prior electroporation.

7.5.2 Electroporation of *Mycobacterium chelonae*

For transformation, 200μL of electrocompetent *M. chelonae* was transformed (2.5kV) with 5μL (0.5-1μg) of pMV306-eGFP plasmid, using a 5mm gap cuvette. Both the transformed sample and control had a transformation time above 4 milliseconds.

The samples were mixed with 1mL of 7H9 broth, and allowed to recover at 30°C for 4h. Once the time was completed, the cultures were centrifuged (14000rpm, 2min) for pelleting the cells. 700μL of the supernatant was discarded, and the remaining volume (500μL), was used to resuspend the bacterial pellet. The suspension was serially diluted (10-fold), and plated 50uL of the dilutions (0, 10⁻³, and 10⁻⁵) in 7H11 agar supplemented with zeocin (50μg/mL) as a selection marker.

Transformant colonies were detected after five days of growth and were propagated in 7H9 broth supplemented with zeocin (Invitrogen, 50μg/mL). Once the cultures reached an OD₆₀₀ of 0.8, we took one volume of the culture and mixed it with one volume of 50% glycerol, prior storage (-80°C).

7.6 Microscopy

7.6.1 Scanning electron microscopy of *M. chelonae* biofilms

7.6.1.1 *Sample preparation*

M. chelonae biofilms were formed in 24-well plates. Once formed, the supernatant was carefully removed, and the pellicle was washed once with phosphate buffer saline (PBS, pH=7.2). The supernatant was replaced by 6% glutaraldehyde in PBS and allowed to fix overnight.

7.6.1.2 *Image acquisition*

The *M. chelonae* pellicles were sent to the Centre for Electron Microscopy at the University of Birmingham, for micrographs to be acquired by Mr. Paul Stanley, using a Philips XL-30 FEG ESEM.

7.6.2 CLSM of *M. chelonae* biofilms

7.6.2.1 *Sample preparation*

M. chelonae::eGFP biofilms were formed in 24-well plates. Once the pellicle was formed (5 days) a coverslip ($\varnothing=16\text{mm}$) was carefully placed at the bottom of each well of the culture plate. The liquid phase was carefully removed with a $200\mu\text{L}$ pipette and washed three times with 1 mL of PBS. After the washings, the eGFP-expressing biofilms were stained with one impermeable fluorophore. We used a volume of $200\mu\text{L}$ for each dye. The concentration for each fluorophore and the incubation time are summarized in Table 7-3.

Table 7-3. Staining conditions.

Fluorophore	Targeted component	Concentration	Time
eGFP	Bacteria	--	--
Nile Red	Lipids	$1\mu\text{M}$	30 min
Propidium iodide	Nucleic acids	$15\mu\text{M}$	15 min
Sypro Ruby	Proteins	As provided by the manufacturer	30 min
Alexa Fluor	α -mannose and α -glucose in the pyranose configuration.	$100\mu\text{g/mL}$	30min

After incubation with the dye, the sample was carefully washed three times more with 1mL of PBS and then fixed with 1mL of a solution of 4% paraformaldehyde in PBS (Thermo ScientificTM) for 30min. The sample was subsequently washed three times more with 1mL of PBS, and the round coverslip was lifted from the bottom of the well to harvest the stained pellicle, which was then mounted on a glass slide. Finally, the coverslip was sealed with clear nail polish to avoid sample desiccation. The ready-to-image coverslips were stored in the dark at 4°C until imaged.

7.6.2.2 Image acquisition

The stained pellicles were imaged in the Birmingham Advanced Light Microscopy Facility, using a Nikon A1R Inverted Confocal/ TIRF microscope. The scan speed for all the samples was 1/8, the scan size 1024, and the pinhole size was 1 Airy units. The lasers used for acquiring each fluorophore and the wavelength range for signal recovery are summarized in Table 7-4.

Table 7-4. Acquisition parameters.

Fluorophore	Target component	Laser wavelength (nm)	Emission (nm)
eGFP	<i>M. chelonae</i>	488	494-524
Nile Red	Lipids	514.5	602-644
Propidium iodide	Nucleic acids	561.4	570-620
SyproRuby	Proteins	457.9	608-638
Alexa Fluor	Carbohydrates	639	663-738

7.6.2.3 Image analysis

The colocalization analysis and calculus of biovolumes were done in Icy (de Chaumont et al., 2012), using the Protocols plug in to create automated pipelines for each analysis. Images from each channel were de-noised using a median filter, and then a threshold was calculated using the Threshold plug in, applying the Li method (Li and Tam, 1998). The image was then binarized to create the region of interest (ROI). The signal within the ROI was extracted for colocalization analysis, using the Colocalization Studio plug in, and calculation of biovolumes, using the Stats plug in. The median comparison of the relative biovolumes was made in Python (Perez and Granger, 2007) using the Numpy (van der Walt et al., 2011), Matplotlib (Hunter, 2007), and StatAnnot modules.

7.7 RNAseq

7.7.1 RNA extraction

We extracted RNA from 200 μ L of bacterial pellet, either biofilm or planktonic samples. The pellets were resuspended in 600 μ L of a lysozyme solution (5mg/mL in TE pH=8.0) and 7 μ L of β -mercaptoethanol. The mixture was transferred to a lysis tube and shaken for one minute (speed=400). Then, 60 μ L of 10% sodium dodecyl sulfate (SDS) were added to the mix which was shaken for two more minutes. The resulting lysate was mixed with 60 μ L of 3M sodium acetate (pH=5.2), and then 720 μ L of acid phenol (pH=4.2). The samples were then incubated at 65°C for 5min, with occasional mixing, and then centrifuged (17000 rfc, 5min). The upper aqueous phase (~650 μ L) was mixed with one volume of acid phenol (pH=4.2) and mixed the two phases by vortexing prior a 2min incubation at 65°C. The samples were centrifuged again (17000rfc, 5min), and the upper aqueous phase (~400 μ L) was mixed with 550 μ L of chloroform:isoamyl alcohol. The suspension was centrifuged (17000rfc, 5min), and the upper aqueous phase (~400 μ L) was transferred into a new tube. 40 μ L of 3M sodium acetate (pH=5.2) and 3 volumes of ethanol were added to the recuperated supernatant and were then left to precipitate overnight at 4°C. The aqueous phase was discarded, and the remaining pellet was washed once with 70% ethanol. The pellet was allowed to air-dry before being resuspended in RNase free water.

7.7.2 rRNA depletion

For depleting the rRNA, the RiboZero® (Illumina®) kit was used, following the manufacturer's instructions. 5µg of total RNA from each sample was put in 0.2mL microcentrifuge tubes. 8µL of the RiboZero® Removal Solution buffer and 4µL of RiboZero® reaction buffer were added to each tube. A final volume of 40µL was obtained after the addition of RNase free water. The samples were placed in a thermocycler at 68°C to allow hybridization. After cooling down, the samples were transferred to a 1.5mL microcentrifuge tube that contained 56µL of magnetic beads provided by the RiboZero® kit.

The tubes were vortexed for ten seconds and were incubated at room temperature for five minutes. Then, the tubes were incubated for five minutes more at 50°C and then placed in a magnetic stand. Once the supernatant was clear, 90µL was transferred to a clean 1.5mL tube and placed on ice. 90µL of RNase-free water was added to each tube, followed by the addition of 18µL of 3M sodium acetate and 2µL of glycogen (10mg/mL). After vortexing, 600µL of 100% ethanol was added to each tube and mixed by vortexing.

The samples were left to precipitate for 1h at -20°C, and were then centrifuged at 10,000 g and 4°C for 30min. The supernatant was discarded, and the samples were washed twice more with 70% ethanol. Once the supernatant was discarded, the samples were allowed to air-dry at room temperature. The dry samples were suspended in 8.5µL of TruSeq Stranded mRNA ® (Illumina®) buffer and kept at -80°C before library preparation.

7.7.3 Library preparation

For the synthesis of the DNA strands from RNA templates, we used the TruSeq RNA® (Illumina®) using the Low sample preparation. 100nG (5µL) of the rRNA-depleted samples was placed in a 96-well PCR plate that was labeled with the RBP barcode, followed by the addition of 19.5µL of the Elute, Prime, Fragment Mix to each sample. The content of each well was mixed, and the plate was sealed. The RBP plate was placed in a thermocycler and was incubated for 8min at 94°C, and then 4°C. When the RBP plate reached 4°C, it was removed from the thermocycler and centrifuged for a minute. 17µL from each well was transferred to the corresponding wells of the CPD plate. 8µL of the SuperScript II mix was added to each well of the CPD plate. The CPD plate was sealed, centrifuged, and incubated at 25°C for 10min, followed by an incubation of 50min at 42°C, and 15min at 70°C.

Once the incubation times were completed, the CPD plate was removed from the thermocycler, and the seal was removed. 25µL of the Second Strand Master Mix was added to each of the wells of the CPD plate. The CPD plate was sealed again and incubated in the thermocycler at 16°C for one hour. After incubation, 90µL of the AMPure XP beads were added to each well of the CPD plate. The plate was incubated at room temperature for 15min and then placed into a magnetic stand for five minutes. The supernatant was discarded, and the beads in the CPD plate were washed with 80% ethanol. The CPD plate was allowed to dry, and then 52.5µL of the Resuspension Buffer was added to each well and incubated for two minutes. The CPD plate was then placed in a magnetic stand, and the supernatant from each tube (50µL) was transferred to the corresponding well of the IMP plate.

40 μ L of the End Repair Mix was added to each well of the IMP plate, which was then sealed, and incubated at 30°C for 30min. Followed incubation, 160 μ L of the AMPure XP beads were added to each well, and further incubated at room temperature for 15min. The IMP plate was then placed in the magnetic stand, and the supernatant was discarded. The content of each plate was washed twice with 80% ethanol. After the washes, the IMP plate was allowed to air-dry, and then 17.5 μ L of the Resuspension Buffer was added to each well of the IMP plate. The mix was incubated for two minutes at room temperature. The IMP plate was transferred to a magnetic stand, and 15 μ L of the supernatant was transferred to the corresponding ALP plate.

12.5 μ L of the A-tailing Mix was added to each well of the ALP plate. The seal plate was incubated in a thermocycler at 37°C for 30min, followed by 5 minutes at 70°C.

After incubation, 2.5 μ L of the Ligation Mix and 2.5 μ L of the RNA Adapter Index was added to each well. After sealing, the ALP plate was incubated at 30°C for 10min. After incubation, 5 μ L of the Stop Ligation Buffer was added to each well, followed by 42 μ L of the AMPure XP beads. After 15min of incubation, the ALP plate was transferred to a magnetic stand, and the supernatant was removed. The samples were washed with 80% ethanol twice. The ALP plate was allowed to air-dry, and then 52.5 μ L of the Resuspension Buffer was added. The ALP was incubated for two minutes and then transferred to a magnetic stand. 50 μ L of the supernatant were transferred to the corresponding well from CAP plate.

50 μ L of the AMPure XP beads were added to each well of the CAP plate. After mixing, the CAP plate was incubated for 15min at room temperature. Once in the magnetic stand, the CAP was incubated for five minutes. The supernatant was removed, and the remaining beads were washed twice with 80% ethanol. After air-drying, 22.5 μ L of the Resuspension

Buffer was added to each well of the CAP plate. After a five minute incubation in a magnetic stand, 20 μ L of the obtained supernatants were transferred to the PCR plate.

5 μ L of the PCR Primer Cocktail was added to each well of the PCR plate, followed by 25 μ L of the PCR Master Mix. After sealing the PCR plate, it was subjected to an amplification program consisting of 15cycles with 60°C as the alignment temperature, and 72°C as the extension temperature. Once the amplification was completed, 50 μ L of AMPure XP beads were added to each well, and the PCR plate was incubated at room temperature for 15min. After incubation, the plate was transferred to a magnetic stand, and the supernatant was removed. The samples were then washed with 80% ethanol, and allowed to air-dry at room temperature. The content of each well was resuspended in 32.5 μ L of Resuspension Buffer and incubated for two minutes. After incubation on the magnetic stand, 30 μ L of the supernatant were transferred to the TSP1 plate. Once sealed, the TSP1 plate, which contains the double-stranded DNA synthesized from ribosome-depleted RNA, was stored at -20°C prior sequencing.

7.7.4 Sequencing

The sequencing of the prepared libraries was done using an Illumina NextSeq Instrument at the Institute of Systems Biology (ISB), Seattle, US.

7.7.5 DEG and pathway enrichment analysis

Dr. Eliza Peterson (Dr. Baliga lab, ISB) did the bioinformatics analysis of the sequenced samples. The estimation of the DEG was done by applying the Deseq2 algorithm (Love et

al., 2014). The pathway enrichment analysis was done by looking for gene homology from the DEG *M. chelonae* in *M. tuberculosis*, followed by the search of enriched subsystems from a metabolic reconstruction of *M. tuberculosis* (Kavvas et al., 2018). Dr. Eliza Peterson kindly provided a list with the DEG and a list including the enriched metabolic subsystems.

7.7.6 Data interpretation and visualization

For visualization of the DEG, heatmaps, and Venn diagrams were generated using the modules Numpy (van der Walt et al., 2011), Pandas (McKinney, 2010), Seaborn (Waskom et al., 2018), and Matplotlib (Hunter, 2007) in Python (Perez and Granger, 2007).

A network was created in String (Szilarczyk et al., 2019) with the set of genes resulting from each pathway analysis (one network for Biofilm t1 and one network for Biofilm t2), and further annotated in Cytoscape (Shannon et al., 2003).

7.8 Raman spectroscopy

7.8.1 Sample preparation

Biofilms were grown in 24-well plates as described before. The biofilms were harvested after 5 and 10 days. Planktonic cultures were harvested after reaching an OD₆₀₀ of 1 and 3. The resulting pellets were washed once with PBS and stored at -80°C before spectra

acquisition. Four different experiments were sent to the Indian Institute of Science (Bangalore, India) for generating the characteristic Raman spectra.

7.8.2 Spectra acquisition

The Raman Spectra acquired using a Renishaw InVia Raman spectrometer by Saumya Singh from Dr. Siva Umapathy's research group, who kindly provided the normalized data for further analysis.

7.8.3 Data visualization and analysis

The spectra from *M. chelonae* cultures were generated after plotting the intensity units for each Raman shift. This was done using the Numpy (van der Walt et al., 2011) and Matplotlib (Hunter, 2007) modules in Python (Perez and Granger, 2007).

7.8.3.1 Principal component analysis

The principal component analysis was done in Python (Perez and Granger, 2007) using the scikit-learn (van der Walt et al., 2014) and Pandas (McKinney, 2010) modules. The ‘elbow rule’ (Nguyen and Holmes, 2019) was applied for selecting the number of principal components for describing the data set, and the resulting graphs were generated using the Matplotlib (Hunter, 2007) module.

7.9 Lipid analysis

7.9.1 Radiolabelling of *M. chelonae* cultures

M. chelonae biofilms and planktonic cultures were grown as described before, only that 1 μ L of 14 [C]-acetate (1 μ Ci/ μ L, Perkin Elmer) was added per milliliter of the bacterial cultures. The planktonic bacteria were labeled after they reached the desired OD₆₀₀, and collected 4h later. *M. chelonae* pellicles were labeled at day 5 for Biofilm t1 or on day 10 for Biofilm t2 and collected a day after labeling.

Once the labeled cultures were collected in a glass tube (\varnothing =16mm), the bacterial pellets were separated from the supernatant by centrifugation (3000rpm, 10min). The resulting supernatants were discarded, and the obtained bacterial pellets were washed with one volume of PBS. The resulting pellets were dried under a stream of air at 50°C.

7.9.2 Lipid extraction

The lipid fractionation process we used has been described by Dobson, et. Al (Dobson et al., 1985). The dried bacterial pellets were suspended in 2mL of petroleum ether (60-80) and mixed. After 2h the tubes were centrifuged (3000 rpm, 5min), and the supernatant was transferred to a new tube. The collected fraction was dried at 50°C under a stream of air, and the resulting material consisted of outer solvent-extractable apolar lipids.

The remaining pellet from the petroleum ether extraction was dried in an air bath. Once dried, 2mL of methanol/0.3% aqueous NaCl (10:1) was added to the pellet, followed by

1mL of petroleum ether (60-80). The samples were mixed in a rotator for 15min and then centrifuged (3000rpm, 5min). The upper layer was transferred to a new tube, and one milliliter more of petroleum ether was added to the remaining lower phase. The resulting mix was agitated again (15min) and centrifuged (3000rpm, 5min). The generated upper layer was pooled with the previously recovered one, and the solvent was evaporated at 50°C under a stream of air. The remaining material is inner apolar lipids.

2.3 mL of chloroform: methanol: 0.3% NaCl (9:10:3) was added to the remaining lower phase with the bacterial pellet mentioned above. The tubes were then mixed in a rotator for an hour before being centrifuged (3000rpm, 5min). The supernatant was transferred to a new tube (called now Tube C) and set aside. 750uL of chloroform: methanol: 0.3% NaCl (5:10:4) were added to the remaining bacterial pellet and then mixed in a rotator for 30min prior centrifugation (3000rpm for 3min). The resulting supernatant was pooled into Tube C, and the remaining bacterial pellet was re-extracted with 750μL of chloroform: methanol: 0.3% NaCl (5:10:4) once for 30 minutes before recovering the supernatant.

1.3mL of chloroform plus 1.3mL of 0.3% NaCl were added to the pooled extracts in Tube C and then mixed 5min before centrifuging. Two phases were generated, and the upper layer was discarded. The lower layer was collected into a new tube, and the resulting material after drying is polar lipids.

7.9.3 Mycolic acid derivatization

Mycolic acids were extracted from the delipidated cell pellets or the apolar fractions of lipids. The starting material was hydrolyzed with 2mL of 5% tetrabutylammonium hydroxide, followed by incubation at 95°C overnight. After cooling down, 2mL of miliQ water, 4mL of CH₂Cl₂, and 500μL of CH₃I were added to each tube. The tubes were mixed for thirty minutes and then centrifuged at 5000rpm for five minutes. The upper aqueous phase was discarded, and the lower organic phase was transferred to a fresh tube. This fraction was washed twice with water. The resulting organic phase was dried and resuspended in 4mL of diethyl ether. Each sample was sonicated for five minutes and then centrifuged at 3000rpm for five minutes. The upper phase was collected in a fresh tube and dried.

7.9.4 Quantification of radioactivity

The extracted lipid fractions were dissolved in 200μL of chloroform/methanol (2:1). 5μL of each sample was added to 10mL of scintillation fluid (Ecoscint A, National Diagnosis). The counts per minute (*CPM*) were measured in the TRI-CARB 2700TR Liquid Scintillation Analyser following a pre-set protocol for ¹⁴[C]-labelled samples. The drops per minute were calculated using the next equation:

$$DPM = \frac{CPM}{0.95}$$

Where 0.95 is the decimal efficiency for ¹⁴[C] samples.

7.9.5 Thin layer chromatography

After quantifying the radioactivity in the extracted lipids, we used 25000cpm (~5-10 μ L) for loading into a 6x6cm squared silica plate F254 (Merck). The lipids were loaded in the bottom left corner of the silica plate, and allowed to air-dry for a couple of minutes. Each silica plate was developed in two directions. The composition of the mobile phases depended on the fraction of the lipids that were being analyzed. Apolar lipids were developed with systems A, B, C and D, and polar lipids were developed with systems D and E. The composition for each mobile phase is shown in Table 7-6.

Table 7-5. Solvents systems for TLC.

System	1 st Dimension	2 nd dimension	Lipid fraction
A	Petroleum ether: ethyl acetate (98:2). Three times.	Petroleum ether: acetone (98:2).	NC bound Apolar
B	Petroleum ether: acetone (98:2). Three times.	Toluene: acetone (95:5).	NC bound Apolar
C	Chloroform: methanol (96:4).	Toluene: acetone (80:20).	NC bound Apolar
D	Chloroform: methanol: water (100:14:0.8).	Chloroform: acetone: methanol: water (50:60:2.5:3).	NC bound Apolar Polar
E	Chloroform: methanol: water (60:30:6).	Chloroform: acetic acid: methanol: water (40:25:3:6).	Polar
---	Petroleum ether (60-80):Acetone (95:5)	Petroleum ether 60-80: Ethyl acetate (95:5). Three times.	MAMES (AgNO ₃ -treated silica gel)

Once the TLCs were developed, they were allowed to air-dry inside of a fume cupboard for 20min. Once dried, the silica plates were exposed to an autoradiography (Carestream Kodak BioMax) for 72h, to allow sample visualization.

7.10 Analysis of the extracellular carbohydrates

7.10.1 Extraction of extracellular polysaccharides

Surface exposed materials from three independent experiments of *Mycobacterium chelonae* cultures were extracted by mechanical forces as described previously for other mycobacteria (Grzegorzewicz and Jackson, 2013; Parish et al., 2003). First, the harvested *M. chelonae* pellets from three different experiments of planktonic cultures and biofilms were mixed with 4mm glass beads and shaken gently for 2min. This mechanical abrasion is known for shedding the surface exposed material from the bacilli, without lysing the later. After this mechanical treatment with the glass beads, the bacterial pellets were suspended in miliQ water to a final volume of 50mL, and the suspended cultures were centrifuged at 3000rpm for 15min at 4°C. The obtained supernatants were recovered and filtered through a 0.22µm pore size filter. The obtained filtrate was concentrated to 1/10th of the original volume using a rota-evaporator. The concentrated filtrate was mixed with chloroform and methanol to a final ratio chloroform/methanol/water 1:2:0.8 (v/v/v). The mix was agitated for 1h and then centrifuged for 10min at 3000rpm. The aqueous phase and the interphase were recovered in separate tubes. The interphase was re-extracted three more times with miliQ water and the obtained supernatants were added to the previously recovered aqueous phase. The pooled extracts were dried and dissolved in 2mL of miliQ water for further digestion for 12h with Proteinase K (Promega) at 50°C. The protein-digested material was dialyzed against MiliQ water for 48h using a 3kDa membrane. We used 100µL of the dialyzed material for further derivatization to alditol acetates.

7.10.2 Synthesis of alditol acetates

To determine the relative composition of the monosaccharides present in our samples, we chose to use gas chromatography (GC) analysis of alditol acetates. Monosaccharides need to be derivatized to volatile molecules to make possible their characterization by GC, and we chose to derivatize our samples to alditol acetates because when hexoses or pentoses (or polyalcohols) are derivatized to their respective alditol acetate, they generate a single peak in the chromatogram (Ruiz-Matute et al., 2011) which eases the interpretation of the data.

We used several standards for easing the identification of the detected peaks in the analyzed samples. The standards were solutions (10mg/mL), of the following molecules: arabinose, fucose, galactose, mannose, rhamnose, ribose, xylose, and Myo-inositol. 10 μ L (1 μ g) of these standard solutions were added to a glass tube (13x100mm). One hundred microliters of the dialyzed material were added to separate tubes (one per sample). One microgram (10 μ L) of the internal standard was added to all the tubes (samples and standard). The tubes were allowed to dry under a stream of air, and then 250 μ L of an aqueous solution of 2M trifluoroacetic acid (TFA) was added. The tubes were closed and kept at 120°C for two hours. Once the time was completed, the content of each tube was dried under a stream of air. The resulting material was suspended in 100 μ L of methanol, and then the tubes were dried. This step was repeated once more.

For reducing the resulting monosaccharides, we added 200 μ L of a reducing agent to each tube and let the reaction happen at room temperature overnight. The reducing agent consisted on sodiumborodeuteride (1mg/mL) in a solution of 1M aqueous ammonium hydroxide/ 95% ethanol (1:1, v/v). Once the time was completed, 50 μ L of glacial acetic acid was added to each tube to stop the reaction. The content of the tube was dried under

a stream of air. Once dry, 100 μ L of 10% glacial acetic acid in methanol was added, and the content of each tube was evaporated again. The addition of 10% glacial acetic acid in ethanol with the subsequent drying, was repeated thrice. 100 μ L of methanol was added to the resulting content of each tube and evaporated later.

To acetylate, a 100 μ L of acetic anhydride was added to each of the tubes and kept at 120°C for two hours. Once the time was completed, the tubes were allowed to cool down, and the liquid contained was dried under a stream of air. Once the solvents evaporated, 1mL of miliQ water and 2mL of chloroform were added to each tube. The tubes were mixed thoroughly and then centrifuged at 3000rpm for 5min. The upper aqueous phase from each tube was discarded. One milliliter more of miliQ water was added to the remaining organic phase, and mixed. The tubes were centrifuged again (3000rpm, 5min), and the generated organic phase was transferred into a new tube, and immediately after the solvent was evaporated under a stream of air. The remaining contents of each tube were sent for GC analysis.

7.10.3 Gas chromatography of alditol acetates

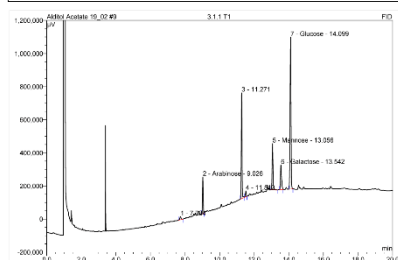
The synthesized alditol acetates were submitted to the Centre for Chemical and Materials Analysis to be analyzed by Gas Chromatography.

Appendices

Appendix 1: Chromatograms of alditol acetates from capsular polysaccharides from 5-day old *M. chelonae* pellicles

Operator:Shimadzu Timebase GC2010_SYSTEM1 Sequence:Alditol Acetate 19_02 Page 1-1
5/2/2019 4:42 PM

9 3.1.1 T1	
Sample Name:	3.1.1 T1
Vial Number:	19
Sample Type:	unknown
Control Program:	Alditol Acetate I
Quantif. Method:	Alditol Acetate
Recording Time:	10/20/19 11:13
Run Time (min):	20.00
Injection Volume:	5.0
Channel:	FID
Wavelength:	n.a.
Bandwidth:	n.a.
Dilution Factor:	1.0000
Sample Weight:	1.0000
Sample Amount:	1.0000



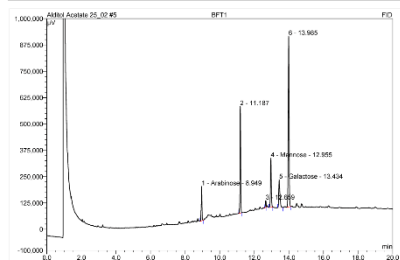
No.	Ret. Time (min)	Peak Name	Height (μV)	Area (μV*min)	Rel. Area (%)	Amount
1	7.79	n.a.	18834.00	157.1	1.21	n.a.
2	9.03	Arabinose	220719.00	10170.6	7.78	n.a.
3	11.27	n.a.	63223.00	30473.3	23.30	n.a.
4	11.51	n.a.	30361.00	2764.5	1.90	n.a.
5	13.06	Mannose	272584.00	17839.9	13.64	n.a.
6	13.54	Galactose	148099.00	10912.3	8.35	n.a.
7	14.10	Glucose	917788.00	51824.4	44.07	n.a.
Total:			2259614.00	130782.04	100.00	0.000

Default Test/Integration

Chromatogram (c) Dionex 1996-2006
Version 6.80 SR8 Build 2623 (156243)

Operator:Shimadzu Timebase GC2010_SYSTEM1 Sequence:Alditol Acetate 25_02 Page 1-1
26/2/2019 10:05 AM

5 BFT1	
Sample Name:	BFT1
Vial Number:	5
Sample Type:	unknown
Control Program:	Alditol Acetate I
Quantif. Method:	Alditol Acetate
Recording Time:	25/2/2019 14:10
Run Time (min):	20.00
Injection Volume:	5.0
Channel:	FID
Wavelength:	n.a.
Bandwidth:	n.a.
Dilution Factor:	1.0000
Sample Weight:	1.0000
Sample Amount:	1.0000



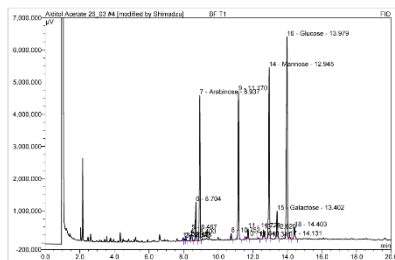
No.	Ret. Time (min)	Peak Name	Height (μV)	Area (μV*min)	Rel. Area (%)	Amount
1	8.95	Arabinose	163094.00	7755.7	7.21	n.a.
2	11.19	n.a.	605640.00	24485.6	22.65	n.a.
3	12.66	n.a.	32387.00	1584.3	1.47	n.a.
4	12.96	Mannose	232970.00	13483.7	12.47	n.a.
5	13.43	Galactose	132178.00	10598.4	9.80	n.a.
6	13.98	n.a.	910970.00	50173.6	46.40	n.a.
Total:			1876940.00	105121.19	100.00	0.000

Default Test/Integration

Chromatogram (c) Dionex 1996-2006
Version 6.80 SR8 Build 2623 (156243)

Operator:Shimadzu Timebase GC2010_SYSTEM1 Sequence:Alditol Acetate 28_03 Page 1-2
28/3/2019 3:59 PM

4 BF T1	
Sample Name:	BF T1
Vial Number:	28
Sample Type:	unknown
Control Program:	Alditol Acetate I
Quantif. Method:	Alditol Acetate
Recording Time:	28/3/2019 17:33
Run Time (min):	20.00
Injection Volume:	5.0
Channel:	FID
Wavelength:	n.a.
Bandwidth:	n.a.
Dilution Factor:	1.0000
Sample Weight:	1.0000
Sample Amount:	1.0000



No.	Ret. Time (min)	Peak Name	Height (μV)	Area (μV*min)	Rel. Area (%)	Amount
1	7.96	n.a.	80397.00	3546.8	0.26	n.a.
2	8.07	n.a.	64820.00	3274.2	0.24	n.a.
3	8.15	n.a.	79428.00	3382.3	0.25	n.a.
4	8.40	n.a.	188559.00	7246.1	0.59	n.a.
5	8.47	n.a.	328304.00	14684.4	1.11	n.a.
6	8.70	n.a.	1209657.00	55611.5	4.11	n.a.
7	8.94	Arabinose	4519829.00	203137.9	15.00	n.a.
8	10.75	n.a.	188914.00	9099.1	0.67	n.a.
9	11.17	n.a.	4594723.00	214114.5	15.81	n.a.
10	11.64	n.a.	37972.00	3727.7	0.28	n.a.
11	11.72	n.a.	321998.00	17604.0	1.30	n.a.
12	12.34	n.a.	43911.00	3263.6	0.24	n.a.
13	12.63	n.a.	278518.00	17624.6	1.30	n.a.
14	12.95	Mannose	6314868.00	301018.2	22.23	n.a.
15	13.40	Galactose	855175.00	50230.6	3.71	n.a.

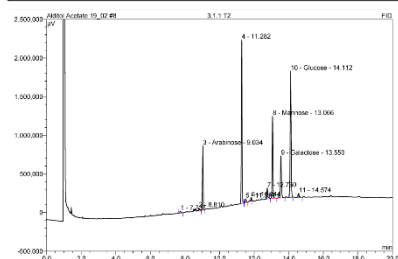
Default Test/Integration

Chromatogram (c) Dionex 1996-2006
Version 6.80 SR8 Build 2623 (156243)

Appendix 2: Chromatograms of alditol acetates from capsular polysaccharides from 10-day old *M. chelonae* pellicles

Operator Shimadzu Timebase GC2010_SYSTEM1 Sequence Alditol Acetate 19_02 Page 1-1
5/2/2019 4:41 PM

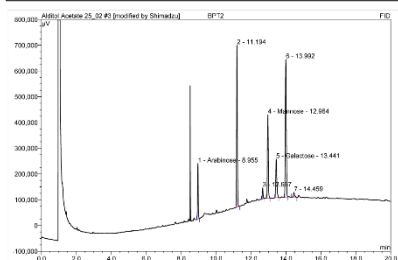
8 3.1.1 T2			
Sample Name:	3.1.1 T2	Injection Volume:	5.0
Vial Number:	14	Channel:	FID
Sample Type:	unknown	Wavelength:	n.a.
Control Program:	Alditol Acetate I	Bandwidth:	n.a.
Quantif. Method:	Alditol Acetate	Dilution Factor:	1.0000
Recording Time:	1/2/2019 10:56	Sample Weight:	1.0000
Run Time (min):	20.00	Sample Amount:	1.0000



No.	Ret.Time min	Peak Name	Height μV	Area $\mu V \cdot min$	Rel.Area %	Amount
1	7.74	n.a.	26381.00	2255.4	0.63	n.a.
2	8.81	n.a.	36870.00	2355.2	0.65	n.a.
3	9.03	Arabinose	233453.00	37548.4	10.45	n.a.
4	11.28	n.a.	2120380.00	101972.8	28.31	n.a.
5	11.52	n.a.	51148.00	3293.5	0.91	n.a.
6	11.84	n.a.	47654.00	2175.5	0.59	n.a.
7	12.76	n.a.	142842.00	8816.9	2.45	n.a.
8	13.07	Mannose	1062794.00	61385.2	17.04	n.a.
9	13.55	Galactose	143327.00	34563.8	9.59	n.a.
10	14.11	Glucose	1535772.00	101877.7	28.29	n.a.
11	14.57	n.a.	52318.00	3889.9	1.08	n.a.
Total:			6552508.00	360172.05	100.00	0.000

Default Test/Integration Chromeleon (c) Dionex 1996-2006
Version 6.80 SR8 Build 2623 (156243)Operator Shimadzu Timebase GC2010_SYSTEM1 Sequence Alditol Acetate 25_02 Page 1-1
26/2/2019 10:03 AM

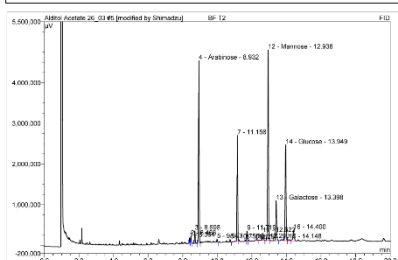
3 BPT2			
Sample Name:	BPT2	Injection Volume:	2.0
Vial Number:	3	Channel:	FID
Sample Type:	unknown	Wavelength:	n.a.
Control Program:	Alditol Acetate I	Bandwidth:	n.a.
Quantif. Method:	Alditol Acetate	Dilution Factor:	1.0000
Recording Time:	25/2/2019 13:24	Sample Weight:	1.0000
Run Time (min):	26.60	Sample Amount:	1.0000



No.	Ret.Time min	Peak Name	Height μV	Area $\mu V \cdot min$	Rel.Area %	Amount
1	8.96	Arabinose	215089.00	9974.2	8.42	n.a.
2	11.19	n.a.	628735.00	29965.2	28.31	n.a.
3	12.67	n.a.	43245.00	2221.7	2.10	n.a.
4	12.95	Mannose	324099.00	18436.0	17.42	n.a.
5	13.44	Galactose	150046.00	10113.3	10.03	n.a.
6	13.99	n.a.	535268.00	32529.7	31.11	n.a.
7	14.45	n.a.	168156.00	17116.4	1.62	n.a.
Total:			1918508.00	105860.48	100.00	0.000

Default Test/Integration Chromeleon (c) Dionex 1996-2006
Version 6.80 SR8 Build 2623 (156243)Operator Shimadzu Timebase GC2010_SYSTEM1 Sequence Alditol Acetate 26_03 Page 1-2
28/3/2019 4:00 PM

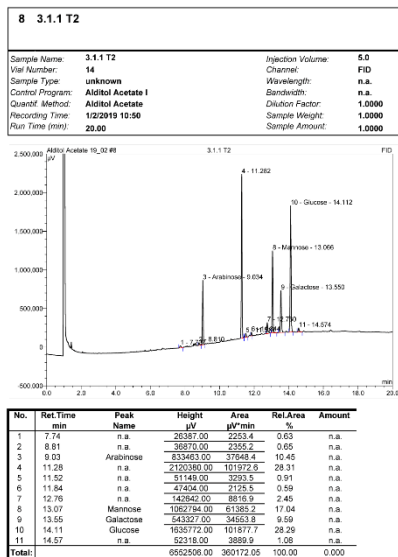
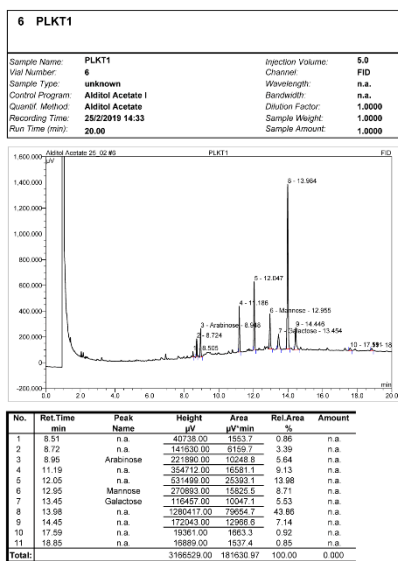
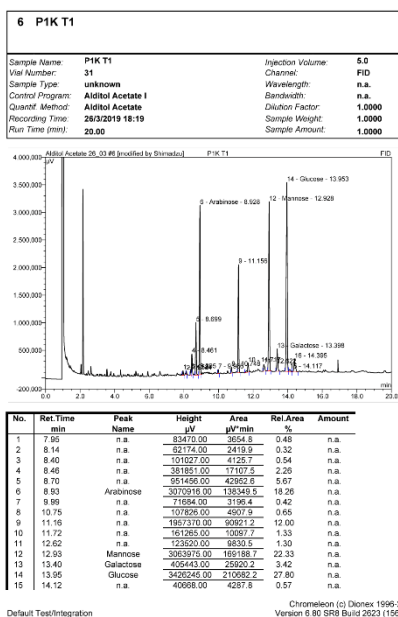
5 BF T2			
Sample Name:	BF T2	Injection Volume:	5.0
Vial Number:	30	Channel:	FID
Sample Type:	unknown	Wavelength:	n.a.
Control Program:	Alditol Acetate I	Bandwidth:	n.a.
Quantif. Method:	Alditol Acetate	Dilution Factor:	1.0000
Recording Time:	28/3/2019 17:56	Sample Weight:	1.0000
Run Time (min):	20.00	Sample Amount:	1.0000



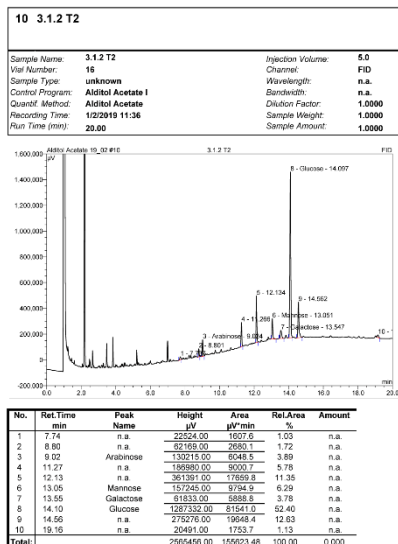
No.	Ret.Time min	Peak Name	Height μV	Area $\mu V \cdot min$	Rel.Area %	Amount
1	8.39	n.a.	133747.00	5694.3	0.65	n.a.
2	8.47	n.a.	178117.00	8285.5	0.92	n.a.
3	8.70	n.a.	309970.00	14951.5	1.70	n.a.
4	8.93	Arabinose	4452942.00	203621.8	23.13	n.a.
5	9.99	n.a.	76516.00	3403.9	0.39	n.a.
6	10.75	n.a.	58672.00	2733.6	0.31	n.a.
7	11.16	n.a.	2591357.00	121185.7	13.76	n.a.
8	11.63	n.a.	19375.00	1076.8	0.12	n.a.
9	11.72	n.a.	245360.00	12361.1	1.40	n.a.
10	12.29	n.a.	30584.00	2437.1	0.28	n.a.
11	12.82	n.a.	174827.00	11779.4	1.34	n.a.
12	12.94	Mannose	4982509.00	250678.5	29.61	n.a.
13	13.40	Galactose	163367.00	67067.0	6.96	n.a.
14	13.95	Glucose	2351970.00	145472.4	16.52	n.a.
15	14.15	n.a.	18537.00	1899.9	0.22	n.a.

Default Test/Integration Chromeleon (c) Dionex 1996-2006
Version 6.80 SR8 Build 2623 (156243)

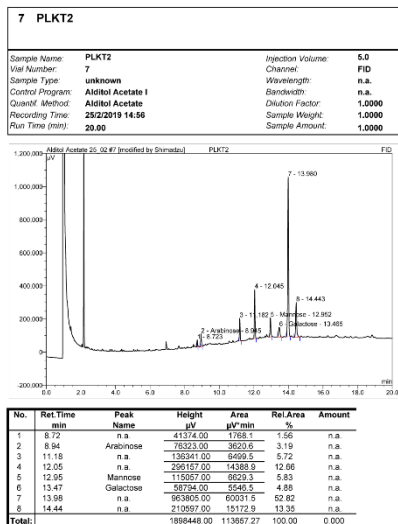
Appendix 3: Chromatograms of alditol acetates from capsular polysaccharides from *M. chelonae* planktonic cultures OD₆₀₀=1.

Operator Shimadzu Timebase GC2010_SYSTEM1 Sequence:Alditol Acetate 19_02 Page 1-1
5/2/2019 4:41 PMOperator Shimadzu Timebase GC2010_SYSTEM1 Sequence:Alditol Acetate 25_02 Page 1-1
26/2/2019 10:05 AMOperator Shimadzu Timebase GC2010_SYSTEM1 Sequence:Alditol Acetate 29_03 Page 1-2
28/3/2019 4:00 PM

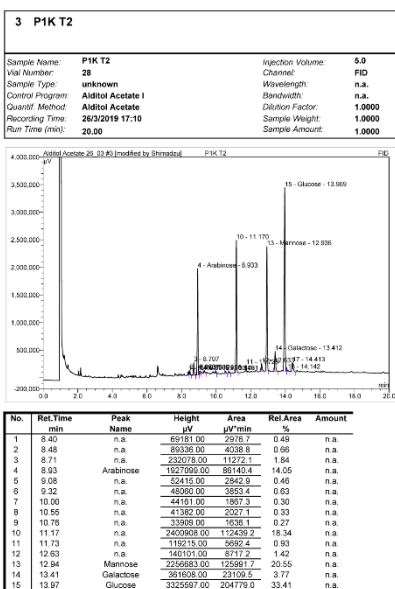
Appendix 3: Chromatograms of alditol acetates from capsular polysaccharides from *M. chelonae* planktonic cultures OD₆₀₀=3.

Operator: Shimadzu Timebase GC2010_SYSTEM1 Sequence: Alditol Acetate 19_02 Page: 1-1
5/2/2019 4:42 PM

Default Test/Integration

Chromleon (c) Dionex 1996-2006
Version 6.80 SR8 Build 2023 (156243)Operator: Shimadzu Timebase GC2010_SYSTEM1 Sequence: Alditol Acetate 25_02 Page: 1-1
26/2/2019 10:06 AM

Default Test/Integration

Chromleon (c) Dionex 1996-2006
Version 6.80 SR8 Build 2023 (156243)Operator: Shimadzu Timebase GC2010_SYSTEM1 Sequence: Alditol Acetate 26_03 Page: 1-2
28/3/2019 3:59 PM

Default Test/Integration

Chromleon (c) Dionex 1996-2006
Version 6.80 SR8 Build 2023 (156243)

Appendix 4: Common DEG in Plancktonic t2, Biofilm t1, and Biofilm t2.

Gene ID	Planktonic t1 (Log2FC)	Biofilm t1 (Log2FC)	Biofilm t1 (Log2FC)	Gene ID	Planktonic t1 (Log2FC)	Biofilm t1 (Log2FC)	Biofilm t1 (Log2FC)
BB28_RS00145	-0.86382	-1.39866	-2.57556	BB28_RS13045	-1.09142	-1.42728	-2.21127
BB28_RS01700	1.592994	2.631764	1.877371	BB28_RS13085	-1.18395	-1.74296	-1.78978
BB28_RS02330	-1.109	-1.58639	-2.53378	BB28_RS13345	-1.12173	-1.33658	-1.55714
BB28_RS03135	1.528366	3.134637	3.631282	BB28_RS13455	1.11644	2.106272	2.428809
BB28_RS03580	1.159861	1.721561	2.190719	BB28_RS14730	-0.76832	-1.56013	-2.02854
BB28_RS03865	1.102697	0.988136	2.019142	BB28_RS15035	-1.18803	-2.07191	-1.4344
BB28_RS04930	-1.25801	-1.54812	-1.59253	BB28_RS16230	-0.81605	-1.18141	-1.51987
BB28_RS05065	5.036193	5.554323	6.606976	BB28_RS16255	-0.951	-1.46519	-1.04864
BB28_RS05070	2.787458	4.745509	4.949974	BB28_RS17085	1.24188	3.360562	3.96485
BB28_RS05625	-1.21917	1.90182	3.704638	BB28_RS17700	1.292062	1.066444	0.945121
BB28_RS07270	-0.99166	-1.83859	-2.37866	BB28_RS17715	-1.09958	-1.39626	-1.22832
BB28_RS08105	-0.66404	-1.22354	-1.06435	BB28_RS18120	-1.13683	-2.06732	-2.42846
BB28_RS09145	1.034457	1.767462	3.115215	BB28_RS19125	-1.18219	-1.53371	-2.00861
BB28_RS09300	1.207552	2.731291	3.181994	BB28_RS19640	4.071299	6.653272	7.00953
BB28_RS09780	-1.10674	-1.77588	-1.15482	BB28_RS21410	0.837207	0.974779	1.249664
BB28_RS10235	-0.85517	-1.30129	-1.54978	BB28_RS22740	1.230089	1.613439	1.691657
BB28_RS10755	-0.95465	-1.19627	-1.5307	BB28_RS24315	-0.79177	-1.60272	-1.13126
BB28_RS11240	1.220136	1.540318	1.18265	BB28_RS24410	1.870165	8.063117	8.603997
BB28_RS12530	1.172827	3.392578	3.519789	BB28_RS24490	-1.00919	-1.78874	-1.89749
BB28_RS12790	-1.14886	-1.48417	-1.08344	BB28_RS24850	-0.90486	-1.28543	-1.24292
BB28_RS13040	-0.77236	-4.8564	-6.12272				

Appendix 5: Common DEG in Plancktonic t2 and Biofilm t1, but not DE in Biofilm t2.

Gene ID	Planktonic t1 (Log2FC)	Biofilm t1 (Log2FC)
BB28_RS02560	0.697938	0.950773
BB28_RS11880	0.670142	1.323779
BB28_RS14660	0.87846	0.950478
BB28_RS14770	-1.35084	-1.6508
BB28_RS15655	1.169495	1.343898
BB28_RS15725	1.372465	1.305596
BB28_RS15945	-0.85357	-0.91363
BB28_RS16210	-0.74816	-1.41346

Appendix 6: Common DEG in Planktonic t2 and Biofilm t2, but not DE in Biofilm t1.

Gene ID	Planktonic t1 (Log2FC)	Biofilm t1 (Log2FC)
BB28_RS00005	-0.9112	-1.52915
BB28_RS07070	2.563874	2.474597
BB28_RS07075	2.636275	2.366342
BB28_RS10780	-1.24844	-1.56758
BB28_RS12785	-0.93957	-0.67217
BB28_RS16195	-1.07986	-0.99554
BB28_RS18895	1.51776	2.003281
BB28_RS19505	-1.53578	1.893032
BB28_RS20535	-1.23867	-1.31945
BB28_RS22455	-1.22506	-1.85624
BB28_RS22850	-0.99802	-0.97164
BB28_RS22870	-1.11557	-1.18014
BB28_RS23395	-0.70722	1.001093
BB28_RS24370	-1.14727	-1.07403

Appendix 7: Common DEG in Biofilm t1 and Biofilm t2, but not in Planktonic t2

Gene ID	Biofilm t1 (Log2FC)	Biofilm t2 (Log2FC)	Gene ID	Biofilm t1 (Log2FC)	Biofilm t2 (Log2FC)
BB28_RS00100	1.84	3.16	BB28_RS13015	-1.21	-1.78
BB28_RS00120	3.05	2.32	BB28_RS13025	-1.99	-1.59
BB28_RS00125	2.14	2.33	BB28_RS13030	-1.34	-0.97
BB28_RS00165	-2.71	-1.44	BB28_RS13035	-1.24	-1.05
BB28_RS00175	-1.03	-1.37	BB28_RS13130	-0.86	-0.86
BB28_RS00215	2.17	2.18	BB28_RS13200	-1.39	-1.17
BB28_RS00300	2.05	3.31	BB28_RS13245	1.12	1.66
BB28_RS00425	2.18	1.66	BB28_RS13280	-1.29	-1.24
BB28_RS00460	1.10	1.07	BB28_RS13390	-1.48	-1.75
BB28_RS00560	-0.80	-1.02	BB28_RS13540	-0.99	-1.25
BB28_RS00615	1.89	1.73	BB28_RS13610	-1.00	-1.29
BB28_RS00650	1.07	1.40	BB28_RS13665	1.71	1.59
BB28_RS01040	-1.29	-1.47	BB28_RS13675	1.90	1.56
BB28_RS01085	-0.88	-1.32	BB28_RS13705	-1.01	-1.70
BB28_RS01095	3.01	2.88	BB28_RS13790	-1.24	-1.95
BB28_RS01160	2.57	3.51	BB28_RS13850	-1.14	-2.08
BB28_RS01295	2.37	3.10	BB28_RS13900	3.56	3.46
BB28_RS01405	1.44	1.45	BB28_RS13905	3.73	3.68
BB28_RS01465	1.33	1.89	BB28_RS13980	1.41	1.06
BB28_RS01510	2.34	2.33	BB28_RS14015	-1.74	-0.88
BB28_RS01525	-1.25	-2.47	BB28_RS14045	-1.30	-1.60
BB28_RS01630	-0.90	-1.23	BB28_RS14125	2.27	3.40
BB28_RS01750	1.28	1.87	BB28_RS14200	-1.78	-1.94
BB28_RS02035	-1.10	-2.27	BB28_RS14245	1.91	1.96
BB28_RS02070	-1.08	-1.71	BB28_RS14365	2.22	1.60
BB28_RS02080	-1.27	-2.55	BB28_RS14370	2.81	2.61
BB28_RS02235	-1.31	-1.37	BB28_RS14380	3.01	2.68
BB28_RS02245	3.09	3.13	BB28_RS14400	3.22	2.86
BB28_RS02290	-0.95	-1.23	BB28_RS14405	6.71	6.71
BB28_RS02295	-1.05	-1.91	BB28_RS14425	1.03	1.17
BB28_RS02320	-0.85	-1.49	BB28_RS14460	1.64	2.26
BB28_RS02350	-1.08	-1.05	BB28_RS14470	3.89	5.24
BB28_RS02375	2.47	4.25	BB28_RS14545	4.03	3.03
BB28_RS02420	-1.35	-1.26	BB28_RS14655	2.96	1.31
BB28_RS02555	-1.10	-1.68	BB28_RS14905	1.78	2.16
BB28_RS02630	3.95	3.04	BB28_RS14935	1.68	4.06
BB28_RS02635	4.92	4.44	BB28_RS14940	1.78	3.85
Gene ID	Biofilm t1	Biofilm t2	Gene ID	Biofilm t1	Biofilm t2

	(Log2FC)	(Log2FC)		(Log2FC)	(Log2FC)
BB28_RS02675	2.96	2.52	BB28_RS14945	1.46	2.61
BB28_RS02680	3.78	3.59	BB28_RS14950	1.54	1.71
BB28_RS02685	3.14	3.80	BB28_RS15055	1.66	1.86
BB28_RS02690	1.65	3.19	BB28_RS15060	-1.23	-1.28
BB28_RS02695	3.13	4.23	BB28_RS15225	-0.92	-1.55
BB28_RS03050	-1.61	-1.02	BB28_RS15260	2.13	2.23
BB28_RS03090	2.14	2.42	BB28_RS15295	-1.79	-1.55
BB28_RS03095	3.85	3.91	BB28_RS15365	3.73	3.87
BB28_RS03100	3.29	3.28	BB28_RS15370	1.83	1.68
BB28_RS03105	2.64	2.68	BB28_RS15455	1.43	2.21
BB28_RS03115	2.82	2.53	BB28_RS15545	-1.33	-1.64
BB28_RS03120	4.64	4.51	BB28_RS15555	-1.91	-2.21
BB28_RS03130	2.49	2.25	BB28_RS15580	4.10	4.31
BB28_RS03140	6.13	6.18	BB28_RS15585	1.58	1.96
BB28_RS03145	3.98	3.99	BB28_RS15590	2.12	2.67
BB28_RS03180	-1.04	-2.26	BB28_RS15595	2.02	2.64
BB28_RS03320	-0.90	-0.83	BB28_RS15690	-1.07	-2.05
BB28_RS03440	1.18	1.29	BB28_RS15775	-0.89	-0.97
BB28_RS03530	3.10	3.10	BB28_RS15910	-1.53	-0.89
BB28_RS03595	2.71	3.83	BB28_RS15930	-1.16	-1.67
BB28_RS03650	1.16	1.17	BB28_RS15980	-1.35	-1.80
BB28_RS03660	2.16	2.69	BB28_RS16030	-1.23	-0.92
BB28_RS03665	2.45	2.31	BB28_RS16225	-1.32	-2.11
BB28_RS03750	-0.91	-0.92	BB28_RS16290	1.75	2.27
BB28_RS03765	1.20	2.59	BB28_RS16320	-1.01	-1.30
BB28_RS03860	-0.89	-0.93	BB28_RS16335	-1.43	-1.70
BB28_RS03940	-0.87	-0.71	BB28_RS16545	1.97	2.05
BB28_RS03950	-0.92	-1.96	BB28_RS16560	1.43	1.67
BB28_RS04030	-0.84	-1.95	BB28_RS16565	-1.22	-1.45
BB28_RS04100	-0.99	-2.05	BB28_RS16580	2.35	2.64
BB28_RS04120	1.94	2.66	BB28_RS16585	2.77	2.76
BB28_RS04125	2.97	3.78	BB28_RS16600	-1.14	-1.50
BB28_RS04210	-1.21	-1.84	BB28_RS16635	-1.01	-1.81
BB28_RS04295	1.21	1.98	BB28_RS16680	-2.35	-2.67
BB28_RS04315	1.27	1.24	BB28_RS16720	1.83	1.88
BB28_RS04320	2.27	2.37	BB28_RS16780	1.41	1.05
BB28_RS04335	2.09	1.74	BB28_RS16800	1.13	1.80
BB28_RS04640	1.20	1.59	BB28_RS16820	1.87	1.88
BB28_RS04680	-0.79	-0.86	BB28_RS16860	1.68	2.88
BB28_RS04990	-1.15	-1.41	BB28_RS16865	3.23	2.96
BB28_RS04995	3.44	3.92	BB28_RS16875	1.98	2.03
BB28_RS05000	5.23	4.57	BB28_RS17045	1.16	2.01
BB28_RS05005	3.37	3.65	BB28_RS17240	1.64	2.20
Gene ID	Biofilm t1	Biofilm t2	Gene ID	Biofilm t1	Biofilm t2

	(Log2FC)	(Log2FC)		(Log2FC)	(Log2FC)
BB28_RS05020	1.69	4.01	BB28_RS17275	-1.40	-1.97
BB28_RS05055	1.43	1.93	BB28_RS17295	-1.37	-2.20
BB28_RS05060	3.07	3.33	BB28_RS17350	-1.21	-2.06
BB28_RS05075	3.63	3.93	BB28_RS17370	-1.20	-1.74
BB28_RS05080	1.90	2.73	BB28_RS17545	2.81	2.94
BB28_RS05185	0.92	1.06	BB28_RS17585	1.52	2.59
BB28_RS05190	3.84	4.38	BB28_RS17640	2.07	3.12
BB28_RS05310	2.42	2.02	BB28_RS17955	1.73	1.72
BB28_RS05420	-1.18	-1.28	BB28_RS18140	-1.21	-1.69
BB28_RS05425	-0.90	-1.39	BB28_RS18185	-1.27	-1.97
BB28_RS05465	-1.52	-2.12	BB28_RS18195	-1.33	-1.64
BB28_RS05500	-1.81	-2.13	BB28_RS18250	3.48	3.93
BB28_RS05550	1.67	2.34	BB28_RS18255	4.34	5.00
BB28_RS05570	-1.93	-1.62	BB28_RS18260	1.67	1.90
BB28_RS05610	1.73	2.67	BB28_RS18265	4.64	6.22
BB28_RS05615	2.23	3.74	BB28_RS18270	1.14	2.45
BB28_RS05635	1.47	1.97	BB28_RS18280	3.62	5.42
BB28_RS05725	-1.28	-1.15	BB28_RS18325	-0.95	-0.79
BB28_RS05805	-1.04	-1.73	BB28_RS18395	-0.76	-1.01
BB28_RS05810	-1.21	-0.92	BB28_RS18510	3.02	2.25
BB28_RS06130	1.56	1.91	BB28_RS18515	1.83	1.16
BB28_RS06300	-1.09	-1.01	BB28_RS18535	-1.29	-1.92
BB28_RS06340	-1.16	-1.46	BB28_RS18590	1.54	1.38
BB28_RS06415	-0.95	-1.48	BB28_RS18670	3.20	2.58
BB28_RS06470	1.22	1.51	BB28_RS18845	2.13	1.99
BB28_RS06475	1.40	2.02	BB28_RS18910	-1.34	-0.81
BB28_RS06495	-0.82	-0.94	BB28_RS18935	-0.85	-1.61
BB28_RS06525	1.36	1.45	BB28_RS18980	-1.26	-1.67
BB28_RS06565	-0.83	-0.76	BB28_RS19035	-1.63	-1.20
BB28_RS06600	-1.20	-1.47	BB28_RS19110	-1.26	-1.63
BB28_RS06620	-1.42	-1.66	BB28_RS19270	1.17	1.27
BB28_RS06700	-2.44	-2.06	BB28_RS19390	-1.22	-0.91
BB28_RS06770	1.92	2.25	BB28_RS19400	-1.53	-1.29
BB28_RS06775	2.50	2.40	BB28_RS19475	1.59	2.18
BB28_RS06785	1.90	1.82	BB28_RS19520	2.32	3.79
BB28_RS06795	3.16	3.07	BB28_RS19525	2.59	2.59
BB28_RS06900	2.91	3.38	BB28_RS19535	2.93	3.01
BB28_RS06905	1.57	2.57	BB28_RS19540	3.02	4.18
BB28_RS06910	1.64	2.47	BB28_RS19590	2.59	2.16
BB28_RS06970	-1.28	-1.26	BB28_RS19595	2.79	2.67
BB28_RS07090	-1.23	-1.10	BB28_RS19600	2.60	3.09
BB28_RS07225	-0.94	-0.84	BB28_RS19610	2.60	3.48
BB28_RS07245	3.57	3.60	BB28_RS19645	1.42	2.13
Gene ID	Biofilm t1	Biofilm t2	Gene ID	Biofilm t1	Biofilm t2

	(Log2FC)	(Log2FC)		(Log2FC)	(Log2FC)
BB28_RS07345	-2.22	-1.91	BB28_RS19650	2.01	3.39
BB28_RS07380	-1.26	-2.24	BB28_RS19655	2.76	3.47
BB28_RS07385	-1.43	-0.88	BB28_RS19665	3.41	4.61
BB28_RS07835	-1.28	-2.73	BB28_RS19670	2.54	3.11
BB28_RS07985	-1.00	-1.47	BB28_RS19745	-1.15	-1.41
BB28_RS07990	-1.03	-1.18	BB28_RS19905	-1.10	-1.59
BB28_RS08155	-0.96	-1.60	BB28_RS19970	3.50	2.82
BB28_RS08165	1.32	2.08	BB28_RS19975	5.18	6.06
BB28_RS08200	-0.94	-2.11	BB28_RS20040	1.63	1.59
BB28_RS08290	-1.12	-1.14	BB28_RS20090	2.69	1.64
BB28_RS08295	-0.89	-0.83	BB28_RS20210	-1.13	-1.72
BB28_RS08320	-0.87	-0.77	BB28_RS20500	-1.20	-1.09
BB28_RS08390	2.95	2.21	BB28_RS20585	1.51	2.44
BB28_RS08455	3.00	1.60	BB28_RS20605	1.26	1.79
BB28_RS08460	1.59	1.48	BB28_RS20625	-1.12	-1.68
BB28_RS08635	-2.74	-2.29	BB28_RS20715	-1.59	-3.06
BB28_RS08665	-1.36	-0.92	BB28_RS20785	-0.92	-1.18
BB28_RS08870	1.48	1.14	BB28_RS20870	2.35	2.17
BB28_RS09020	-1.07	-2.47	BB28_RS20955	-1.33	-1.51
BB28_RS09090	1.55	1.54	BB28_RS21040	-0.92	-1.20
BB28_RS09120	1.96	3.85	BB28_RS21165	-1.37	-2.45
BB28_RS09130	3.42	5.63	BB28_RS21170	-1.35	-2.20
BB28_RS09230	1.41	1.53	BB28_RS21175	-1.21	-1.07
BB28_RS09245	1.40	1.27	BB28_RS21195	-1.33	-1.15
BB28_RS09250	-1.61	-2.68	BB28_RS21255	-1.44	-1.30
BB28_RS09285	1.16	2.46	BB28_RS21445	-1.20	-1.19
BB28_RS09310	2.97	2.84	BB28_RS21500	-1.40	-2.41
BB28_RS09340	2.97	4.68	BB28_RS21610	1.38	2.31
BB28_RS09425	1.83	3.08	BB28_RS21620	1.97	1.69
BB28_RS09475	2.85	2.75	BB28_RS21630	0.91	1.10
BB28_RS09725	2.30	2.92	BB28_RS21730	3.39	3.79
BB28_RS09865	-1.48	-1.54	BB28_RS21775	2.38	2.18
BB28_RS09925	0.91	1.31	BB28_RS21780	1.54	1.30
BB28_RS09960	-1.32	-1.18	BB28_RS21800	3.87	4.23
BB28_RS10020	-0.82	-2.07	BB28_RS21820	1.78	2.37
BB28_RS10035	-1.06	-2.04	BB28_RS21825	2.63	2.01
BB28_RS10085	-1.64	-1.93	BB28_RS21840	1.75	2.76
BB28_RS10100	-1.22	-0.96	BB28_RS21875	1.17	2.64
BB28_RS10115	1.49	1.56	BB28_RS22085	-1.13	-1.95
BB28_RS10250	1.94	2.38	BB28_RS22115	1.22	1.33
BB28_RS10400	-1.19	-1.22	BB28_RS22120	1.60	1.36
BB28_RS10735	1.46	1.42	BB28_RS22125	2.24	2.67
BB28_RS10760	-0.84	-1.89	BB28_RS22175	0.95	1.18
Gene ID	Biofilm t1	Biofilm t2	Gene ID	Biofilm t1	Biofilm t2

	(Log2FC)	(Log2FC)		(Log2FC)	(Log2FC)
BB28_RS10785	-1.25	-1.65	BB28_RS22215	2.03	2.91
BB28_RS10840	-1.47	-2.47	BB28_RS22260	1.67	2.63
BB28_RS10870	1.18	1.72	BB28_RS22340	1.51	2.02
BB28_RS10920	1.98	1.01	BB28_RS22370	-0.97	-1.62
BB28_RS10925	3.46	2.95	BB28_RS22395	-1.39	-1.73
BB28_RS10930	1.20	2.13	BB28_RS22450	-1.03	-1.27
BB28_RS10935	1.49	2.24	BB28_RS22540	-1.19	-1.14
BB28_RS10945	2.06	2.90	BB28_RS22655	-1.16	-2.27
BB28_RS10950	2.02	2.20	BB28_RS22750	-1.25	-1.45
BB28_RS11035	-1.97	-1.66	BB28_RS22765	-1.11	-1.95
BB28_RS11060	-1.34	-1.68	BB28_RS22860	-1.18	-1.75
BB28_RS11105	2.25	2.51	BB28_RS22885	-0.99	-1.81
BB28_RS11110	1.69	1.75	BB28_RS22960	-1.13	-1.22
BB28_RS11125	1.94	4.59	BB28_RS23110	2.47	2.45
BB28_RS11185	2.39	2.83	BB28_RS23145	1.55	1.56
BB28_RS11285	1.94	1.95	BB28_RS23235	3.21	3.17
BB28_RS11330	1.08	1.23	BB28_RS23240	4.76	4.02
BB28_RS11365	-0.91	-1.02	BB28_RS23320	-1.25	-1.36
BB28_RS11440	1.40	1.87	BB28_RS23435	-1.09	-2.24
BB28_RS11540	-0.87	-1.39	BB28_RS23505	2.78	2.87
BB28_RS11630	1.41	1.18	BB28_RS23520	-1.18	-0.80
BB28_RS11885	1.34	1.09	BB28_RS23840	-1.08	-1.32
BB28_RS11895	1.31	1.42	BB28_RS23860	1.98	3.72
BB28_RS11925	-1.72	-1.74	BB28_RS24125	2.64	2.85
BB28_RS12080	-1.05	-1.19	BB28_RS24145	-1.39	-1.69
BB28_RS12215	4.39	4.07	BB28_RS24200	-1.29	-1.85
BB28_RS12230	2.63	3.28	BB28_RS24270	-0.78	-1.05
BB28_RS12335	-0.92	-1.18	BB28_RS24300	-1.30	-2.22
BB28_RS12520	2.80	3.53	BB28_RS24350	1.09	1.24
BB28_RS12525	2.79	4.20	BB28_RS24455	1.92	2.05
BB28_RS12540	2.84	2.56	BB28_RS24460	2.36	2.24
BB28_RS12545	2.44	1.58	BB28_RS24465	1.02	1.29
BB28_RS12550	1.73	1.61	BB28_RS24520	1.83	1.88
BB28_RS12750	2.14	1.73	BB28_RS24550	-1.53	-2.01
BB28_RS12755	1.04	1.76	BB28_RS24725	-1.37	-1.53
BB28_RS12845	2.50	2.81	BB28_RS24735	-1.42	-2.04
BB28_RS12850	1.59	2.43	BB28_RS24755	-1.19	-1.09
BB28_RS12855	1.47	2.31	BB28_RS24770	2.55	2.32
BB28_RS12870	3.03	4.82	BB28_RS24780	6.76	7.27
BB28_RS12875	1.02	1.43	BB28_RS24830	-1.59	-1.98
BB28_RS12950	1.93	1.15	ffs	2.68	2.46
BB28_RS12960	-0.95	-1.45	ssrA	2.25	2.17

Appendix 8: DEG only in Planktonic t2.

Gene ID	Biofilm t1 (Log2FC)
BB28_RS01090	1.240005
BB28_RS01155	-1.59252
BB28_RS01290	-1.97396
BB28_RS01605	1.587311
BB28_RS03600	-1.10331
BB28_RS04035	-1.36114
BB28_RS04055	1.151279
BB28_RS06150	1.095813
BB28_RS06210	1.146762
BB28_RS06305	0.847264
BB28_RS07400	1.489112
BB28_RS08540	-1.573
BB28_RS12345	-2.14966
BB28_RS13050	1.295696
BB28_RS16410	0.858077
BB28_RS17070	1.008574
BB28_RS17160	-1.18149
BB28_RS18540	-1.48569
BB28_RS18955	-1.49932
BB28_RS20590	1.316039
BB28_RS21160	-1.64299
BB28_RS21460	1.126396
BB28_RS21580	-0.78905
BB28_RS22770	-0.92237
BB28_RS23890	-0.97581
BB28_RS23985	1.017709
BB28_RS24395	-1.16963
BB28_RS24740	-1.16767

Appendix 9: DEG only in Biofilm t1.

Gene ID	Biofilm t1 (Log2FC)	Gene ID	Biofilm t1 (Log2FC)	Gene ID	Biofilm t1 (Log2FC)
BB28_RS00430	1.110917	BB28_RS07020	1.673855121	BB28_RS15420	-1.36937439
BB28_RS00580	1.306248	BB28_RS07025	1.347902618	BB28_RS16295	2.76369041
BB28_RS00760	1.620231	BB28_RS07030	1.113450756	BB28_RS16555	1.09301442
BB28_RS00830	-1.19911	BB28_RS07040	1.07241493	BB28_RS16715	-1.41162518
BB28_RS00910	-1.77378	BB28_RS07905	2.641916931	BB28_RS16795	1.00136916
BB28_RS00915	1.571835	BB28_RS08110	2.815201183	BB28_RS16910	-1.276292
BB28_RS00985	-0.91498	BB28_RS08535	-1.13651773	BB28_RS16925	-1.29181018
BB28_RS01100	2.625909	BB28_RS08705	-1.00932034	BB28_RS16995	1.3313529
BB28_RS02355	-1.10542	BB28_RS08865	-1.22933762	BB28_RS17005	2.22995335
BB28_RS02530	1.090521	BB28_RS09015	1.311476361	BB28_RS17035	-0.83020813
BB28_RS02620	1.639369	BB28_RS09885	1.280136819	BB28_RS17420	1.14875507
BB28_RS03055	-1.76973	BB28_RS09970	1.264380403	BB28_RS17730	-0.97529369
BB28_RS03085	1.380092	BB28_RS09975	1.39993082	BB28_RS17790	1.31184188
BB28_RS03125	2.248046	BB28_RS09990	-0.84728354	BB28_RS17900	-1.58289445
BB28_RS03155	1.434102	BB28_RS10080	1.871134503	BB28_RS18830	1.89265297
BB28_RS03295	1.945678	BB28_RS10580	1.272836995	BB28_RS19300	1.14884161
BB28_RS03315	1.084694	BB28_RS11055	-2.03381785	BB28_RS19835	1.66236213
BB28_RS03410	1.361512	BB28_RS11160	1.228348602	BB28_RS21350	1.31291815
BB28_RS03495	1.559922	BB28_RS11310	1.120185399	BB28_RS21600	1.24536179
BB28_RS03550	1.30858	BB28_RS11415	1.242000281	BB28_RS21855	0.98964202
BB28_RS03610	-1.08099	BB28_RS11770	1.474639589	BB28_RS22145	1.71716096
BB28_RS04195	2.086935	BB28_RS11870	2.197831387	BB28_RS22150	1.62420836
BB28_RS04555	2.721495	BB28_RS11875	1.709288581	BB28_RS22170	1.30945158
BB28_RS04635	1.906666	BB28_RS12365	1.701731976	BB28_RS22635	1.09449434
BB28_RS04665	-2.02977	BB28_RS12475	-1.29037061	BB28_RS22640	2.07164684
BB28_RS04675	-0.88031	BB28_RS13450	-0.93366994	BB28_RS22820	-0.93226395
BB28_RS04775	-0.82742	BB28_RS14145	2.755748034	BB28_RS23105	2.93890812
BB28_RS04890	-1.1914	BB28_RS14155	1.541848829	BB28_RS23605	1.2014345
BB28_RS05050	1.519397	BB28_RS14305	1.319341962	BB28_RS23980	2.36086909
BB28_RS05085	2.387072	BB28_RS14535	2.876022712	BB28_RS24010	-1.26815336
BB28_RS05360	1.695193	BB28_RS14540	1.79224702	BB28_RS24385	-0.81044449
BB28_RS05975	1.249914	BB28_RS14570	1.454110318	BB28_RS24560	1.10767217
BB28_RS06135	-1.47909	BB28_RS15075	1.834217443	BB28_RS24805	2.8234673
BB28_RS06200	1.660559	BB28_RS15080	1.218060872		

Appendix 10: DEG only in Biofilm t2.

Gene ID	Biofilm t2 (Log2FC)	Gene ID	Biofilm t2 (Log2FC)	Gene ID	Biofilm t2 (Log2FC)	Gene ID	Biofilm t2 (Log2FC)
BB28_RS00155	1.42	BB28_RS06190	-1.14	BB28_RS13840	1.47	BB28_RS19050	-1.80
BB28_RS00200	-0.85	BB28_RS06235	-1.79	BB28_RS13870	-0.70	BB28_RS19055	-1.48
BB28_RS00210	-0.88	BB28_RS06275	-0.92	BB28_RS13875	1.02	BB28_RS19060	-1.52
BB28_RS00260	-1.13	BB28_RS06290	-1.14	BB28_RS13910	-1.74	BB28_RS19065	-0.99
BB28_RS00305	-0.80	BB28_RS06430	-1.30	BB28_RS13930	-0.82	BB28_RS19100	-1.64
BB28_RS00345	1.88	BB28_RS06505	1.33	BB28_RS13975	-1.65	BB28_RS19105	-1.47
BB28_RS00390	-1.32	BB28_RS06540	-1.40	BB28_RS14005	1.48	BB28_RS19130	-1.99
BB28_RS00410	-1.67	BB28_RS06550	1.26	BB28_RS14010	1.55	BB28_RS19135	-1.84
BB28_RS00655	-1.38	BB28_RS06560	-1.22	BB28_RS14035	1.62	BB28_RS19140	-1.60
BB28_RS00670	-1.06	BB28_RS06590	-1.69	BB28_RS14040	-0.68	BB28_RS19145	-2.02
BB28_RS00720	1.57	BB28_RS06675	1.94	BB28_RS14050	-1.64	BB28_RS19150	-1.97
BB28_RS00810	1.25	BB28_RS06695	-1.08	BB28_RS14060	-1.13	BB28_RS19155	-1.63
BB28_RS00815	1.43	BB28_RS06730	-1.58	BB28_RS14080	-0.58	BB28_RS19160	-1.50
BB28_RS00835	-0.75	BB28_RS06765	2.18	BB28_RS14090	-0.97	BB28_RS19165	-2.34
BB28_RS00875	-1.68	BB28_RS06780	1.94	BB28_RS14095	-0.63	BB28_RS19175	-1.40
BB28_RS00880	-1.25	BB28_RS06810	1.91	BB28_RS14135	-1.82	BB28_RS19180	-1.54
BB28_RS00885	-1.46	BB28_RS06895	-0.59	BB28_RS14385	1.53	BB28_RS19250	2.31
BB28_RS00890	-1.12	BB28_RS06955	1.80	BB28_RS14410	1.26	BB28_RS19255	-0.78
BB28_RS00895	-0.89	BB28_RS06960	1.81	BB28_RS14415	1.89	BB28_RS19305	-1.08
BB28_RS00900	-0.67	BB28_RS07105	-0.73	BB28_RS14445	1.45	BB28_RS19315	-1.33
BB28_RS00905	-1.16	BB28_RS07130	1.22	BB28_RS14450	1.95	BB28_RS19325	-0.93
BB28_RS00935	-1.55	BB28_RS07265	-0.98	BB28_RS14475	1.41	BB28_RS19340	-0.98
BB28_RS00955	1.10	BB28_RS07335	-2.18	BB28_RS14550	-1.06	BB28_RS19375	2.22
BB28_RS00980	-1.57	BB28_RS07375	-3.36	BB28_RS14590	-1.01	BB28_RS19415	-1.31
BB28_RS00995	-1.78	BB28_RS07405	-1.10	BB28_RS14625	-1.26	BB28_RS19440	-1.27
BB28_RS01000	-1.01	BB28_RS07435	-2.02	BB28_RS14630	-1.00	BB28_RS19450	-2.15
BB28_RS01005	-0.71	BB28_RS07465	-0.81	BB28_RS14635	-1.22	BB28_RS19455	-2.04
BB28_RS01115	-1.38	BB28_RS07475	-0.84	BB28_RS14640	-0.94	BB28_RS19460	1.85
BB28_RS01165	1.34	BB28_RS07550	-2.77	BB28_RS14700	-0.88	BB28_RS19465	1.45
BB28_RS01195	0.99	BB28_RS07660	-1.23	BB28_RS14735	-0.97	BB28_RS19470	1.53
BB28_RS01200	3.32	BB28_RS07665	-1.13	BB28_RS14750	-1.27	BB28_RS19480	-0.86
BB28_RS01220	1.37	BB28_RS07930	-0.86	BB28_RS14760	-1.35	BB28_RS19490	3.18
BB28_RS01225	1.78	BB28_RS07980	-1.10	BB28_RS14775	-0.87	BB28_RS19495	3.19
BB28_RS01265	-1.24	BB28_RS08125	-0.60	BB28_RS14815	-1.34	BB28_RS19500	3.12
BB28_RS01270	-0.88	BB28_RS08130	-1.08	BB28_RS14820	-0.65	BB28_RS19515	3.98
BB28_RS01305	1.77	BB28_RS08170	2.97	BB28_RS14850	1.50	BB28_RS19530	1.22
BB28_RS01340	-1.00	BB28_RS08175	2.87	BB28_RS14855	2.29	BB28_RS19545	-1.62
BB28_RS01345	-1.75	BB28_RS08180	1.65	BB28_RS14860	2.76	BB28_RS19550	-0.92
BB28_RS01350	-1.31	BB28_RS08185	2.59	BB28_RS14895	-1.09	BB28_RS19570	-1.64
BB28_RS01355	2.01	BB28_RS08195	3.12	BB28_RS14910	1.76	BB28_RS19760	-1.36
BB28_RS01435	-1.21	BB28_RS08205	1.27	BB28_RS14920	1.26	BB28_RS19780	-1.03

Appendices

Gene ID	Biofilm t2 (Log2FC)	Gene ID	Biofilm t2 (Log2FC)	Gene ID	Biofilm t2 (Log2FC)	Gene ID	Biofilm t2 (Log2FC)
BB28_RS01440	-1.25	BB28_RS08215	1.42	BB28_RS14925	2.41	BB28_RS19800	1.91
BB28_RS01455	-1.14	BB28_RS08325	-1.38	BB28_RS14975	1.58	BB28_RS19875	2.33
BB28_RS01475	1.71	BB28_RS08350	-1.60	BB28_RS15015	-1.28	BB28_RS19910	-1.34
BB28_RS01625	-0.62	BB28_RS08380	-1.03	BB28_RS15040	1.42	BB28_RS19940	4.70
BB28_RS01675	1.67	BB28_RS08400	-0.91	BB28_RS15045	1.52	BB28_RS19945	4.14
BB28_RS01755	-0.97	BB28_RS08440	1.64	BB28_RS15050	1.90	BB28_RS19955	2.14
BB28_RS01800	1.63	BB28_RS08490	1.72	BB28_RS15110	1.35	BB28_RS20015	-1.09
BB28_RS01810	3.51	BB28_RS08500	1.39	BB28_RS15255	1.22	BB28_RS20030	-0.97
BB28_RS01815	3.74	BB28_RS08580	-1.18	BB28_RS15300	-1.09	BB28_RS20080	-0.73
BB28_RS01820	4.63	BB28_RS08585	2.51	BB28_RS15395	-0.79	BB28_RS20085	-0.62
BB28_RS01825	4.05	BB28_RS08640	1.52	BB28_RS15425	-1.50	BB28_RS20160	-0.98
BB28_RS01830	4.90	BB28_RS08660	1.76	BB28_RS15460	3.38	BB28_RS20165	1.54
BB28_RS01835	4.45	BB28_RS08695	-0.87	BB28_RS15465	1.17	BB28_RS20270	-1.46
BB28_RS01840	5.03	BB28_RS08815	-0.77	BB28_RS15480	1.28	BB28_RS20385	-1.83
BB28_RS01880	1.29	BB28_RS08820	-1.45	BB28_RS15485	1.68	BB28_RS20505	-1.28
BB28_RS01885	1.55	BB28_RS09135	1.83	BB28_RS15540	-0.64	BB28_RS20565	4.82
BB28_RS01910	2.15	BB28_RS09170	1.71	BB28_RS15570	1.93	BB28_RS20570	3.60
BB28_RS01945	-1.13	BB28_RS09290	2.20	BB28_RS15605	1.56	BB28_RS20575	1.91
BB28_RS01950	-2.18	BB28_RS09315	1.67	BB28_RS15610	-1.81	BB28_RS20665	2.39
BB28_RS02010	-1.28	BB28_RS09320	2.74	BB28_RS15660	-1.39	BB28_RS20675	-0.85
BB28_RS02065	-1.34	BB28_RS09335	2.78	BB28_RS15665	-1.64	BB28_RS20690	-0.73
BB28_RS02085	1.01	BB28_RS09390	1.79	BB28_RS15745	1.66	BB28_RS20725	-1.58
BB28_RS02150	2.76	BB28_RS09395	2.79	BB28_RS15800	1.48	BB28_RS20730	-1.85
BB28_RS02155	1.89	BB28_RS09400	-1.15	BB28_RS15820	-1.30	BB28_RS20765	-1.15
BB28_RS02160	2.69	BB28_RS09405	1.29	BB28_RS15825	-1.82	BB28_RS20780	-2.73
BB28_RS02170	-1.18	BB28_RS09440	-1.21	BB28_RS15850	1.31	BB28_RS20790	-1.20
BB28_RS02200	-1.20	BB28_RS09450	1.44	BB28_RS15875	1.99	BB28_RS20860	-1.77
BB28_RS02230	-0.91	BB28_RS09455	1.70	BB28_RS15915	-0.66	BB28_RS20905	-1.30
BB28_RS02310	1.30	BB28_RS09500	-1.43	BB28_RS15940	1.93	BB28_RS20910	-1.20
BB28_RS02335	-0.95	BB28_RS09720	-0.96	BB28_RS15975	-0.81	BB28_RS20980	-1.14
BB28_RS02385	-0.75	BB28_RS09765	-1.39	BB28_RS16170	-0.83	BB28_RS21060	1.97
BB28_RS02405	2.13	BB28_RS09870	-1.43	BB28_RS16175	-1.37	BB28_RS21090	-0.72
BB28_RS02415	-1.37	BB28_RS09895	1.64	BB28_RS16215	2.23	BB28_RS21180	-0.81
BB28_RS02455	-1.31	BB28_RS09930	-1.16	BB28_RS16220	1.92	BB28_RS21200	-1.38
BB28_RS02475	-1.63	BB28_RS10135	-1.23	BB28_RS16275	2.57	BB28_RS21265	-1.15
BB28_RS02615	2.30	BB28_RS10200	-1.64	BB28_RS16280	2.39	BB28_RS21300	-1.39
BB28_RS02700	3.32	BB28_RS10260	-0.95	BB28_RS16285	1.88	BB28_RS21305	-1.45
BB28_RS02705	2.29	BB28_RS10365	-0.94	BB28_RS16350	1.16	BB28_RS21325	-1.03
BB28_RS02725	-1.66	BB28_RS10390	-0.99	BB28_RS16355	1.92	BB28_RS21330	-1.10
BB28_RS02735	2.15	BB28_RS10470	1.79	BB28_RS16360	2.54	BB28_RS21340	-0.62
BB28_RS02750	2.07	BB28_RS10490	1.11	BB28_RS16365	2.31	BB28_RS21355	-1.34
BB28_RS02780	-0.87	BB28_RS10540	-1.38	BB28_RS16420	1.83	BB28_RS21360	-0.75
BB28_RS02790	1.44	BB28_RS10570	-1.19	BB28_RS16435	-1.16	BB28_RS21400	-0.77
BB28_RS02845	2.03	BB28_RS10615	1.58	BB28_RS16450	-0.87	BB28_RS21440	-0.75

Appendices

Gene ID	Biofilm t2 (Log2FC)	Gene ID	Biofilm t2 (Log2FC)	Gene ID	Biofilm t2 (Log2FC)	Gene ID	Biofilm t2 (Log2FC)
BB28_RS02915	-1.17	BB28_RS10645	-1.08	BB28_RS16525	-1.00	BB28_RS21465	-1.16
BB28_RS03040	-0.88	BB28_RS10675	1.92	BB28_RS16530	-0.83	BB28_RS21525	-1.62
BB28_RS03170	2.71	BB28_RS10705	2.60	BB28_RS16685	1.89	BB28_RS21540	-0.87
BB28_RS03190	2.17	BB28_RS10710	2.06	BB28_RS16740	-0.79	BB28_RS21605	-1.38
BB28_RS03210	2.11	BB28_RS10715	1.36	BB28_RS16750	1.46	BB28_RS21635	-1.00
BB28_RS03240	1.79	BB28_RS10790	-0.76	BB28_RS16755	-1.12	BB28_RS21700	2.21
BB28_RS03280	-0.82	BB28_RS10805	1.23	BB28_RS16815	2.54	BB28_RS21710	1.42
BB28_RS03285	-0.78	BB28_RS10820	2.54	BB28_RS16840	1.68	BB28_RS21720	1.89
BB28_RS03325	3.27	BB28_RS10825	1.65	BB28_RS16855	1.54	BB28_RS21725	1.62
BB28_RS03385	1.60	BB28_RS10830	1.93	BB28_RS16895	-0.97	BB28_RS21735	1.66
BB28_RS03435	3.13	BB28_RS10835	1.73	BB28_RS16905	-0.85	BB28_RS21790	2.34
BB28_RS03470	1.44	BB28_RS10875	-1.81	BB28_RS16915	-0.72	BB28_RS21795	1.66
BB28_RS03490	-1.97	BB28_RS10940	1.40	BB28_RS16955	1.50	BB28_RS21805	2.09
BB28_RS03535	1.51	BB28_RS10955	1.74	BB28_RS16985	-1.50	BB28_RS21930	1.60
BB28_RS03590	3.44	BB28_RS10965	1.53	BB28_RS17020	2.64	BB28_RS22060	1.23
BB28_RS03615	-1.13	BB28_RS10970	1.49	BB28_RS17050	1.48	BB28_RS22110	1.94
BB28_RS03800	-1.26	BB28_RS11075	-1.38	BB28_RS17075	-1.20	BB28_RS22135	-0.74
BB28_RS03885	1.02	BB28_RS11085	-1.44	BB28_RS17090	2.36	BB28_RS22205	1.77
BB28_RS03910	-0.89	BB28_RS11090	-1.26	BB28_RS17095	1.31	BB28_RS22225	-1.86
BB28_RS03955	-1.47	BB28_RS11130	5.02	BB28_RS17100	3.09	BB28_RS22250	-1.02
BB28_RS04015	-1.41	BB28_RS11135	4.41	BB28_RS17140	-0.62	BB28_RS22265	2.44
BB28_RS04020	1.13	BB28_RS11140	4.47	BB28_RS17145	-0.79	BB28_RS22295	1.55
BB28_RS04025	-0.60	BB28_RS11145	3.41	BB28_RS17180	1.64	BB28_RS22335	1.52
BB28_RS04085	-1.90	BB28_RS11150	3.43	BB28_RS17210	-1.28	BB28_RS22350	-1.70
BB28_RS04110	1.15	BB28_RS11190	2.69	BB28_RS17315	1.28	BB28_RS22645	-2.02
BB28_RS04135	-0.95	BB28_RS11205	-1.25	BB28_RS17320	3.36	BB28_RS22660	-1.28
BB28_RS04160	-1.11	BB28_RS11215	1.88	BB28_RS17390	1.55	BB28_RS22695	-0.73
BB28_RS04200	1.15	BB28_RS11280	1.06	BB28_RS17435	-1.20	BB28_RS22720	-1.42
BB28_RS04205	1.47	BB28_RS11350	3.41	BB28_RS17460	-1.65	BB28_RS22730	1.22
BB28_RS04215	-1.07	BB28_RS11355	1.82	BB28_RS17465	-1.40	BB28_RS22815	-1.55
BB28_RS04240	1.23	BB28_RS11370	-0.89	BB28_RS17535	-1.15	BB28_RS22965	-0.90
BB28_RS04245	-1.57	BB28_RS11405	2.25	BB28_RS17565	1.43	BB28_RS22970	-1.45
BB28_RS04260	1.22	BB28_RS11475	-1.33	BB28_RS17570	4.19	BB28_RS23000	-1.13
BB28_RS04285	1.25	BB28_RS11645	1.64	BB28_RS17575	2.18	BB28_RS23050	-1.42
BB28_RS04290	-1.74	BB28_RS12110	1.25	BB28_RS17580	3.00	BB28_RS23065	2.39
BB28_RS04345	-0.83	BB28_RS12135	-0.84	BB28_RS17615	-1.35	BB28_RS23070	1.70
BB28_RS04445	-1.27	BB28_RS12145	1.38	BB28_RS17635	2.85	BB28_RS23080	2.94
BB28_RS04455	-0.91	BB28_RS12160	1.83	BB28_RS17690	-0.65	BB28_RS23090	2.62
BB28_RS04550	-2.80	BB28_RS12165	2.87	BB28_RS17695	-0.65	BB28_RS23095	3.60
BB28_RS04585	-0.67	BB28_RS12170	2.19	BB28_RS17720	2.42	BB28_RS23115	2.27
BB28_RS04645	2.40	BB28_RS12175	3.16	BB28_RS17725	2.33	BB28_RS23140	1.36
BB28_RS04650	3.08	BB28_RS12180	2.49	BB28_RS17735	-1.31	BB28_RS23150	-1.18
BB28_RS04660	-0.64	BB28_RS12185	1.92	BB28_RS17740	2.16	BB28_RS23155	2.16
BB28_RS04755	-1.24	BB28_RS12225	1.47	BB28_RS17745	1.28	BB28_RS23360	-0.74

Appendices

Gene ID	Biofilm t2 (Log2FC)	Gene ID	Biofilm t2 (Log2FC)	Gene ID	Biofilm t2 (Log2FC)	Gene ID	Biofilm t2 (Log2FC)
BB28_RS04795	-1.08	BB28_RS12235	3.66	BB28_RS17770	-0.63	BB28_RS23410	-1.34
BB28_RS04865	1.86	BB28_RS12240	1.70	BB28_RS17785	1.21	BB28_RS23440	-1.90
BB28_RS04895	-0.79	BB28_RS12280	1.41	BB28_RS17840	-0.82	BB28_RS23445	-2.62
BB28_RS04905	-1.23	BB28_RS12330	1.56	BB28_RS17980	-0.78	BB28_RS23450	-1.24
BB28_RS04970	1.57	BB28_RS12340	1.49	BB28_RS18000	-1.35	BB28_RS23550	1.34
BB28_RS05015	1.88	BB28_RS12385	1.48	BB28_RS18005	1.47	BB28_RS23590	1.89
BB28_RS05045	1.53	BB28_RS12405	1.58	BB28_RS18075	1.53	BB28_RS23625	4.97
BB28_RS05090	2.18	BB28_RS12465	-0.67	BB28_RS18090	-1.16	BB28_RS23630	1.73
BB28_RS05095	3.01	BB28_RS12495	-0.77	BB28_RS18135	-0.72	BB28_RS23655	3.05
BB28_RS05100	2.02	BB28_RS12515	1.43	BB28_RS18275	2.92	BB28_RS23845	2.22
BB28_RS05110	1.69	BB28_RS12570	-1.06	BB28_RS18285	1.86	BB28_RS23865	2.86
BB28_RS05165	-0.87	BB28_RS12600	-0.61	BB28_RS18290	2.60	BB28_RS23915	3.13
BB28_RS05195	3.42	BB28_RS12685	-0.81	BB28_RS18295	2.19	BB28_RS23920	4.38
BB28_RS05200	3.78	BB28_RS12710	1.74	BB28_RS18300	3.69	BB28_RS23925	3.53
BB28_RS05205	3.69	BB28_RS12730	-1.07	BB28_RS18330	-1.23	BB28_RS23930	-0.85
BB28_RS05210	3.92	BB28_RS12840	1.61	BB28_RS18355	2.10	BB28_RS24080	-1.45
BB28_RS05215	3.00	BB28_RS12860	1.59	BB28_RS18360	1.20	BB28_RS24090	-1.10
BB28_RS05220	2.33	BB28_RS12865	2.16	BB28_RS18375	1.49	BB28_RS24120	2.20
BB28_RS05265	1.83	BB28_RS12880	3.19	BB28_RS18440	2.52	BB28_RS24130	1.84
BB28_RS05270	1.50	BB28_RS12885	1.79	BB28_RS18450	-1.24	BB28_RS24175	-1.64
BB28_RS05275	2.61	BB28_RS12900	2.83	BB28_RS18485	1.74	BB28_RS24185	1.88
BB28_RS05280	1.64	BB28_RS13010	-0.87	BB28_RS18490	-0.85	BB28_RS24250	-0.79
BB28_RS05325	2.00	BB28_RS13055	1.84	BB28_RS18620	-0.98	BB28_RS24325	1.05
BB28_RS05350	1.42	BB28_RS13065	-1.57	BB28_RS18630	1.70	BB28_RS24360	-1.79
BB28_RS05385	-0.86	BB28_RS13080	-0.91	BB28_RS18710	-1.50	BB28_RS24380	1.00
BB28_RS05640	1.39	BB28_RS13105	-0.94	BB28_RS18720	-1.01	BB28_RS24440	-0.68
BB28_RS05655	1.83	BB28_RS13125	1.53	BB28_RS18730	-1.21	BB28_RS24450	2.41
BB28_RS05685	-1.42	BB28_RS13170	1.23	BB28_RS18745	-0.83	BB28_RS24475	-1.39
BB28_RS05700	1.37	BB28_RS13380	2.10	BB28_RS18805	-1.41	BB28_RS24570	-1.58
BB28_RS05730	1.38	BB28_RS13435	1.77	BB28_RS18840	-1.09	BB28_RS24655	-1.02
BB28_RS05740	1.91	BB28_RS13445	1.60	BB28_RS18880	0.99	BB28_RS24685	-0.97
BB28_RS05840	-1.47	BB28_RS13465	-0.72	BB28_RS18920	-1.44	BB28_RS24695	-0.65
BB28_RS05845	-0.87	BB28_RS13545	-1.50	BB28_RS18925	-1.26	BB28_RS24700	-1.21
BB28_RS05985	-1.09	BB28_RS13625	1.58	BB28_RS18940	-1.37	BB28_RS24800	-2.42
BB28_RS06010	-0.80	BB28_RS13715	-1.03	BB28_RS18945	-1.91	rnpB	3.14
BB28_RS06030	-0.90	BB28_RS13730	1.24	BB28_RS18990	-1.86	rrf	4.91
BB28_RS06080	-0.76	BB28_RS13740	-0.85	BB28_RS19010	-0.97		
BB28_RS06090	-0.81	BB28_RS13830	1.79	BB28_RS19040	-1.17		

References

- Abate G, Hamzabegovic F, Eickhoff CS, Hoft DF. BCG Vaccination Induces *M. avium* and *M. abscessus* Cross-Protective Immunity. *Front Immunol* 2019;10:1–10. <https://doi.org/10.3389/fimmu.2019.00234>.
- Abidi SH, Ahmed K, Sherwani SK, Bibi N, U.Kazmi S. Detection of *Mycobacterium Smegmatis* Biofilm and its Control by Natural Agents. *Int J Curr Microbiol Appl Sci* 2014;3:801–12.
- Abrahams KA, Besra GS. Mycobacterial cell wall biosynthesis: a multifaceted antibiotic target. *Parasitology* 2018;116–33. <https://doi.org/10.1017/S0031182016002377>.
- Ackart DF, Hascall-Dove L, Caceres SM, Kirk NM, Podell BK, Melander C, et al. Expression of antimicrobial drug tolerance by attached communities of *Mycobacterium tuberculosis*. *Pathog Dis* 2014a. <https://doi.org/10.1111/2049-632X.12144>.
- Ackart DF, Lindsey EA, Podell BK, Melander RJ, Basaraba RJ, Melander C. Reversal of *Mycobacterium tuberculosis* phenotypic drug resistance by 2-aminoimidazole-based small molecules. *Pathog Dis* 2014b;70:370–8. <https://doi.org/10.1111/2049-632X.12143>.
- Alderwick LJ, Harrison J, Lloyd GS, Birch HL. The Mycobacterial Cell Wall — Peptidoglycan and Arabinogalactan. *Cold Spring Harb Perspect Med* 2015;5:1–16. <https://doi.org/10.1101/cshperspect.a021113>.
- Alderwick LJ, Lloyd GS, Lloyd AJ, Lovering AL, Eggeling L, Besra GS. Biochemical characterization of the *Mycobacterium tuberculosis* phosphoribosyl-pyrophosphate synthetase. *Glycobiology* 2010;21:410–25.
- Anand A, Verma P, Singh AK, Kaushik S, Pandey R, Shi C, et al. Polyketide Quinones Are Alternate Intermediate Electron Carriers during Mycobacterial Respiration in Oxygen-Deficient Niches. *Mol Cell* 2015;60:637–50. <https://doi.org/10.1016/j.molcel.2015.10.016>.
- Anderson GG, Palermo JJ, Schilling JD, Roth R, Heuser J, Hultgren S. Intracellular Bacterial Biofilm-Like Pods in Urinary Tract Infections. *Science* (80-) 2001;301:105–7.
- Aparna MS, Yadav S. Biofilms: microbes and disease. *Brazilian J Infect Dis* 2008;12:526–30. <https://doi.org/10.1590/S1413-86702008000600016>.
- Aung TT, Chor WHJ, Yam JKH, Givskov M, Yang L, Beuerman RW. Discovery of novel antimycobacterial drug therapy in biofilm of pathogenic nontuberculous mycobacterial keratitis. *Ocul Surf* 2017;1–14. <https://doi.org/10.1016/j.jtos.2017.06.002>.
- Aung TT, Kuok J, Yam H, Lin S, Salleh SM, Givskov M, et al. Biofilms of Pathogenic Nontuberculous Mycobacteria Targeted by New Therapeutic Approaches. *Antimicrob Agents Chemother* 2016;60:24–35. <https://doi.org/10.1128/AAC.01509-15>.Address.
- Aylward GW, Stacey AR, Marsh RJ. *Mycobacterium chelonae* infection of a corneal graft. *Br J Ophthalmol* 1987;71:690–3.
- Banerjee A, Dubnau E, Quemard A, Balasubramanian V, Um K, Wilson T, et al. *inhA*, a gene encoding a target for isoniazid and ethionamide in *Mycobacterium tuberculosis*. *Science* (80-) 1994;263:227–30. <https://doi.org/10.1126/science.8284673>.
- Bansal-mutalik R, Nikaido H. Mycobacterial outer membrane is a lipid bilayer and the inner membrane is unusually rich in diacyl phosphatidylinositol dimannosides. *PNAS* 2014;111:4958–63. <https://doi.org/10.1073/pnas.1403078111>.
- Barry CE, Lee RE, Mdluli K, Sampson AE, Schroeder BG, Slayden RA, et al. Mycolic acids: structure, biosynthesis and physiological functions. *Prog Lipid Res* 1998;37:143–79. [https://doi.org/10.1016/S0163-7827\(98\)00008-3](https://doi.org/10.1016/S0163-7827(98)00008-3).
- Basu P, Sandhu N, Bhatt A, Singh A, Balhana R, Gobe I, et al. The anaplerotic node is essential for the intracellular survival of *Mycobacterium tuberculosis*. *J Biol Chem* 2018;293:5695–704. <https://doi.org/10.1074/jbc.RA118.001839>.
- Beier BD, Quivey RG, Berger AJ. Identification of different bacterial species in biofilms using confocal Raman microscopy. *J Biomed Opt* 2010;15:066001. <https://doi.org/10.1117/1.3505010>.
- Belisle JT, Vissa VD, Sievert T, Takayama K, Brennan PJ, Besra GS. Role of the major antigen of *Mycobacterium tuberculosis* in cell wall biogenesis. *Science* 1997;276:1420–2.

<https://doi.org/10.1126/science.276.5317.1420>.

Besra G, KH K, McNeil M, Dell A, Morris H, Brennan P. A new interpretation of the structure of the mycolyl-arabinogalactan complex of *Mycobacterium tuberculosis* as revealed through characterization of oligoglycosylalditol fragments by fast-atom bombardment mass spectrometry and ¹H nuclear magnetic resonan. *Biochemistry* 1995;4257–66.

Betts JC, Lukey PT, Robb LC, McAdam R a., Duncan K. Evaluation of a nutrient starvation model of *Mycobacterium tuberculosis* persistence by gene and protein expression profiling. *Mol Microbiol* 2002;43:717–31. <https://doi.org/10.1046/j.1365-2958.2002.02779.x>.

Bhamidi S, Scherman MS, Rithner CD, Prenni JE, Chatterjee D, Khoo K-H, et al. The identification and location of succinyl residues and the characterization of the interior arabinan region allow for a model of the complete primary structure of *Mycobacterium tuberculosis* mycolyl arabinogalactan. *J Biol Chem* 2008;283:12992–3000. <https://doi.org/10.1074/jbc.M800222200>.

Bhatt A, Brown AK, Singh A, Minnikin DE, Besra GS. Loss of a mycobacterial gene encoding a reductase leads to an altered cell wall containing beta-oxo-mycolic acid analogs and accumulation of ketones. *Chem Biol* 2008;15:930–9.

Bhatt A, Molle V, Besra GS, Jacobs WRJ, Kremer L. *Mycobacterium tuberculosis* FAS-II condensing enzymes: their role in mycolic acid biosynthesis, acid-fastness, pathogenesis and in future drug development. *Mol Microbiol* 2007;64:1442–54.

Billman-Jacobe H, McConville M, Haites R, Kovacevic S, Coppel R. Identification of a peptide synthetase involved in the biosynthesis of glycopeptidolipids of *Mycobacterium smegmatis*. *Mol Microbiol* 1999;33:1244–53.

Binić I, Janković A, Ljubenović M, Gligorićević J, Jančić S, Janković D. *Mycobacterium chelonae* Infection Due to Black Tattoo Ink Dilution. *Am J Clin Dermatol* 2011;12:1. <https://doi.org/10.2165/11589500-000000000-00000>.

Bjarnsholt T, Ciofu O, Molin S, Givskov M, Høiby N. Applying insights from biofilm biology to drug development — can a new approach be developed? *Nat Rev Drug Discov* 2013;12:791–808. <https://doi.org/10.1038/nrd4000>.

Blanc P, Dutronc H, Peuchant O, Dauchy F-A, Cazanave C, Neau D, et al. Nontuberculous *Mycobacterial* Infections in a French Hospital: A 12-Year Retrospective Study. *PLoS One* 2016;11:e0168290. <https://doi.org/10.1371/journal.pone.0168290>.

Brady RA, Leid JG, Calhoun JH, Costerton JW, Shirtliff ME. Oteomyelitis and the role of biofilms in chronic infection. *FEMS Immunol* 2007;52.

Brennan PJ, Nikaido H. The envelope of mycobacteria. *Annu Rev Biochem* 1995;64:29–63. <https://doi.org/10.1146/annurev.bi.64.070195.000333>.

Brown-Elliott B a., Nash K a., Wallace RJ. Antimicrobial susceptibility testing, drug resistance mechanisms, and therapy of infections with nontuberculous mycobacteria. *Clin Microbiol Rev* 2012;25:545–82. <https://doi.org/10.1128/CMR.05030-11>.

Brown-Elliott BA, Philley J V. Rapidly Growing *Mycobacteria*. *Microbiol Spectr* 2017;5. <https://doi.org/10.1128/microbiolspec.TNMI7-0027-2016>.

Brown AK, Bhatt A, Singh A, Saparia E, Evans AF, Besra G. Identification of the dehydratase component of the mycobacterial mycolic acid-synthesizing fatty acid synthase-II complex. *Microbiology* 2007;153:4166–73.

Brown L, Wolf JM, Prados-Rosales R, Casadevall A. Through the wall: Extracellular vesicles in Gram-positive bacteria, mycobacteria and fungi. *Nat Rev Microbiol* 2015;13:620–30. <https://doi.org/10.1038/nrmicro3480>.

Buijtel PCAM, Willemse-Erix HFM, Petit PLC, Endtz HP, Puppels GJ, Verbrugh HA, et al. Rapid Identification of *Mycobacteria* by Raman Spectroscopy. *J Clin Microbiol* 2008;46:961–5. <https://doi.org/10.1128/JCM.01763-07>.

Butler HJ, Ashton L, Bird B, Cinque G, Curtis K, Dorney J, et al. Using Raman spectroscopy to

- characterize biological materials. *Nat Protoc* 2016;11:664–87. <https://doi.org/10.1038/nprot.2016.036>.
- Bylund J, Burgess LA, Cescutti P, Ernst RK, Speert DP. Exopolysaccharides from *Burkholderia cenocepacia* inhibit neutrophil chemotaxis and scavenge reactive oxygen species. *J Biol Chem* 2006;281:2526–32.
- Calmette A. L'infection bacillaire et la tuberculose chez l'homme et chez les animaux: processus d'infection, et de defense, étude biologique et expérimentale. Masson, et cie; 1922.
- Campbell SM, Winkelmann RR, Sammons DL. Erythema induratum caused by *Mycobacterium chelonae* in an immunocompetent patient. *J Clin Aesthet Dermatol* 2013;6:38–40.
- Chakraborty P, Kumar A. The extracellular matrix of mycobacterial biofilms: could we shorten the treatment of mycobacterial infections? *Microb Cell* 2019;6:105–22. <https://doi.org/10.15698/mic2019.02.667>.
- Chatterjee D, Lowell K, Rivoire B, McNeil MR, Brennan PJ. Lipoarabinomannan of *Mycobacterium tuberculosis*. Capping with mannosyl residues in some strains. *J Biol Chem* 1992;267:6234–9.
- de Chaumont F, Dallongeville S, Chenouard N, Hervé N, Pop S, Provoost T, et al. Icy: an open bioimage informatics platform for extended reproducible research. *Nat Methods* 2012;9:690–6. <https://doi.org/10.1038/nmeth.2075>.
- Chen JM, German GJ, Alexander DC, Ren H, Tan T, Liu J. Roles of Lsr2 in Colony Morphology and Biofilm Formation of *Mycobacterium smegmatis*. *J Bacteriol* 2006;188:633–41. <https://doi.org/10.1128/JB.188.2.633>.
- Chowdhury H, Comyn O, Jones G, Nanavaty M. *Mycobacterium chelonae* in a tectonic corneal graft. *Oman J Ophthalmol* 2016;9:177. <https://doi.org/10.4103/0974-620X.192292>.
- Chua SL, Hoong Yam JK, Chen Y, Munk Vejborg R, Chyuan Tan BG, Kjelleberg S, et al. Dispersed cells represent a distinct stage in the transition from bacterial biofilm to planktonic lifestyle. *Nat Commun* 2014;5:4462.
- Cornforth DM, Dees JL, Ibberson CB, Huse HK, Mathiesen IH, Kirketerp-Møller K, et al. *Pseudomonas aeruginosa* transcriptome during human infection. *Proc Natl Acad Sci U S A* 2018;115. <https://doi.org/10.1073/pnas.1717525115>.
- Cowman S, Burns K, Benson S, Wilson R, Loebinger MR. The antimicrobial susceptibility of non-tuberculous mycobacteria. *J Infect* 2016;72:324–31. <https://doi.org/10.1016/j.jinf.2015.12.007>.
- Crellin PK, Luo C, Morita YS. Metabolism of Plasma Membrane Lipids in *Mycobacteria* and *Corynebacteria*. *Lipid Metab* 2013;460. <https://doi.org/10.5772/52781>.
- Crichton RR, Charleatoux-wauters M. Iron transport and storage. *Nature* 1976;260:466–466. <https://doi.org/10.1038/260466b0>.
- Cui T, He Z. C-di-GMP signaling and implications for pathogenesis of *Mycobacterium tuberculosis*. *Chinese Sci Bull* 2012;57:4387–93. <https://doi.org/10.1007/s11434-012-5298-5>.
- Dabó H, Santos V, Marinho A, Ramos A, Carvalho T, Ribeiro M, et al. Nontuberculous mycobacteria in respiratory specimens: clinical significance at a tertiary care hospital in the north of Portugal. *J Bras Pneumol* 2015;41:292–4. <https://doi.org/10.1590/S1806-37132015000000005>.
- Daffe M, Brennan P, McNeil M. Predominant structural features of the cell wall arabinogalactan of *Mycobacterium tuberculosis* as revealed through characterization of oligoglycosyl alditol fragments by gas chromatography/mass spectrometry and by ¹H and ¹³C NMR analyses. *J Biol Chem* 1990;265:4334–43.
- Daffé M, Crick DC, Jackson M. Genetics of Capsular Polysaccharides and Cell Envelope (Glyco)lipids. *Microbiol Spectr* 2014;2:1–78. <https://doi.org/10.1128/microbiolspec.MGM2-0021-2013>.
- Daniel J, Oh TJ, Lee CM, Kolattukudy PE. AccD6, a member of the Fas II locus, is a functional carboxyltransferase subunit of the acyl-coenzyme A carboxylase in *Mycobacterium tuberculosis*. *J Bacteriol* 2007;189:11–7.
- Davey ME, O'toole G a. Microbial biofilms: from ecology to molecular genetics. *Microbiol Mol Biol*

Rev 2000;64:847–67.

Deshayes C, Bach H, Euphrasie D, Attarian R, Coureuil M, Sougakoff W, et al. Mmps4 promotes glycopeptidolipids biosynthesis and export in *Mycobacterium smegmatis*. *Mol Microbiol* 2010;78:989–1003.

Diem M. *Modern Vibrational Spectroscopy and Micro-Spectroscopy*. Chichester, UK: John Wiley & Sons, Ltd; 2015. <https://doi.org/10.1002/9781118824924>.

Dietrich G, Mollenkopf H-J, Weber H, Knapp B, Diehl K-D, Hess J, et al. Cultivation of *Mycobacterium bovis* BCG in bioreactors. *J Biotechnol* 2002;96:259–70.

Dinadayala P, Sambou T, Daffé M. Comparative structural analyses of the α -glucan and glycogen from *Mycobacterium bovis*. *Glycobiology* 2008;18:502–8. <https://doi.org/10.1093/glycob/cwn031>.

Distel JW, Hatton JF, Gillespie MJ. Biofilm formation in medicated root canals. *J Endod* 2002;28:689–93. <https://doi.org/10.1097/00004770-200210000-00003>.

Dobson G, Minnikin DE, Minnikin SM, Parlett JH, Goodfellow MR, Scott S, et al. Systematic analysis of complex mycobacterial lipids. *Acad Press* 1985.

Draper P, Rees RJW. The nature of the electron-transparent zone that surrounds *Mycobacterium lepraemurium*. *J Gen Microbiol* 1973;7:79–87.

Eckstein T, Belisle J, Inamine J. Proposed pathway for the biosynthesis of serovar-specific glycopeptidolipids in *Mycobacterium avium* serovar 2. *Microbiology* 2003;149:2797–807.

Van Ende C, Wilmes D, Lecouvet FE, Labriola L, Cuvelier R, Van Ingelgem G, et al. Cutaneous *Mycobacterium chelonae* infection distal to the arteriovenous fistula. *Clin Kidney J* 2016;9:sfw073. <https://doi.org/10.1093/ckj/sfw073>.

Esteban J, García-Coca M. *Mycobacterium* biofilms. *Front Microbiol* 2018;8:1–8. <https://doi.org/10.3389/fmicb.2017.02651>.

Falkinham JO. Challenges of NTM drug development. *Front Microbiol* 2018;9:1–7. <https://doi.org/10.3389/fmicb.2018.01613>.

Falkinham JO. Surrounded by mycobacteria: Nontuberculous mycobacteria in the human environment. *J Appl Microbiol* 2009;107:356–67. <https://doi.org/10.1111/j.1365-2672.2009.04161.x>.

Fang Z, Sampson SL, Warren RM, Gey van Pittius NC, Newton-Foot M. Iron acquisition strategies in mycobacteria. *Tuberculosis* 2015;1–8. <https://doi.org/10.1016/j.tube.2015.01.004>.

Faria S, Joao I, Jordao L. General Overview on Nontuberculous Mycobacteria, Biofilms, and Human Infection. *J Pathog* 2015;2015:1–10. <https://doi.org/10.1155/2015/809014>.

Fernández-Cabezón L, Galán B, García JL. New insights on steroid biotechnology. *Front Microbiol* 2018;9. <https://doi.org/10.3389/fmicb.2018.00958>.

Flemming HC, Wingender J. The biofilm matrix. *Nat Rev Microbiol* 2010;8:623–33. <https://doi.org/10.1038/nrmicro2415>.

Flores-Valdez M a, Aceves-Sánchez MDJ, Montero-Pérez S a, Sánchez-López a D, Gutiérrez-Pabello J a, Hernández-Pando R. Vaccination of mice with recombinant bacille Calmette-Guérin harboring Rv1357c protects similarly to native BCG. *Int J Tuberc Lung Dis* 2012;16:774–6. <https://doi.org/10.5588/ijtld.11.0735>.

Flores-Valdez MA, de Jesús Aceves-Sánchez M, Pedroza-Roldán C, Vega-Domínguez PJ, Prado-Montes de Oca E, Bravo-Madrigal J, et al. The cyclic di-GMP phosphodiesterase gene R v1357c / BCG 1419c affects BCG Pellicle production and In Vivo maintenance. *IUBMB Life* 2015;67:129–38. <https://doi.org/10.1002/iub.1353>.

Fogelson SB, Camus AC, Walter Lorenz W, Vasireddy R, Vasireddy S, Smith T, et al. Variation among human, veterinary and environmental *Mycobacterium chelonae*-abscessus complex isolates observed using core genome phylogenomic analysis, targeted gene comparison, and anti-microbial susceptibility patterns. *PLoS One* 2019;14:1–20. <https://doi.org/10.1371/journal.pone.0214274>.

- Franklin M, Chang C, Akiyama T, Bothner B. New Technologies for Studying Biofilms. *Microbiol Spectr* 2015;3:1–41.
- Freeman R, Geier H, Weigel KM, Do J, Ford TE, Cangelosi G a. Roles for cell wall glycopeptidolipid in surface adherence and planktonic dispersal of *Mycobacterium avium*. *Appl Environ Microbiol* 2006;72:7554–8. <https://doi.org/10.1128/AEM.01633-06>.
- Fujiwara N, Ohara N, Ogawa M, Maeda S, Naka T, Taniguchi H, et al. Glycopeptidolipid of *Mycobacterium smegmatis* J15cs affects morphology and survival in host cells. *PLoS One* 2015;10:1–11. <https://doi.org/10.1371/journal.pone.0126813>.
- Gago G, Diacovich L, Gramajo H. Lipid metabolism and its implication in mycobacteria – host interaction. *Curr Opin Microbiol* 2018;41:36–42. <https://doi.org/https://doi.org/10.1016/j.mib.2017.11.020>.
- Gambino M, Cappitelli F. Mini-review : Biofilm responses to oxidative stress. *Biofouling* 2016;7014:1–13. <https://doi.org/10.1080/08927014.2015.1134515>.
- Gande R, Gibson KJ, Brown AK, Krumbach K, Dover LG, Sahm H, et al. Acyl-CoA carboxylases (accD2 and accD3), together with a unique polyketide synthase (Cg-pks), are key to mycolic acid biosynthesis in *Corynebacteriaceae* such as *Corynebacterium glutamicum* and *Mycobacterium tuberculosis*. *J Biol Chem* 2004;279:44847–57.
- Gao LY, Laval F, Lawson EH, Groger RK, Woodruff A, Morisaki JH, et al. Requirement for kasB in *Mycobacterium* mycolic acid biosynthesis, cell wall impermeability and intracellular survival: implications for therapy. *Mol Microbiol* 2003;49:1547–63.
- García-Fernández J, Papavinasasundaram K, Galán B, Sassetti CM, García JL. Molecular and functional analysis of the mce4 operon in *Mycobacterium smegmatis*. *Environ Microbiol* 2017;19:3689–99. <https://doi.org/10.1111/1462-2920.13869>.
- Gomes LC, Moreira JMR, Simões M, Melo LF, Mergulhão FJ. Biofilm Localization in the Vertical Wall of Shaking 96-Well Plates. *Scientifica (Cairo)* 2014;2014:1–6. <https://doi.org/10.1155/2014/231083>.
- González-Machado C, Capita R, Riesco-Peláez F, Alonso-Calleja C. Visualization and quantification of the cellular and extracellular components of salmonella agona biofilms at different stages of development. *PLoS One* 2018;13. <https://doi.org/10.1371/journal.pone.0200011>.
- Goodfellow M. Phylum XXVI. Actinobacteria phyl. nov. *Bergey's Manual® Syst. Bacteriol.*, New York, NY: Springer New York; 2012, p. 33–2028. https://doi.org/10.1007/978-0-387-68233-4_3.
- Goude R, Amin AG, Chatterjee D, Parish T. The Arabinosyltransferase EmbC Is Inhibited by Ethambutol in *Mycobacterium tuberculosis*. *Antimicrob Agents Chemother* 2009;53:4138–46. <https://doi.org/10.1128/AAC.00162-09>.
- Griffith DE, Aksamit T, Brown-Elliott B a., Catanzaro A, Daley C, Gordin F, et al. An official ATS/IDSA statement: Diagnosis, treatment, and prevention of nontuberculous mycobacterial diseases. *Am J Respir Crit Care Med* 2007;175:367–416. <https://doi.org/10.1164/rccm.200604-571ST>.
- Grzegorzewicz AE, Jackson M. Subfractionation and Analysis of the Cell Envelope (Lipo)polysaccharides of *Mycobacterium tuberculosis*. *Science (80-.)*, vol. 214, 2013, p. 309–24. https://doi.org/10.1007/978-1-62703-245-2_19.
- Guérardel Y, Maes E, Ellass E, Leroy Y, Timmerman P, Besra GS, et al. Structural Study of Lipomannan and Lipoarabinomannan from *Mycobacterium chelonae*. *J Biol Chem* 2002a;277:30635–48. <https://doi.org/10.1074/jbc.M204398200>.
- Guérardel Y, Maes E, Ellass E, Leroy Y, Timmerman P, Besra GS, et al. Structural study of lipomannan and lipoarabinomannan from *Mycobacterium chelonae*: Presence of unusual components with α 1,3-mannopyranose side chains. *J Biol Chem* 2002b;277:30635–48. <https://doi.org/10.1074/jbc.M204398200>.
- Guilbaud M, Piveteau P, Desvaux M, Brisse S, Briandet R. Exploring the diversity of *Listeria monocytogenes* biofilm architecture by high-throughput confocal laser scanning microscopy and the predominance of the honeycomb-like morphotype. *Appl Environ Microbiol* 2015;81:1813–9. <https://doi.org/10.1128/AEM.03173-14>.

- Gupta KR, Baloni P, Indi SS, Chatterji D. Regulation of growth, cell shape, cell division and gene expression by second messengers (p)ppGpp and c-di-GMP in *Mycobacterium smegmatis*. *J Bacteriol* 2016;198:JB.00126-16. <https://doi.org/10.1128/JB.00126-16>.
- Gupta KR, Kasetty S, Chatterji D. Novel Functions of (p)ppGpp and Cyclic di-GMP in Mycobacterial Physiology Revealed by Phenotype Microarray Analysis of Wild-Type and Isogenic Strains of *Mycobacterium smegmatis*. *Appl Environ Microbiol* 2015;81:2571–8. <https://doi.org/10.1128/AEM.03999-14>.
- Gupta RS, Lo B, Son J. Phylogenomics and comparative genomic studies robustly support division of the genus *Mycobacterium* into an emended genus *Mycobacterium* and four novel genera. *Front Microbiol* 2018;9:1–41. <https://doi.org/10.3389/fmicb.2018.00067>.
- Hall-stoodley L, Brun OS, Polshyna G, Barker LP. *Mycobacterium marinum* biofilm formation reveals cording morphology. *FEMS Microbiol Lett* 2006;257:43–9. <https://doi.org/10.1111/j.1574-6968.2006.00143.x>.
- Hall-Stoodley L, Keevil CW, Lappin-Scott HM. *Mycobacterium fortuitum* and *Mycobacterium chelonae* biofilm formation under high and low nutrient conditions. *J Appl Microbiol* 1999;85 Suppl 1:60S-69S. <https://doi.org/10.1111/j.1365-2672.1998.tb05284.x>.
- Hänzelman S, Castelo R, Guinney J. GSEA: gene set variation analysis for microarray and RNA-Seq data. *BMC Bioinformatics* 2013;14:7.
- Herbert BY, Crabtree G. OBSERVATIONS ON THE CARBOHYDRATE METABOLISM OF TUMOURS. *Biochem J* 1929;23:8–11.
- Holland SP, Pulido JS, Miller D, Ellis B, Alfonso E, Scott M, et al. Biofilm and Scleral Buckle-associated Infections. *Ophthalmology* 2017;98:933–8. [https://doi.org/10.1016/S0161-6420\(91\)32199-7](https://doi.org/10.1016/S0161-6420(91)32199-7).
- Hong Y, Zhou X, Fang H, Yu D, Li C, Sun B. Cyclic di-GMP mediates *Mycobacterium tuberculosis* dormancy and pathogenicity. *Tuberculosis (Edinb)* 2013;93:625–34. <https://doi.org/10.1016/j.tube.2013.09.002>.
- Hooda a., Pati PK, John B, George P V., Michael JS. Disseminated *Mycobacterium chelonae* infection causing pacemaker lead endocarditis in an immunocompetent host. *Case Reports* 2014;2014:bcr2014206042–bcr2014206042. <https://doi.org/10.1136/bcr-2014-206042>.
- Hove-Jensen B. Mutation in the phosphoribosylpyrophosphate synthetase gene (prs) that results in simultaneous requirements for purine and pyrimidine nucleosides, nicotinamide nucleotide, histidine, and tryptophan in *Escherichia coli*. *J Bacteriol* 1988;170:1148–52.
- Howard ST, Rhoades E, Recht J, Pang X, Alsup A, Kolter R, et al. Spontaneous reversion of *Mycobacterium abscessus* from a smooth to a rough morphotype is associated with reduced expression of glycopeptidolipid and reacquisition of an invasive phenotype. *Microbiology* 2006;152:1581–90. <https://doi.org/10.1099/mic.0.28625-0>.
- Hsueh P, Teng L, Yang P, Chen Y, Ho S, Luh K. Recurrent Catheter-Related Infection Caused by a Single Clone of *Mycobacterium Chelonae* With Two Colonial Morphotypes. *J Clin Microbiol* 1998;36:1422.
- Hunter JD. Matplotlib: A 2D Graphics Environment. *Comput Sci Eng* 2007;9:90–5. <https://doi.org/10.1109/MCSE.2007.55>.
- Hunter SW, Fujiwara T, Brennan PJ. Structure and antigenicity of the major specific glycolipid antigen of *Mycobacterium leprae*. *J Biol Chem* 1982;257:15072–8.
- Ishii T. Chapter 11: Transcriptome Analysis of Adrenocortical Cells in Health and Disease. *Cell. Endocrinol. Heal. Dis.*, 2014, p. 169–92.
- Islam MS, Richards JP, Ojha AK. Targeting drug tolerance in mycobacteria: a perspective from mycobacterial biofilms. *Expert Rev Anti Infect Ther* 2012;10:1055–66. <https://doi.org/10.1586/eri.12.88>.
- Ivan M, Dancer C, Koehler AP, Hobby M, Lease C. *Mycobacterium chelonae* abscesses associated with biomesotherapy, Australia, 2008. *Emerg Infect Dis* 2013;19:1493–5. <https://doi.org/10.3201/eid1909.120898>.

- Jackson M, Crick DC, Brennan PJ. Phosphatidylinositol is an essential phospholipid of mycobacteria. *J Biol Chem* 2000;275:30092–9. <https://doi.org/10.1074/jbc.M004658200>.
- Jaén-Luchoro D, Salva-Serra F, Aliaga-Lozano F, Seguí C, Busquets A, Ramírez A, et al. Complete Genome Sequence of *Mycobacterium chelonae* Type Strain CCUG 47445, a Rapidly Growing Species of Nontuberculous *Mycobacteria*. *Am Soc Microbiol* 2016;Genome Ano.
- Jagadeesan N, Patra S, Singh AP, Nagesh CM, Reddy B, Badnur SC, et al. Spontaneous endocarditis caused by rapidly growing non-tuberculous *Mycobacterium chelonae* in an immunocompetent patient with rheumatic heart disease. *J Cardiovasc Dis Res* 2013;4:254–6. <https://doi.org/10.1016/j.jcdr.2013.06.003>.
- James GA, Swogger E, Wolcott R, deLancey Pulcini E, Secor P, Sestrich J, et al. Biofilms in chronic wounds. *Wound Repair Regen* 2007;16.
- Jankute M, Cox JAG, Harrison J, Besra GS. Assembly of the *Mycobacterial* Cell Wall. *Annu Rev Microbiol* 2015;69:405–23. <https://doi.org/10.1146/annurev-micro-091014-104121>.
- Jarlier V, Nikaido H. Permeability barrier to hydrophilic solutes in *Mycobacterium chelonae*. *J Bacteriol* 1990;172:1418–23.
- Julián E, Roldán M, Sánchez-Chardi A, Astola O, Agustí G, Luquin M. Microscopic cords, a virulence-related characteristic of *Mycobacterium tuberculosis*, are also present in nonpathogenic mycobacteria. *J Bacteriol* 2010;192:1751–60. <https://doi.org/10.1128/JB.01485-09>.
- Jung GB, Nam SW, Choi S, Lee G-J, Park H-K. Evaluation of antibiotic effects on *Pseudomonas aeruginosa* biofilm using Raman spectroscopy and multivariate analysis. *Biomed Opt Express* 2014;5:3238. <https://doi.org/10.1364/BOE.5.003238>.
- Kalscheuer R, Palacios A, Anso I, Cifuentes J, Anguita J, Jacobs WR, et al. The *Mycobacterium tuberculosis* capsule: a cell structure with key implications in pathogenesis. *Biochem J* 2019;476:1995–2016. <https://doi.org/10.1042/bcj20190324>.
- Kalscheuer R, Syson K, Veeraraghavan U, Weinrick B, Karolin E, Liu Z, et al. Self-poisoning of *Mycobacterium tuberculosis* by targeting GlgE in an α -glucan pathway. *Nat Chem Biol* 2010a;6:376–84. <https://doi.org/10.1038/nchembio.340>.
- Kalscheuer R, Weinrick B, Veeraraghavan U, Besra GS, Jacobs WRJ. Trehalose-recycling ABC transporter LpqY-SugA-SugB-SugC is essential for virulence of *Mycobacterium tuberculosis*. *PNAS* 2010b;107:21761–6.
- Kaneda K, Naito S, Imaizumi S, Yano I, Mizuno S, Tomiyasu I, et al. Determination of Molecular Species Composition of C80 or Longer-Chain α -Mycolic Acids in *Mycobacterium* spp. by Gas Chromatography-Mass Spectrometry and Mass Chromatography. *J Clin Microbiol* 1986;24:1060–70.
- Kang C-M, Nyayapathy S, Lee J-Y, Suh J-W, Husson RN. Wag31, a homologue of the cell division protein DivIVA, regulates growth, morphology and polar cell wall synthesis in mycobacteria. *Microbiology* 2008;154:725–35. <https://doi.org/10.1099/mic.0.2007/014076-0>.
- Kannaiyan K, Ragunathan L, Sakthivel S, Sasidar AR, Venkatachalam GK. Surgical Site Infections Due to Rapidly Growing *Mycobacteria* 2015:7–10. <https://doi.org/10.7860/JCDR/2015/10572.5638>.
- Katoch VM. Infections due to non-tuberculous mycobacteria (NTM). *Indian J Med Res* 2004;290–304.
- Kaur D, Guerin ME, Kovierov H, Brennan PJ, Jackson M. Chapter 2 Biogenesis of the Cell Wall and Other Glycoconjugates of *Mycobacterium tuberculosis*. *Adv Appl Microbiol* 2009a;69:23–78. [https://doi.org/10.1016/S0065-2164\(09\)69002-X](https://doi.org/10.1016/S0065-2164(09)69002-X).
- Kaur D, Guerin ME, Škovierová H, Brennan PJ, Jackson M. Chapter 2 Biogenesis of the Cell Wall and Other Glycoconjugates of *Mycobacterium tuberculosis*. *Adv. Appl. Microbiol.*, vol. 69, 2009b, p. 23–78. [https://doi.org/10.1016/S0065-2164\(09\)69002-X](https://doi.org/10.1016/S0065-2164(09)69002-X).
- Kavvas ES, Seif Y, Yurkovich JT, Norsigian C, Poudel S, Greenwald WW, et al. Updated and standardized genome-scale reconstruction of *Mycobacterium tuberculosis* H37Rv, iEK1011, simulates flux states indicative of physiological conditions 2018:1–15.

- Keating LA, Wheeler PR, Mansoor H, Inwald JK, Dale J, Hewinson RG, et al. The pyruvate requirement of some members of the *Mycobacterium tuberculosis* complex is due to an inactive pyruvate kinase: implications for in vivo growth. *Mol Microbiol* 2005;56:163–74. <https://doi.org/10.1111/j.1365-2958.2005.04524.x>.
- Keshavjee S, Farmer PE. Tuberculosis, drug resistance, and the history of modern medicine. *N Engl J Med* 2012;367:931–6. <https://doi.org/10.1056/NEJMra1205429>.
- Khatoun Z, McTiernan CD, Suuronen EJ, Mah T-F, Alarcon EI. Bacterial biofilm formation on implantable devices and approaches to its treatment and prevention. *Heliyon* 2018;4.
- Kheir WJ, Sheheitli H, Abdul Fattah M, Hamam RN. Nontuberculous *Mycobacterial* Ocular Infections: A Systematic Review of the Literature. *Biomed Res Int* 2015;2015:1–17. <https://doi.org/10.1155/2015/164989>.
- Khoo K-H, Dell A, Morris HR, Brennan PJ, Chatterjee D. Inositol Phosphate Capping of the Nonreducing Termini of Lipoarabinomannan from Rapidly Growing Strains of *Mycobacterium*. *J Biol Chem* 1995;270:12380–9. <https://doi.org/10.1074/jbc.270.21.12380>.
- Kim HS, Lee Y, Lee S, Kim YA, Sun YK. Recent trends in clinically significant nontuberculous mycobacteria isolates at a Korean general hospital. *Ann Lab Med* 2014;34:56–9. <https://doi.org/10.3343/alm.2014.34.1.56>.
- Kim MJ, Mascola L. *Mycobacterium chelonae* Wound Infection after Liposuction. *Emerg Infect Dis* 2010;16:1173–5. <https://doi.org/10.3201/eid1607.090156>.
- Kinane DF, Stathopoulou PG, Panos N. Periodontal diseases. *Nat Rev Dis Prim* 2017;3.
- Klepp LI, Forrellad MA, Osella A V., Blanco FC, Stella EJ, Bianco MV, et al. Impact of the deletion of the six mce operons in *Mycobacterium smegmatis*. *Microbes Infect* 2012;14:590–9. <https://doi.org/10.1016/j.micinf.2012.01.007>.
- Kobayashi K. *Bacillus subtilis* Pellicle Formation Proceeds through Genetically Defined Morphological Changes. *J Bacteriol* 2007;189:4920–31. <https://doi.org/10.1128/JB.00157-07>.
- Koliwer-brandl H, Syson K, Weerd R Van De, Chandra G, Geurtsen J, Bornemann S, et al. Metabolic Network for the Biosynthesis of Intra- and Extracellular α -Glucans Required for Virulence of *Mycobacterium tuberculosis* 2016:1–26. <https://doi.org/10.1371/journal.ppat.1005768>.
- Kovács ÁT, Dragoš A. Evolved Biofilm: Review on the Experimental Evolution Studies of *Bacillus subtilis* Pellicles. *J Mol Biol* 2019:16–8. <https://doi.org/10.1016/j.jmb.2019.02.005>.
- Kremer L, Nampoothiri KM, Lesjean S, Dover LG, Graham S, Betts JC, et al. Biochemical characterization of acyl carrier protein (AcpM) and malonylCoA:AcpM transacylase (mtFabD), two major components of *Mycobacterium tuberculosis* fatty acid synthase II. *Biol Chem* 2001;276:27967–74.
- Kuhar N, Sil S, Verma T, Umapathy S. Challenges in application of Raman spectroscopy to biology and materials. *R Soc Chem* 2018;8:25888–908. <https://doi.org/10.1039/c8ra04491k>.
- Kumar A, Farhana A, Guidry L, Saini V, Hondalus M, Steyn AJC. Redox homeostasis in mycobacteria: the key to tuberculosis control? *Expert Rev Mol Med* 2011;13:1–25. <https://doi.org/10.1017/S1462399411002079>.
- Kumar M, Chatterji D. Cyclic di-GMP: a second messenger required for long-term survival, but not for biofilm formation, in *Mycobacterium smegmatis*. *Microbiology* 2008;154:2942–55. <https://doi.org/10.1099/mic.0.2008/017806-0>.
- Kumar S, Matange N, Umapathy S, Visweswariah SS. Linking carbon metabolism to carotenoid production in mycobacteria using Raman spectroscopy. *FEMS Microbiol Lett* 2015;362:1–6. <https://doi.org/10.1093/femsle/fnu048>.
- Lage R, Biccigo DGZ, Santos FBC, Chimara E, Pereira ESP, Costa A da. *Mycobacterium chelonae* cutaneous infection in a patient with mixed connective tissue disease. *An Bras Dermatol* 2012;90:104–7. <https://doi.org/10.1590/abd1806-4841.20152276>.
- Lake MA, Ambrose LR, Lipman MCI, Lowe DM. ‘ ‘Why me, why now?’ ’ Using clinical immunology

- and epidemiology to explain who gets nontuberculous mycobacterial infection. *BMC Med* 2016;14:54. <https://doi.org/10.1186/s12916-016-0606-6>.
- Lee J-H, Kim Y-G, Cho MH, Wood TK, Lee J. Transcriptomic Analysis for Genetic Mechanisms of the Factors Related to Biofilm Formation in *Escherichia coli* O157:H7. *Curr Microbiol* 2011;62:1321–30.
- Leid JG, Willson CJ, Shirliff ME, Hassett DJ, Parsek MR, Jeffers AK. The exopolysaccharide alginate protects *Pseudomonas aeruginosa* biofilm bacteria from IFN- γ -mediated macrophage killing. *J Immunol* 2005;175:7512–7518.
- Lemassu A, Daffé M. Structural features of the exocellular polysaccharides of *Mycobacterium tuberculosis*. *Biochem J* 1994;297 (Pt 2):351–7. <https://doi.org/10.1089/hyb.1994.13.81>.
- Lemassu A, Ortalo-magne A, Bardou F, Silve G. Extracellular and surface-exposed polysaccharides of non-tuberculous mycobacteria. *Microbiology* 1996a;1513–20.
- Lemassu A, Ortalo-Magné A, Bardou F, Silve G, Lanéelle MA, Daffé M. Extracellular and surface-exposed polysaccharides of non-tuberculous mycobacteria. *Microbiology* 1996b;142:1513–20. <https://doi.org/10.1099/13500872-142-6-1513>.
- Lenaerts AJ, Hoff D, Aly S, Ehlers S, Andries K, Cantarero L, et al. Location of persisting mycobacteria in a Guinea pig model of tuberculosis revealed by r207910. *Antimicrob Agents Chemother* 2007;51:3338–45. <https://doi.org/10.1128/AAC.00276-07>.
- Li CH, Tam PKS. An iterative algorithm for minimum cross entropy thresholding. *Pattern Recognit Lett* 1998;19:771–6. [https://doi.org/10.1016/S0167-8655\(98\)00057-9](https://doi.org/10.1016/S0167-8655(98)00057-9).
- Li Y, Duan X, Huang Q, Liu Z, Xu M, Guo S, et al. *Mycobacterium* Lysine ϵ -aminotransferase is a novel alarmone metabolism related persist gene via dysregulating the intracellular amino acid level. *Sci Rep* 2016;6:1–10. <https://doi.org/10.1038/srep19695>.
- Liao S, Klein MI, Heim KP, Fan Y, Bitoun JP, Ahn SJ, et al. *Streptococcus mutans* extracellular DNA is upregulated during growth in biofilms, actively released via membrane vesicles, and influenced by components of the protein secretion machinery. *J Bacteriol* 2014;196:2355–66. <https://doi.org/10.1128/JB.01493-14>.
- de Lisle G, Wards B, Buddle B, Collins D. The efficacy of live tuberculosis vaccines after presensitization with *Mycobacterium avium*. *Tuberculosis (Edinb)* 2005;85:73–9.
- Liu Y, Landick R, Raman S. A Regulatory NADH/NAD⁺ Redox Biosensor for Bacteria. *ACS Synth Biol* 2019;8:264–73. <https://doi.org/10.1021/acssynbio.8b00485>.
- Lo MW, Mak SK, Wong YY, Lo KC, Chan SF, Tong GMW, et al. Atypical mycobacterial exit-site infection and peritonitis in peritoneal dialysis patients on prophylactic exit-site gentamicin cream. *Perit Dial Int* 2013;33:267–72. <https://doi.org/10.3747/pdi.2011.00184>.
- Lopez-Marin LM, Gautier N, Laneelle MA, Silve G, Daffe M. Structures of the glycopeptidolipid antigens of *Mycobacterium abscessus* and *Mycobacterium chelonae* and possible chemical basis of the serological cross-reactions in the *Mycobacterium fortuitum* complex. *Microbiology* 1994;140:1109–18. <https://doi.org/10.1099/13500872-140-5-1109>.
- López D, Vlamakis H, Kolter R. Biofilms. *Cold Spring Harb Perspect Biol* 2010;2:a000398. <https://doi.org/10.1101/cshperspect.a000398>.
- López Marin LM, Lanéelle MA, Promé D, Daffé M, Lanéelle G, Promé JC. Glycopeptidolipids from *Mycobacterium fortuitum*: a variant in the structure of C-mycoside. *Biochemistry* 1991;30:10536–42. <https://doi.org/10.1021/bi00107a024>.
- Love MI, Huber W, Anders S. Moderated estimation of fold change and dispersion for RNA-seq data with DESeq2. *Genome Biol* 2014;15:1–21. <https://doi.org/10.1186/s13059-014-0550-8>.
- Luo TL, Eisenberg MC, Hayashi MAL, Gonzalez-Cabezas C, Foxman B, Marrs CF, et al. A Sensitive Thresholding Method for Confocal Laser Scanning Microscope Image Stacks of Microbial Biofilms. *Sci Rep* 2018;8:1–14. <https://doi.org/10.1038/s41598-018-31012-5>.
- Mah TF, O'Toole G a. Mechanisms of biofilm resistance to antimicrobial agents. *Trends Microbiol*

2001;9:34–9.

Mali S, Doctor T, Doshi A, Sharma R. Extensive infection of face by mycobacterium chelonae: An unusual presentation. *Indian J Dermatol* 2014;59:495. <https://doi.org/10.4103/0019-5154.139904>.

Mangtani P, Abubakar I, Ariti C, Al. E. Protection by BCG vaccine against tuberculosis: a systematic review of randomized controlled trials. *Clin Infect Dis* 2014;58:470–80.

Manzoor SE, Lambert PA, Griffiths PA, Gill MJ, Fraise AP. Reduced glutaraldehyde susceptibility in *Mycobacterium chelonae* associated with altered cell wall polysaccharides. *J Antimicrob Chemother* 1999;4:759–65.

Marrakchi H, Ducasse S, Labesse G, Montrozier H, Margeat E, Emorine L, et al. MabA (FabG1), a *Mycobacterium tuberculosis* protein involved in the long-chain fatty acid elongation system FAS-II. *Microbiology* 2002;148:951–60.

Marrakchi H, Lan  elle G, Qu  mard A. InhA, a target of the antituberculous drug isoniazid, is involved in a mycobacterial fatty acid elongation system, FAS-II. *Microbiology* 2000;146:289–96. <https://doi.org/10.1099/00221287-146-2-289>.

Marrakchi H, Lan  elle MA, Daff   M. Mycolic acids: Structures, biosynthesis, and beyond. *Chem Biol* 2014;21:67–85. <https://doi.org/10.1016/j.chembiol.2013.11.011>.

Marsollier L, Brodin P, Jackson M, Kordul  kov   J, Tafelmeyer P, Carbonnelle E, et al. Impact of *Mycobacterium ulcerans* biofilm on transmissibility to ecological niches and Buruli ulcer pathogenesis. *PLoS Pathog* 2007;3:e67.

Mart  n-de-Hijas NZ, Garc  a-Almeida D, Ayala G, Fern  ndez-Roblas R, Gadea I, Celdr  n a, et al. Biofilm development by clinical strains of non-pigmented rapidly growing mycobacteria. *Clin Microbiol Infect* 2009;15:931–6. <https://doi.org/10.1111/j.1469-0691.2009.02882.x>.

Maurya AK, Nag VL, Kant S, Kushwaha RAS, Kumar M, Singh AK, et al. Prevalence of nontuberculous mycobacteria among extrapulmonary tuberculosis cases in tertiary care centers in Northern India. *Biomed Res Int* 2015;2015. <https://doi.org/10.1155/2015/465403>.

McCallum C, Johnson B. *Mycobacterium chelonae* bacteremia in a patient taking infliximab and prednisone. *Can Med Assoc J* 2016;188:E538–E538. <https://doi.org/10.1503/cmaj.150978>.

McKinney W. Data Structures for Statistical Computing in Python. *Proc 9th Python Sci Conf* 2010:51–6.

McNeil M, Daffe M, Brennan P. Evidence for the nature of the link between the arabinogalactan and peptidoglycan of mycobacterial cell walls. *J Biol Chem* 1990a;18200–6.

McNeil M, Daffe M, Brennan PJ. Location of the mycolyl ester substituents in the cell walls of mycobacteria. *J Biol Chem* 1991;266:13217–23.

McNeil M, Daffe M, Brennan PJ. Evidence for the nature of the link between the arabinogalactan and peptidoglycan of mycobacterial cell walls. *J Biol Chem* 1990b;265:18200–6.

McNeil M, Wallner S, Hunter S, Brennan P. Demonstration that the galactosyl and arabinosyl residues in the cell-wall arabinogalactan of *Mycobacterium leprae* and *Mycobacterium tuberculosis* are furanoid. *Carbohydr Res* 1987;166:299–308.

Meyer A, Prasad KG, Antisdel J. *Mycobacterium chelonae* dacryocystitis after endoscopic dacryocystorhinostomy 2011:1–4. <https://doi.org/10.2500/ar.2014.5.0081>.

Meyers H, Brown-Elliott BA, Moore D, Curry J, Truong C, Zhang Y, et al. An outbreak of *Mycobacterium chelonae* infection following liposuction. *Clin Infect Dis* 2002;34:1500–7.

Mikusova K, Huang H, Yagi T, Holsters M, Brennan PJ, McNeil M, et al. Decaprenylphosphoryl Arabinofuranose, The donor of the D-Arabinoguranosyl Residues of Mycobacterial Arabinan, Is formed via a Two-Step Epimerization of Decaprenylphosphoryl Ribose. *J Bacteriol* 2005;187:8020–5.

Minnikin DE, Lee OY-C, Wu HHT, Nataraj V, Donoghue HD, Ridell M, et al. Pathophysiological Implications of Cell Envelope Structure in *Mycobacterium tuberculosis* and Related Taxa. *Tuberc. - Expand. Knowl.*, 2015. <https://doi.org/10.5772/59585>.

- Mirate DJ, Hull DS, Steel Jr. JH, Carter MJ. *Mycobacterium chelonae* keratitis: a case report. *Br J Ophthalmol* 1983;67:324–6.
- Misaki A, Azuma I, Yamamura Y. Structural and Immunochemical Studies on D-Arabino-D-Mannans and D-Mannans of *Mycobacterium tuberculosis* and Other *Mycobacterium* Species I. *J Biochem* 1977;82:1759–70. <https://doi.org/10.1093/oxfordjournals.jbchem.a131874>.
- Miyamoto Y, Mukai T, Nakata N, Maeda Y, Kai M, Naka T, et al. Identification and characterization of the genes involved in glycosylation pathways of mycobacterial glycopeptidolipid biosynthesis. *J Bacteriol* 2006;188:86–95. <https://doi.org/10.1128/JB.188.1.86-95.2006>.
- Moorthy RS, Rao NA. Atypical mycobacterial wound infection after blepharoplasty. *Br J Ophthalmol* 1995;93.
- Murback NDN, Higa Júnior MG, Pompílio MA, Cury ESJ, Hans Filho G, Takita LC. Disseminated cutaneous atypical mycobacteriosis by *M. chelonae* after sclerotherapy of varicose veins in a immunocompetent patient: a case report. *An Bras Dermatol* 2015;90:138–42. <https://doi.org/10.1590/abd1806-4841.20153504>.
- Murthy SI, Jain R, Swarup R, Sangwan VS. Recurrent non-tuberculous mycobacterial keratitis after deep anterior lamellar keratoplasty for keratoconus. *BMJ Case Rep* 2013;1–3. <https://doi.org/10.1136/bcr-2013-200641>.
- Narasimhan SL, Austin TW. Prosthetic valve endocarditis due to *Mycobacterium fortuitum*. *Can Med Assoc J* 1978;119:154–5.
- Nasiri MJ, Dabiri H, Darban-Sarokhalil D, Shahraki AH. Prevalence of Non-Tuberculosis Mycobacterial infections among tuberculosis suspects in Iran: Systematic review and meta-analysis. *PLoS One* 2015;10:1–9. <https://doi.org/10.1371/journal.pone.0129073>.
- Nataraj V, Varela C, Javid A, Singh A, Besra GS, Bhatt A. Mycolic acids: Deciphering and targeting the Achilles' heel of the tubercle bacillus. *Mol Microbiol* 2015;98:7–16. <https://doi.org/10.1111/mmi.13101>.
- Nessar R, Reytrat J-M, Davidson LB, Byrd TF. Deletion of the *mmpL4b* gene in the *Mycobacterium abscessus* glycopeptidolipid biosynthetic pathway results in loss of surface colonization capability, but enhanced ability to replicate in human macrophages and stimulate their innate immune response. *Microbiology* 2011;157:1187–95. <https://doi.org/10.1099/mic.0.046557-0>.
- Nguyen LH, Holmes S. Ten quick tips for effective dimensionality reduction. *PLOS Comput Biol* 2019;15:e1006907. <https://doi.org/10.1371/journal.pcbi.1006907>.
- Nouioui I, Carro L, García-López M, Meier-Kolthoff JP, Woyke T, Kyrpides NC, et al. Genome-based taxonomic classification of the phylum actinobacteria. *Front Microbiol* 2018;9:1–119. <https://doi.org/10.3389/fmicb.2018.02007>.
- Odriozola JM, Ramos JA, Bloch K. Fatty acid synthetase activity in *Mycobacterium smegmatis*. Characterization of the acyl carrier protein-dependent elongating system. *Biochim Biophys Acta* 1977;488:207–17.
- Ojha A, Anand M, Bhatt A, Kremer L, Jacobs WR, Hatfull GF. GroEL1: a dedicated chaperone involved in mycolic acid biosynthesis during biofilm formation in mycobacteria. *Cell* 2005;123:861–73. <https://doi.org/10.1016/j.cell.2005.09.012>.
- Ojha A, Hatfull GF. The role of iron in *Mycobacterium smegmatis* biofilm formation: The exochelin siderophore is essential in limiting iron conditions for biofilm formation but not for planktonic growth. *Mol Microbiol* 2007;66:468–83. <https://doi.org/10.1111/j.1365-2958.2007.05935.x>.
- Ojha AK, Baughn AD, Sambandan D, Hsu T, Trivelli X, Guerardel Y, et al. Growth of *Mycobacterium tuberculosis* biofilms containing free mycolic acids and harbouring drug-tolerant bacteria. *Mol Microbiol* 2008;69:164–74. <https://doi.org/10.1111/j.1365-2958.2008.06274.x>.
- Ojha AK, Trivelli X, Guerardel Y, Kremer L, Hatfull GF. Enzymatic hydrolysis of trehalose dimycolate releases free mycolic acids during mycobacterial growth in biofilms. *J Biol Chem* 2010;285:17380–9. <https://doi.org/10.1074/jbc.M110.112813>.
- Ojha AK, Varma S, Chatterji D. Synthesis of an unusual polar glycopeptidolipid in glucose-limited

- culture of *Mycobacterium smegmatis*. *Microbiology* 2002;148:3039–48. <https://doi.org/10.1099/00221287-148-10-3039>.
- Okado T, Iimori S, Nishida H, Yui N, Sohara E, Rai T, et al. Successful Treatment of *Mycobacterium chelonae* Peritoneal Dialysis-Related Infection by a Combination Regimen Including Local Thermal Therapy. *Perit Dial Int* 2015;35:114–6. <https://doi.org/10.3747/pdi.2013.00161>.
- Okshevsy M, Meyer RL. The role of extracellular DNA in the establishment, maintenance and perpetuation of bacterial biofilms. *Crit Rev Microbiol* 2015;41:341–52. <https://doi.org/10.3109/1040841X.2013.841639>.
- Orme IM. A new unifying theory of the pathogenesis of tuberculosis. *Tuberculosis (Edinb)* 2013;1–7. <https://doi.org/10.1016/j.tube.2013.07.004>.
- Orme IM, Ordway DJ. Host Response to Nontuberculous Mycobacterial Infections of Current Clinical Importance. *Infect Immun* 2014;82:3516–22. <https://doi.org/10.1128/IAI.01606-13>.
- Ortalo-Magne A, Dupont MA, Lemassu A, Andersen AB, Gounon P, Daffe M. Molecular composition of the outermost capsular material of the tubercle bacillus. *Microbiology* 1995;141:1609–20. <https://doi.org/10.1099/13500872-141-7-1609>.
- Ortalo-Magné A, Lemassu A, Lanée M-A, Bardou F, Silve G, Gounon P, et al. Identification of the surface-exposed lipids on the cell envelopes of *Mycobacterium tuberculosis* and other mycobacterial species. *J Bacteriol* 1996;178:456–61.
- Pacheco S a., Hsu FF, Powers KM, Purdy GE. MmpL11 protein transports mycolic acid-containing lipids to the mycobacterial cell wall and contributes to biofilm formation in *Mycobacterium smegmatis*. *J Biol Chem* 2013;288:24213–22. <https://doi.org/10.1074/jbc.M113.473371>.
- Pang JM, Layre E, Sweet L, Sherrid A, Moody DB, Ojha A, et al. The polyketide Pks1 contributes to biofilm formation in *Mycobacterium tuberculosis*. *J Bacteriol* 2012;194:715–21. <https://doi.org/10.1128/JB.06304-11>.
- Parish T, Stoker NG, Daffé M, Lanée M-A. Analysis of the Capsule of *Mycobacterium tuberculosis*. *Mycobacterium Tuberc Protoc* 2003;54:217–27. <https://doi.org/10.1385/1-59259-147-7:217>.
- Patnaik S, Mohanty I, Panda P, Sahu S, Dash M. Disseminated *Mycobacterium chelonae* infection: Complicating a case of hidradenitis suppurativa. *Indian Dermatol Online J* 2013;4:336. <https://doi.org/10.4103/2229-5178.120672>.
- Pearlman MD. *Mycobacterium chelonae* Breast Abscess Associated With Nipple Piercing. *Infect Dis Obstet Gynecol* 1995;3:116–8. <https://doi.org/10.1155/S1064744995000433>.
- Perez F, Granger BE. IPython: A System for Interactive Scientific Computing. *Comput Sci Eng* 2007;9:21–9. <https://doi.org/10.1109/MCSE.2007.53>.
- Perumal J, Dinish U, Bendt AK, Kazakeviciute A, Yaw Fu C, Hao Ong IL, et al. Identification of mycolic acid forms using surface-enhanced Raman scattering as a fast detection method for tuberculosis. *Int J Nanomedicine* 2018;13:6029–38.
- Peterson EJ, Bailo R, Rothchild AC, Arrieta-Ortiz ML, Kaur A, Pan M, et al. Path-seq identifies an essential mycolate remodeling program for mycobacterial host adaptation. *Mol Syst Biol* 2019;15:1–19. <https://doi.org/10.15252/msb.20188584>.
- Pier GB, Coleman F, Grout M, Franklin M, Ohman DE. Role of alginate O acetylation in resistance of mucoid *Pseudomonas aeruginosa* to opsonic phagocytosis. *Infect Immun* 2001;69:1895–901.
- Piersimoni C, Scarparo C. Extrapulmonary infections associated with nontuberculous mycobacteria in immunocompetent persons. *Emerg Infect Dis* 2009;15:1351–8. <https://doi.org/10.3201/eid1509.081259>.
- Pinto-Gouveia M, Gameiro A, Ramos L, Cardoso JC, Brites MM, Tellechea A, et al. *Mycobacterium chelonae* Is an Ubiquitous Atypical Mycobacterium. *Case Rep Dermatol* 2015;7:207–11. <https://doi.org/10.1159/000438898>.
- Pisithkul T, Schroeder JW, Trujillo EA, Yeesin P, Stevenson DM, Chaiamarit T, et al. Metabolic Remodeling during Biofilm Development of *Mycobacterium* *genus-species* id="named-

- content-1">*Bacillus subtilis*. *MBio* 2019;10:e00623-19. <https://doi.org/10.1128/mBio.00623-19>.
- Portevin D, de Sousa-D'Auria C, Houssin C, Grimaldi C, Chami M, Daffé M, et al. A polyketide synthase catalyzes the last condensation step of mycolic acid biosynthesis in *Mycobacteria* and related organisms. *Proc Natl Acad Sci* 2004;101:314–9.
- Potera C. Studying slime. *Environ Heal Perspect* 1998;106:A604–6.
- Poyntz HC, Stylianou E, Grif KL, Marsay L, Checkley AM, Mcshane H. Non-tuberculous mycobacteria have diverse effects on BCG efficacy against *Mycobacterium tuberculosis*. *Tuberculosis* 2014;94:226–37. <https://doi.org/10.1016/j.tube.2013.12.006>.
- Prados-Rosales R, Baena A, Martinez LR, Luque-Garcia J, Kalscheuer R, Veeraraghavan U, et al. *Mycobacteria* release active membrane vesicles that modulate immune responses in a TLR2-dependent manner in mice. *J Clin Invest* 2011;121:1471–83. <https://doi.org/10.1172/JCI44261>.
- Puech V, Guilhot C, Perez E, Tropis M, Armitige LY, Gicquel B, et al. Evidence for a partial redundancy of the fibronectin-binding proteins for the transfer of mycoloyl residues onto the cell wall arabinogalactan termini of *Mycobacterium tuberculosis*. *Mol Microbiol* 2002;44:1109–22. <https://doi.org/10.1046/j.1365-2958.2002.02953.x>.
- Qvist T, Eickhardt-Sørensen S, Pressler T, Katzenstein TL, Andersen CB, Iversen M, et al. First evidence of *Mycobacterium abscessus* biofilm in the lungs of chronically infected CF patients. *JCystFibros* 2013;12:S2–S2. [https://doi.org/10.1016/S1569-1993\(13\)60006-5](https://doi.org/10.1016/S1569-1993(13)60006-5).
- Qvist T, Eickhardt S, Kragh KN, Andersen CB, Iversen M, Høiby N, et al. Chronic pulmonary disease with *Mycobacterium abscessus* complex is a biofilm infection. *Eur Respir J* 2015;46:1823–6. <https://doi.org/10.1183/13993003.01102-2015>.
- Rai V, Dey N. The Basics of Confocal Microscopy. *Laser Scanning, Theory Appl.*, 2011.
- Rajendran R, May A, Sherry L, Kean R, Williams C, Jones BL, et al. Integrating *Candida albicans* metabolism with biofilm heterogeneity by transcriptome mapping. *Nat Publ Gr* 2016:1–11. <https://doi.org/10.1038/srep35436>.
- Rashid AM, Batey SFD, Syson K, Koliwer-brandl H, Miah F, Barclay JE, et al. Assembly of α - Glucan by GlgE and GlgB in *Mycobacteria* and *Streptomyces*. *Biochemistry* 2016;55:3270–84. <https://doi.org/10.1021/acs.biochem.6b00209>.
- Raymond JB, Mahapatra S, Crick DC, Pavelka MSJ. Identification of the *namH* gene, encoding the hydrioxylase responsible for the N-glycolation of the mycobacterial peptidoglycan. *J Biol Chem* 2005;280:326–33.
- Recht J, Kolter R. Glycopeptidolipid acetylation affects sliding motility and biofilm formation in *Mycobacterium smegmatis*. *J Bacteriol* 2001;183:5718–24. <https://doi.org/10.1128/JB.183.19.5718-5724.2001>.
- Recht J, Martínez A, Torello S, Kolter R. Genetic Analysis of Sliding Motility in *Mycobacterium smegmatis* 2000;182:4348–51.
- Reimand J, Isserlin R, Voisin V, Kucera M, Tannus-Lopes C, Rostamianfar A, et al. Pathway enrichment analysis and visualization of omics data using g:Profiler, GSEA, Cytoscape and EnrichmentMap. *Nat Protoc* 2019;14:482–517.
- Rieck B, Degiacomi G, Zimmermann M, Cascioferro A, Boldrin F, Lazar-Adler NR, et al. PknG senses amino acid availability to control metabolism and virulence of *Mycobacterium tuberculosis*. vol. 13. 2017. <https://doi.org/10.1371/journal.ppat.1006399>.
- Rindi L, Garzelli C. Increase in non-tuberculous mycobacteria isolated from humans in Tuscany, Italy, from 2004 to 2014. *BMC Infect Dis* 2016;16:44. <https://doi.org/10.1186/s12879-016-1380-y>.
- Ringshausen FC, Wagner D, de Roux A, Diel R, Hohmann D, Hickstein L, et al. Prevalence of Nontuberculous Mycobacterial Pulmonary Disease, Germany, 2009-2014. *Emerg Infect Dis* 2016;22:1102–5. <https://doi.org/10.3201/eid2206.151642>.
- Ripoll F, Deshayes C, Pasek S, Laval F, Beretti J-L, Biet F, et al. Genomics of glycopeptidolipid

- biosynthesis in *Mycobacterium abscessus* and *M. chelonae*. BMC Genomics 2007;8:114. <https://doi.org/10.1186/1471-2164-8-114>.
- Rodriguez JM, Xie YL, Winthrop KL, Schafer S, Sehdev P, Solomon J, et al. *Mycobacterium chelonae* Facial Infections Following Injection of Dermal Filler. Aesthetic Surg J 2013;33:265–9. <https://doi.org/10.1177/1090820X12471944>.
- Römling U, Balsalobre C. Biofilm infections, their resilience to therapy and innovative treatment strategies. J Intern Med 2012;272:541–61. <https://doi.org/10.1111/joim.12004>.
- Rösch P, Harz M, Schmitt M, Ronneberger O, Burkhardt H, Lankers M, et al. Chemotaxonomic Identification of Single Bacteria by Micro-Raman Spectroscopy : Application to Clean-Room-Relevant Biological Contaminations Chemotaxonomic Identification of Single Bacteria by Micro-Raman Spectroscopy : Application to Clean-Room-Relevant B. Appl Environ Microbiol 2005;71:1626–37. <https://doi.org/10.1128/AEM.71.3.1626>.
- Röse L, Kaufmann SHE, Daugelat S. Involvement of *Mycobacterium smegmatis* undecaprenyl phosphokinase in biofilm and smegma formation. Microbes Infect 2004;6:965–71. <https://doi.org/10.1016/j.micinf.2004.05.011>.
- Rose SJ, Babrak LM, Bermudez LE. *Mycobacterium avium* Possesses Extracellular DNA that Contributes to Biofilm Formation, Structural Integrity, and Tolerance to Antibiotics. PLoS One 2015;10:e0128772. <https://doi.org/10.1371/journal.pone.0128772>.
- Rose SJ, Bermudez LE. Identification of Bicarbonate as a Trigger and Genes Involved with Extracellular DNA Export in *Mycobacterial* Biofilms. MBio 2016;7:e01597-16. <https://doi.org/10.1128/mBio.01597-16>.
- Roukens AH, Mendels EJ, Verbeet NL, von dem Borne PA, Nicolae-Cristea AR, Bentvelsen RG, et al. Disseminated Cutaneous *Mycobacterium chelonae* Infection in a Patient With Acute Myeloid Leukemia. 2014. <https://doi.org/10.1093/ofid/ofu103>.
- Ruiz-Matute AI, Hernández-Hernández O, Rodríguez-Sánchez S, Sanz ML, Martínez-Castro I. Derivatization of carbohydrates for GC and GC-MS analyses. J Chromatogr B Anal Technol Biomed Life Sci 2011;879:1226–40. <https://doi.org/10.1016/j.jchromb.2010.11.013>.
- Runyon EH. Anonymous mycobacteria in pulmonary disease. Med Clin North Am 1959;43:273–90. [https://doi.org/10.1016/S0025-7125\(16\)34193-1](https://doi.org/10.1016/S0025-7125(16)34193-1).
- Sacco E, Covarrubias AS, O'Hare HM, Carroll P, Eynard N, Jones TA, et al. The missing piece of the type II fatty acid synthase system from *Mycobacterium tuberculosis*. Proc Natl Acad Sci 2007;104:14628–33.
- Sambandan D, Dao DN, Weinrick BC, Vilchère C, Gurucha SS, Ojha A, et al. Keto-Mycolic acid-dependent pellicle formation confers tolerance to drug-sensitive *Mycobacterium tuberculosis*. MBio 2013;4:1–10. <https://doi.org/10.1128/mBio.00222-13>.
- Sambou T, Dinadayala P, Stadthagen G, Barilone N, Bordat Y, Constant P, et al. Capsular glucan and intracellular glycogen of *Mycobacterium tuberculosis* : biosynthesis and impact on the persistence in mice. Mol Microbiol 2008;70:762–74. <https://doi.org/10.1111/j.1365-2958.2008.06445.x>.
- Samek O, Bernatová S, Ježek J, Šiler M, Šerý M, Krzyžánek V, et al. Identification of individual biofilm-forming bacterial cells using Raman tweezers. J Biomed Opt 2015;20:051038. <https://doi.org/10.1117/1.jbo.20.5.051038>.
- Sani M, Houben ENG, Geurtsen J, Pierson J, De Punder K, Van Zon M, et al. Direct visualization by Cryo-EM of the mycobacterial capsular layer: A labile structure containing ESX-1-secreted proteins. PLoS Pathog 2010;6. <https://doi.org/10.1371/journal.ppat.1000794>.
- Sauer K. The genomics and proteomics of biofilm formation. Genome Biol 2003.
- Schaudinn C, Dittmann C, Jurisch J, Laue M, Günday-Türel N, Blume-Peyvati U, et al. Development, standardization and testing of a bacterial wound infection model based on ex vivo human skin. PLoS One 2017;1–13.
- Schlafer S, Meyer RL. Confocal microscopy imaging of the biofilm matrix. J Microbiol Methods

- 2017;138:50–9. <https://doi.org/10.1016/j.mimet.2016.03.002>.
- Schooling SR, Beveridge TJ. Membrane vesicles: An overlooked component of the matrices of biofilms. *J Bacteriol* 2006;188:5945–57. <https://doi.org/10.1128/JB.00257-06>.
- Schorey JS, Sweet L. The mycobacterial glycopeptidolipids: Structure, function, and their role in pathogenesis. *Glycobiology* 2008;18:832–41. <https://doi.org/10.1093/glycob/cwn076>.
- Shah JA, Arlehamn CSL, Horne DJ, Sette A, Hawn TR. Nontuberculous Mycobacteria and Heterologous Immunity to Tuberculosis. *J Infect Dis* 2019;220:1091–8. <https://doi.org/10.1093/infdis/jiz285>.
- Shannon P, Markiel A, Ozier A, Baliga NS, Wang JT, Ramage D, et al. Cytoscape: a software environment for integrated models of biomolecular interaction networks. *Genome Res* 2003;13:2498–504.
- Singh A, Varela C, Bhatt K, Veerapen N, Lee OYC, Wu HHT, et al. Identification of a Desaturase Involved in Mycolic Acid Biosynthesis in *Mycobacterium smegmatis*. *PLoS One* 2016;11:e0164253. <https://doi.org/10.1371/journal.pone.0164253>.
- Singh PK, Shaefer AL, Parsek MR, Moninger TO, Welsh MJ, Greenberg EP. Quorum-sensing signals indicate that cystic fibrosis lungs are infected with bacterial biofilms. *Nature* 2000;407:762–4.
- Sochorová Z, Petráčková D, Sitařová B, Buriánková K, Bezoušková S, Benada O, et al. Morphological and proteomic analysis of early stage air-liquid interface biofilm formation in *Mycobacterium smegmatis*. *Microbiol (United Kingdom)* 2014;160:1346–56. <https://doi.org/10.1099/mic.0.076174-0>.
- Sonden B, Kocincova D, Deshayes C, Euphrasie D, Rhayat L, Laval F, et al. Gap, a mycobacterial specific integral membrane protein, is required for glycolipid transport to the cell surface. *Mol Microbiol* 2005;58:426–40.
- Sousa S, Bandeira M, Carvalho PA, Duarte A, Jordao L. Nontuberculous mycobacteria pathogenesis and biofilm assembly. *Int J Mycobacteriology* 2015;4:36–43. <https://doi.org/10.1016/j.ijmyco.2014.11.065>.
- Stöckel S, Meisel S, Lorenz B, Klotz S, Henk S, Dees S, et al. Raman spectroscopic identification of *Mycobacterium tuberculosis*. *J Biophotonics* 2017;10:727–34. <https://doi.org/10.1002/jbio.201600174>.
- Stormer RS, Falkinham JO. Differences in antimicrobial susceptibility of pigmented and unpigmented colonial variants of *Mycobacterium avium*. *J Clin Microbiol* 1989;27:2459–65.
- Streit E, Millet J, Rastogi N. Nontuberculous mycobacteria in guadeloupe, martinique, and French Guiana from 1994 to 2012. *Tuberc Res Treat* 2013;2013:472041. <https://doi.org/10.1155/2013/472041>.
- Surman SB, Walker JT, Goddard DT, Morton LHG, Keevil CW, Weaver W, et al. Comparison of microscope techniques for the examination of biofilms. *J Microbiol Methods* 1996;25:57–70. [https://doi.org/10.1016/0167-7012\(95\)00085-2](https://doi.org/10.1016/0167-7012(95)00085-2).
- Szlarczyk D, Gable AL, Lyon D, Junge A, Wyder S, Huerta-Cepas J, et al. String v11: protein-protein association networks with increased coverage, supporting functional discovery in genome-wide experimental data sets. *Nucleic Acids Res* 2019;47.
- Takayama K, Wang C, Besra GS. Pathway to Synthesis and Processing of Mycolic Acids in *Mycobacterium tuberculosis*. *Am Soc Microbiol* 2005;18:81–101. <https://doi.org/10.1128/CMR.18.1.81>.
- Talari ACS, Movasaghi Z, Rehman S, Rehman IU. Raman spectroscopy of biological tissues. *Appl Spectrosc Rev* 2015;50:46–111. <https://doi.org/10.1080/05704928.2014.923902>.
- Tamayo R, Pratt JT, Camilli A. Roles of cyclic diguanylate in the regulation of bacterial pathogenesis. *Annu Rev Microbiol* 2007;61:131–48. <https://doi.org/10.1146/annurev.micro.61.080706.093426>.
- Tebruegge M, Pantazidou A, MacGregor D, Gonis G, Leslie D, Sedda L, et al. Nontuberculous mycobacterial disease in children - Epidemiology, diagnosis & management at a tertiary center. *PLoS One* 2016;11:1–14. <https://doi.org/10.1371/journal.pone.0147513>.
- Thomson RM. Changing Epidemiology of Pulmonary Nontuberculous Mycobacteria Infections. *Emerg Infect Dis* 2010;16:1576–83. <https://doi.org/10.3201/eid1610.091201>.

- Totani T, Nishiuchi Y, Tateishi Y, Yoshida Y, Kitanaka H, Niki M, et al. Effects of nutritional and ambient oxygen condition on biofilm formation in *Mycobacterium avium* subsp. *hominissuis* via altered glycolipid expression. *Sci Rep* 2017;7:41775. <https://doi.org/10.1038/srep41775>.
- Tripathi SM, Ramachandran R. Overexpression, purification and crystallization of lysine ϵ -aminotransferase (Rv3290c) from *Mycobacterium tuberculosis* H37Rv. *Acta Crystallogr Sect F Struct Biol Cryst Commun* 2006;62:572–5. <https://doi.org/10.1107/S1744309106016824>.
- Trivedi A, Mavi PS, Bhatt D, Kumar A. Thiol reductive stress induces cellulose-anchored biofilm formation in *Mycobacterium tuberculosis*. *Nat Commun* 2016;7:11392. <https://doi.org/10.1038/ncomms11392>.
- Umrao J, Singh D, Zia A, Saxena S, Sarsaiya S, Singh S, et al. Prevalence and species spectrum of both pulmonary and extrapulmonary nontuberculous mycobacteria isolates at a tertiary care center. *Int J Mycobacteriology* 2016;5:288–93. <https://doi.org/10.1016/j.ijmyco.2016.06.008>.
- Vandenabeele P. Raman spectroscopy. *Anal Bioanal Chem* 2010;397:2629–30. <https://doi.org/10.1007/s00216-010-3872-8>.
- Varela C, Rittman D, Singh A, Krumbach K, Bhatt K, Eggeling L, et al. MmpL Genes Are Associated with Mycolic Acid Metabolism in *Mycobacteria* and *Corynebacteria*. *Chem Biol* 2012;19:498–506.
- Varghese B, Memish Z, Abuljadayel N, Al-Hakeem R, Alrabiah F, Al-Hajj SA. Emergence of Clinically Relevant Non-Tuberculous Mycobacterial Infections in Saudi Arabia. *PLoS Negl Trop Dis* 2013;7:3–7. <https://doi.org/10.1371/journal.pntd.0002234>.
- Ventura M, Rieck B, Boldrin F, Degiacomi G, Bellinzoni M, Barilone N, et al. GarA is an essential regulator of metabolism in *mycobacterium tuberculosis*. *Mol Microbiol* 2013;90:356–66. <https://doi.org/10.1111/mmi.12368>.
- Vilch  ze C, Morbidoni HR, Weisbrod TR, Iwamoto H, Kuo M, Sacchettini JC, et al. Inactivation of the *inhA*-encoded fatty acid synthase II (FASII) enoyl-acyl carrier protein reductase induces accumulation of the FASI end products and cell lysis of *Mycobacterium smegmatis*. *J Bacteriol* 2000;187:4059–67.
- Villeneuve C, Etienne G, Abadie V, Montrozier H, Bordier C, Laval F, et al. Surface-exposed glycopeptidolipids of *Mycobacterium smegmatis* specifically inhibit the phagocytosis of mycobacteria by human macrophages: Identification of a novel family of glycopeptidolipids. *J Biol Chem* 2003;278:51291–300. <https://doi.org/10.1074/jbc.M306554200>.
- van der Walt S, Colbert SC, Varoquaux G. The NumPy Array: A Structure for Efficient Numerical Computation. *Comput Sci Eng* 2011;13:22–30. <https://doi.org/10.1109/MCSE.2011.37>.
- van der Walt S, Sch  nberger JL, Nunez-Iglesias J, Boulogne F, Warner JD, Yager N, et al. scikit-image: image processing in Python. *PeerJ* 2014;2:e453. <https://doi.org/10.7717/peerj.453>.
- Wang Z, Gerstein M, Snyder M. RNA-Seq: a revolutionary tool for transcriptomics. *Nat Rev Genet* 2009;10:57–63.
- Waskom M, Botvinnik O, O’Kane D, Hobson P, Ostblom J, Lukauskas S, et al. *mwaskom/seaborn: v0.9.0* (July 2018) 2018. <https://doi.org/10.5281/ZENODO.1313201>.
- Watters C, Fleming D, Bishop D, Rumbaugh KP. Host Responses to Biofilm. vol. 142. Elsevier Inc.; 2016. <https://doi.org/10.1016/bs.pmbts.2016.05.007>.
- van der Werf MJ, K  dm  n C, Katalini  -Jankovi   V, Kummik T, Soini H, Richter E, et al. Inventory study of non-tuberculous mycobacteria in the European Union. *BMC Infect Dis* 2014;14:62. <https://doi.org/10.1186/1471-2334-14-62>.
- Whitaker J, Rickaby W, Robson A, Bakr F, White J, Rinaldi CA. Recurrent pocket infection due to *Mycobacterium chelonae* at the site of an explanted cardiac implantable electrical device in proximity to a long-standing tattoo. *Hear Case Reports* 2016;2:132–4. <https://doi.org/10.1016/j.hrcr.2015.10.012>.
- WHO. Global Tuberculosis Report 2015. *World Heal Organ* 2015;53:160.
- WHO. WHO declares tuberculosis a global emergency. *Sozial- Und Pr  ventivmedizin SPM* 1993;38:251–2. <https://doi.org/10.1007/BF01624546>.

- Wiercigroch E, Szafranec E, Czamara K, Pacia MZ, Majzner K, Kochan K, et al. Raman and infrared spectroscopy of carbohydrates: A review. *Spectrochim Acta - Part A Mol Biomol Spectrosc* 2017;185:317–35. <https://doi.org/10.1016/j.saa.2017.05.045>.
- Wolff KA, de la Peña AH, Nguyen HT, Pham TH, Amzel LM, Gabelli SB, et al. A Redox Regulatory System Critical for Mycobacterial Survival in Macrophages and Biofilm Development. *PLoS Pathog* 2015;11:1–20. <https://doi.org/10.1371/journal.ppat.1004839>.
- World Health Organization. Global Tuberculosis Report 2019. Geneva: 2019.
- Wouters K, Maes E, Spitz J, Roeffaers MJB, Wattiau P, Hofkens J, et al. A non-invasive fluorescent staining procedure allows Confocal Laser Scanning Microscopy based imaging of Mycobacterium in multispecies biofilms colonizing and degrading polycyclic aromatic hydrocarbons. *J Microbiol Methods* 2010;83:317–25. <https://doi.org/10.1016/j.mimet.2010.09.014>.
- Wright CC, Hsu FF, Arnett E, Dunaj JL, Davidson PM, Pacheco SA, et al. The Mycobacterium tuberculosis MmpL11 Cell Wall Lipid Transporter Is Important for Biofilm Formation, Intracellular Growth, and Nonreplicating Persistence. *Infect Immun* 2017;85:1–17. <https://doi.org/10.1128/IAI.00131-17>.
- Wyk N Van, Navarro D, Blaise M, Berrin J, Henrissat B, Drancourt M, et al. Characterization of a mycobacterial cellulase and its impact on biofilm- and drug-induced cellulose production 2017;27:392–9. <https://doi.org/10.1093/glycob/cwx014>.
- Van Wyk N, Navarro D, Blaise M, Berrin JG, Henrissat B, Drancourt M, et al. Characterization of a mycobacterial cellulase and its impact on biofilm- and drug-induced cellulose production. *Glycobiology* 2017;27:392–9. <https://doi.org/10.1093/glycob/cwx014>.
- van Wyk R, van Wyk M, Mashele SS, Nelson DR, Syed K. Comprehensive comparative analysis of cholesterol catabolic genes/proteins in mycobacterial species. *Int J Mol Sci* 2019;20. <https://doi.org/10.3390/ijms20051032>.
- Xu S, Mescheryakov VA, Poce G, Chng S-S. MmpL3 is the plippase for mycolic acids in mycobacteria. *PNAS* 2017;114:7993–8.
- Yamada T, Ushijima K, Uemura O. A hospital-acquired outbreak of catheter-related nontuberculous mycobacterial infection in children on peritoneal dialysis. *CEN Case Reports* 2015;4:43–7. <https://doi.org/http://dx.doi.org/10.1007/s13730-014-0137-y>.
- Yang Y, Richards JP, Gundrum J, Ojha AK. GlnR activation induces peroxide resistance in mycobacterial biofilms. *Front Microbiol* 2018;9:1–13. <https://doi.org/10.3389/fmicb.2018.01428>.
- Yang Y, Thomas J, Li Y, Vilchèze C, Derbyshire KM, Jacobs WR, et al. Defining a temporal order of genetic requirements for development of mycobacterial biofilms. *Mol Microbiol* 2017;105:794–809. <https://doi.org/10.1111/mmi.13734>.
- Yuan S-M. Mycobacterial endocarditis: a comprehensive review. *Rev Bras Cir Cardiovasc* 2014;30:93–103. <https://doi.org/10.5935/1678-9741.20140113>.
- Zambrano MM, Kolter R. Mycobacterial biofilms: a greasy way to hold it together. *Cell* 2005;123:762–4. <https://doi.org/10.1016/j.cell.2005.11.011>.
- Zeng S, Constant P, Yang D, Baulard A, Lefèvre P, Daffé M, et al. Cpn60.1 (GroEL1) Contributes to Mycobacterial Crabtree Effect: Implications for Biofilm Formation. *Front Microbiol* 2019;10:1–15. <https://doi.org/10.3389/fmicb.2019.01149>.
- Zimhony O, Vilcheze C, Jacobs WRJ. Characterization of Mycobacterium smegmatis expressing the Mycobacterium tuberculosis fatty acid synthase I (fasI) gene. *J Bacteriol* 2004;4051–5.